AQUIFER TEST INTERPRETATION WITH SPECIAL EMPHASIS ON THE DRAWDOWN EVALUATION FOR WELLS WITHIN FRACTURE NETWORKS SMALLER THAN THE REPRESENTATIVE ELEMENTARY VOLUME (REV)

by

Ingo Bardenhagen

Thesis submitted in fulfilment of the requirements for the degree of Doctor of Philosophy in the Faculty of Natural and Agricultural Sciences, Department of Geohydrology, University of the Free State, Bloemfontein, South Africa

Promoter: Prof. G.J. van Tonder

May 2002

Herewith I ensure that I compiled the present thesis on my own effort, without any external non-academic help. I did not employ any tools other than the listed in this work. I have precisely marked all sentences that, either in words or meaning, are quoted from published or unpublished reports. No part of this thesis has been published in another thesis or habilitation before.

Acknowledgement

My stay in Namibia and the 5-years of activity as a geohydrologist at the Department of Water Affairs Namibia introduced me to the interesting topic of pumping tests in fractured aquifers. I am indebted to Prof. Dr. Gerrit van Tonder from the Institute of Groundwater Studies (IGS) at the University Bloemfontein, Republic of South Africa, who motivated me to investigate in this theme under the umbrella of a PhD. thesis. I very much appreciate his discussions and leading throughout the whole research period.

I would like to thank Prof. Dr. Wen-Hsing Chiang, Priv.-Doz. Dr. Ingrid Stober, and Mr. Cornelius Riemann for the encouraging discussions. My colleagues at the IGS are thanked for the nice working atmosphere, which I had the opportunity to enjoy during my short stays in Bloemfontein.

I would like to thank the Department of Water Affairs Namibia, Department of Water Affairs Botswana, and the IGS for allowing me the publication of pumping test data included in this work.

Thanks go also to Mr. Piet Heyns and Mr. Greg Christelis, who encouraged me on the investigation and publication of parts of the finding of this thesis.

Dr. Reiner Baumann and Mr. Erik Böker are thanked for the reading and corrections of this work.

Last but not least I would like to thank my wife, Dr. Sara Vassolo, who untiring supported and encouraged me on the long way to the finalization of this work. She was always available for discussions, reading, and corrections, and would even motivate me over points of no return.

AQUIFER TEST INTERPRETATION WITH SPECIAL EMPHASIS ON THE DRAWDOWN EVALUATION FOR WELLS WITHIN FRACTURE NETWORKS SMALLER THAN THE REPRESENTATIVE ELEMENTARY VOLUME (REV)

TABLE OF CONTENTS

LIST OF FIGURES

NOMENCLATURE

α = empirical parameter (generally $\alpha = 0.94$) [-]
β = shape factor: 1/3 for spherical blocks 1 for slab blocks [-]
Γ = Gamma function
Δh = potential or head difference over the length of interest [L]
Δl = length of interest [L]
Δt = time increment after the recovery phase starts [T]
ξ = skin factor at the well [-]
ξ_f = fracture skin factor [-]
ξ_{pp} = partial penetration skin factor [-]
ξ_T = total skin factor [-]
ρ = density of the fluid [ML^{-3}]
μ = dynamic viscosity [$ML^{-1}T^{-1}$]
A = through-flow area [L^2]
a = side length of the square fracture [L]
a_f = side half-length of the square fracture [L]
a_w = width length of the square fracture [L]
a_{wf} = width half-length of the square fracture [L]
b = extent of the flow region [L]
b_h = average half thickness of the block [L]
b_r = relative fracture half-width [L]
b_s = thickness of the skin [L]
CD_f = relative fracture storage capacity
Cr = relative fracture conductivity
d = drawdown over one log cycle [-]
d' = residual drawdown over one log cycle [L]
d_f = separation between fractures [L]
dt = integration variable [-]
Ei = exponential integral
F(u)= Theis well function [-]
F_L = function for partial penetration skin in the Laplace space
g = acceleration of the gravity [LT^{-2}]
h = aquifer or formation thickness [L]
h_d = dimensionless aquifer thickness [-]
$h_{d\text{-}hor}$ = dimensionless aquifer thickness for a horizontal fracture [-]
h_f = fracture height [L]
h_h = hydraulic head [L]
$\overline{H}_h$ = dimensionless drawdown at the source in the Laplace space [-]
$\overline{h}_h$ = dimensionless drawdown in the reservoir in Laplace space [-]
i = integer value
I_0 = modified Bessel function of the first kind of zero order
k = permeability [L^2]
K = conductivity of the matrix [LT^{-1}]
K_e = equivalent conductivity [LT^{-1}]
K_f = conductivity of the fracture system [LT^{-1}]
K_h = horizontal conductivity of the matrix or formation [LT^{-1}]
K_{hf} = horizontal conductivity of the fracture [LT^{-1}]
K_s = conductivity of the skin [LT^{-1}]

K_v = vertical conductivity of the matrix or formation [LT^{-1}]
K_{vf} = vertical conductivity of the fracture [LT^{-1}]
K_x = hydraulic conductivity of the formation in x-direction [LT^{-1}]
K_y = hydraulic conductivity of the formation in y-direction [LT^{-1}]
K_z = hydraulic conductivity of the formation in z-direction [LT^{-1}]
K_v = modified Bessel function of fractal order
K_1 = Bessel function of second kind and first order
K_o = modified Bessel function of second kind and zero order
L = Laplace transform
l_d = distance of the pumped well screen bottom to the top of the aquifer [L]
l_d' = distance of the observation well screen bottom to the top of the aquifer [L]
l_f = fracture length [L]
l_l = distance of the pumped well screen top to the top aquifer [L]
l_l' = distance of the observation well screen top to the top of the aquifer [L]
m = integer number
M = number of fracture segments
N = even number
n = dimension of the fracture flow system
p = Laplace transform variable
Q = discharge rate [L^3T^{-1}]
$\bar{q}$ = dimensionless block-to-fracture flow in the Laplace space [-]
$\bar{Q}$ = extraction rate in the Laplace space [L^3T^{-1}]
q_b = additional source function [L^3T^{-1}]
q_d, q_{fd} = dimensionless matrix-to-fracture flux [-]
Q_i = constant discharge rate of the i^{th} period [L^3T^{-1}]
q_m = influx rate per fracture segment [L^2T^{-1}]
Q_n = last constant discharge rate [L^3T^{-1}]
r = distance of an observation well to the pumped well [L]
r_c = casing radius [L]
r_d = dimensionless radius, r/r_w [-]
r', r_d', t_d', τ, u, x' = integration variables
r_{eff} = effective radius [L]
r_f = radius of the horizontal penny-shape fracture [L]
r_{pp} = radius of influence of partial penetration [L]
r_w = drilled radius or radius of the source [L]
r_x = distance of an observation well to the pumped well along the fracture [L]
s = drawdown [L]
s_{add} = additional drawdown due to skin [L]
s_d = dimensionless drawdown [-]
S_f = storage coefficient of the fracture system [-]
s_f = drawdown due to skin at the fracture [L]
s_{fd} = dimensionless drawdown in the fracture [-]
s_r = dimensionless relative separation [-]
s_w = drawdown due to skin at the well [L]
S = storage coefficient of the matrix or formation [-]
S_s = specific storage coefficient of the matrix or formation [L^{-1}]
S_{sf} = specific storage of the fracture system [L^{-1}]
S_w = storage capacity of the source [-]
t = time [T]
t' = time corrected for the superposition effects in the drawdown phase [T]

t_0 = time at which the straight-line intercepts the time axis [T]
t_{01} = time at which the first straight-line intercepts the time axis [T]
t_{02} = time at which the second straight-line intercepts the time axis [T]
t_{corr} = corrected time [T]
t_d = dimensionless time [-]
t_d' = integration variable
t_i = start time of the i^{th} discharge period [T]
t_i' = end time of the i^{th} discharge period [T]
T = matrix or formation transmissivity [L^2T^{-1}]
T_f = fracture or feature transmissivity [L^2T^{-1}]
V_f = fracture volume [L^3]
V_i = weighting factor
w = fracture aperture [L]
W_d = dimensionless well bore storage coefficient [-]
$x^{1/2}$ = function for reservoir properties
x_d = Cartesian dimensionless distance, x/x_f [-]
x_f = fracture half-length [L]
x_L = dimensionless half-length of the model area [-]
y_d = Cartesian dimensionless distance, y/x_f [-]
z = vertical position of the observation well [L]
z_f = distance from the fracture to the lower boundary of the reservoir [L]

1. INTRODUCTION

Pumping tests are the most important experiments for aquifer investigation in the ground water industry. They are the only method that, based on the drawdown analysis, provides simultaneous information on the hydraulic behavior of the well, the reservoir, and the reservoir boundaries, which are essential for an efficient aquifer and well field management. The drawdown behavior in primary aquifers has been widely investigated and is well-known. However, research is still needed to completely understand the drawdown development in secondary or fractured aquifers, due to the complexity of the flow situation.

Fractured aquifers are characterized by the fact that the water flows along fractures, faults, or other open geological features. These features are embedded in a matrix that has either porous nature, like in sandstone, or is almost impermeable (inert), as in the case of granite.

Fractures, faults, or bedding planes are geological features that have been developed either by tectonic forces or artificially (hydraulic fracturing) and often act as high or extremely high conductive conduits. These geological structures can appear either as a single feature or interconnected to give way to clustered systems of various complexity, from discontinuous fracture networks to continuously fractured reservoirs. The continuous fractured aquifer is the most interconnected case and is often described as a homogeneous fractured network (for example the double porosity case).

The drawdown behavior in wells that intersect single preferential flow paths has been investigated quite well by various authors (Prats, 1961; Gringarten *et al.*, 1974; Cinco-Ley *et al.*, 1978; Raghavan *et al.*, 1978; Agarwal *et al.*, 1979; Cinco-Ley & Samaniego, 1981a; Valkó & Economides (1997)). On the other side, the homogeneous fractured case has also been intensely treated (Barenblatt *et al.*, 1960, Warren & Root, 1962; Kazemi, 1969; Boulton & Streltsova, 1977; Moench, 1984; Bourdet, 1985; Cinco-Ley & Samaniego, 1985; Olarewaju, 1996; Olarewaju *et al.*, 1997). However, very little is known about the drawdown behavior in wells situated in an aquifer that is neither a continuous fractured nor a single fractured case (discontinuous fracture networks).

Aim of this thesis is the investigation of the drawdown behavior in discontinuous fracture networks below the representative elementary volume (REV). It is emphasized that a proper evaluation of the aquifer properties is not possible without a thorough analysis and diagnosis of the test curves. To achieve the goal, this work is subdivided into four major parts. The first part (Chapter 2) summarizes known reservoir and well effects on ground water flow that affect drawdown and recovery data. Basic instructions for pumping test planning and interpretation are given in the second part (Chapter 3), which also includes the use of various diagnostic tools. In the third part (Chapter 4), a selection of analytical models used for the analyses of drawdown curves in wells that intersect single fractures or are located in homogeneous fractured aquifers is presented. Methodologies for the analysis of pumping test data for each of these analytical models are described step by step in a kind of a handbook. Theoretical and field examples are evaluated using the computer program TPA (**T**est **P**umping **A**nalysis)[1]. The program, which was compiled under the

[1] TPA was developed using Pascal language applying object oriented programming (OOP) with the Borland Delphi 3 compiler. It can be downloaded for free from the IGS (Institute of Groundwater Studies) web page. The program allows the edition of own pumping test data by hand, but also the import of data from Excel spread sheet and ASCII files. The pumping test evaluation curves can be

umbrella of this thesis provides powerful tools for the diagnostic and analysis of pumping test data and a simulator that can be used for the forward modelling of test curves. The simulator provides solutions for a variety of fractured aquifer models like the double porosity, the single vertical and horizontal fracture with both finite and infinite conductivity, and the generalised radial flow (Barker, 1988). The influences of reservoir boundaries, well bore storage, well bore and fracture skin, and partial penetration can be considered in some of these solutions[2]. Most of the drawdown curves presented in this thesis were drown using TPA.

The fourth part (Chapter 5) of this thesis studies the influence of various realistic combinations of discontinuous fracture networks on the drawdown behavior with the help of numerical modelling. Numerical models are flexible enough to accommodate to complex study cases and thus, they are an appropriate tool for these investigations. Furthermore, boundary conditions are clearly set and defined, so that even minor effects on the drawdown curves can be explained. Additionally, they are affordable compared to the usually very expensive detailed field investigations.

Although turbulent and non-laminar flows can occur within fractures (Wollrath & Zielke, 1990), many experimental works demonstrate that laminar flow is also common along these features (Witherspoon *et al.*, 1979). Further, Guppy *et al.* (1982) have shown that, for single fractures, the drawdown curves computed using non-laminar flow are coincident with those obtained with the Darcian law. Therefore, instead of using numerical models based on non-laminar flow like ROCKFLOW (Zielke *et al.*, 1984-1994), FRAC3DVS (Therrien and Sudicky, 1996), or Spring (2000), this chapter will use MODFLOW (Harabaugh *et al.*, 1999) in a first approach, which is based on the Darcian law. This thesis demonstrates that the application of MODFLOW is sufficient for the examples studied in this thesis. However, it cannot be applied for inclined fractures or crossings others than perpendicular. For such cases the use of any of the above mentioned models is imperative.

This chapter shows that analytical results can be reproduced using numerical modelling based on the Darcian law in combination with an appropriate set up. This is demonstrated using single vertical fracture cases (Gringarten *et al.*, 1974, Cinco-Ley *et al.*, 1978). In addition, the influences of fracture aperture and relative storage capacity on the drawdown curve in a single vertical fracture are presented. To complete the analysis of vertical structures, the drawdown curves in a series of parallel and crossed features are shown. Further, the single horizontal fracture case is modelled to confirm the semi analytical solution from Valkó & Economides (1997). The effects of the structure shape on the drawdown curve are investigated. Furthermore, the results obtained using a series of parallel horizontal structures is presented. Finally, combinations of intersected vertical and horizontal structures are described.

directly printed from the program environment, or saved as a WMF file, or transferred as a WMF file via clip-board.

[2] The simulator also provides solutions for primary aquifers like confined, leaky, delayed response, and two aquifers. It is possible to combine this solutions with the influences from reservoir boundaries, well bore storage, well bore skin, partial penetration, and horizontal well.

2. BASICS ON RESERVOIR AND WELL EFFECTS

The rock properties that influence the ground water flow in fractured reservoirs are introduced in this chapter. Further, the governing laws and flow situations that describe the drawdown behavior in such aquifers are presented. Finally, the influence of various well and reservoir boundaries on the drawdown curves is described.

All drawdown curves presented in this chapter are produced using the program TPA, which was developed under the umbrella of this thesis.

2.1 Fracture Network Properties

Characteristic for fractured aquifers is the fact that a substantial volume of water flows along fractures. Those fractures are usually embedded in porous matrix blocks (sandstone) or micro fissured blocks (quartzite), which have a low permeability compared to the fracture conductivity but capable to store water in the uncountable pores or micro fractures. In extreme cases the blocks between the fractures have such a low permeability (granite) that very little water can be exchanged between fracture network and matrix, which is in this case called 'inert'.

If fractures are densely interconnected they form a 'fracture network continuum' characterized by a large storage capacity that contributes substantially to the volume extracted by a pumped well. Whether a fracture network is a continuum or not, is determined by the following three properties:

- representative elementary volume (REV)
- fracture connectivity
- conductivity contrast between fracture and matrix

The REV is the characteristic volume of fractured rock that can be represented by a homogeneous isotropic medium whose hydraulic properties do not change significantly if an additional volume of rock is added (Fig. 2.1) (Long *et al.*, 1982). According to Long & Witherspoon (1985), a fractured reservoir can have various REV depending on the scale of the investigation and, in some instances, it is not possible to define a REV at all.

The fracture connectivity describes the interconnection between fractures in a given volume of rock, which is a function of the fracture length and fracture density. Generally the fracture network continuity of a rock volume increases with increasing fracture length and fracture density (Long & Witherspoon, 1985).

The conductivity contrast between fracture and matrix can diminish or increase the continuous behavior of a fracture network. Wei *et al.* (1998) by means of numerical modelling observed linear flow in a well situated in a parallel fracture system embedded in a matrix with a high conductivity contrast between fracture (K_f) and matrix (K) (K_f/K = 10000). The same fracture distribution with a lower contrast (K_f/K = 100) resulted in a long bilinear flow phase followed by a radial flow phase. A similar situation was observed in a perpendicular two-dimensional fracture network with low contrast, whereas using a high contrast the system behaved a homogeneous media alike. However, both extremes the continuum and the single fracture case have very characteristic flow behavior that can be observed during pumping tests and will be presented in the following section.

It is often observed that in fractured aquifers the initially measured air lift yield is a strong overestimation of the long-term sustainable yield of the well. The explanation

lies on the fact that the storage of a single fracture or fracture cluster is very limited, which can be demonstrated by the following calculation:

$$V_f = l_f \cdot h_f \cdot w = 2000m \cdot 200m \cdot 0.002m = 800m^3$$

where
V_f = fracture volume [L^3]
l_f = fracture length [L]
h_f = fracture height [L]
w = fracture aperture [L]

A well located in such a fracture, which extracts water at a rate of 10 m^3/h would empty it within 80 hours. However, if the matrix in which the fracture is embedded is not inert, this does not happen because the matrix is drained by the fracture. In this instance the fracture acts as a conduit or preferential flow path.

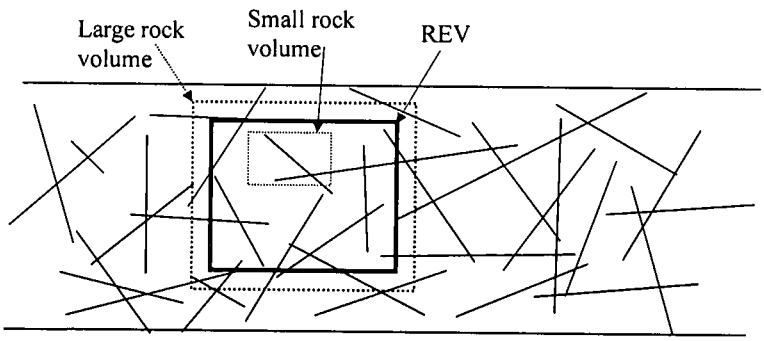

Figure 2.1. The representative elementary volume REV of a fractured rock is considered as hydraulically homogeneous (continuously fractured). A volume of rock larger than the REV would maintain the same hydraulic properties, but not a smaller volume

2.2 Governing Equation for Flow in Fractured Aquifers

The Poiseuille equation or 'cubic law' governs the laminar flow within a single fracture (Witherspoon *et al.*, 1979). This law is a special case of the 'Darcian Law', which is written as:

$$Q = K \cdot \frac{\Delta h}{\Delta l} \cdot A \qquad (2.1)$$

where
Q = discharge rate [L^3T^{-1}]
A = through-flow area [L^2]
Δh = potential or head difference over the length of interest l [L]
Δl = length of interest [L]
K = hydraulic conductivity of the matrix or formation [LT^{-1}]

The hydraulic conductivity is defined as $K = k\rho g / \mu$, where
ρ = density of the fluid [ML^{-3}]
g = acceleration of the gravity [LT^{-2}]
μ = dynamic viscosity [$ML^{-1}T^{-1}$]
k = permeability [L^2]

In the 'cubic law' the hydraulic conductivity is defined as $K = (2 \cdot w)^2 \cdot \rho \cdot g / 12 \cdot \mu$ [L/T] and $A = w \cdot h_f$ [L^2]. Replacing K and A in equation (2.1):

$$Q = \frac{w^3 \cdot \rho \cdot g \cdot h_f}{3 \cdot \mu} \cdot \frac{\Delta h}{\Delta l} \qquad (2.2)$$

where
w = fracture aperture [L]
h_f = fracture height [L]

Equation (2.2) represents the Poiseuille equation, which is valid for laminar flow or Reynold numbers smaller than 2300 (Wendland, 1996). The rate Q is a function of the cube of the fracture aperture, hence the name 'cubic law'.

Taking into consideration equation (2.2), the cone of depression produced by a pumped well at a certain observation point P(r,z) in a fracture continuum can be described by the following diffusivity equation in cylindrical coordinates (Moench & Ogata, 1984):

$$K_{hf} \frac{1}{r} \frac{\partial}{\partial r}\left[r \frac{\partial h_h(r,t)}{\partial r} \right] + K_{vf} \frac{\partial^2 h_h(r,t)}{\partial z_o^{\,2}} = S_s \frac{\partial h_h(r,t)}{\partial t} + q_b \qquad (2.3)$$

where
h_h = hydraulic head [L]
r = distance of an observation well to the pumped well [L], with $r \geq r_w$
r_w = drilled radius or radius of the source [L]
z_o = vertical position of the observation point P [L]
K_{hf} = horizontal conductivity of the fracture network [LT^{-1}]
K_{vf} = vertical conductivity of the fracture network [LT^{-1}]
S_s = specific storage coefficient of the reservoir [L^{-1}]
q_b = additional source function

Equation (2.3) is valid under following conditions

- negligible change in the gravity acceleration
- constant fluid properties
- laminar flow
- confined conditions

In a fully penetrating well the hydraulic head does not vary with depth. Therefore, the second term on the left hand side in equation (2.3) becomes zero and the equation reduces to an ordinary linear inhomogeneous differential equation.

The solutions of equation (2.3) that will be discussed in this chapter were derived by several authors using either the Laplace transformation or Green's functions under different boundary conditions.

The Laplace transformation L applied to the hydraulic head function $h_h(t)$ is often used to solve radial symmetric boundary conditions. It reads

$$L\{h_h(t)\} = \bar{h}_h(p) = \int_0^\infty e^{-p \cdot t} \cdot h_h(t) \cdot dt \qquad (2.4)$$

The advantage of the Laplace transformation lies in the elimination of one of the integration variables, which in many cases results in an ordinary arithmetic function. The inversion of this function can be done either analytically or numerically. Mavor

& Cinco-Ley (1979) and Moench & Ogata (1984) showed that the Stehfest (1970) algorithm used for the numerical inversion of the Laplace transform is extremely fast and usually accurate enough to be used in these cases. The Stehfest algorithm reads:

$$h_h(t) \approx \left(\frac{\ln 2}{t}\right) \cdot \sum_{i=1}^{N} V_i \cdot \bar{h}_h(p) \cdot \left[\frac{i \cdot \ln 2}{t}\right] \qquad (2.5)$$

where V_i are weighting factors calculated as:

$$V_i = -1^{(\frac{N}{2})+i} \cdot \sum_{n=\frac{i+1}{2}}^{\min(i,\frac{N}{2})} \frac{n^{\frac{N}{2}+1} \cdot (2n)!}{(\frac{N}{2}-n)!\,n!\,(n-1)!\,(i-n)!\,(2n-i)!}$$

with
N = even number
i,n = integer values

The advantage of the algorithm lies in the fact that V_i is calculated only once for a given even number N, becoming hence very fast. Stehfest (1970) and Walton (1996) report that the quality of the results decreases with increasing number of N due to rounding errors. For this reason solutions derived in TPA use a range of N from 4 to 26 depending on the time interval calculated.

Green's functions were first applied to boundary flow problems in fractured aquifers by Gringarten & Ramey (1973) and have the advantage that they allow the combination of two source functions by simply multiplication, which is known as Newman product. Using this technique Gringarten *et al.* (1974) and Gringarten & Ramey (1974) derived solutions for the drawdown in wells situated in single vertical and horizontal fractures. The drawdown solutions for pumping wells located in vertical fractures with uniform flux and infinite flux are generally analytically derived, whereas in most cases the drawdown in observation wells within the matrix is numerically determined.

2.3 Flow Behavior in Fractured Media

The following flow types can occur during pumping tests in fractured reservoirs (Barker, 1988):

- linear flow
- radial flow
- spherical flow

2.3.1 Linear flow

The name 'linear flow' derives from the way in which the pressure drops along fractures: linear-proportional to the extraction rate. Linear flow is also described as 'parallel flow' (Kruseman & de Ridder, 1991) because of the parallelism between the streamlines.

The typical geological features where linear flow is observed are sub-vertical fractures, faults, or dikes. The different flow phases that can be distinguished during pumping tests in those features are listed below (Fig 2.2):

- linear fracture flow is observed when the feature has a finite conductivity and is either embedded in a inert formation (matrix) or in a low conductivity formation (Boehmer & Boonstra, 1986; Cinco-Ley & Samaniego, 1981a)

- if the matrix is permeable enough, the linear flow in the fracture is superposed by a perpendicular linear flow from the formation to the fracture. This flow situation is described as the 'bilinear flow' (Cinco-Ley & Samaniego, 1977)
- linear flow from the formation to the fracture is also observed in the case of infinite conductivity single features with negligible storage (Gringarten *et al.*, 1974)
- a special case of bilinear flow occurs in reservoirs that consist of a continuous fracture network embedded in porous matrix blocks (Fig. 2.3), which is known as double porosity reservoir (Barenblatt *et al.*, 1960) or naturally fractured reservoir (Mavor & Cinco, 1979)

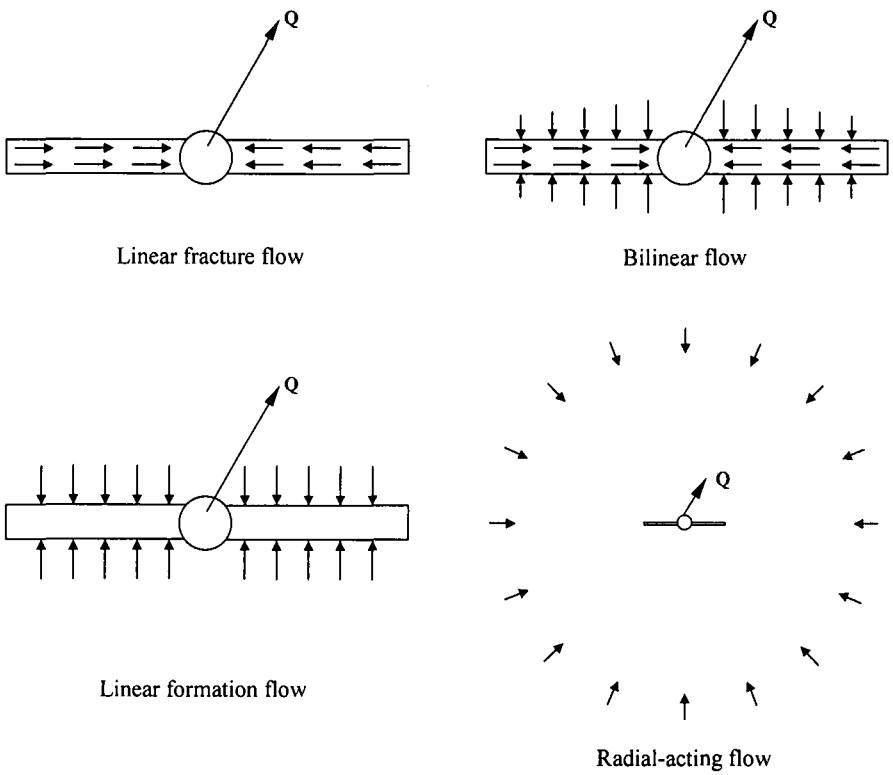

Figure 2.2. Different flow phases observed in a single fracture of finite extension embedded in an infinite formation (after Cinco-Ley & Samaniego, 1981a)

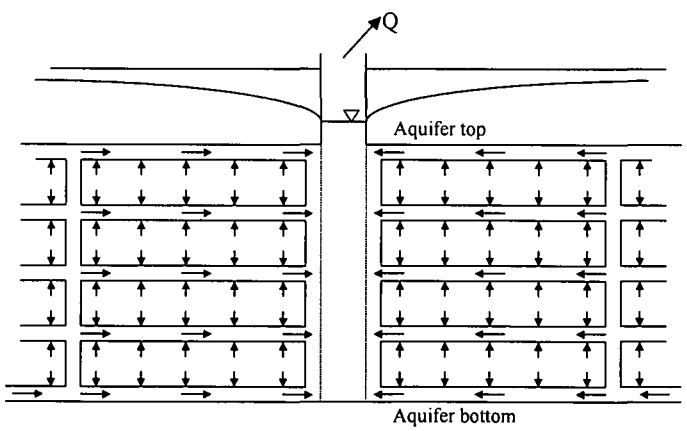

Figure 2.3. Ground water flow in an idealised double porosity aquifer

2.3.2 Radial Flow

Radial flow (also known as pseudo-radial flow or radial-acting flow) appears when the cone of depression is approximately circular (Prats, 1961). It is generally observed in a fully penetrating well (line source) located in homogeneous reservoirs, but also in a well in any fractured reservoir that can be considered as continuum. Prats (1961) demonstrated that radial-acting flow also appears for a single fracture case at late time, when the cone of depression becomes almost radial (Figure 2.2).

2.3.3 Spherical Flow

In cases where the extraction source is a point in an isotropic medium, the cone of depression becomes a sphere (Gringarten & Ramey, 1973). In sedimentary rock aquifers or igneous rock aquifers with an upper weathered zone, spherical flow will be observed only within small dimensions and over a short period of time because the spherical cone of depression will reach the bottom of the aquifer and the cone will become an ordinary radial flow (Fig. 2.4). Furthermore, due to anisotropy effects in the aquifer the sphere will become an ellipsoid. Therefore, the spherical flow can be considered as a special case of a partial penetrating well in a formation with isotropic conductivity ($K_x = K_y = K_z$ or $K_h = K_v$).

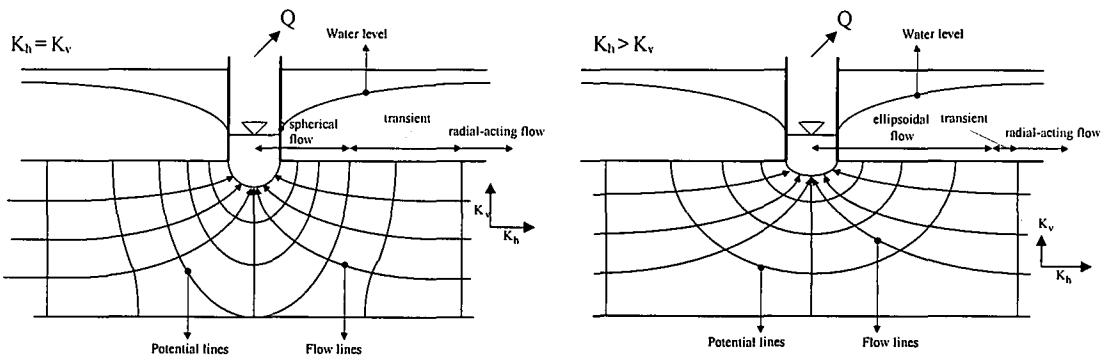

Figure 2.4. Spherical flow behavior in a bounded aquifer under isotropic ($K_h = K_v$) and anisotropic ($K_h > K_v$) conditions

2.4 Influence of Well and Reservoir Boundaries

Following well and additional reservoir effects can affect the drawdown and recovery data within fractured aquifers:

- well bore storage
- well bore skin
- partial penetration skin
- fracture skin
- pseudo-skin
- fracture dewatering
- reservoir boundaries

2.4.1 Well bore storage

Often the early time drawdown in a pumped well graphs with a slope of 1 in a log-log plot (Fig. 2.5), which indicates that the drawdown is linear proportional to the discharge time. This behavior is described as well bore storage effect and is perceptible for a longer period in low transmissivity media. The well bore storage effect can also be seen in observation wells. However, this effect decreases with increasing distance to the pumped well and disappears at approximately 1000 times the well radius (Fig. 2.5) (Streltsova, 1988).

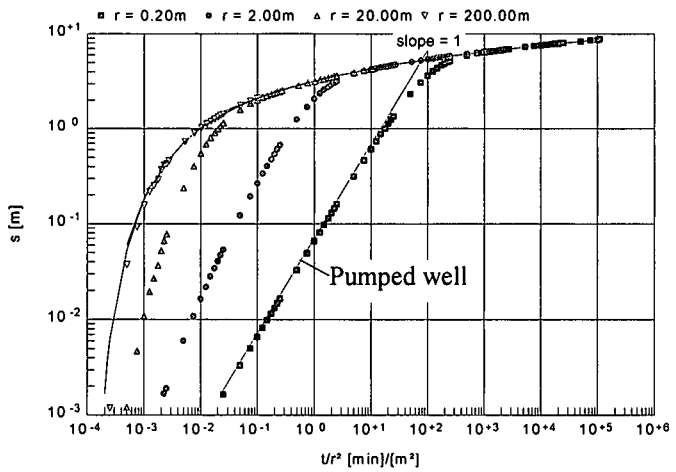

Figure 2.5. Well bore storage effect in a pumped well and observation wells at various distances. Straight-line slope 1 indicates the well bore storage in the pumped well. The solid curve shows the drawdown in the four wells without well bore storage effect. Aquifer type: confined, infinite extended; Discharge Q = 12.5 m^3/h; Transmissivity T = 50 m^2/d; Storage coefficient S = 10^{-4}; Drilled radius r_w = 0.2 m. The well bore storage effect disappears at a relative distance r/r_w = 1000.

The unit slope, which is also typical for closed reservoirs, is the basis for the explanation of the well bore storage effect. When the pumping process starts, all the water is extracted from the well bore that acts as a closed reservoir at this stage. This results in a steep gradient between the water level in the well and the aquifer next to the well. At this early time the gradient within the aquifer is still too small to provide enough water to cover the demand in the well. With time, the gradient in the aquifer increases and more and more water can be provided, which results in a decrease of the well bore storage effect. The well bore storage effect disappears when the water level in the well coincides with the water level in the reservoir next to the well (Fig. 2.6). Due to this behavior, the well bore storage effect can be considered as a kind of delayed response of the aquifer to the extraction in the well.

The time span in which the well bore storage is visible cannot be shorten by increasing the extraction rate, as shown in Fig. 2.7.

Given wells with different radius pumped at the same rate, the well with a smaller casing radius will show the larger drawdown at early time (Fig. 2.8A). This results in a larger gradient between the water level in the well and the aquifer next to the well, which forces a deeper cone of depression in the aquifer. Therefore, after a time t_i, the portion of the discharge rate provided by the aquifer is larger in the well with the smaller casing radius (Fig. 2.8B). This is true during the phase, where the drawdown is affected by well bore storage.

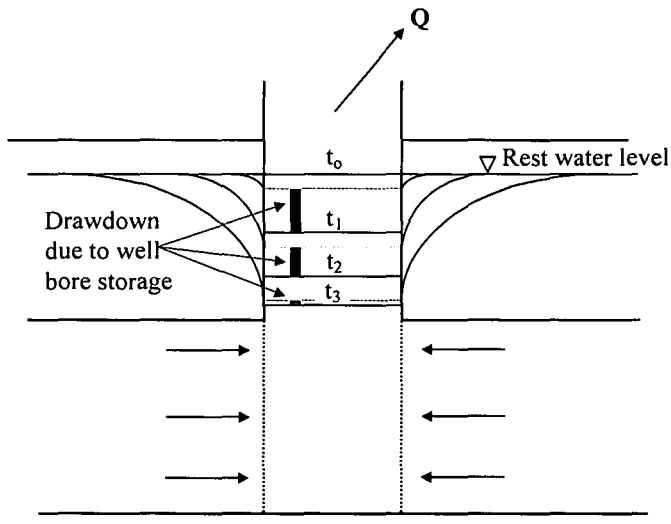

Figure 2.6. Relationship between gradient changes in the reservoir and well bore storage

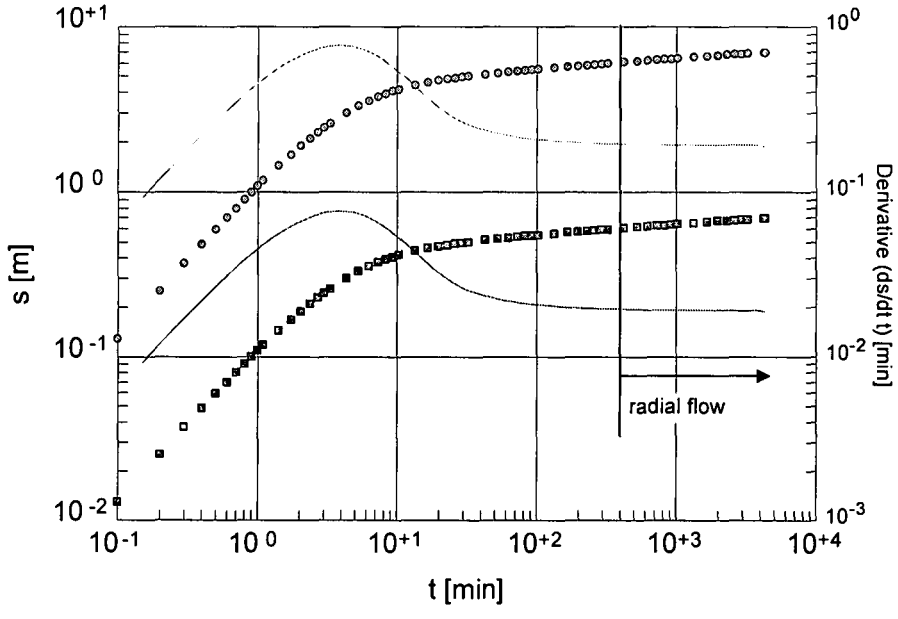

Figure 2.7. Drawdown in a pumping well which shows well bore storage effect with extraction rates of 10 m³/h (dots) and 1 m³/h (squares). The example shows that the well bore storage effect is not affected by discharge rate or, in other words, the well bore storage effect in a given well is only related to the pumping time but not to the extraction rate. Therefore a higher pumping rate produces only a deeper drawdown, but does not overcome the well bore storage effect earlier. The well bore storage effect should rather be understood as delayed response of the aquifer storage

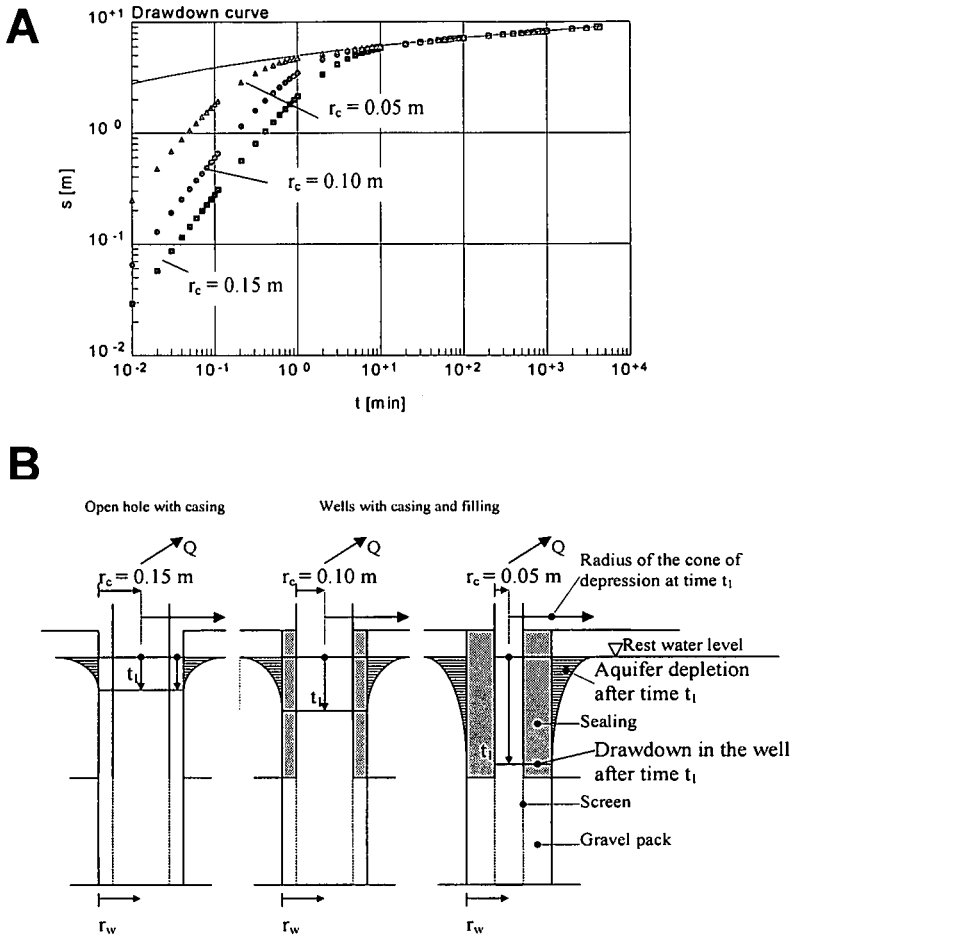

Figure 2.8. Well bore storage effect, illustrated as drawdown A and sketch B in three pumping wells with different casing radius r_c. Aquifer type: confined, infinite extended; Discharge rate Q = 12.5 m^3/h; Transmissivity T = 50 m^2/d; Storage coefficient S = 10^{-4}; Drilled radius r_w = 0.15 m. Solid curve in A indicates the drawdown without well bore storage effect

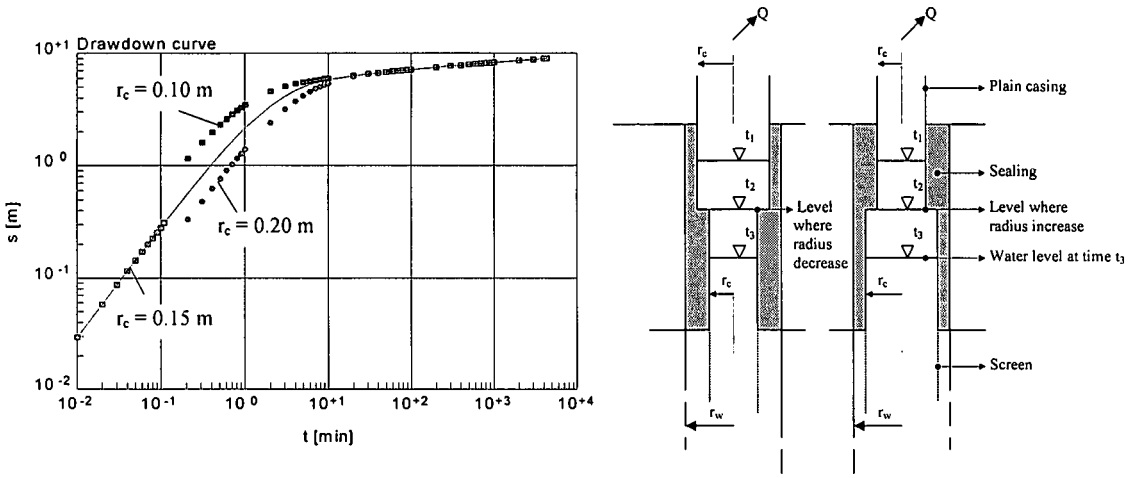

Figure 2.9. Drawdown in a pumping well during the well bore storage phase due to changes of the casing radius. Solid curve indicates the drawdown without changes in the casing radius. Aquifer type: confined, infinite extended; Discharge Q = 12.5 m^3/h; Transmissivity T = 50 m^2/d; Storage coefficient S = 10^{-4}; Drilled radius r_w = 0.15 m

If the water level in a telescoped casing drops from a bigger diameter into a smaller diameter the drawdown increases suddenly (Fig. 2.9). Contrarily, if the water level drops from a smaller diameter into a bigger diameter the drawdown decreases until the well bore storage effect vanishes (Fig. 2.9) (Earlougher, 1977). The same effects will appear if the diameter of the drilled radius changes in relation to the casing radius.

Ramey & Gringarten (1976) found that well bore storage effect can also occur when the water-well system is substantially compressible, e.g. extremely hot ground water from geysers that is heated up and contains volatile components or the pumping test is performed in a section delimited by compressible packer systems. However, ground water under typical physical conditions is almost incompressible for all practical purposes (Papadopulos & Cooper, 1967; Moench, 1984). For this case, Moench & Ogata (1984) defined the dimensionless well bore storage coefficient W_d:

$$W_d = \frac{r_c^2}{2 \cdot r_w^2 \cdot S} \qquad (2.6)$$

where
r_c = casing radius [L] in which the water level change occur
r_w = drilled radius [L]
S = storage coefficient of the reservoir [-]

The dimensionless well bore storage coefficient W_d is included in the determination of the drawdown affected by well bore storage (Section 2.4.2).

2.4.2 Well bore skin

Well bore skin can be caused by a thin layer with a very small storage capacity, which is located between borehole wall and aquifer and restricts the inflow to the pumped well. In the presence of a high conductivity zone around the pumped well, non-laminar or turbulent flow can give place to a similar effect (Kruseman & de Ridder, 1991). As a result of any of these effects, an additional drawdown is observed within the well (Fig. 2.10). It averages the effects of various sources as clogged screens, gravel pack, too small open area of the screens and mineral precipitation between borehole wall and formation. Mathematically the losses caused by well bore skin are described by a linear and a non-linear term (Jacob, 1946) that are constant as long as the discharge rate is constant (Kawecki, 1995). The sum of both well loss components can be represented by a constant total well skin factor ξ [-], which is simply added to a given well function F (van Everdingen, 1952) to calculate the total drawdown within the pumped well:

$$F(u,\xi) = F(u) + \xi \qquad (2.7)$$

Here u is the argument, which is a function of the aquifer parameters T and S as well as the geometry of the extraction source over the extraction period. The drawdown affected by a skin is a curve parallel to that without skin effects, whereas no effects appear during the recovery phase, except during the well bore storage period (Fig. 2.11). Due to the parallel shift, the determination of the transmissivity is not affected by the presence of well bore skin. However, the storage coefficient will be wrongly evaluated, as it will be explained in Section 3.1.3.

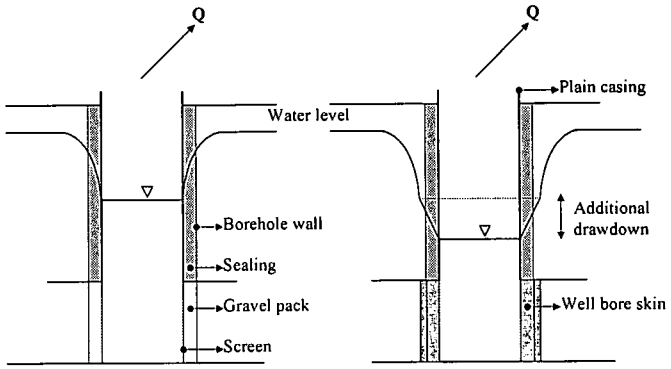

Figure 2.10. Well bore skin and its effect on the drawdown in a pumped well

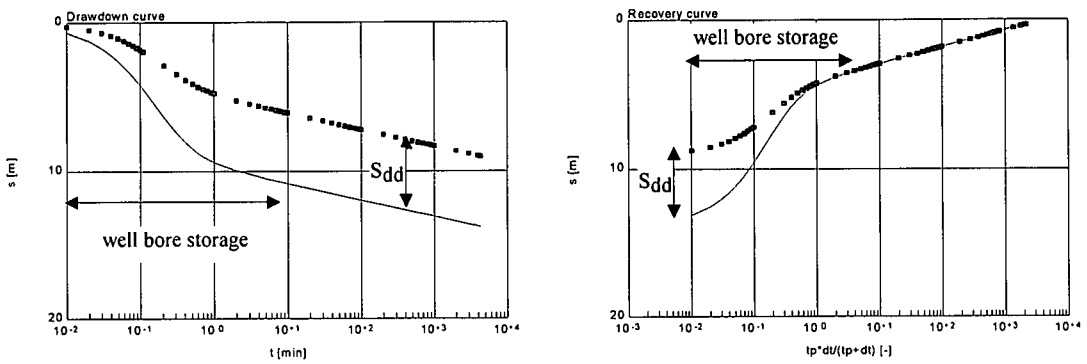

Figure 2.11. Drawdown and recovery curve in a pumping well with and without additional drawdown caused by a skin

The drawdown s for a fully penetrating well in a homogeneous confined aquifer pumped at constant discharge rate and affected by skin, writes (van Everdingen, 1956)

$$s = \frac{Q}{4 \cdot \pi \cdot T} \cdot \left[Ei(u) + 2\xi \right] \qquad (2.8)$$

where

$$u = \frac{S \cdot r_w^2}{4 \cdot T \cdot t}$$

$$F(u) = Ei(u), \quad with \quad Ei = \int_u^{\infty} \frac{e^x}{x} dx$$

Q = discharge rate [L^3T^{-1}]
T = matrix or formation transmissivity [L^2T^{-1}]
t = time [T]
r_w = drilled radius or radius of the source [L]
S = storage coefficient of the matrix or formation [-]

The dimensionless well skin factor ξ derived from equation (2.8) reads:

$$\xi = \frac{2 \cdot \pi \cdot T \cdot s}{Q} - 0.5 \cdot Ei(u) \qquad (2.9)$$

If $u \leq 0.03$, the exponential integral Ei(u) is satisfied by the Cooper & Jacob (1946) approximation: $Ei(u) \approx -\ln(1/u)-0.5772$ within 1% error. The corresponding additional

drawdown s_{add} in metre can be calculated from following relationship (Kruseman & de Ridder, 1991)

$$s_{add} = \frac{\xi \cdot Q}{2 \cdot \pi \cdot T} \qquad (2.10)$$

In a homogeneous aquifer and an ideal well ξ is zero. Physically this would mean that the effective radius r_{eff} is equal to the drilled radius r_w because ξ can be related to drilled radius as follows (Sabet, 1991):

$$r_{eff} = r_w \cdot e^{-\xi} \qquad (2.11)$$

By restricted inflow, ξ becomes positive, which according to equation (2.11) results in an effective radius smaller than the drilled radius, what is known as negative skin effect (de Marsilly, 1986). In cases where the permeability of the formation around the well is improved, for example with well development, a negative skin factor ξ will be observed (de Marsilly, 1986; Gustafson & Anderson, 1997), which results in an enlarged effective radius (positive skin effect). However, for practical purposes it is unlikely that the development would produce a negative skin factor smaller than -0.5 (Fig. 2.12). An increased effective radius will be observed in a well situated in single fracture that acts as a conduit (Horne, 1995).

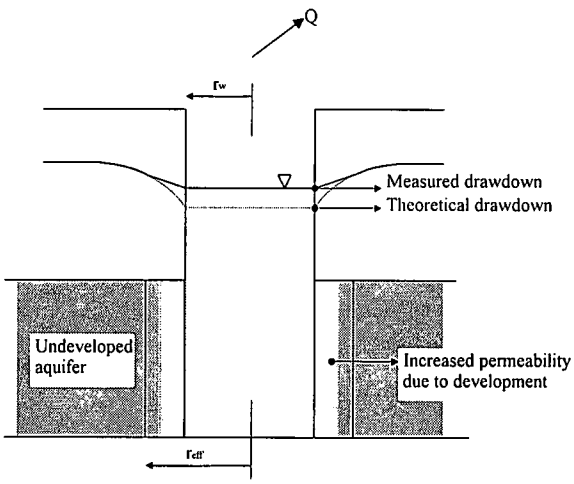

Figure 2.12. Increased effective radius (or positive skin effect), due to an increased permeability zone around the well caused by development or fracture influence

The additional drawdown caused by skin is almost instantaneous, due to the limited storage capacity of the skin layer. During the radial-acting flow phase the calculated skin effect using equation (2.9) will plot always as a horizontal line in a semi-log plot, but not for those parts of the curve affected by well bore storage or other reservoir effects (Fig. 2.13). This effect can be used for identification of the radial-acting flow phase.

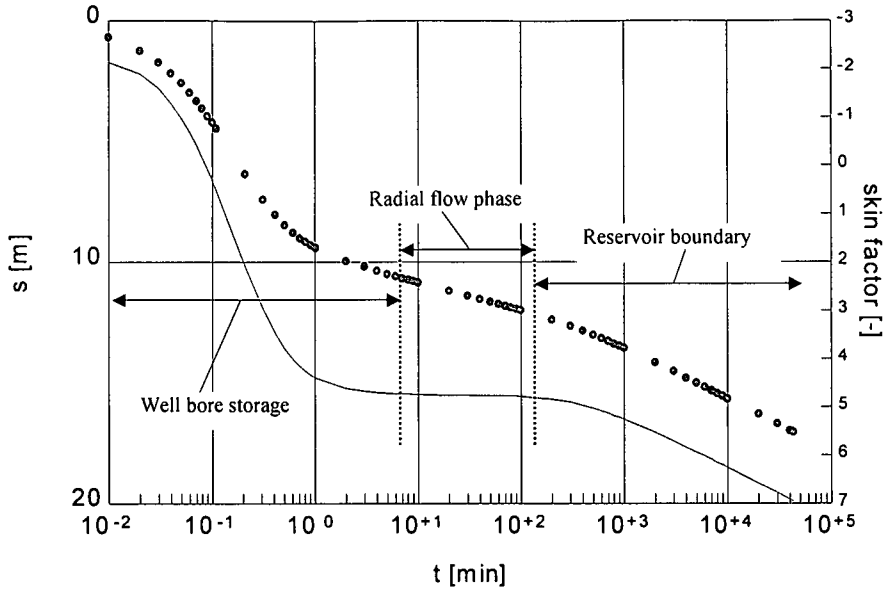

Figure 2.13. Drawdown data (dots) and skin factor ξ (solid line) for a pumping well with well bore storage in a confined homogeneous aquifer and one closed boundary. The skin factor (solid line) plots as a horizontal during the radial-acting flow phase

2.4.3 Partial penetration skin

The reduced entrance area in a partial penetrating well causes an additional drawdown due to high velocity losses at the bottom of the well and anisotropy effects of the aquifer in the area closed to the well (Fig. 2.14).

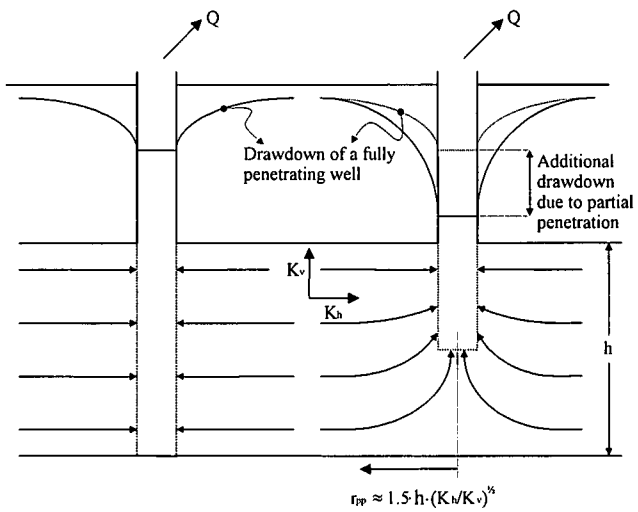

Figure 2.14. Flow to a fully penetrating well and a partial penetrating well

Under partial penetration effects, the slope of the drawdown at the pumped and observation wells within the critical distance r_{pp} is increased and not only shifted as in the case of well bore skin (Fig. 2.15). This effect, if not considered, can lead to an underestimation of the reservoir transmissivity, which might not be dangerous in the design of a water supply scheme, but certainly it is in the design of a dewatering scheme for mining or engineering purposes. For late time data only, an additional drawdown shown as a parallel shift is observed (Fig. 2.15). Moench & Ogata (1984) give following equation for the calculation of the partial penetration skin in the Laplace space:

$$F_L = \frac{2}{(l_l - l_d)(l_l' - l_d')} \sum_{n=1}^{\infty} \frac{1}{n^2} \left[\sin(x_l n) - \sin(x_d n)\right] \cdot \left[\sin(x_l' n) - \sin(x_d' n)\right] \cdot K_o(\varphi) \qquad (2.12)$$

$$\varphi = \left[r^2 x + \Omega \left(\frac{n\pi r}{h} \right)^2 \right]^{\frac{1}{2}}$$

where

$x^{1/2}$ = function that describes the reservoir properties. For a line source in a homogenous confined aquifer $x^{1/2} = (p \cdot S/T)^{1/2}$

K_o = modified Bessel function of second kind and zero order

T = matrix or formation transmissivity [L^2T^{-1}]

S = storage coefficient of the matrix or formation [-]

p = Laplace transform variable [-]

Ω = K_v/K_h [-]

K_v = vertical reservoir conductivity [LT^{-1}]

K_h = horizontal reservoir conductivity [LT^{-1}]

l_l = top of the screen related to the top aquifer in the pumped well [L]

l_l' = top of the screen related to the top aquifer in the observation well [L]

l_d = bottom of the screen related to the top aquifer in the pumped well [L]

l_d' = bottom of the screen related to the top aquifer in the observation well [L]

h = aquifer or formation thickness [L]

n = integer value from 1 to infinite, for practical purposes n = 30 is sufficient

The application of the numerical inversion algorithm of Stehfest (1970) to equation (2.12) expressed as

$$\bar{h}(p) = \frac{F_L}{p} \qquad (2.13)$$

gives the additional drawdown due to the partial penetration skin ξ_{pp}.

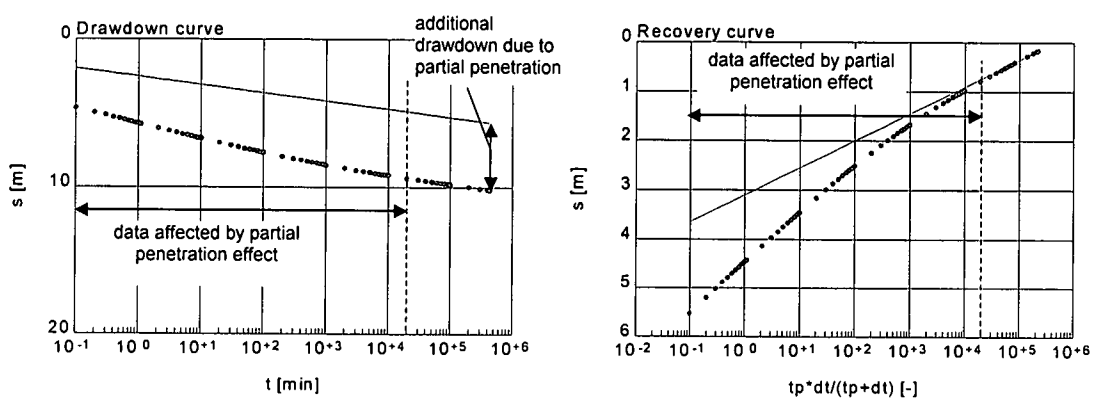

Figure 2.15. Increased drawdown and recovery slope in a pumped well at early time due to partial penetration skin (dots). Solid line indicates the drawdown and recovery for a fully penetrating well. Aquifer type: confined, infinite extended; Transmissivity T = 100 m^2/d; Storativity S = $7 \cdot 10^{-4}$; Vertical conductivity 1 m/d; Aquifer thickness h = 100 m; Partial penetration depth = 50 m. Partial penetration effect is negligible after $2 \cdot 10^4$ minutes (~14 days)

2.4.4 Fracture skin

Fracture skin is a thin layer between fracture and matrix with reduced conductivity and very small storage capacity. Such a skin can be created by mineral precipitation (Moench, 1984) or by clay minerals from weathering. Fracture skin in a single fracture causes an additional drawdown similar to that of a well bore skin (Fig. 2.16) (Cinco-Ley & Samaniego, 1977). It increases clogging phenomena and, in extreme cases, can even destroy the stimulation effect of drilling in a fracture zone (Economides & Nolte, 1989). Cinco-Ley & Samaniego (1977) defined the fracture skin factor ξ_f as follows

$$\xi_f = \frac{\pi \cdot b_s}{2 \cdot x_f} \cdot \left(\frac{K}{K_s} - 1 \right) \qquad (2.14)$$

where
b_s = thickness of the skin [L]
x_f = fracture half-length [L]
K = conductivity of the matrix or formation [LT^{-1}]
K_s = conductivity of the skin [LT^{-1}]

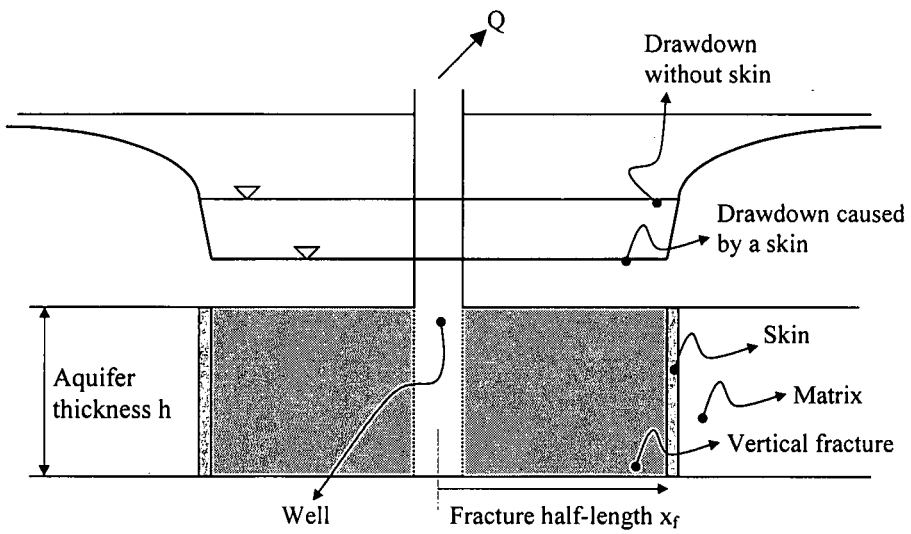

Figure 2.16. Drawdown in a single vertical fracture affected by skin between fracture and matrix

In continuous fractured rock with double porosity behavior, the fracture skin results in a pseudo-steady flow exchange between fracture and matrix blocks (Fig. 2.17) (Moench, 1984). Moench (1984) introduced the fracture skin factor for the double porosity solution as

$$\xi_f = \frac{2 \cdot K \cdot b_s}{K_s \cdot w} \qquad (2.15)$$

where
w = fracture aperture [L]

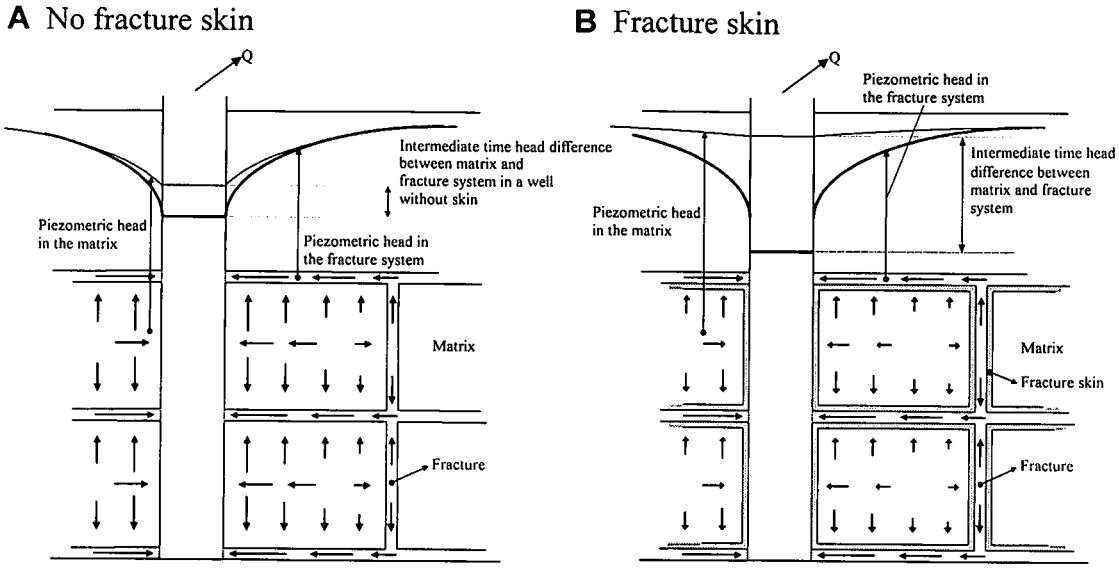

Figure 2.17. Effect of fracture skin on the drawdown of the matrix and fracture system in a double porosity aquifer, both pumped with the same discharge rate

2.4.5 Pseudo-skin

An observation well located within or in the proximity of a fracture that acts as a conduit shows less drawdown than that expected for observation wells in a homogeneous formation (Fig. 2.18). This effect is known as pseudo-skin (Gringarten & Ramey, 1974). The determination of the skin using equation (2.9) leads to a negative skin factor ξ [-] which, after equation (2.11), results in a larger effective radius.

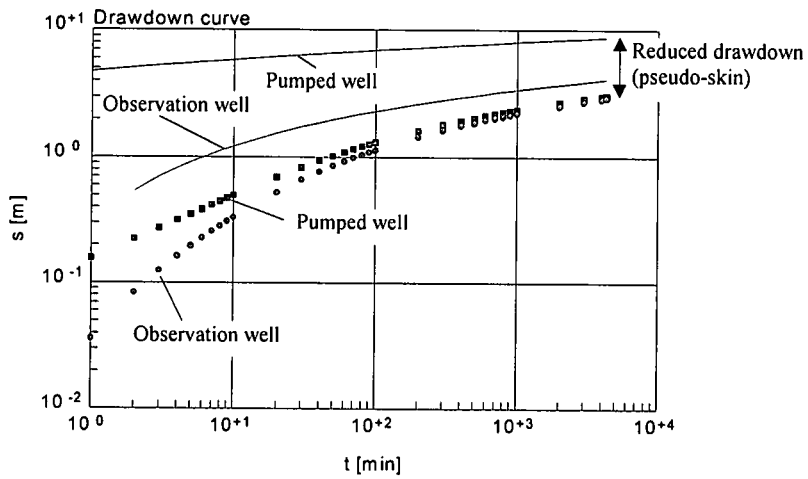

Figure 2.18. Drawdown in a pumped well situated in a homogeneous aquifer and an observation well 25 m apart (solid curves). Drawdown in a pumped well (squares) situated in a single fracture (fracture half-length x_f = 200 m) with infinite conductivity and an observation well (dots) located in the matrix at a distance of 25 m perpendicular to the fracture strike direction. Transmissivity of the matrix T = 50 m^2/d; Storage coefficient S = 10^{-4}. The difference in the drawdown is known as pseudo-skin effect

This effect can be used to determine whether a well is located in a fracture zone, as in principle no negative skin factor smaller than -0.5 (or enlarged effective radius) is observed in a continuous fractured aquifer. If the REV is equal or smaller than the drilled radius r_w (Section 3.1.3, Fig. 3.6), ξ will be zero. An exception might be a zone of higher permeability due to caving processes during the drilling works.

2.4.6 Fracture dewatering

Fracture dewatering should be avoided whenever feasible because of the danger of mineral precipitation that can cause fracture and well clogging. These effects are directly related to the water chemistry. Precipitation occurs especially when ground water with high manganese, iron, or bicarbonate contents are oxygenated.

If a continuous fracture network (homogenous aquifer) is dewatered, the physical conditions change gradually with time due to the reduction of the down-hole influx area. Under these circumstances the dewatering phenomena can be approached applying the Jacob correction $s' = s - s^2/2h$ to the drawdown data, as for an unconfined aquifer.

If a discontinuous fracture network is dewatered (Fig. 2.19), a sudden drop of the water level in the borehole is observed when it reaches the fracture (van Tonder *et al.*, 1998). This effect is characteristic for discrete down-hole water strikes. In these cases, the physical conditions in the vertical direction change instantaneously due to following reasons:

- the aquifer above the dewatered fracture becomes a perched aquifer that releases water into the fracture and borehole
- unconfined conditions in the dewatered fracture
- turbulent flow in the dewatered fracture and along the borehole wall
- reduced influx area

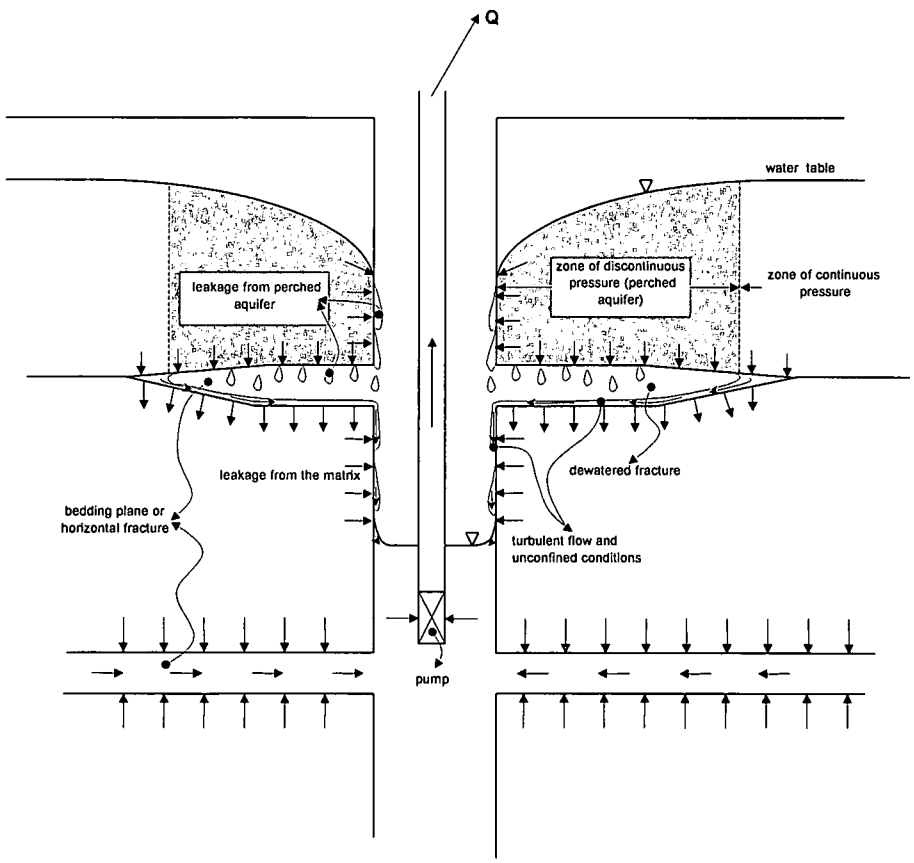

Figure 2.19. Effects caused by the dewatering of a bedding plane or horizontal fracture

The drawdown scenario can be described as follows:

- as soon the water level in the borehole reaches the water strike e.g. a bedding plane, the flow conditions in the dewatered fracture change from confined to unconfined
- if the storage capacity of the fracture is small compared to the discharge rate the drawdown will drop continuously below the water strike at the cost of the well bore storage (this part of the curve in a log-log plot shows usually a slope of 1) until the gradient between the water level in the borehole and the matrix is large enough to cover the discharge rate
- if radial flow is observed in both before and after the dewatering of the fracture, the drawdown curve after the dewatering in the semi-log plot will show an increased slope compared to the initial one (Fig. 2.20). The slope increment depends on the importance of the dewatered water strike

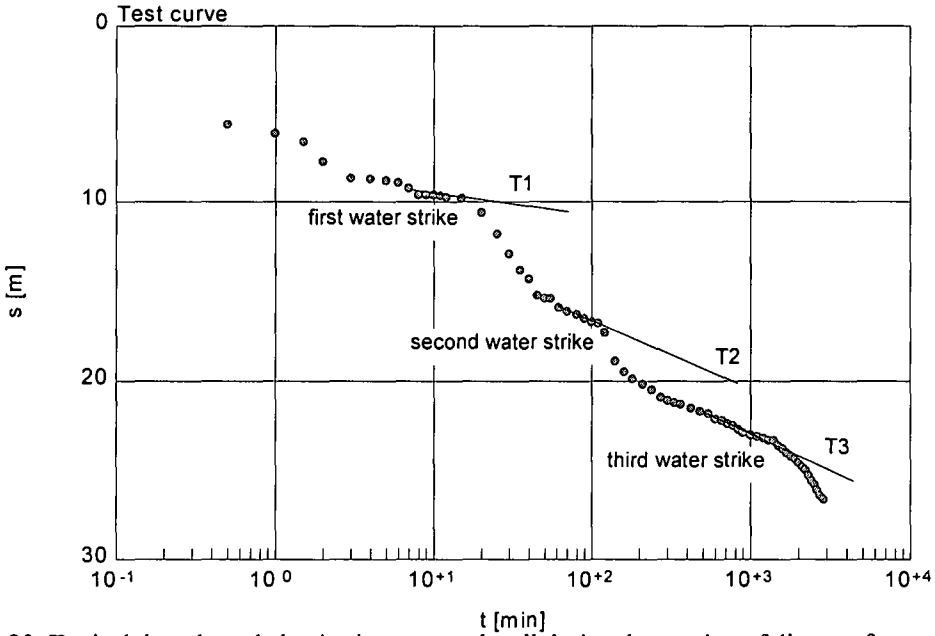

Figure 2.20. Typical drawdown behavior in a pumped well during dewatering of discrete fractures

The determination of aquifer parameters using such disturbed drawdown curves is sometimes possible applying conventional methods for parts of the curve. But in general the evaluation is extremely complicated and it is rather recommended to repeat the drawdown test using a smaller pumping rate to avoid the dewatering of the fractures. Step tests are usually very helpful for the proper adjustment of the pumping rate. The rate to be chosen should lead to a drawdown that does not reach the water strikes.

Some fracture dewatering effects on drawdown curves will be demonstrated later using field examples (compare Section 4.1.4).

2.4.7 Reservoir boundaries

All ground water reservoirs are limited. Whether the influence of reservoir boundaries is seen in a pumping test curve is a function of the pumping time, the transmissivity, the storage coefficient and the distance to the boundaries, but not of the discharge rate. This can be demonstrated by the calculation of the distance at which the cone of depression is zero (drawdown $s = 0$). The Cooper-Jacob (1946) equation, which is the solution for the differential equation (2.3) for long pumping time ($u < 0.03$), gives:

$$s = \frac{0.183 \cdot Q}{T} \cdot \log\left(\frac{2.25 \cdot T \cdot t}{S \cdot r^2}\right) \qquad (2.16)$$

If a well is discharged (Q > 0), the term 0.183·Q/T cannot become zero. Therefore, the logarithm should be set equal to zero:

$$\log\left(\frac{2.25 \cdot T \cdot t}{S \cdot r^2}\right) = 0 = s \qquad (2.17)$$

Applying exponential:

$$\frac{2.25 \cdot T \cdot t}{S \cdot r^2} = 1 \qquad (2.18)$$

The radius at which the drawdown disappears is given by the positive result of the square root:

$$r = \sqrt{\frac{2.25 \cdot T \cdot t}{S}} \qquad (2.19)$$

Equation (2.19) proves that the discharge rate has no influence on the time at which a reservoir boundary is reached. This equation is useful to estimate the extension of a cone of depression after a given period of pumping or, knowing the distance from the well to the boundary, to determine at which time t the cone of depression will reach the boundary assuming that T/S (diffusivity) remains constant. Further, Equation (2.19) shows that the larger T and smaller S, the larger the cone of depression for a given time.

Ferris *et al.* (1962) introduced the widely used concept of mirror wells to include the effect of positive (recharge) boundaries or negative (closed) boundaries. Earlougher (1977), Streltsova (1988), and Kruseman & de Ridder (1991) presented a detailed overview on how the mirror well concept can be used. The effects of positive and negative boundaries on a drawdown curve are shown in Figures 2.21 to 2.24. Basically, recharge boundaries show a flattening of the curve, whereas closed boundaries show an increase of the drawdown when the cone of depression reaches the boundary.

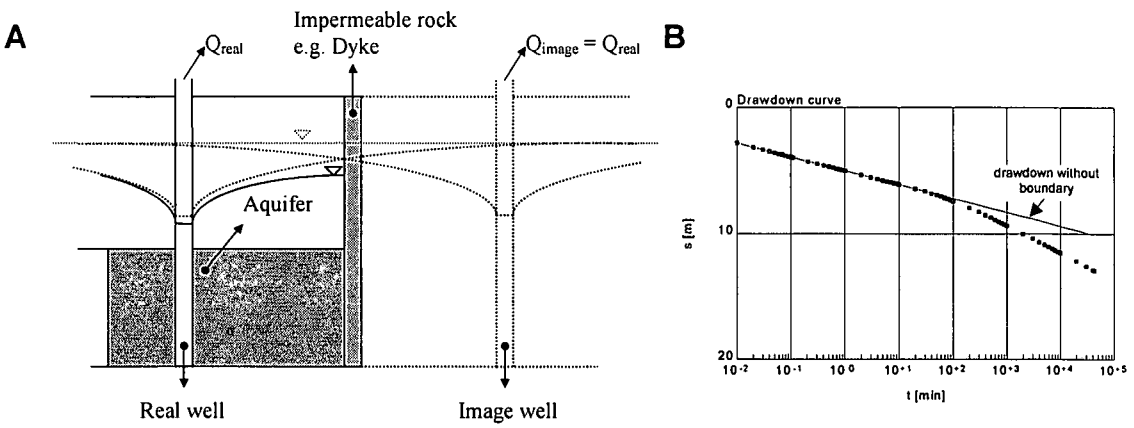

Figure 2.21. A: One closed boundary and its representation as superposed image well. B: Example of a drawdown curve in a pumped well affected by one closed boundary (squares)

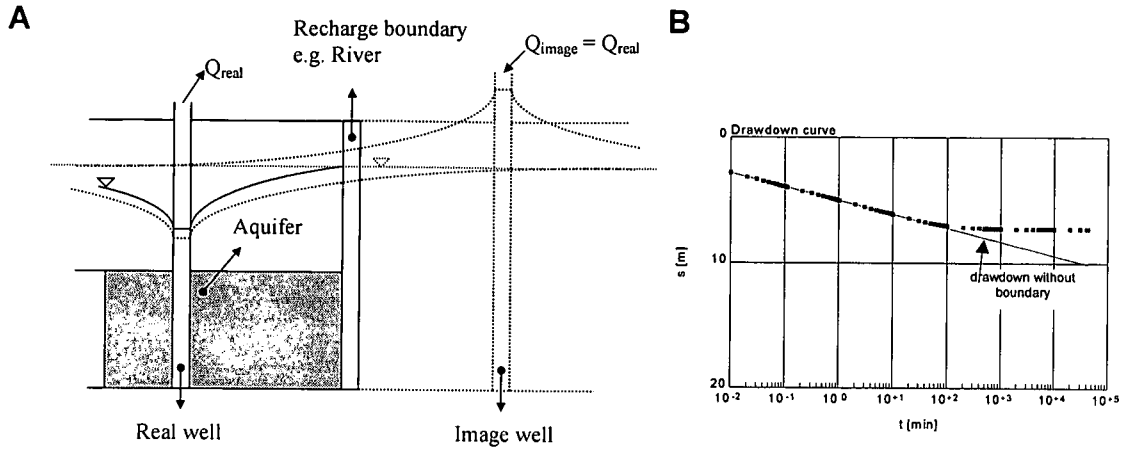

Figure 2.22. A: One recharge boundary and its representation as superposed image well. B: Example of a drawdown curve in a pumped well affected by one recharge boundary (squares)

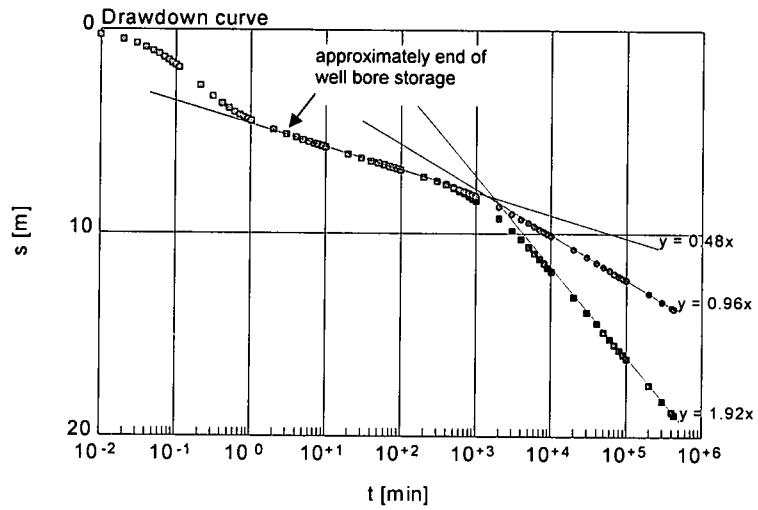

Figure 2.23. Diagnostic straight-lines in a semi-log plot for the identification of reservoir boundaries, which are valid for pumped and observation wells. In this example, the slope of 0.48 indicates radial flow not affected by boundaries. A doubled slope (0.96) indicates one closed boundary. A quadruple slope (1.92) indicates two perpendicular closed boundaries

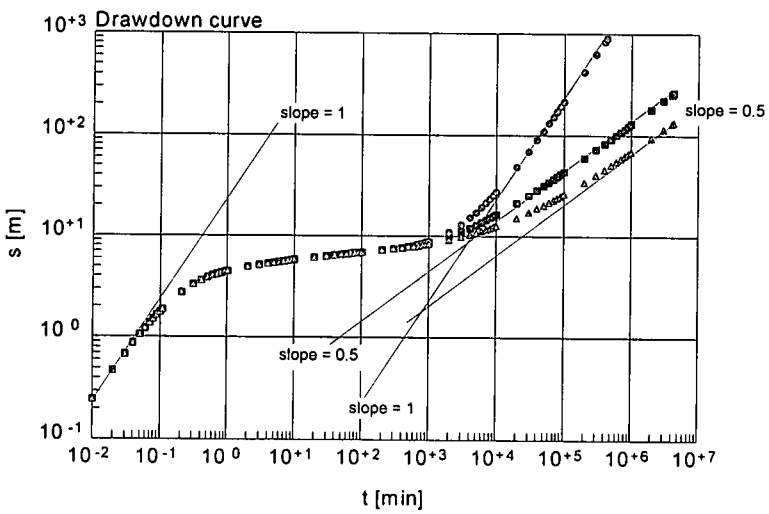

Figure 2.24. Diagnostic straight-lines in a log-log plot for the identification of various reservoir boundaries, which are valid for pumped and observation wells. The slope 1 at early time indicates well bore storage effect. The slope 1 at late time indicates a closed reservoir (four boundaries). The slope 0.5 at late time indicates two parallel boundaries or channel flow (triangles) or three boundaries perpendicular to each other (squares)

3. FLOW DIAGNOSTICS

This chapter explains principles and tools that should be followed during the planning, performance, and evaluation of pumping tests in fracture media.

All drawdown curves presented in this chapter are produced using the program TPA, which was developed under the umbrella of this thesis.

3.1 Basic Instructions for the Analysis of Pumping Test Data

3.1.1 Discharge rate

As it is shown in Figure 3.1A, an increase of the discharge rate in a given well does not accelerate flow effects. The influence of the well bore storage is overcome simultaneously in both curves, as already explained in Section 2.4.1. Similarly, any aquifer boundaries (positive or negative) will be reached at the same time with both discharge rates, as explained in Section 2.4.7. The only effect that an increase in the discharge rate has is the development of a steeper cone of depression, as shown in Figure 3.1B. These effects should be considered in the planning and performance of a pumping test.

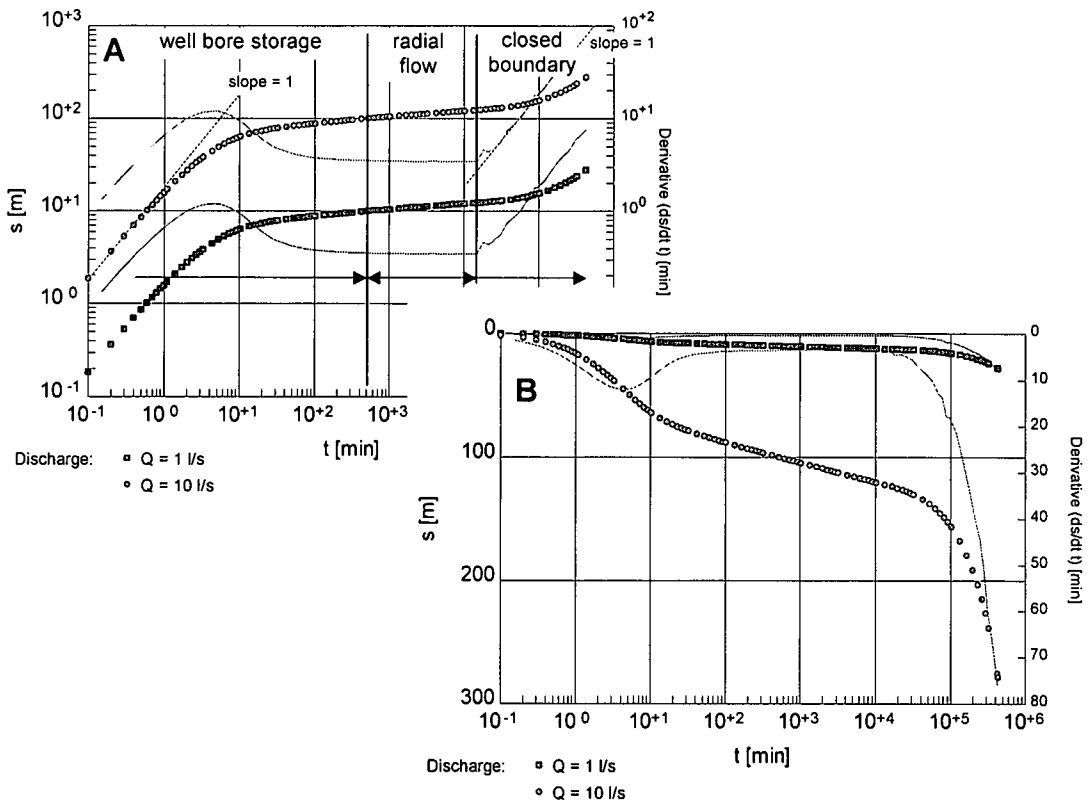

Figure 3.1. Drawdown in a pumped well for different discharge rates. An increase of the extraction rate cannot accelerate the overcoming of well bore storage or reaching of a boundary

3.1.2 Correction for discharge variations

For step drawdown tests or in cases of variations larger than 10% in the extraction rates during a constant discharge test (pump failure, etc.), only the recovery or build up curve is suitable for common analysis methods like Theis (1935) or Agarwal (1980). However, these methods would lead to correct results, if the influence of the

discharge variations in the pumping time are eliminated. The time correction can be computed using the Birsoy & Summers (1980) correction, which writes:

$$t_{corr} = \prod_{i=1}^{n-1} \left(\frac{t - t_i}{t - t_i'} \right)^{\frac{Q_i}{Q_n}} \qquad (3.1)$$

where
t_i = start time of the i^{th} discharge period [T]
t_i' = end time of i^{th} discharge period [T]
Q_i = constant discharge rate of i^{th} period [L^3T^{-1}]
Q_n = last constant discharge rate [L^3T^{-1}]

If the time correction is ignored, significant differences in the recovery behavior are observed (Fig. 3.2), which would result in a wrong determination of the transmissivity.

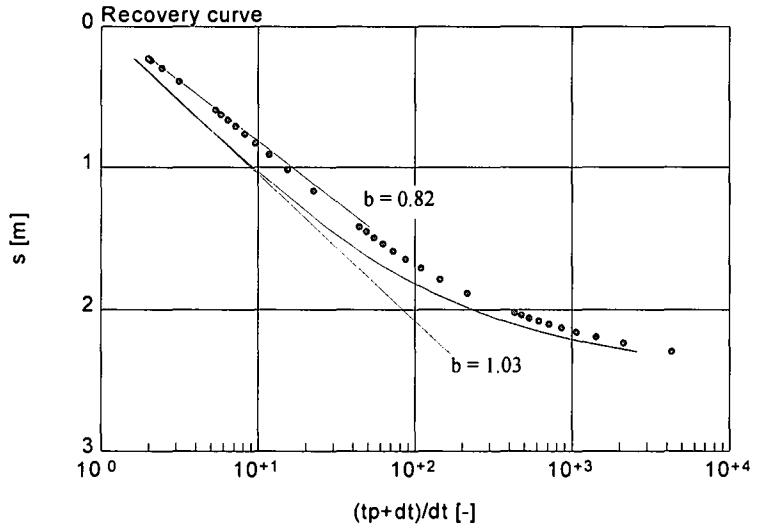

Figure 3.2. Pumped well recovery curve from a step test run at Q = 4 m^3/h, Q = 8 m^3/h, and Q = 12 m^3/h. The dots graph the recovery considering a constant average discharge of Q = 8 m^3/h and no time correction. The solid curve shows the same recovery data with time correction. The Theis recovery method estimates transmissivity values of T = 50 m^2/d for corrected data and T = 43 m^2/d for uncorrected data, due to the differences in the applied discharge rate (Q = 12 m^3/h for corrected data and an average of Q = 8 m^3/h for uncorrected data)

The corrected time t_{corr} replaces the pumping time t_p in the Theis (1935) time correction for the recovery curve, which then reads

$$t' = \frac{t_{corr} + dt}{dt} \qquad (3.2)$$

where
t' = time corrected for the superposition effects in the drawdown phase
dt = time increment after the recovery (build up) phase starts

The time correction for the recovery curve in the Agarwal (1980) method reads

$$t' = \frac{t_{corr} \cdot dt}{t_{corr} + dt} \qquad (3.3)$$

The advantage of the Agarwal method lies in the possibility of using common type curve fitting for the determination of the transmissivity and storage coefficient (if skin effects are negligible).

3.1.3 Influence of the pseudo-skin effect

Common analysis methods for primary aquifers (Cooper-Jacob or Theis) can be applied to pumping test results from a fracture network with limited extent for the determination of the transmissivity T, but only after the establishment of the radial-acting flow phase. However, these methods cannot be used for the estimation of the storage coefficient S, due to the pseudo-skin effects (Section 2.4.5).

After Cooper-Jacob (1946), the storage coefficient is calculated using following equation:

$$S = \frac{2.25 \cdot T \cdot t_0}{r^2} \qquad (3.4)$$

where

T = matrix or formation transmissivity [L^2T^{-1}]
r = distance of the observation well to the pumped well [L]
t_0 = time at which the straight-line intercepts the time axis [T]

The value of t_0 in the presence of pseudo-skin will be wrongly evaluated (Gustafson & Anderson, 1997) and consequently also S will be wrongly estimated, as illustrated in Figure 3.3.

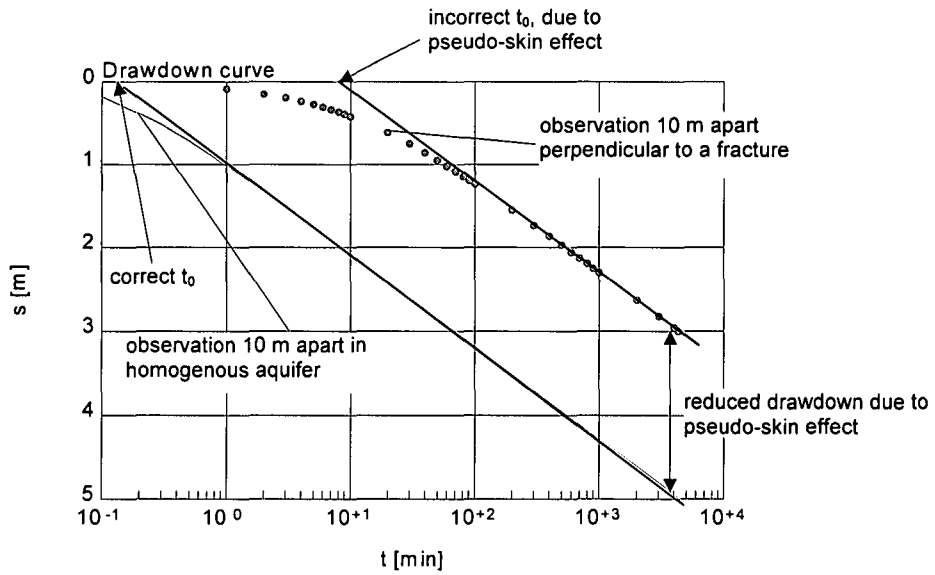

Figure 3.3. The application of Cooper-Jacob approach for the determination of the storage coefficient in pumped and observation wells gives wrong results due to pseudo-skin effect

Figure 3.4 shows the extremely large error made in the calculation of S, when the Cooper-Jacob (1946) straight-line method is applied to the drawdown data measured in observation wells located in various directions around an infinite conductivity vertical fracture with uniform flux. Indeed, common methods are only applicable for the calculation of S, when the observation well is located at a distance of 1.5 to 5 times the fracture half-length, depending on the direction of the fracture. For practical purposes, a distance of 3 times the fracture half-length can be applied, as the error for larger distances becomes less than 1% for all directions. This distance represents the

REV of such system or, in other words it is the distance at which the cone of depression reaches the radial-acting flow phase.

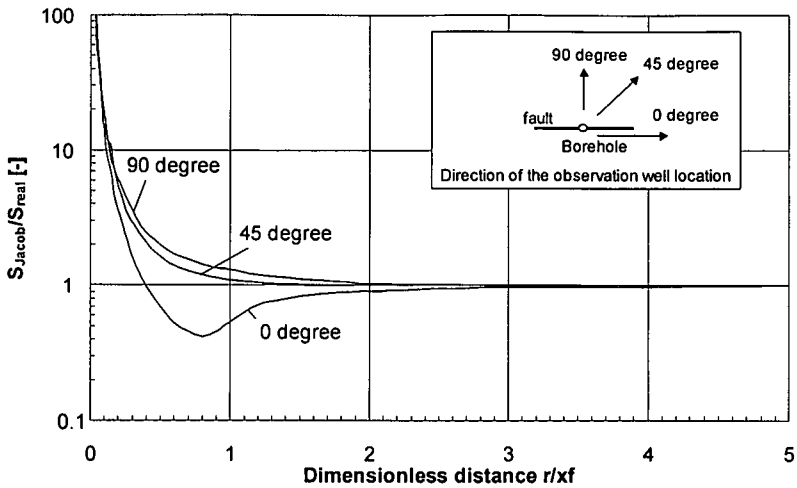

Figure 3.4. Deviation from the real storage coefficient calculated using the Cooper-Jacob straight-line method for data of the radial-acting flow phase in observation wells in the vicinity of a single vertical infinite conductivity fracture with uniform flux

It must be beared in mind that once the radial-acting flow phase in the observation well located in a discontinuous fractured aquifer has been reached, the drawdown is only a function of its location and not of the extraction time. Figure 3.4 can also be used to either determine the correct storage coefficient, if the relative position of the observation well to the fracture is known, or to determine the fracture half-length if the storage coefficient is known.

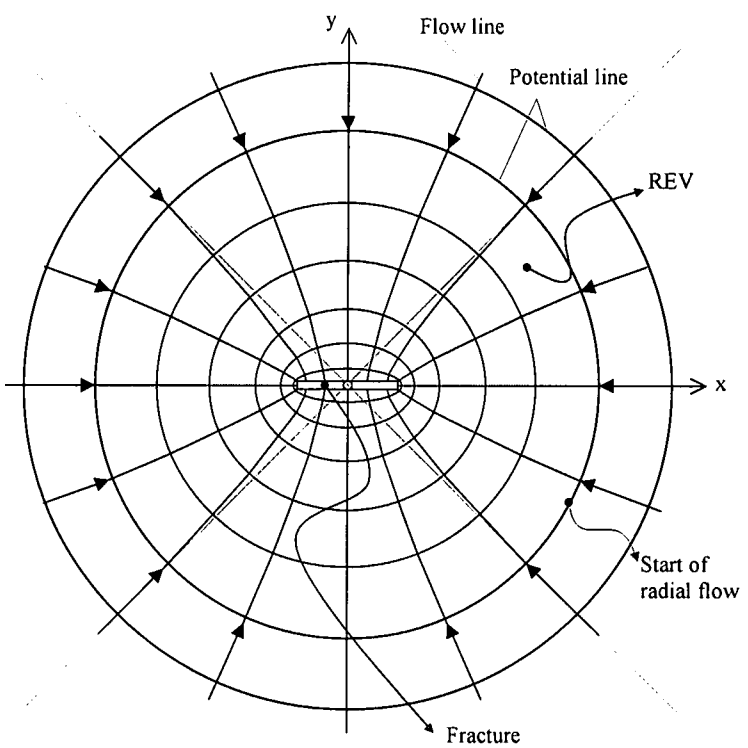

Figure 3.5. REV for a single vertical fracture with infinite conductivity. An observation point beyond the grey area would show only radial-acting flow behavior

The start of the radial flow indicates the time at which the fractured reservoir behaves as homogeneous. The distance from the pumped well to the point where radial flow starts defines the size of the REV, as demonstrated in Figure 3.5.

Whether the influence of a fracture network can be observed or not depends on the location of the observation point. Is the REV smaller than the drilled radius (Fig. 3.6A) or is the observation well located outside of the REV (Fig. 3.6B), the influence of the fracture network cannot be observed and the drawdown curve will follow a Theis curve. Therefore, in Figure 3.6B only the data in the pumped well can show the influence of the fracture network. In instances where the REV coincides with the drilled radius r_w, any observation well will show radial-acting flow.

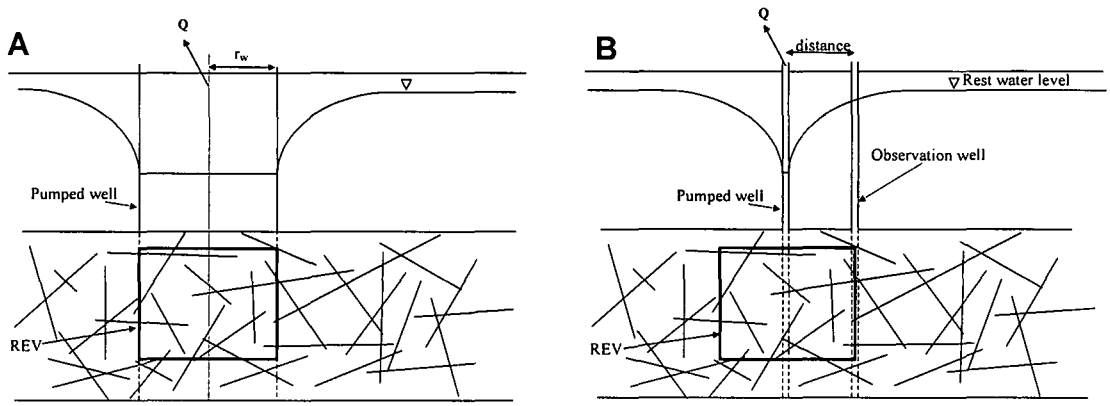

Figure 3.6. If the REV is smaller than the drilled radius (A) or the observation well is located outside of the REV (B), the influence of the fracture network cannot be observed

Radial-acting flow data can then be analysed with methods usually applied to primary aquifers, whereas for observations within the REV the influence of the fracture network must be considered.

3.2 Diagnosis Tools

3.2.1 Comparison of drawdown and recovery data

Under continuous pumping rate both the drawdown and the time-corrected recovery curves must show the same behavior, even if boundaries are present, due to the superposition theory (Fig. 3.7). An exception is represented by a closed reservoir (Streltsova, 1988), for which these curves differ from each other once the boundaries are reached as illustrated in Figure 3.8. Often the drawdown curve is disturbed by variations in the pumping rate. This effect can also be easily recognised by comparison of the drawdown and recovery curves.

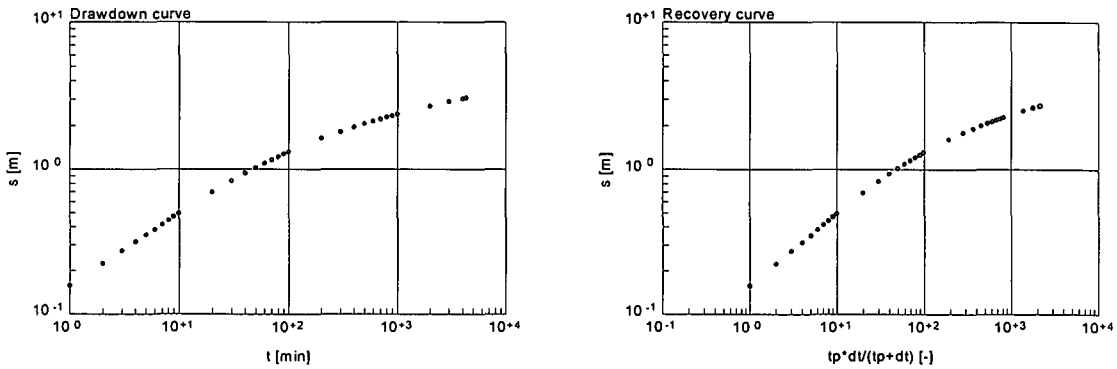

Figure 3.7. The superposition theory implies that the shapes of the drawdown and recovery curves in pumped and observation wells are similar. This effect can be used to determine the quality of the drawdown data

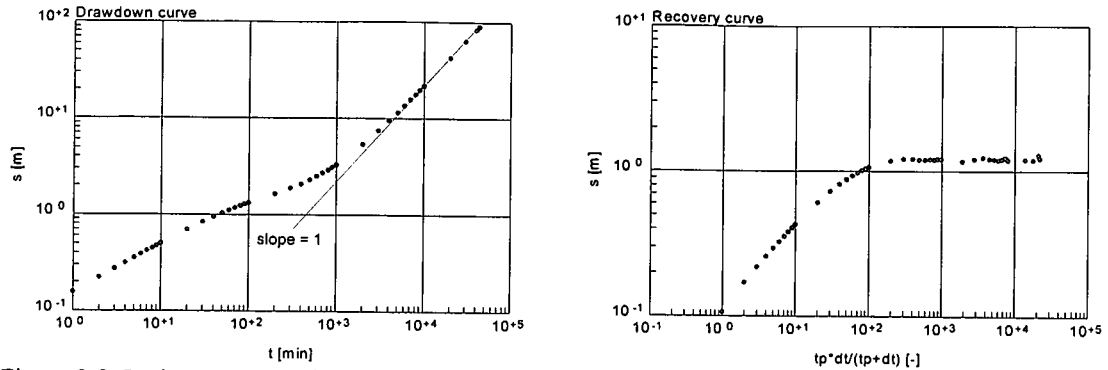

Figure 3.8. In the presence of four boundaries (limited reservoir), the drawdown and recovery curves in pumped and observation wells behave differently once the boundaries are reached

3.2.2 Diagnosis by straight-lines

As already described in Chapter 2, flow boundaries as well as flow types influence the drawdown and recovery data by plotting as straight-lines in the various diagnosis plots, which often have typical slopes as follows:

Straight-lines in a log-log plot identify following effects:

- linear fracture flow plots as a slope of 0.5 (Cinco-Ley & Samaniego, 1981a)
- linear formation flow graphs as a slope of 0.5 (Gringarten *et al.*, 1974)
- bilinear flow plots with a slope of 0.25 (Cinco-Ley & Samaniego, 1981a)
- well bore storage shows a slope of 1 at early time
- two parallel closed boundaries show a slope of 0.5 known as channel flow (Ehlig-Economides & Economides, 1985)
- three closed boundaries perpendicular to each other show a slope of 0.5
- limited reservoir (four closed boundaries) shows a slope of 1 at late time

The straight-lines in a semi-log plot provide following information:

- radial-acting flow appears as a straight-line (Cooper-Jacob, 1946)
- one closed boundary doubles the slope of the radial-acting flow straight-line
- two perpendicular closed boundaries quadruple the slope of the radial-acting flow straight-line

Pumping tests data should be systematically examined to the presence of the characteristic straight-lines, as these are the most powerful tools for the determination of the various aquifer boundaries and flow phases. Only the correct identification of the flow phases will allow a proper test evaluation. The practical use of diagnosis by straight-lines will be illustrated in Chapter 4.

3.2.3 Special plots and skin analysis

Besides the log-log and semi-log plots, following three additional plots are very useful for the diagnosis of pumping test data in fractured aquifers (Cinco, 1982):

- linear drawdown versus square root of time
- linear drawdown versus fourth square root of time
- linear drawdown versus the inverse of the square root of time

The first plot is useful for the determination of linear flow behavior; as the drawdown data will plot on a straight-line that starts in the origin of the diagram. In the second plot the drawdown data of the bilinear flow phase plot on a straight-line starting in the origin. The drawdown data of a spherical flow plot on a straight-line that starts in the origin in the third plot. The practical use of these diagnostic plots will be illustrated in Chapter 4.

Cinco-Ley & Samaniego (1981b) demonstrated that the first two diagrams are very useful to determine skin effects in drawdown data of wells in single fractures with either linear or bilinear drawdown behaviors.

Cinco-Ley & Samaniego (1981b) found that, due to skin effects, the early time linear flow data in a log-log plot graphs as an almost horizontal line that develops into the radial acting phase (bilinear flow would plot similarly). Plotting the same data in a linear drawdown versus square root of time diagram, a straight-line shifted downwards from the origin will be shown. Both authors stated further that data only from the pumped well does not provide a unique solution for the determination of the skin location, which could be located at the well, between fracture and formation, or at both. Bardenhagen (1999) showed an unique evaluation method for the skin location in a single vertical fault by using drawdown data of a pumped well and an observation well located in the same fault, both plotted on a linear drawdown versus square root of time plot.

These considerations are also valid in the case of horizontal fractures, as they are only related to the flow regime and not to the fracture position.

3.2.4 Curve derivatives

The same plots mentioned above can be applied to recovery data after time correction. In most practical cases the quality of the recovery data is better than that of the drawdown, as they are not influenced by fluctuations in the pumping rate. This holds especially for the application of derivatives that are commonly used as diagnosis tools of drawdown phases. The use of derivatives is of great advantage due to their sensitive reaction to small changes in the drawdown or recovery, while they are independent of skin effects. Usually, the first derivative is computed as $(\Delta s/\Delta t \cdot t)$ (Economides & Nolte, 1989) and its plot provides following information:

- all characteristics of the straight-line slopes remain the same
- the radial-acting flow phase is plotted as a horizontal line, which eases the identification for the human eye

Unfortunately, derivatives are often noisy when applied to real data. Smoothing of the derivatives would overcome this problem, but it cannot be ensured that the applied mathematical algorithm would not produce misleading artifacts. Nevertheless, with some experience even noisy derivatives can be interpreted.

4. ANALYTICAL MODELS FOR EVALUATION OF PUMPING TEST IN FRACTURED AQUIFERS

In this chapter, various analytical and semi analytical models that describe flow and drawdown in wells intersecting single fractures or are located in homogeneous fractured aquifers are presented. Methodologies for the analysis of pumping test data applying these models are described using the program TPA, which was developed under the umbrella of this thesis. The ability of the program to evaluate pumping tests performed in fractured aquifers is shown for both published data and pumping test data collected in the field.

4.1 Double porosity model (Moench, 1984)

4.1.1 Theory

The concept of double porosity introduced by Barenblatt *et al.* (1960) considers homogenous distributed conductive fractures embedded in a homogenous distributed matrix. For both, fracture and matrix, different conductivity and storage coefficients can be adopted. Two matrix types are generally discussed, the spherical block matrix (Warren & Root, 1962) used to represent aquifers like quartzite and the layered matrix (Kazemi, 1969) adopted for example for sandstone with bedding planes (Fig. 4.1).

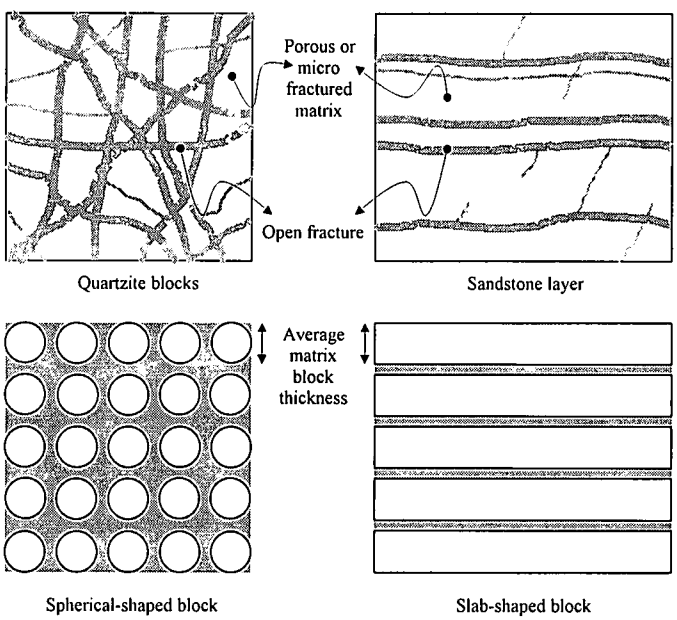

Figure 4.1. Natural fractured systems and their simplification into spherical-shaped block and slab-shaped blocks

Olarewaju (1997) introduced a solution that explains the flow exchange between matrix and a fractal fracture system which, although representing a more realistic approach for the description of double porosity behavior, requires detailed knowledge of the fracture system and therefore its discussion lies beyond the scope of this work.

The concept of double porosity was extended to a triple porosity by Abdassah & Ershaghi (1984), which was recently reinterpreted by Al-Ghamdi & Ershaghi (1996) with the introduction of a dual fracture model connected to matrix blocks. Both models concentrate on the interpretation of the very early time data behavior, which

are unfortunately often masked by well bore storage effects. Therefore, the practical use of these interpretations is questionable and will not be further discussed.

Warren & Root (1962) introduced a pseudo-steady state block-to-fracture flow solution, which seems to adequately represent field data but, using numerical models, Kazemi (1969) and Wei *et al.* (1998) found that the flow in the double porosity reservoirs is of transient block-to-fracture type. However, Moench (1984) shows that the pseudo-steady flow case is in fact a special case of the transient flow restricted by a skin between fracture and matrix (Fig. 2.17, Section 2.4.4) caused by mineral precipitation on the matrix blocks' surfaces.

For the mathematical description of the drawdown behavior, Moench (1984) considers two representative elementary volumes (REV) one for the fractures and one for the matrix. However, the classic concept of double porosity cannot be applied if the cone of depression is not larger than both REV. If this is not the case, the influence of the individual fractures is not negligible, as demonstrated by Wei *et al.* (1998).

Furthermore, Moench (1984) assumes an infinite extent of the matrix and fracture system under confined conditions. To be able to deal with well bore storage, well losses (skin at the well), and partial penetration he derived a solution in the Laplace space using the Stehfest (1970) algorithm for the numerical inversion. The solution infers that only water from the fracture network reaches the well and that the contribution of the matrix is negligible. Combining the findings from Mavor & Cinco-Ley (1979), Moench & Ogata (1984), and Moench (1984), the drawdown in a pumped well with well bore storage, skin effect, and partial penetration in the Laplace space can be written as:

$$\bar{h}_h(p) = \frac{2\left[K_0(x) + x \cdot \xi \cdot K_1(x) + F_L\right]}{p\left\{p \cdot W_d\left[K_0(x) + x \cdot \xi \cdot K_1(x)\right] + x \cdot K_1(x)\right\}} \qquad (4.1)$$

and in an observation well as

$$\bar{h}_h(p) = \frac{2\left[K_0(r_d \cdot x) + F_L\right]}{p\left\{p \cdot W_d\left[K_0(x) + x \cdot \xi \cdot K_1(x)\right] + x \cdot K_1(x)\right\}} \qquad (4.2)$$

where

$\bar{h}_h(p)$ = dimensionless drawdown in the Laplace space [-]
K_o = modified Bessel function of second kind and zero order [-]
K_1 = Bessel function of second kind and first order [-]
F_L = partial penetration skin function (Section 2.4.3)
ξ = dimensionless skin factor at the well (well bore skin factor) [-]
W_d = dimensionless well bore storage coefficient [-]
p = Laplace transform variable [-]
x = $(p+\bar{q}d)^{½}$
$\bar{q}$ = dimensionless block-to-fracture flow in the Laplace space [-]
r_d = dimensionless radius, r/r_w [-]
r = distance of an observation well to the pumped well [L]
r_w = drilled radius or radius of the source [L]

The dimensionless transient block-to-fracture flow $\bar{q}$ for sphere-shaped blocks is given by Moench (1984) in the Laplace space as

$$\bar{q} = \frac{3 \cdot \gamma^2 [f \cdot \coth(f) - 1]}{\{1 + \xi_f [f \cdot \coth(f) - 1]\}} \qquad (4.3)$$

and for slab-shaped blocks

$$\bar{q} = \frac{\gamma^2 \cdot f \cdot \tanh(f)}{[1 + \xi_f \cdot f \cdot \tanh(f)]} \qquad (4.4)$$

Moench (1984) also presents a solution for the pseudo-steady flow exchange, which seems to contradict the general findings of his work. The solution produces an almost horizontal flattening of the transient phase for small dimensionless fracture skin value ξ_f, which in some instances may fit data better than the transient solution. The flow $\bar{q}$ for sphere-blocks under pseudo-steady state flow situation reads:

$$\bar{q} = \frac{3 \cdot \gamma^2 \cdot f^2}{(3 + \xi_f \cdot f)} \qquad (4.5)$$

and for slab-shaped blocks

$$\bar{q} = \frac{\gamma^2 \cdot f^2}{(1 + \xi_f \cdot f)} \qquad (4.6)$$

where

ξ_f = dimensionless fracture skin
γ = $r_w/b_h\,(K/K_f)^{1/2}$ [-]
f = $(S/S_f\,p)^{1/2}/\gamma$ [-]
r_w = drilled radius or radius of the source [L]
b_h = average half thickness of the block [L]
K = conductivity of the matrix block [LT^{-1}]
K_f = conductivity of the fracture system [LT^{-1}]
S = storage coefficient of the matrix block [-]
S_f = storage coefficient of the fracture system [-]

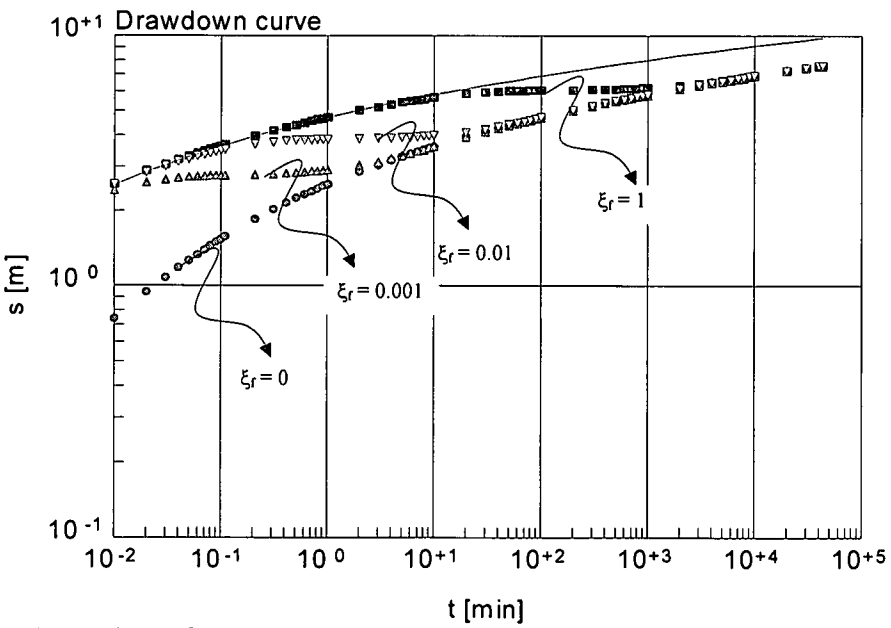

Figure 4.2. Comparison of the drawdown behavior in a pumped well with and without skin in the pseudo-steady case. The solid curve represents the flow in a confined infinite aquifer without skin

Unfortunately, if no skin is present the matrix responds immediately to pressure changes, which results in an almost instantaneous water release from the matrix into the fracture network masking the flattening effects (Fig. 4.2).

The double porosity model presented by Moench (1984) was implemented in TPA because it considers a fracture skin thus, it is a more realistic approach as it produces a restricted flow exchange between matrix and fracture.

4.1.2 Diagnosis

In a double porosity aquifer, when pumping starts mainly the fracture network releases water. Thus, the drawdown at early time data is characterized by a straight-line in a semi-log plot that is proportional to the transmissivity of the fracture system. The flattening of the curve is originated by the ever-increasing additional contribution from the matrix storage. The later drawdown, which is also proportional to the transmissivity of the fracture system, is the response of both the matrix and the fracture storage, and plots as a straight-line parallel to the initial one in the semi-log plot. In a log-log plot, both the initial and the late drawdown are characterized by Theis curves shifted horizontally from each other. The distance between the two parallels or two Theis curves depends on the fracture/matrix storage coefficient ratio (Fig. 4.3).

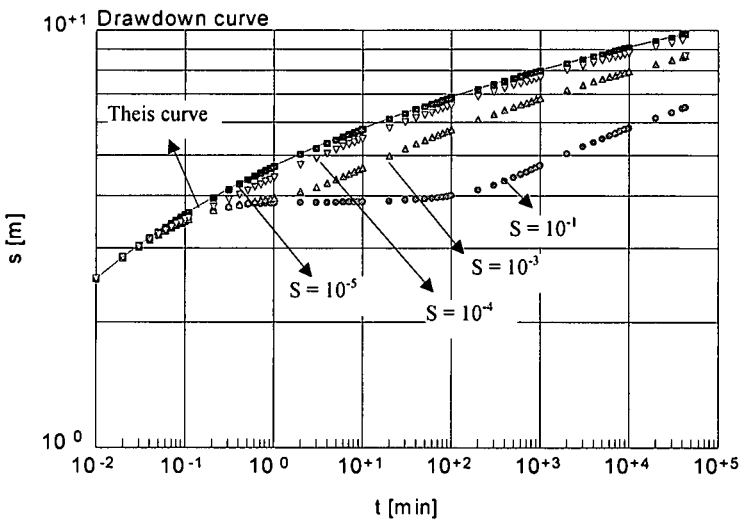

Figure 4.3. Drawdown curves in a pumped well for various matrix storage coefficients S. Storage coefficient of the fracture $S_f = 10^{-4}$

Both the pseudo-steady state and the transient model with fracture skin show an almost horizontal flattening (Fig. 4.4). However, the flattening does not appear in the transient model without block-to-fracture skin. In this case, the late time data plot on a straight-line that doubles the slope of the early time data (Fig. 4.5). If well bore storage masks the first straight-line this behavior can be mistaken as a drawdown in a confined aquifer with one closed boundary (Fig. 4.6). In fact, there is no unique diagnosis method applicable, if data from observation wells are not available. Figure 4.7 shows that if double porosity data is plotted in a log-log plot, the extension of the late time data joins the distance dependent time axis = t/r^2, whereas in case of a boundary effect it is the medium time data that joins this axis. However, this diagnosis method can be applied to identify double porosity if either data from a pumped well and one observation well are available and the well losses or skin at the pumped well are negligible, or data of at least two observation wells are present (Fig 4.7).

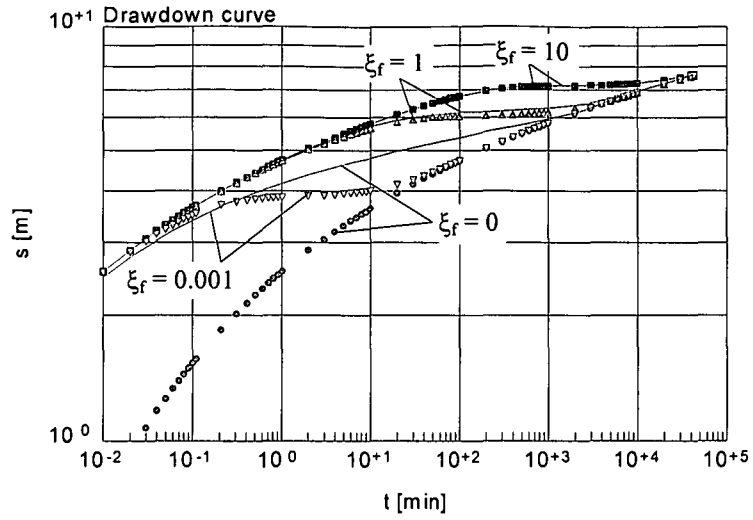

Figure 4.4. Drawdown in a pumped well. Comparison between pseudo-steady state flow (marker) and transient flow (solid curves) for various fracture skins

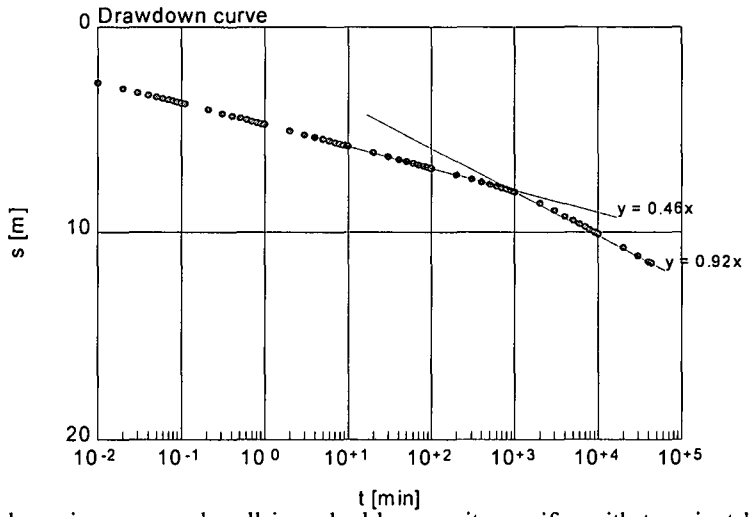

Figure 4.5. Drawdown in a pumped well in a double porosity aquifer with transient block-to-fracture flow and no fracture skin. The correct transmissivity is obtained using the late time data

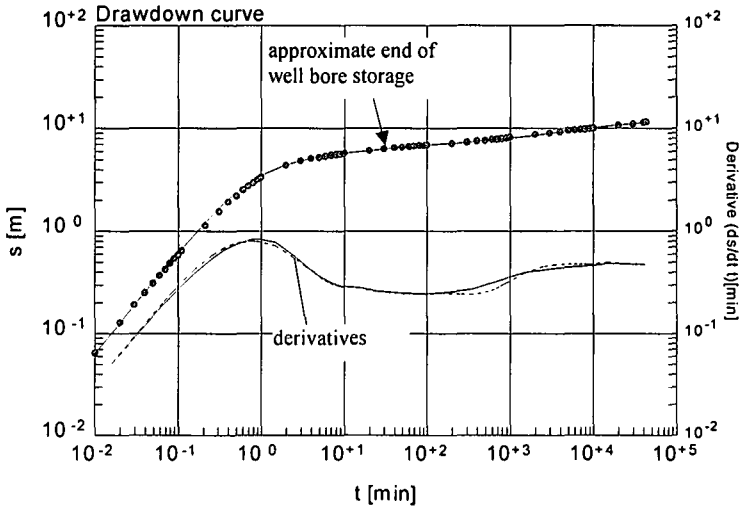

Figure 4.6. Drawdown in a pumped well. Comparison between the drawdown in a confined aquifer with one closed boundary (marker) and in a double porosity aquifer (solid line), both with well bore storage. For all practical purposes, it is not possible to distinguish between both cases

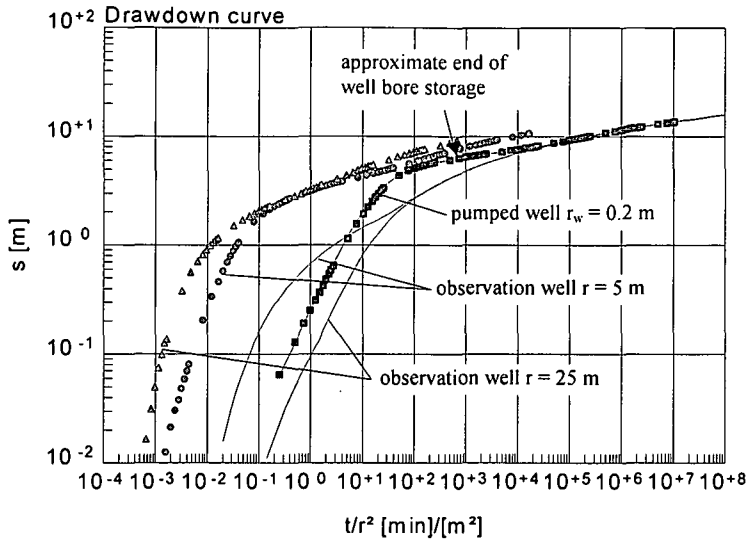

Figure 4.7. Comparison between the drawdown in a pumped well and two observation wells in a confined aquifer with one closed boundary (marker) and in a double porosity aquifer (solid curves), both with well bore storage. It is clearly seen that the double porosity curves merge the time dependent axis at late time, whereas in the confined case the merge occurs at medium time, while the boundary is not yet affecting the drawdown

4.1.3 Method of analysis

Moench (1984) proposed a type curve approach for the analysis of double porosity data, which includes well bore storage, well skin, and fracture skin and therefore is more advanced than the simple straight-line approach proposed by Warren & Root (1962) and Kazemi (1969). However, the tremendous increase of computer calculation power allows a combined approach of straight-line and forward modelling. This approach will be described in this work using TPA. The advantage of this proposed method lies in the ability to calculate different drawdown scenarios after model calibration to find the optimal extraction rate of a particular well.

4.1.3.1 Application of straight-line methods

If a double porosity case is diagnosed and it has been determined that the influence of the well bore storage is negligible, the Warren & Root straight-line method can be applied to the pumped well data. The method allows to determine the transmissivity T of the fracture system and the storage coefficients S_f and S for the fracture system and the matrix, respectively (Fig. 4.8).

The steps to follow in the application of the Warren & Root method to the pumped well data using a semi-log plot are:

- one straight-line must be fitted to the early time data (first branch) of the curve
- a second parallel straight-line must be fitted to the late time data (second branch)

Both straight-lines must have the same slope, as they reflect the transmissivity of the fracture system. In the presence of skin at the well, the Warren & Root method gives wrong results for the two storage coefficients, as demonstrated in Figure 4.9. A simple method for the skin determination will be presented in the following section.

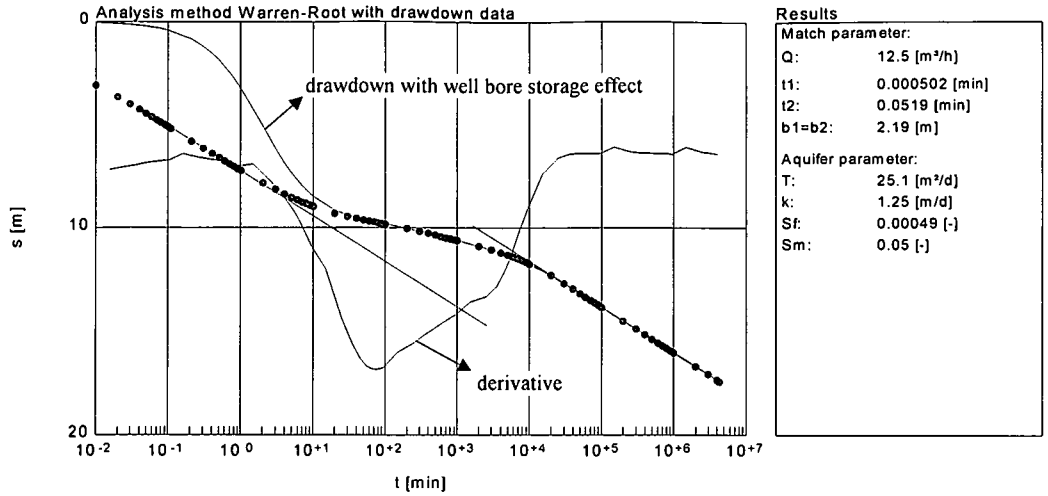

Figure 4.8. Application of the Warren & Root method to a pumped well that shows double porosity behavior. The solid curve indicates drawdown affected by well bore storage. It is clear that in this case it is not possible to fit a straight-line to the early time data

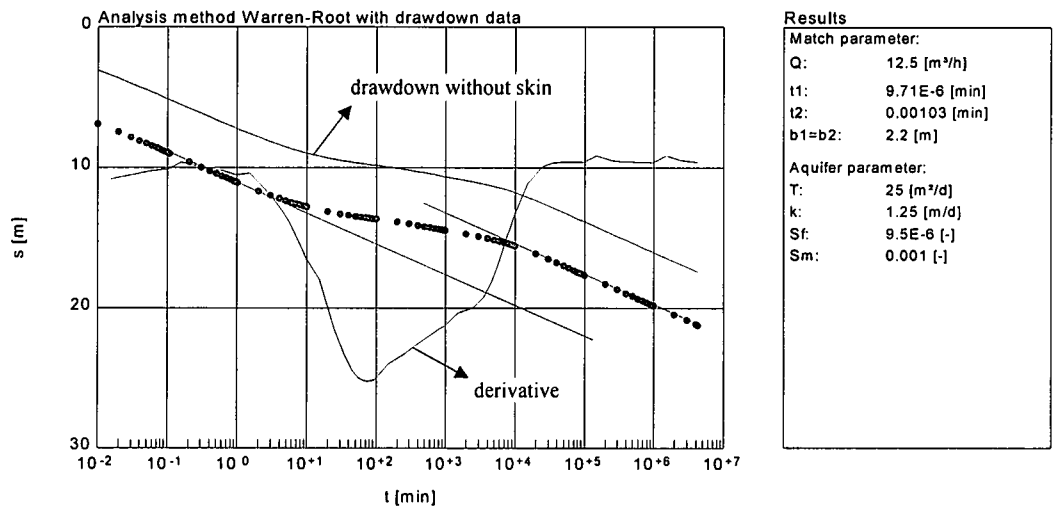

Figure 4.9. The solid curve is drawn using the same aquifer parameters as in Figure 4.8. An additional drawdown of 2 m due to well bore skin still gives the same transmissivity T = 25 m^2/d, but both storage coefficients S and S_f are much smaller due to the fact that the extrapolated time value to be used in equations 4.8 and 4.9 are wrongly determined

Kazemi (1969) showed that the Warren & Root method (1962) can also be applied for observation well data. Both methods are in fact similar to the Cooper-Jacob (1946) straight-line method. The aquifer parameters for both methods are calculated as follows:

$$T_f = \frac{0.183 \cdot Q}{d} \qquad (4.7)$$

$$S_f = \frac{2.25 \cdot t_{01} \cdot T_f}{r^2} \qquad (4.8)$$

$$S = \left[\frac{2.25 \cdot t_{02} \cdot T_f}{r^2} - S_f \right] \cdot \beta \qquad (4.9)$$

where
d = drawdown over one log cycle [L]

r = effective well radius (Warren & Root method) or distance of the observation well to the pumped well (Kazemi method) [L]
T_f = transmissivity of the fracture system [L^2T^{-1}]
S_f = storage coefficient of the fracture system [-]
S = storage coefficient of the matrix or formation [-]
β = shape factor: 1/3 for spherical blocks 1 for slab blocks [-]. This parameter implies that the conceptual model of the geological situation is known
t_{01} = time at which the first straight-line intercepts the time axis [T]
t_{02} = time at which the second straight-line intercepts the time axis [T]

Both methods can be applied, if following conditions are true:

- aquifer is infinite
- aquifer is confined
- Darcian flow prevails in fracture network and matrix
- fracture network acts as continuum during the whole extraction period
- matrix acts as continuum during the whole extraction period
- well penetrates the aquifer fully
- well bore storage is negligible
- well bore skin is negligible
- first straight-line can be applied if $u < 0.03$, where u is defined as $S_f r^2/(4t T_f)$ with t = time since extraction started. The time is equal to the time at which the first derivative becomes horizontal
- second straight-line can be applied if $1/u > 100$, where u is defined as $(S_f+\beta S)r^2/(4t T_f)$ and t is the time at which the first derivative for late time data becomes horizontal

4.1.3.2 Determination of the well bore skin

Equation (2.9) can be applied for the determination of the well bore skin in a double porosity aquifer. The transmissivity T is set equal to the fracture transmissivity T_f, calculated as described above. Two storage coefficients are available, S_f and S for the fracture system and the matrix, respectively, and both can be used in equation (2.9) to determine the correct well bore skin. Similar to Figure 2.13, the early time and late time radial-flow phases plot horizontal, when the time series of the skin factor ξ is graphed (Figure 4.10). Which of these horizontals gives the correct well bore skin, depends on the storage coefficient adopted in equation (2.9), as shown in following example.

The example assumes a zero value for the well bore skin factor. If the storage coefficient for the fracture system S_f is used to determine Ei(u) in equation (2.9), the correct zero skin factor ξ is given by the first horizontal, whereas the transient and late time data result in a wrong negative skin value (Fig. 4.10A). When S in equation (2.9) is replaced by the sum of $S_f + \beta S$, a wrong positive skin is obtained in the first horizontal (early time and transient data) and the correct zero value is given by the late time data (Fig. 4.10B).

If the well bore skin data is different from zero, the methodology applied is the same, but the resulting graph will plot as a parallel curve shifted along the vertical axes.

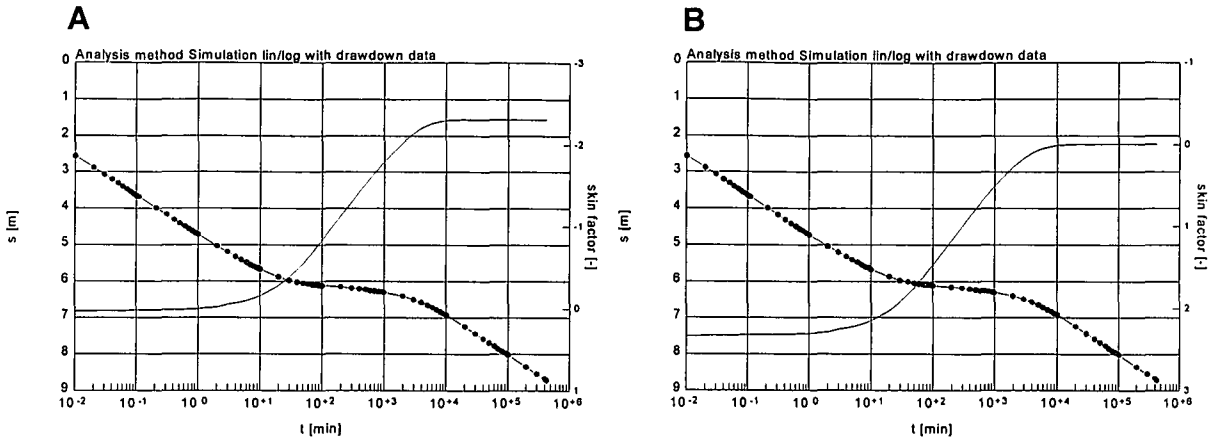

Figure 4.10. Determination of the skin factor for early time and late time in a pumped well

Another approach for the determination of the well bore skin is shown in Figure 4.11, where the offset between the late time data of the pumped well and an observation well gives an approximate value of the skin effect in meter. Equation (2.10) can be used to evaluate the dimensionless skin factor ξ.

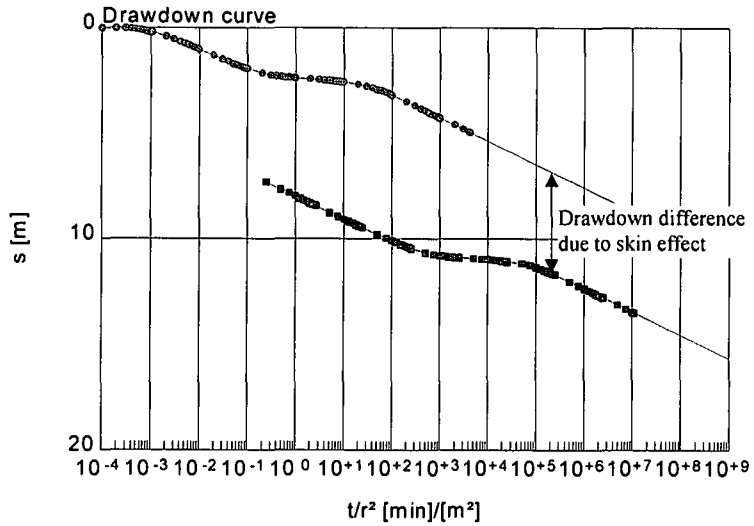

Figure 4.11. The offset between the late time data in a pumped well (squares) and an observation well (dots) indicates the additional drawdown in metres that can be used as an initial approximation of the skin factor ξ

4.1.3.3 Application of the forward modelling

The aquifer properties obtained with the straight-line approach, the well bore skin value, and the conceptual model of the aquifer geology constitute the 'known aquifer parameter' for the forward modelling. These are:

- transmissivity of fracture network T_f [L^2T^{-1}]
- storage coefficient of the fracture network S_f [-]
- storage coefficient of the matrix block S [-]
- well bore skin factor ξ [-]
- principle geometry of the matrix block
- characteristic thickness of the matrix block ($2 \cdot b_h$) [L]

The unknown parameters for the Moench model are:

- conductivity of the matrix block K [LT^{-1}]
- fracture skin ξ_f [-]

These two unknowns must be estimated via trial and error to fit the measured data until the simulated curve and its derivative satisfactorily fit the measured data and its derivative. This procedure is very fast for the experienced user. Generally 3 to 5 runs are enough to get a good fit.

4.1.4 Field examples

First example: Effects of well bore skin and well bore storage

Figure 4.12 illustrates the forward modelling results for the drawdown and its derivatives using TPA. Drawdown data of a pumped well (UE-25b) and an observation well (UE-25a) published by Moench (1984) are analysed. Both wells are situated in a drilling site in Nevada, USA. The aquifer is composed of layered volcanic rocks that show double porosity behavior. The curve fit was achieved using the aquifer parameters listed by Moench:

Discharge rate [m^3/h]	Q	= 129
Fracture transmissivity [m^2/d]	T_f	= 345.6
Fracture storage coefficient [-]	S_f	= 0.0006
Matrix storage coefficient [-]	S	= 0.12
Matrix conductivity [m/d]	K	= 0.7
Well bore skin factor [-]	ξ	= 0
Fracture skin factor [-]	ξ_f	= 1
Aquifer thickness [m]	h	= 400
Slab thickness [m]	$2b_h$	= 80
Drilled well bore radius [m]	r_w	= 0.11
Distance of the observation well [m]	r	= 110

Both curves do not show horizontal derivatives, therefore the straight-line methods of Warren & Root (1962) and Kazemi (1969) cannot be applied. The solution was obtained by forward modelling instead. Although the results for both wells are acceptable, the fit for the pumped well can be improved, if a negative well bore skin factor ξ = -0.5 is applied. This indicates that either the drilled radius is larger than the published value or the REV for the fracture network is larger than the drilled radius. The drawdown data of the pumped well at early time show an increase of the casing radius to approximately 0.14 m, thus data are still affected by well bore storage (Fig. 4.13). An increase of the matrix storage coefficient S to 0.25 leads to a better fit of the late time data from the observation well without worsening the fit in the pumping well.

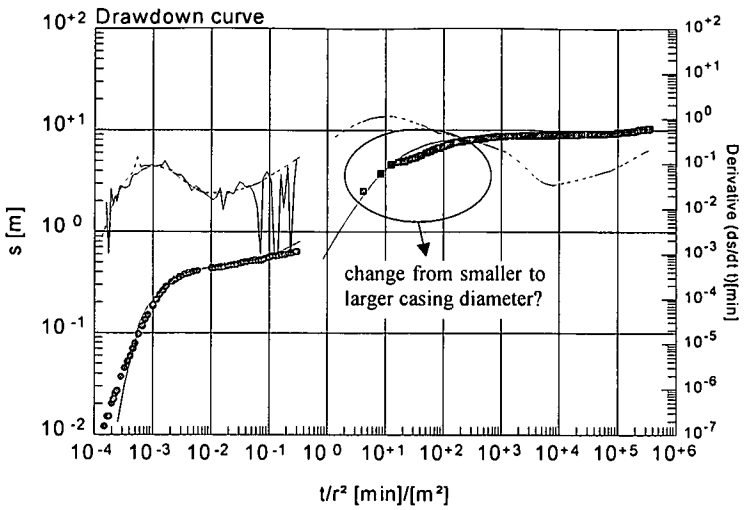

Figure 4.12. Forward modelling results for the data published by Moench. The pumping well data are indicated by squares and the observation well data by dots. Both curves do not show horizontal derivatives, therefore the straight-line methods of Warren & Root and Kazemi cannot be applied

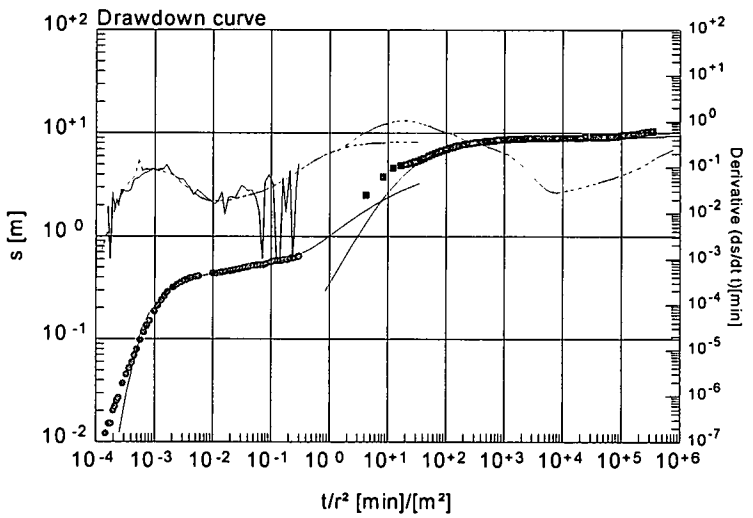

Figure 4.13. Forward modelling with matrix storage coefficient S increased to 0.25 and casing radius of the pumped well increased to 0.14 m leads to an improved fit in the early time pumping well data. The very early time data does not fit probably due to a larger upper well diameter (see text above). The pumping well data are indicated by squares and the observation well data by dots

Second example: Effect of dewatered water strike

Figure 4.14 presents data of a pumped well and an observation well situated in a layered Karoo sandstone aquifer in Botswana. Both curves do not show horizontal derivatives, therefore the straight-line methods of Warren & Root (1962) and Kazemi (1969) cannot be applied. The solution is obtained applying forward modelling instead and the parameters listed in the table below. Using these parameters, it is possible to fit the observation well data, but not the pumped well data due to the dewatering of the main water strike, which was recorded at 9 m below the rest water level. This example illustrates that in the case of strikes dewatering, it is difficult to determine the aquifer parameters, if only data from the pumped well are available. The early time data in the pumped well can be fitted with a well bore skin factor of $\xi = 3.7$, but not the medium and late time data (Fig. 4.14).

Discharge rate [m^3/h]	Q	= 19.2
Fracture transmissivity [m^2/d]	T_f	= 35
Fracture storage coefficient [-]	S_f	= 0.0003
Matrix storage coefficient [-]	S	= 0.015
Matrix conductivity [m/d]	K	= 0.011
Well bore skin factor [-]	ξ	= 3.7
Fracture skin factor [-]	ξ_f	= 0.3
Aquifer thickness [m]	h	= 70
Slab thickness [m]	$2b_h$	= 11
Drilled well bore radius [m]	r_w	= 0.155
Distance of the observation well [m]	r	= 14.1

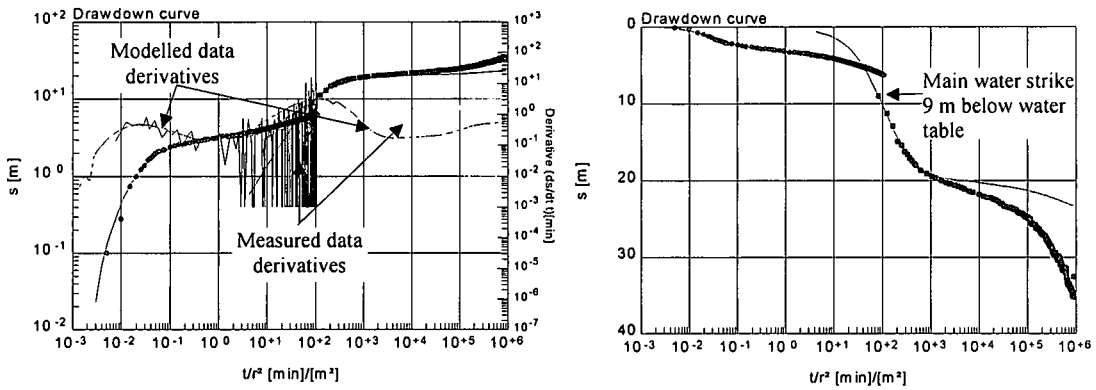

Figure 4.14. The simulated curve (solid line) fits the observation well data (dots) very well, but not the pumped well data (squares) due to additional well losses caused by dewatering of the main water strike. Early time data of the pumped well are fitted using a well bore skin factor of $\xi = 3.7$

The Jacob's correction ($s' = s - s^2/2h$) applied to the drawdown data of the pumped well is not sufficient to overcome the additional losses due to the dewatering of a water strike. The correction leads to a reduction of the well bore skin factor to $\xi = 2.4$, but the medium and late time data still cannot be fitted (Fig. 4.15).

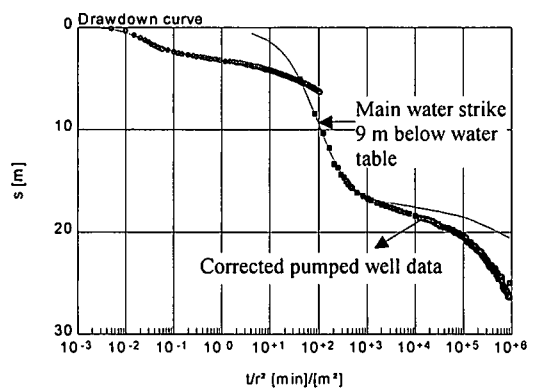

Figure 4.15. Jacob's correction ($s' = s - s^2/2h$) applied to the drawdown data of the pumped well is not sufficient to overcome the additional losses due to the dewatering of a water strike. In this case the early time data of the pumped well are fitted using a well bore skin factor of $\xi = 2.4$

4.2 Single vertical fracture with infinite conductivity and finite extent (Gringarten *et al.*, 1974)

4.2.1 Theory

The drawdown behavior in wells connected to a single vertical fracture (Fig. 4.16) became a focus of interest in the petroleum industry after the introduction of hydraulic fracturing, which is used to enhance the yield of production boreholes in low permeable formations. Stober (1986), Merton (1987), and other researchers showed that the solutions applied to hydraulic fracturing could be utilized for natural vertical fracture cases as well.

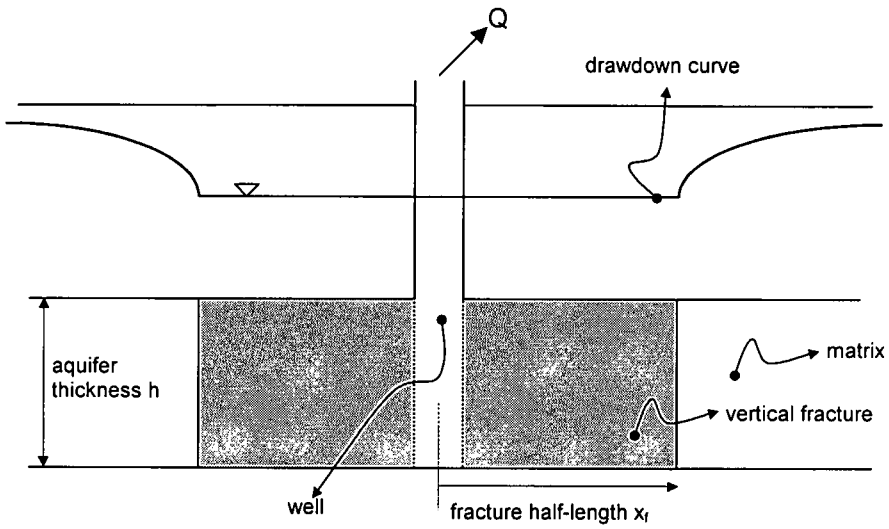

Figure 4.16. Drawdown behavior in a system composed of a single vertical fracture with infinite conductivity embedded in a matrix

Prats (1961) investigated the drawdown behavior of single vertical fractures with finite extent using an electrical analogue model. Based on Green's source function and applying the Neuman product, Gringarten *et al.* (1974) produced following general solutions for the dimensionless drawdown s_d in a vertical fracture with infinite conductivity and finite length:

$$s_d(x_d, y_d, t_d) = \int_0^{t_d} e^{-\frac{y_d^2}{4(t-t')_d}} \sum_{m=1}^{M} Q_m(t_d) \cdot F(x_d, t_d) \cdot \frac{dt_d'}{4\sqrt{(t-t')_d}} \qquad (4.10)$$

where

$$Q_m(t_d) = \frac{2q_m(t_d') \cdot h_f \cdot x_f}{Q}$$

q_m = influx rate per fracture segment [L^2T^{-1}]
Q = influx rate over the entire length of the fracture equivalent to the discharge at the well [L^3T^{-1}]
h_f = fracture height [L]
x_f = fracture half-length [L]

$$F(x_d,t_d)=erf\left(\frac{x_d+\frac{m}{M}}{2\sqrt{(t-t')_d}}\right)-erf\left(\frac{x_d+\frac{m-1}{M}}{2\sqrt{(t-t')_d}}\right)-erf\left(\frac{x_d-\frac{m}{M}}{2\sqrt{(t-t')_d}}\right)+erf\left(\frac{x_d-\frac{m-1}{M}}{2\sqrt{(t-t')_d}}\right)$$

x_d = Cartesian dimensionless distance, x/x_f [-]
y_d = Cartesian dimensionless distance, y/x_f [-]
t_d = dimensionless time,

$$t_d=\frac{T\cdot t}{S\cdot x_f^{\,2}}[-]$$

T = matrix or formation transmissivity [L^2T^{-1}]
t = time [T]
S = storage coefficient of the matrix or formation [-]
M = number of fracture segments
m = integer number
t_d' = integration parameter
e = exponential function
erf = error function,

$$erf(x)=\frac{2}{\sqrt{\pi}}\int_0^x e^{-u^2}du$$

The transformation of equation (4.10) in real world coordinates is given by

$$s=\frac{Q}{2\cdot\pi\cdot T}\cdot s_d(x_d,y_d,t_d) \qquad (4.11)$$

Gringarten *et al.* (1974) presented solutions for two different flux conditions along the fracture surface:

- uniform flux, where the flux distribution is homogeneous along the fracture and constant in time
- infinite flux, where the flux distribution is uniform along the fracture during the linear flow phase, but not in the transient and radial-acting flow phases. Simultaneously, it varies with time until the radial-acting flow phase is reached

In the uniform flux case the flux Q_m is independent of time. Thus, it can be taken out of the integral in equation (4.10) and the solution reduces to

$$s_d(x_d,y_d,t_d)=\int_0^{t_d} e^{-\frac{y_d^2}{4t_d'}}\cdot\left[erf\left(\frac{1-x_d}{2\sqrt{t_d'}}\right)+erf\left(\frac{1+x_d}{2\sqrt{t_d'}}\right)\right]\frac{dt'}{4\sqrt{\frac{t_d'}{\pi}}} \qquad (4.12)$$

Generally, equation (4.12) must be solved by numerical integration. However, analytical solutions exist for the pumped well and observation wells located along the fracture. For the pump well the analytical solution reads

$$s_d(0,0,t_d)=\sqrt{\pi\cdot t_d}\cdot erf\left(\frac{1}{2\sqrt{t_d}}\right)-\frac{1}{2}Ei\left(-\frac{1}{4\cdot t_d}\right) \qquad (4.13)$$

For observation wells along the fracture the solution is given by:

$$s_d(x_d,0,t_d) = \frac{1}{2}\sqrt{\pi \cdot t_d} \cdot \left[erf\left(\frac{1-x_d}{2\sqrt{t_d}}\right) + erf\left(\frac{1+x_d}{2\sqrt{t_d}}\right)\right] - \frac{(1-x_d)}{4} \cdot Ei\left[-\frac{1-x_d}{4 \cdot t_d}\right] - \frac{(1+x_d)}{4} \cdot Ei\left[-\frac{1+x_d}{4 \cdot t_d}\right] \qquad (4.14)$$

Gringarten *et al.* (1974) found that the uniform flux drawdown at a dimensionless distance $x_d = 0.732$ is equal to the infinite flux drawdown at the well (Fig. 4.17). Substituting this x_d value in equation (4.14) the drawdown reads:

$$s_d(0,0,t_d) = \frac{1}{2}\sqrt{\pi \cdot t_d} \cdot \left[erf\left(\frac{0.134}{\sqrt{t_d}}\right) + erf\left(\frac{0.866}{\sqrt{t_d}}\right)\right] - 0.067 \cdot Ei\left(-\frac{0.018}{t_d}\right) - 0.433 \cdot Ei\left(-\frac{0.75}{t_d}\right) \qquad (4.15)$$

Although the drawdown for both cases does not differ much (Fig. 4.18), data measured in a pumping well can usually be described by only one of the two models (Gringarten *et al.*, 1974).

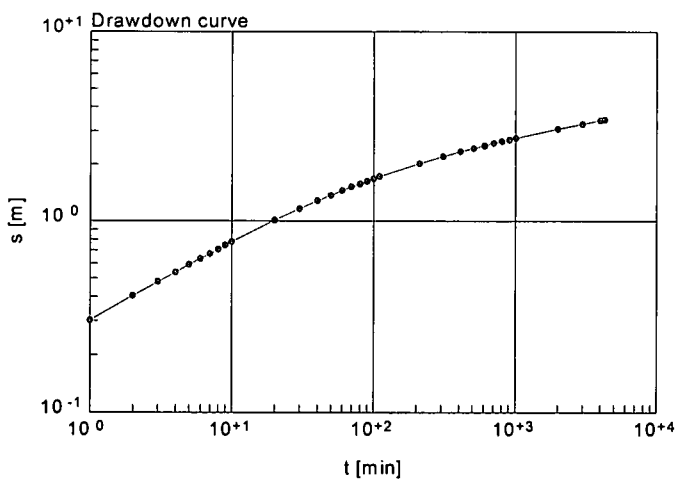

Figure 4.17. Comparison of drawdown in an infinite conductivity vertical fracture for uniform flux at $x_d = 0.732$ (dots) and infinite flux at the pumped well (solid line)

The drawdown s in a fracture at early time is given by Gringarten *et al.* (1974) for both the uniform and infinite flux cases and reads

$$s = \frac{Q}{2 \cdot \pi \cdot T} \cdot \sqrt{\pi \cdot t_d} \qquad (4.16)$$

with
$t_d < 10^{-2}$ for uniform flux
$t_d < 2 \cdot 10^{-1}$ for infinite flux

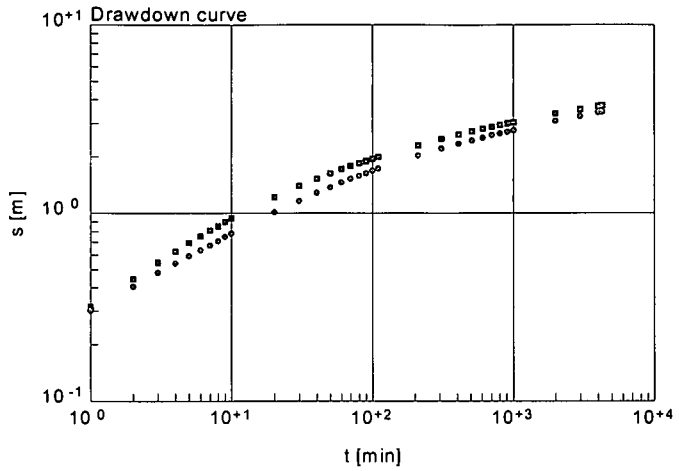

Figure 4.18. Comparison of drawdown in an infinite conductivity vertical fracture with uniform flux (squares) and infinite flux (dots), both at the pumped well

Equation (4.16) describes the drawdown during the linear flow phase, which implies uniformity of flux along the fracture for both, the infinite flux case and the uniform flux case. Due to the fact that the fracture has infinite conductivity, there is an infinite small pressure gradient along the fracture that can be neglected ($\Delta p/\Delta x_f = 0$). Therefore, at early time the same drawdown is observed along the entire length of the fracture and an observation well located in the fracture will show the same curve as the pumped well.

The long-term solution describes the radial-acting flow phase ($t_d \geq 10$) on the fracture as

$$s = \frac{Q}{2 \cdot \pi \cdot T} \cdot \left[\frac{1}{2} \ln(t_d) + 1.1 \right] \qquad (4.17)$$

Equation (4.17) plots as a straight-line in a semi-log plot. Analogue to a homogeneous aquifer, the transmissivity value for the formation can be obtained using the Cooper-Jacob (1946) method, which will be demonstrated later.

The concept of relative storage capacity was initially introduced by Ramey & Gringarten (1976) for compressible fluids. However, due to the fact that the compressibility of ground water is negligible, the relative storage capacity CD_f defined by Cinco-Ley *et al.* (1978) will be used in this work. It is defined as:

$$CD_f = \frac{S_f \cdot w}{\pi \cdot S \cdot x_f} \qquad (4.18)$$

where
S = storage coefficient of the matrix or formation [-]
S_f = storage coefficient of the fracture system [-]
w = fracture aperture [L]
x_f = fracture half-length [L]

4.2.2 Diagnosis

The drawdown in a pumped well situated in a vertical fracture with infinite conductivity and finite extent is dominated by two different flow phases:

- linear flow at early time, which shows a typical slope of 0.5 in a log-log plot (Fig. 4.19A) or a straight-line in a lin $t^{1/2}$ plot (Fig. 4.19B)
- radial flow after a transition period, which plots as a straight-line in a semi-log plot (Fig. 4.19C)

Unfortunately drawdown data at early time plot often on an almost horizontal line due to skin effects at the well (well bore skin; Section 2.4.2), at the fracture interface (fracture skin; Section 2.4.4), or at both (Cinco-Ley & Samaniego, 1977). In these cases, the data draw as a straight-line in a lin $t^{1/2}$ plot with a positive shift from the origin (Fig 4.20). This plot can also be used to uniquely identify the skin location (Bardenhagen, 1999), as shown in Figure 4.21. Alternatively, the derivative of the curve can be used to determine the linear flow phase, due to the fact that it is not affected by the skin effects. The derivative will plot as a straight-line with a slope of 0.5 in a log-log plot (Fig 4.22A) or as a straight-line from the origin in a lin $t^{1/2}$ plot (Fig 4.22B).

Whether the radial-acting flow phase is present or not, can be determined using the derivative in a log-log plot, as it graphs horizontal during the radial flow phase. The data beyond the point where the radial-acting flow starts can be used for the estimation of the transmissivity applying the Cooper-Jacob (1946) straight-line method. If the radial-acting flow phase is not fully developed, the Gringarten type curve method should be applied, whose handling is basically the same as the common Theis type curve approach.

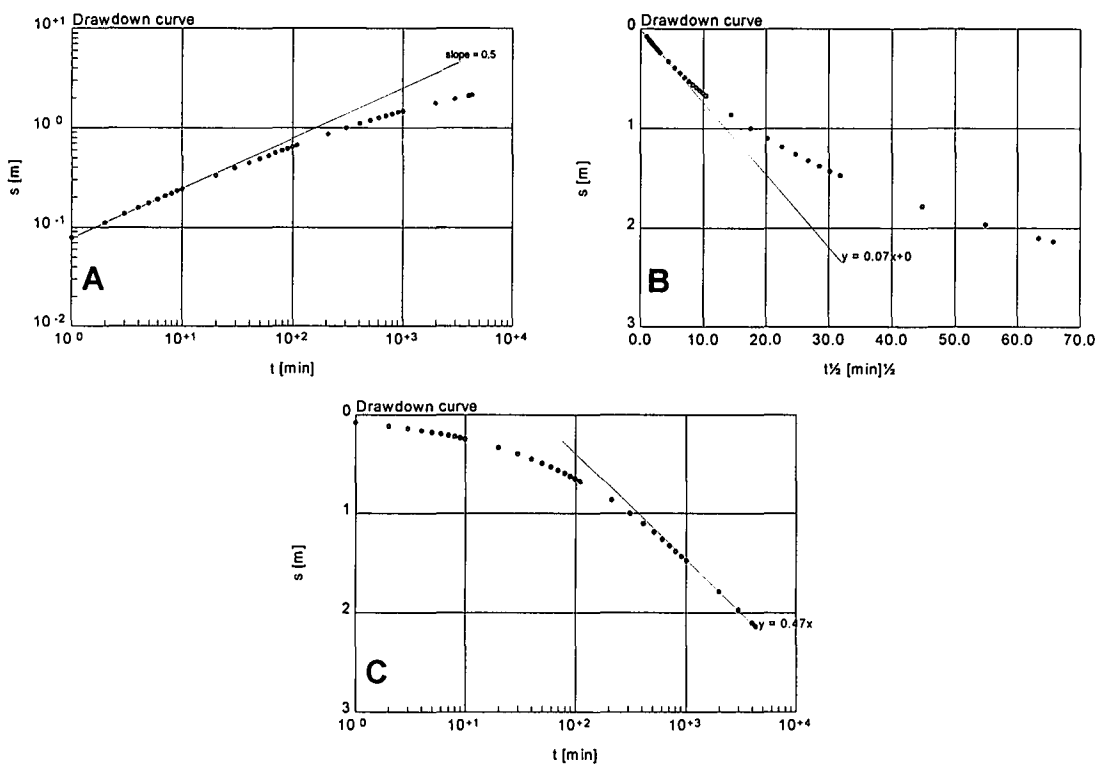

Figure 4.19. Pumped well flow phases in various diagnosis plots. Linear flow is shown in graphs A and B. Graph C shows radial-acting flow

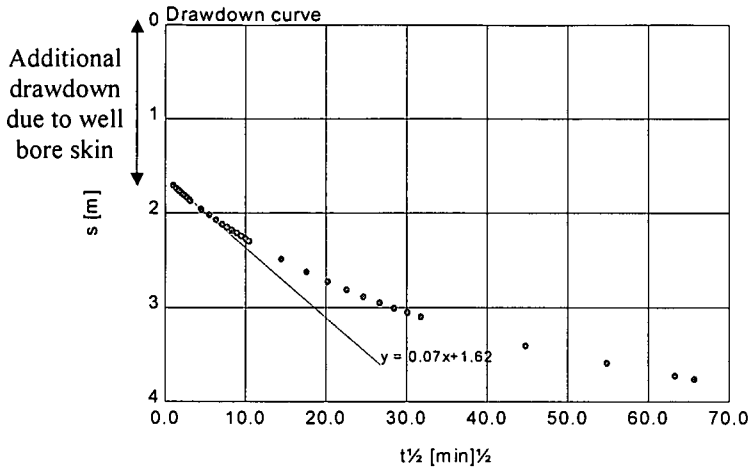

Figure 4.20. Drawdown in a pumped well located in an infinite conductivity vertical fracture. The positive shift of the drawdown curve from the origin indicates the presence of skin effects

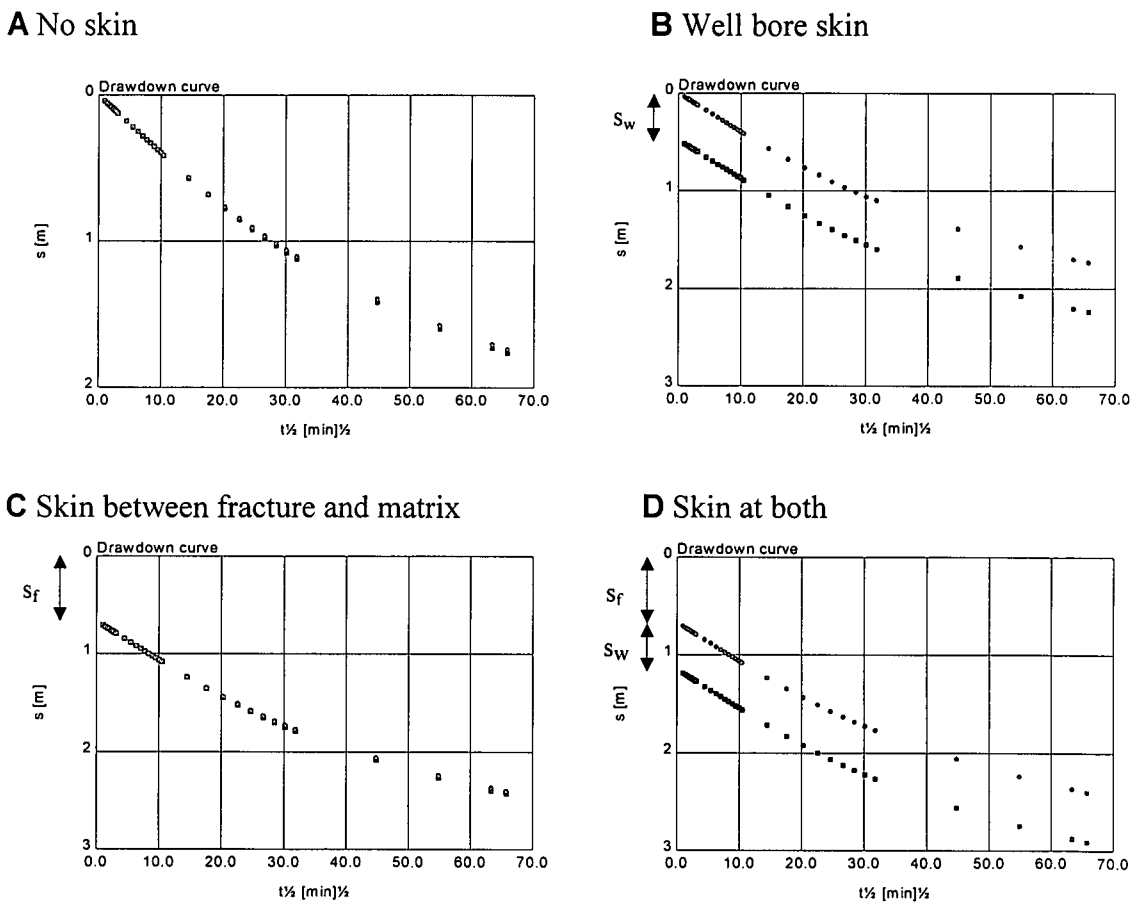

Figure 4.21. Skin effects on drawdown curves from pumped well (squares) and observation well (dots) located at a distance $x/x_f = 0.5$. Both wells are drilled in the same fracture

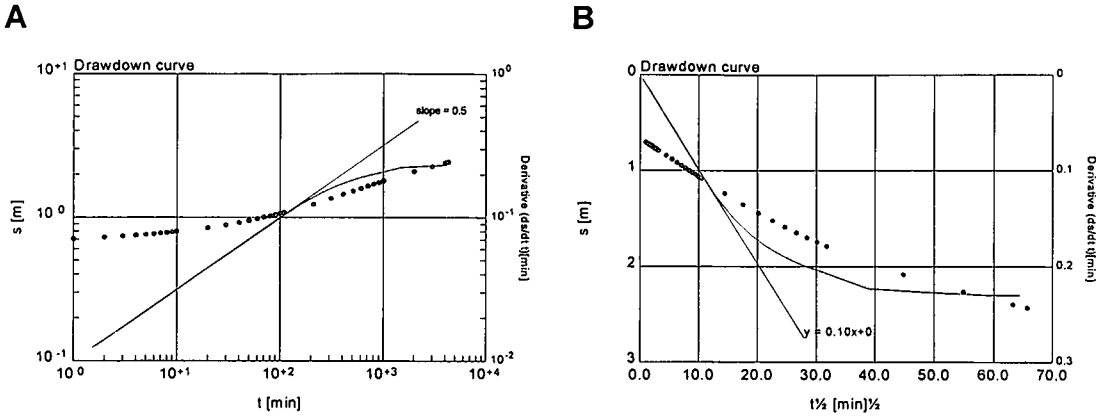

Figure 4.22. Drawdown in a pumped well. The derivative is not affected by the skin effects and therefore, it can be used to determine the linear flow phase at early time

It must be beared in mind that no unique evaluation of the aquifer parameters is possible, if only the linear flow phase is observed (Streltsova, 1988), as demonstrated in the various recovery curves in Figure 4.23. For example, the Agarwal straight-line method can only be used for the determination of the aquifer transmissivity, if the pumping time is long enough to allow for radial-acting flow as indicated by the horizontal derivative in curve A (solid line A). The pumping time in curves B and C was not long enough to reach the radial-acting flow and therefore, the derivatives (solid lines B and C) are not horizontal.

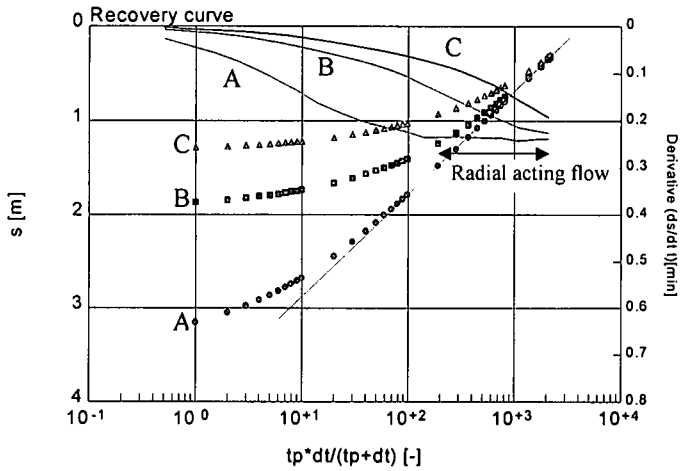

Figure 4.23. Various recovery in a pumped well for different pumping times. Radial-acting flow phase was only reached in curve A as indicated by the horizontal derivative (solid line A). The pumping time in curves B and C was not long enough

The influence of the fracture storage on the drawdown is described by the relative fracture storage capacity CD_f. At early time the drawdown curves differ significantly depending on the CD_f value. The early time drawdown data for $CD_f = 10^{-4}$ does not plot on a straight-line with slope 0.5 (Ramey & Gringarten, 1976). Indeed, between $10^{-4} \leq CDf \leq 10^{-2}$ the drawdown curves are not characterized by straight-lines for times of interest. If $CD_f > 10^{-2}$ the data will plot as a straight-line with slope of 1, which indicates that the cone of depression has reached the edges of the very high conductive fracture (Fig. 4.24). In these cases, the drawdown at early time is similar to that of pumping from a limited reservoir (closed boundaries). As soon as the

gradient between matrix and fracture builds up, the influx from the matrix to the fracture increases and the slope of 1 vanishes, similar to the well bore storage effect case.

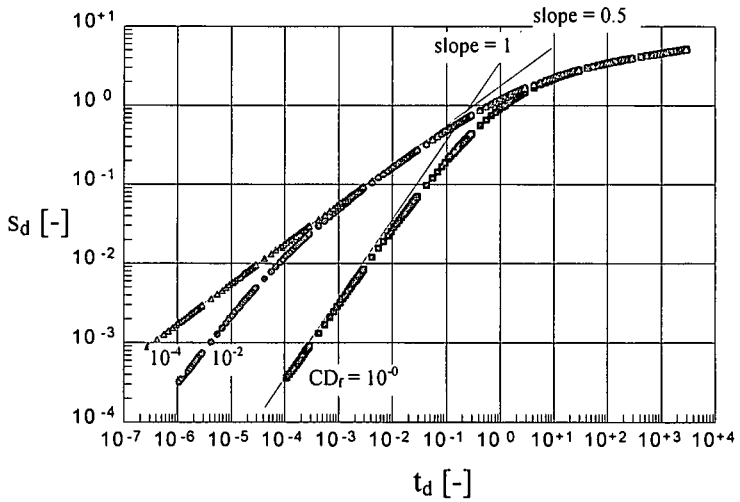

Figure 4.24. Various dimensionless drawdown curves in a pumped well for different relative fracture storage capacity CD_f ($s_d = 2 \cdot \pi \cdot T \cdot s/Q$ and $t_d = T \cdot t / S \cdot x_f^2$)

4.2.3 Method of analysis

Basically two methods of analysis for the drawdown data can be used to determine the formation or matrix transmissivity T: a straight-line method using a semi-log plot and a type curve method using a log-log plot. If recovery (build up) data are available, the recovery method of Theis (1935) or Agarwal (1980) can be used. Alternatively, a forward modelling using TPA can be applied to determine the aquifer parameter for both the drawdown and recovery phase. The determination of the actual fracture transmissivity T_f is not possible because it is a priori considered infinite.

The methods can be applied if following conditions are true:

- matrix is infinite
- aquifer (fracture and matrix) is confined
- Darcian flow prevails in fracture and matrix
- well and fracture penetrate the aquifer fully
- well bore storage and fracture storage are negligible
- well bore skin and fracture skin are negligible
- straight-line can be applied if td $\geq$ 10 (radial-acting flow). Cross-check that the first derivative becomes horizontal

4.2.3.1 Straight-line application

Straight-line methods can be applied to both pumped well and observation well data, but only if a significant part of the curve shows radial-acting flow (see previous section). The handling is similar to that of the Cooper-Jacob (1946) method. The transmissivity T of the formation can be determined by following equation:

$$T = \frac{0.183 \cdot Q}{d} \qquad (4.19)$$

where
T = matrix or formation transmissivity [L^2T^{-1}]
Q = discharge rate [L^3T^{-1}]
d = drawdown over one log cycle [L]

It must be beared in mind that the common Cooper-Jacob (1946) method for the determination of the storage coefficient is only applicable, if the distance of the observation well to the pumped well is larger than 3 times that of the fracture half-length x_f (Section 3.1.3).

The Theis (1935) and Agarwal (1980) recovery methods are applicable for the determination of the formation transmissivity T, if a significant portion of the recovery curve shows radial-acting flow behavior, as demonstrated in Figure 4.22. The handling of the straight-line recovery method is similar to the drawdown approach. The transmissivity of the formation is determined by following equation:

$$T = \frac{0.183 \cdot Q}{d'} \qquad (4.20)$$

where
d' = residual drawdown over one log cycle [L]

4.2.3.2 Type curve application

The advantage of the Gringarten type curve approach lies in the fact that only data of the transient phase from linear flow to radial-acting flow is needed (Fig. 4.25). In other words, the method is applicable even if a test was run too short to fully reach the radial-acting flow phase.

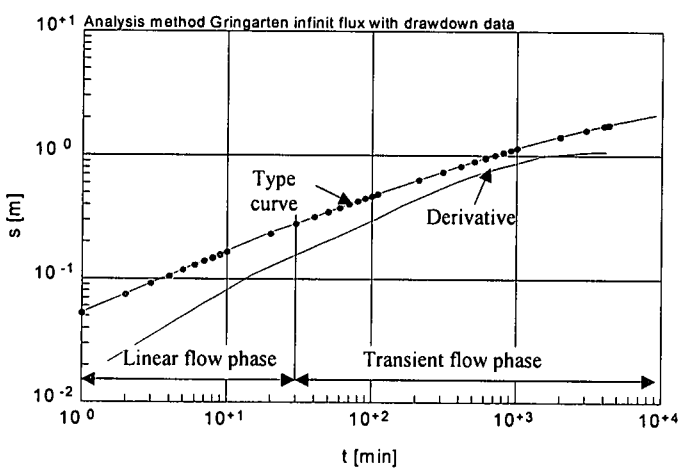

Figure 4.25. Example of the Gringarten type curve method for a pumped well data set (dots) that does not reach the radial-acting flow

The application of Gringarten type curve method for pumped wells is similar to that of the Theis type curve method (Fig. 4.26). After matching the data curve with

the type curve the transmissivity T and storage coefficient S can be determined by substituting the values for the match point coordinates in following equations:

$$T = \frac{Q}{2 \cdot \pi \cdot d} \cdot s_d(0,0,t_d) \qquad (4.21)$$

$$S = \frac{T \cdot t}{t_d \cdot x_f^{\,2}} \qquad (4.22)$$

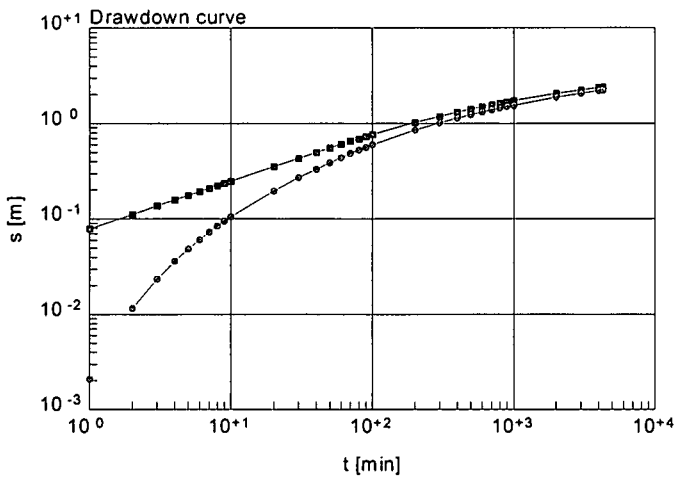

Figure 4.26. Example of Gringarten forward simulation (solid lines) for a pumped well (squares) and an observation well (dots). Simulation parameters are: T = 50 m^2/d, S = 0.0001, x_f = 400 m, distance between pumped and observation wells r = 50 m (perpendicular to the fracture)

The fracture half-length x_f is usually an unknown parameter, which can only be determined if data from an observation well is available and its relative location to the fracture is known. Unfortunately, for each observation well location a new set of type curves have to be drawn, which is not very effective. In such cases the forward modelling represents a more appropriate approach (Fig. 4.26).

4.2.3.3 Determination of skin effects

Skin effects can appear at the well (well bore skin), between fracture and matrix (fracture skin) or at both, as described in Bardenhagen (1999). If drawdown data from wells situated in a vertical fracture with infinite conductivity are obscured by skin effects, the curve shows an almost horizontal drawdown at the early time data followed by a transition period and the radial-acting flow phase. Figure 4.27 shows the various possible drawdown shapes graphed in log-log plots. The total skin factor ξ_t can be graphically determined using the pumped well data represented in a lin $t^{1/2}$ plot (Fig. 4.21D) and following equation

$$\xi_t = \frac{s_{add} \cdot 2 \cdot \pi \cdot T}{Q} \qquad (4.23)$$

where

s_{add} = additional drawdown = $s_w + s_f$ [L]
T = matrix or formation transmissivity [L^2T^{-1}]
Q = discharge rate [L^3T^{-1}]

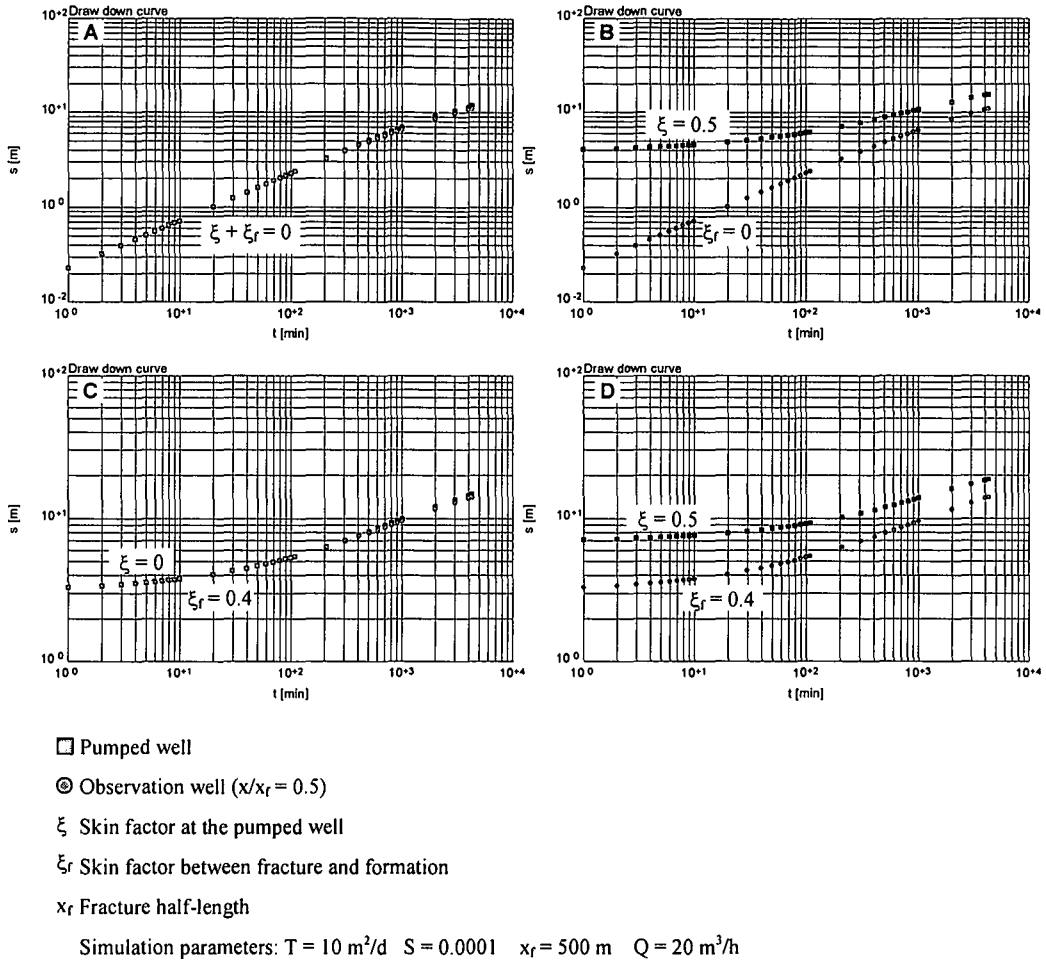

Figure 4.27. Skin effect at pumped well and observation well located in the same infinite conductivity fracture

In the presence of an observation well located in the same fracture the additional drawdown caused by fracture skin ξ_f can be determined after equation (4.24), similar to ξ_t. The well bore skin ξ is then calculated as

$$\xi = \xi_t - \xi_f \qquad (4.24)$$

4.2.3.4 Forward modelling application

If the transmissivity value is known either from the straight-line method or the type curve approach, this value should be used as known parameter in the forward modelling to accelerate the fitting process. In the worst case, the known parameters are:

- hydrogeological concept of a single vertical fracture with infinite transmissivity
- transmissivity T of the matrix
- skin factor ξ_f

The unknown parameters are

- storage coefficient S of the matrix
- fracture half-length x_f

However, these parameters cannot be uniquely determined without data of an observation well located in the matrix.

4.2.4 Field example

First example: Skin effect at well bore

Two boreholes (BH1 and BH2) located 133.5 m apart were sited on a 15 km long, 5 m wide, sub-vertical (77°S) fault zone crossing the Fish River in the southern part of Namibia (Bardenhagen, 1999). The river might represent a potential recharge source. The fault partly separates two low yielding formations composed by horizontal intercalated layers of claystone, siltstone and sandstone. Both boreholes intersect the fault at 27m below the surface. The water level in both boreholes rose immediately after the fault was struck to a level of 906.1 m amsl (8.3 m below surface in BH1 and 5.3 m below surface in BH2). The airlift yield was estimated at more than 100 m^3/h in each borehole. Screens with 0.5 mm slots were installed to avoid borehole collapse. Figure 4.28 shows the drawdown measured during a constant discharge test. Only the drawdown in the observation well shows a slope of 0.5 indicating linear formation flow. However, the drawdown in the pumped well starts almost horizontal and develops at late time to radial-acting flow. This behavior is typical for a skin that is located at the well.

Discharge rate [m^3/h]	Q	= 67
Matrix transmissivity [m^2/d]	T	= 200
Fracture storage coefficient [-]	S_f	= 0.0007
Fracture half-length [m]	x_f	= 460
Well bore skin factor [-]	ξ	= 1.78
Fracture skin factor [-]	ξ_f	= 0
Drilled well bore radius [m]	r_w	= 0.11
Distance of the observation well [m]	r	= 133.5

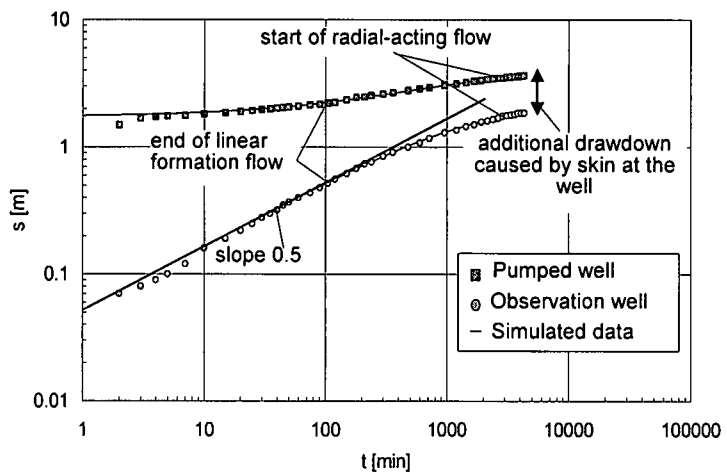

Figure 4.28. Example for a restricted drawdown in a pumped well, hence the almost horizontal shape of the early time data. The slope of 0.5 in the drawdown data of the observation well indicates linear formation flow. The solid line represents the simulated drawdown for a vertical infinite conductivity fracture with uniform flux

Second example: Well bore skin and fracture dewatering effects

A borehole was drilled into the dolomites of the Tsumeb Karst area, Namibia. Water strikes were recorded at depths between 14 m and 27 m below the water table. A constant discharge test was performed at a rate of 20 m^3/h. The data indicate a short period of linear flow at early time. As soon as the water level in the pumped well drops to the level of the first water strike, a significant increase in the drawdown is observed with a further increase as the water level drops below the second strike (Fig. 4.29). This behavior is a clear indication for over-extraction at the used rate. An additional drawdown of 7 m caused by skin effects can be determined from the special plot. However, it is not possible to uniquely locate this skin, due to the lack of observation borehole data. The determination of the aquifer parameters (T and S) for this test is not possible with any of the above mentioned methods because the transient and radial-acting flow phases are masked by the effects of fracture dewatering.

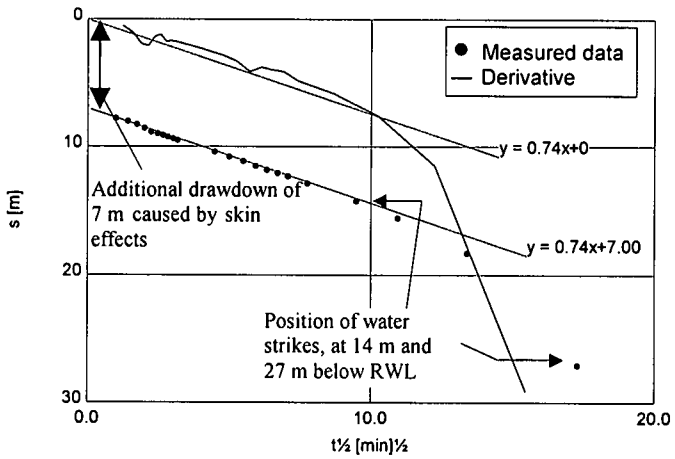

Figure 4.29. Graphical skin evaluation in a pumped well using the linear flow period of drawdown curve

4.3 Single vertical fracture with finite conductivity and finite extent (Cinco-Ley *et al.*, 1978)

4.3.1 Theory

Cinco-Ley *et al.* (1978) introduced a semi-analytical model that describes the drawdown in a single vertical fracture with finite conductivity and length (Fig. 4.30), which is embedded in an infinite, isotropic, homogeneous, horizontal matrix limited by upper and lower impermeable boundaries (top and bottom of the aquifer, respectively). It considers bilinear flow in the system and is, therefore, a generalised solution for this type of aquifer's geometry. The Gringarten *et al.* (1974) infinite flux solution is a special case of this model.

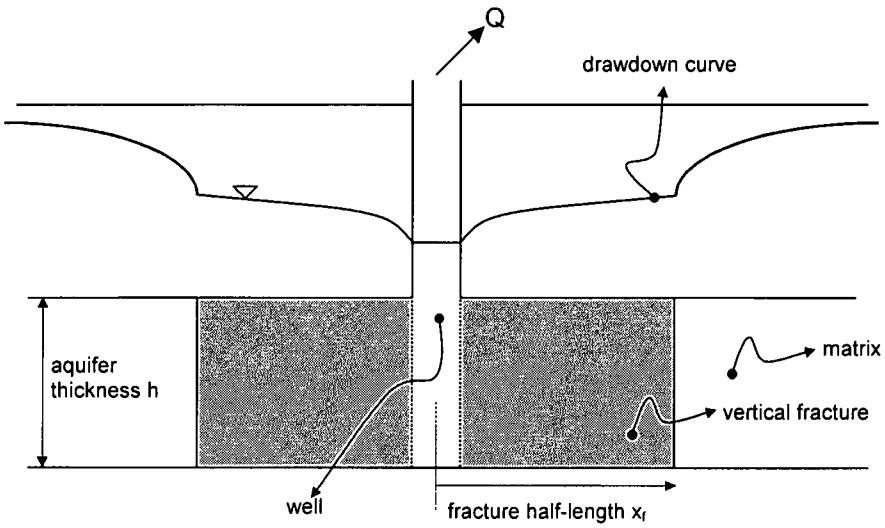

Figure 4.30. Drawdown behavior in a system composed of a single vertical fracture with finite conductivity embedded in a matrix

Assuming that the drawdown distribution in the fracture (equation. 4.25) coincides with the drawdown distribution in the matrix-fracture interface (equation 4.26), the matrix-fracture flux distribution can be obtained by simultaneously solving both equations. The model developed by Cinco-Ley *et al.* (1978) solves this equation by means of a special form of the finite difference method. The drawdown is obtained using the calculated fluxes in either equation 4.25 or 4.26. The equations for the fracture and reservoir are derived with the help of the Green and source functions and the Newman product. The equations for the fracture and matrix-fracture interface, respectively, read:

$$s_{fd}(x_d,t_d)=\frac{x_f}{w}\sqrt{\frac{\pi\cdot S\cdot T\cdot}{S_f\cdot T_f}}\cdot\sum_{m=1}^{\infty}\int_0^{t_d}\left\{\frac{e^{-\left[\frac{(x_d-2m)^2}{4(T_fS/TS_f)\tau}\right]}}{\sqrt{\tau}}-\int_{2m-1}^{2m+1}q_{fd}(x',\tau)\frac{e^{-\left[\frac{(x_d-x')^2}{4(T_fS/TS_f)\tau}\right]}}{2\sqrt{t_d-\tau}}dx'\right\}d\tau \qquad (4.25)$$

$$s_d(x_d,y_d,t_d)=\frac{1}{4}\int_0^{t_d}\int_{-1}^{1}q_d(x',\tau)\frac{e^{-\left[\frac{(x_d-x')^2+y_d^2}{4(t_d-\tau)}\right]}}{t_d-\tau}dx'\cdot d\tau \qquad (4.26)$$

where
s_{fd} = dimensionless drawdown in the fracture [-]
s_d = dimensionless drawdown in the matrix [-]
x_d = Cartesian dimensionless distance, x/x_f [-]
y_d = Cartesian dimensionless distance, y/x_f [-]
t_d = dimensionless time, $T \cdot t/S \cdot x_f^2$ [-]
w = fracture aperture [L]
T = matrix or formation transmissivity [L^2T^{-1}]
T_f = fracture transmissivity [L^2T^{-1}]
S = storage coefficient of the matrix or formation [-]
S_f = storage coefficient of the fracture [-]
m = integer value [-]
q_d, q_{fd} = dimensionless matrix-to-fracture flux [-]
τ, x'= integration variables

The solution of equations 4.25 and 4.26 uses the concept of relative conductivity Cr (Cinco-Ley *et al.*, 1978) to relate the conductivities of fracture and matrix as follows

$$Cr = \frac{T_f \cdot w}{\pi \cdot T \cdot x_f} \qquad (4.27)$$

where
T_f = fracture transmissivity [L^2T^{-1}]
w = fracture aperture [L]
T = matrix or formation transmissivity [L^2T^{-1}]
x_f = fracture half-length [L]

Cinco-Ley *et al.* (1978) presented a series of type curves calculated at the pumped well for Cr values in the range of 0.1 to 100 and dimensionless time t_d between 10^{-3} and 10^3. The curves that corresponds to Cr ≥ 100 practically coincide with the infinite flux solution from Gringarten *et al.* (1974). Agarwal *et al.* (1979) extended these type curves to smaller dimensionless times ($t_d = 10^{-5}$) based on numerical results obtained with the finite difference method.

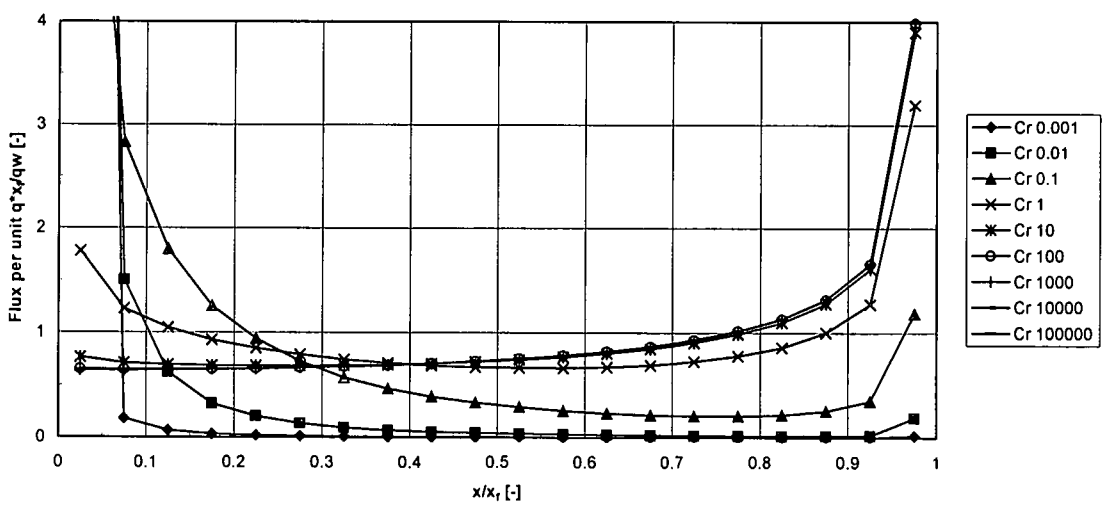

Figure 4.31. Stabilized flux distribution for different relative conductivities Cr. The stabilized flux distribution along the fracture remains constant for all values of Cr ≥ 100

In general, the influence of the fracture storage capacity on the drawdown behavior can be described by the relative fracture storage capacity CD_f (equation 4.18, Section 4.2.1), as shown by Cinco-Ley *et al.* (1978). However, they proved that this influence can be neglected for practical values of dimensionless time t_d.

The gradient along the fracture cannot be neglected, due to its finite conductivity. Thus, the solution requires the knowledge of the temporal flux distribution along the fracture. However, the flux distribution remains constant once the radial-acting flow phase starts (Fig. 4.31) and is then known as stabilized flux distribution.

4.3.2 Diagnosis

The drawdown in a pumped well situated in a vertical fracture with finite conductivity and finite length is characterized by the relative conductivity Cr (Cinco-Ley & Samaniego, 1981a) as follows:

- linear fracture flow at very early time, which shows a typical slope of 0.5 in a log-log plot or a straight-line in a lin $t^{1/2}$ plot. It is observed for $Cr < 100$, but is usually masked by well bore storage
- bilinear flow at early time, which shows a typical slope of 0.25 in a log-log plot (Fig. 4.32A) or a straight-line in a lin $t^{1/4}$. It is observed for $Cr < 100$
- linear formation flow at intermediate time, which shows a typical slope of 0.5 in a log-log plot (Fig. 4.32A) or a straight-line in a lin $t^{1/2}$ plot. It develops if $Cr \geq 100$
- radial flow at late time, which plots as a straight-line in a semi-log plot (Fig. 4.32B). It appears for all Cr, if the discharge time is sufficiently long ($t_d \geq 10$)

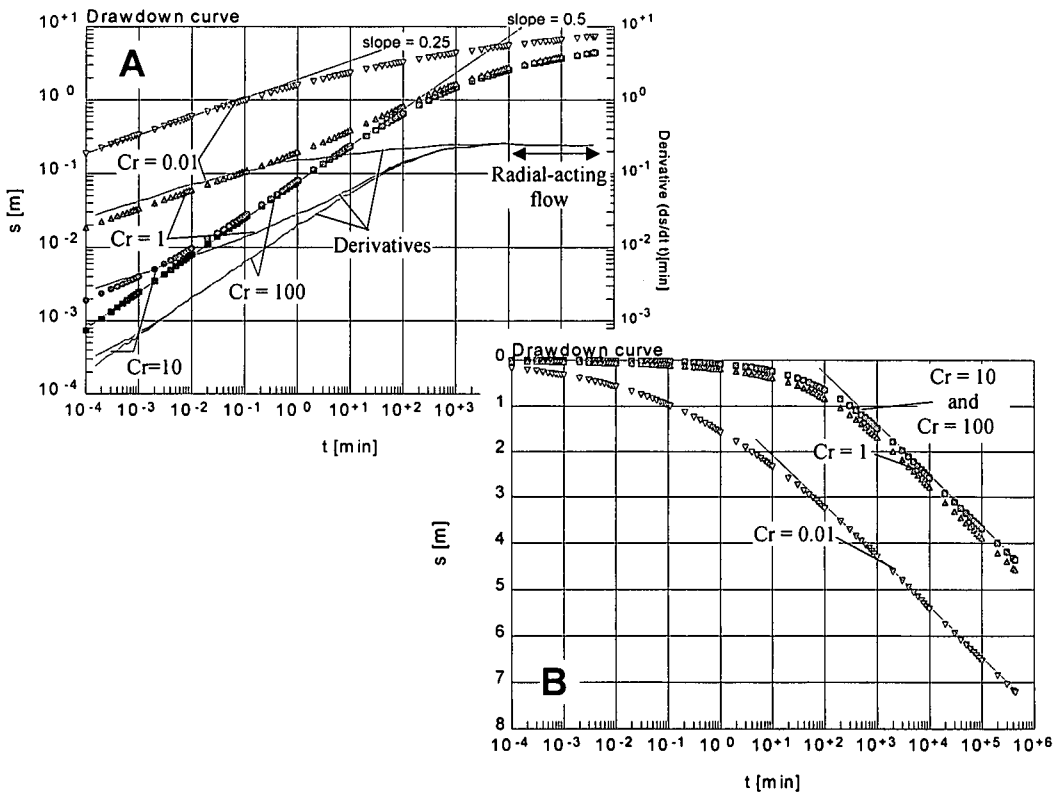

Figure 4.32. Drawdown curves in pumped wells located in a vertical finite conductivity fracture for various relative conductivities Cr. The drawdown curves show transition zones between all the different flow phases

The fracture has a finite conductivity, therefore the reaction in an observation well located in the same fracture is not instantaneous like in the infinite conductivity fracture case (Gringarten *et al.* 1974) (Fig. 4.33).

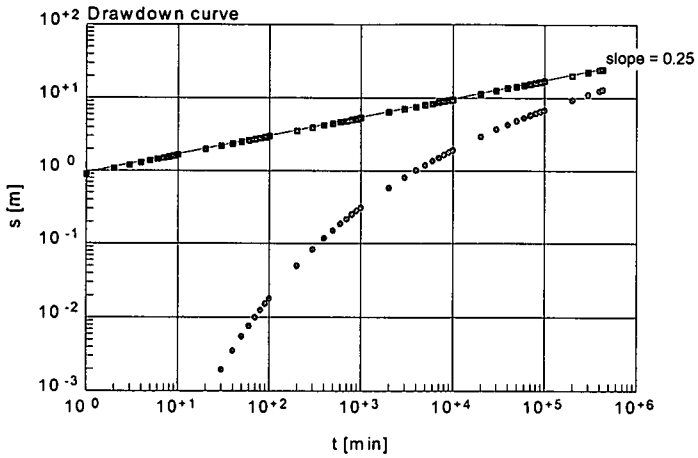

Figure 4.33. Drawdown in a pumped well (squares) and an observation well (dots) both located in the same vertical finite conductivity fracture. The curves differ at early time, due to the finite conductivity of the fracture

Whenever affected by skin, the drawdown in the pumped well develops similar to the infinite conductivity fracture case. In a log-log plot it graphs initially as a horizontal straight-line to show the normal radial flow shape after a transition phase (Fig. 4.34A). In a lin $t^{1/4}$ plot the early time bilinear flow plots as a straight-line with a positive shift from the origin (Fig. 4.34B). However, the derivative of the drawdown curve can be used to determine the different flow phases, as it is not affected by skin.

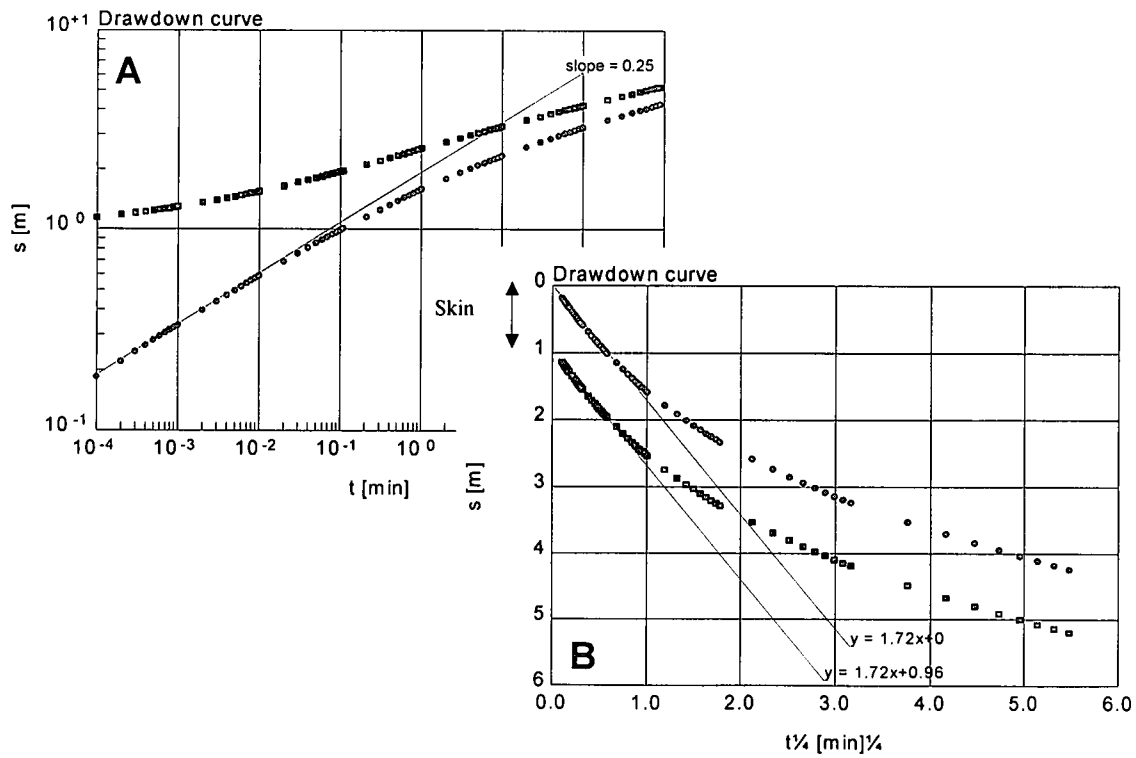

Figure 4.34. Drawdown from pumped well affected by skin (squares) and without skin (dots), both located in a finite conductivity fracture

Due to the finite conductivity of the fracture, it is not possible to graphically determine the location of the skin as described in Section 4.2.2 for the infinite conductivity fracture case.

In cases where the storage capacity of the fracture cannot be neglected, the influence of this parameter on the drawdown behavior can be described by the relative fracture storage capacity CD_f (equation 4.18, Section 4.2.1). In log-log plots (Fig. 4.35) the effects are as follows:

- for values of $CD_f > 10^{-4}$ the bilinear flow at early time data does not plot on a straight-line with slope 0.25
- for values between $10^{-4} \leq CD_f \leq 10^{-2}$ the drawdown curves cannot be characterized by any straight-line as they only show transient flow behavior
- for values of $CD_f > 10^{-2}$ the data plot as a straight-line with slope 0.5

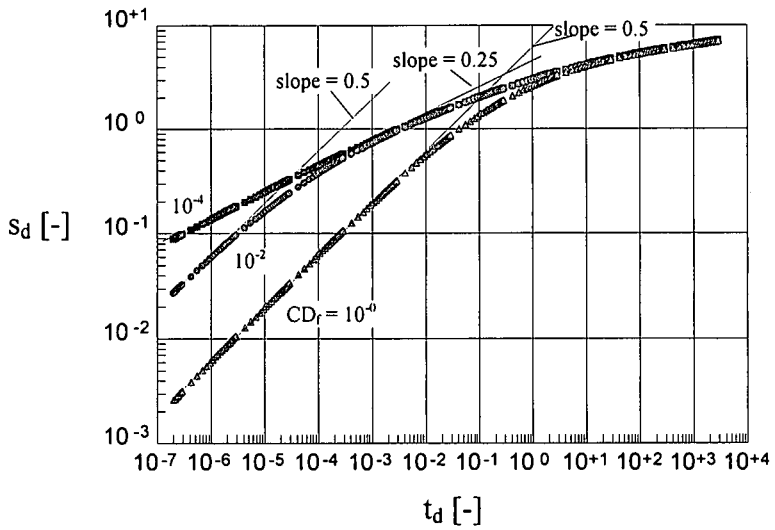

Figure 4.35. Various dimensionless drawdown curves in a pumped well and their derivatives for different relative fracture storage capacity CD_f ($s_d = 2 \cdot \pi \cdot T \cdot s/Q$ and $t_d = T \cdot t / S\, x_f^2$)

4.3.3 Method of analysis

Using the Cinco-Ley *et al.* (1978) model in those cases where bilinear flow and radial-acting flow are present ($Cr < 100$), following parameters can be determined:

- reservoir transmissivity
- reservoir storage coefficient
- fracture half-length
- fracture transmissivity
- fracture storage coefficient

Basically two methods of analysis for the drawdown data can be used to determine these parameters: a straight-line method using a semi-log plot and a type curve method using a log-log plot. If recovery (build up) data are available, the recovery method of Theis (1935) or Agarwal (1980) can be utilized. Alternatively, a forward modelling using TPA can be applied to determine the aquifer parameter for both the drawdown and recovery phase in the pumped well.

The application of the methods is possible, if following conditions are true:

- matrix is infinite
- aquifer (fracture and matrix) is confined
- Darcian flow prevails in fracture and matrix
- well and fracture penetrate the aquifer fully
- well bore storage and fracture storage are negligible
- well bore skin and fracture skin are negligible
- straight-line can be applied if td $\geq$ 10 (radial-acting flow). Cross-check that the first derivative becomes horizontal

4.3.3.1 Straight-line application

The straight-line application allows the determination of the reservoir transmissivity using the radial-acting flow phase of drawdown or recovery curves graphed in a semi-log plot. Both pumped well and/or observation well data can be utilized. The approach is similar to the methods of Cooper-Jacob (1946) and Theis (1935). The transmissivity T of the formation can be determined using equation 4.19 (Section 4.2.3.1).

It must be beared in mind that the common Cooper-Jacob (1946) method for the determination of the storage coefficient is only applicable, if the distance of the observation well to the pumped well is larger than 3 times the fracture half-length x_f (Section 3.1.3).

The Theis (1935) and Agarwal (1980) recovery methods are applicable for the determination of the formation transmissivity T, if a significant portion of the recovery curve shows radial-acting flow behavior (Section 4.2.2). The handling of the straight-line recovery method is similar to the drawdown approach. The transmissivity of the formation can be determined using equation 4.20 (Section 4.2.3.1).

4.3.3.2 Type curve application

The advantage of the Cinco-Ley *et al.* (1978) type curve approach lies in the fact that only data of the transient phase from linear flow to radial-acting flow is needed. In other words, the method is applicable even if the test did not reach the radial-acting flow phase.

The application of Cinco-Ley *et al.* (1978) type curve method for a pumped well is similar to that of the Theis type curve method. After matching a type curve to the data, the transmissivity T and storage coefficient S of the formation are calculated by substituting the values of the match point coordinates in equations 4.21 and 4.22 (Section 4.2.3.2). The evaluation of the storage coefficient requires the knowledge of the fracture half-length x_f, which can only be determined, if data from at least one observation well are available and the relative location to the fracture is known.

The transmissivity of the fracture T_f can be determined using the transmissivity of the formation and estimated values for the fracture's aperture and half-length in the equation for the relative conductivity Cr (equation 4.27). The storage coefficient of the fracture S_f can be uniquely determined using equation 4.18, if the relative storage capacity $CD_f > 10^{-4}$.

4.3.3.3 Determination of skin effects

Skin effects can appear at the well (well bore skin), between fracture and matrix (fracture skin), or at both (Cinco-Ley & Samaniego, 1981b). If drawdown data from wells situated in a vertical fracture with finite conductivity are obscured by skin effects, the curve shows an almost horizontal drawdown at the early time data followed by a transition phase and the radial-acting flow period. The total skin factor

ξ_t can be graphically determined using the pumped well data represented in a lin $t^{1/4}$ plot (Fig. 4.34) and equation 4.23 (Section 4.2.3.3).

4.3.3.4 Forward modelling application

If the transmissivity value is known either from the straight-line method or the type curve approach, this value should be used as known parameter in the forward modelling to accelerate the fitting process. The model implemented in TPA (Fig. 4.36) simplifies the method presented by Cinco-Ley *et al.* (1978) by neglecting the influence of the fracture's storage coefficient. It is considered that for the practical times, this parameter does not influence the drawdown behavior. Furthermore, at this stage TPA is not able to model the drawdown in observation wells, Thus, a unique evaluation of the unknown parameters is not viable yet.

In the worst case, the known parameters are:

- hydrogeological concept of a single vertical fracture with finite transmissivity
- transmissivity T of the matrix
- skin factor ξ_t

Following unknown parameters must be estimated

- storage coefficient S of the matrix
- transmissivity T_f of the fracture
- fracture aperture w
- fracture half-length x_f

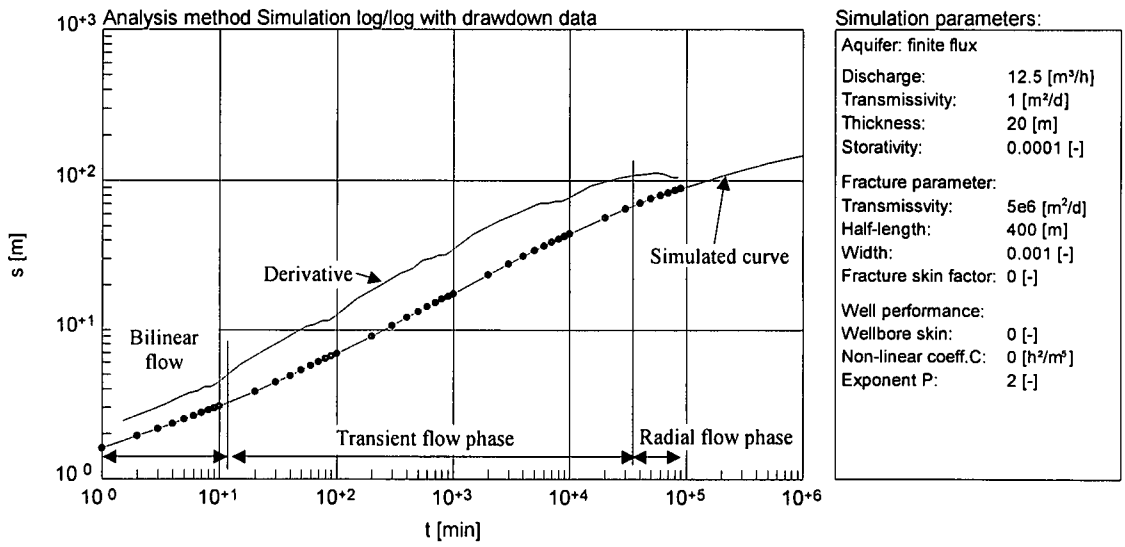

Figure 4.36. Example of the Cinco-Ley *et al.* (1978) forward modelling for a data set (dots) measured in a pumped well that does not reach a fully radial-acting flow phase

4.3.4 Field example (Cinco-Ley *et al.*, 1978)

Cinco-Ley *et al.* (1978) evaluated a pumping test performed in an oil well. The published parameters are:

Discharge rate [m^3/h]	Q	= 2.5
Oil density [kg/m^3]	ρ	= 0.9
Oil viscosity [cp]	μ	= 0.85
Acceleration of the gravity [m/s^2]	g	= 9.8
Formation transmissivity [m^2/d]	T	= 0.042
Formation storage coefficient [-]	S	= 0.0002
Fracture transmissivity [m^2/d]	T_f	= 260
Well bore skin factor [-]	ξ	= 0
Fracture skin factor [-]	ξ_f	= 0
Fracture aperture [m]	w	= 0.02
Fracture half-length [m]	x_f	= 48

The test was modelled using forward modelling and the above listed parameters. The evaluation is presented in Figure 4.37.

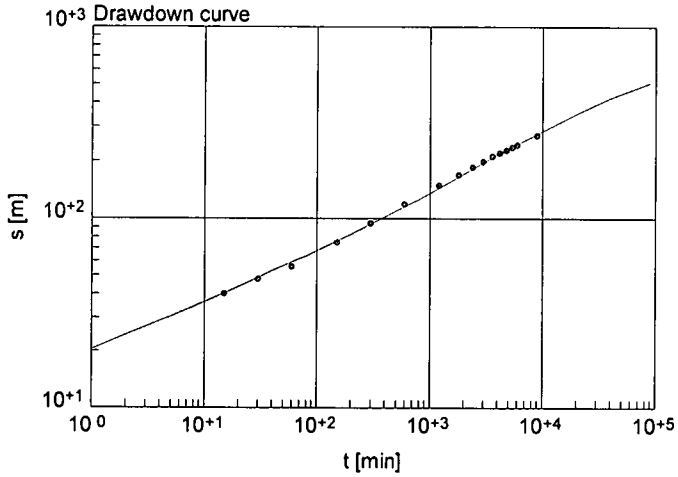

Figure 4.37. Example of the Cinco-Ley *et al.* (1978) pumping test evaluation for Cr = 0.82. The dots represent the data measured in the pumped well and the solid line the modelled curve

4.4 Single vertical dike with finite conductivity and infinite extent (Boonstra & Boehmer, 1986)

4.4.1 Theory

Boonstra & Boehmer (1986) introduced a semi-analytical model that describes the drawdown in a single vertical feature with finite conductivity, infinite length, and a considerable uniform width (Fig. 4.38). The feature is embedded in an infinite, isotropic, homogeneous, horizontal matrix limited by upper and lower impermeable boundaries (top and bottom of the aquifer, respectively). The model considers linear flow at early time and bilinear flow at intermediate time. Although originally presented to analyse drawdown in dikes, the method is also applicable to model the drawdown in vertical fractures with significant width.

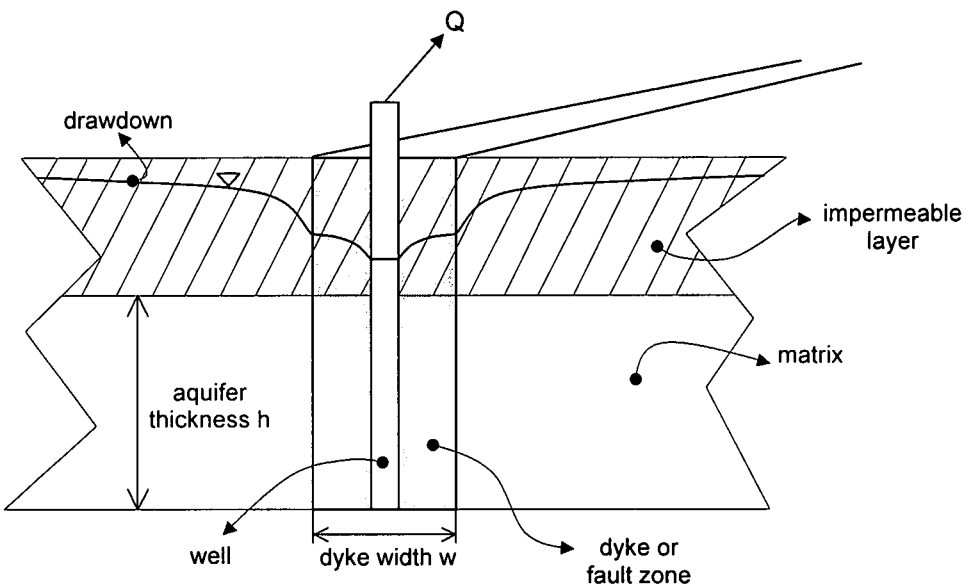

Figure 4.38. Drawdown behavior in a cross section of a system composed of a finite conductivity dyke or fault zone with considerable width and infinite length embedded in a matrix

The equation presented by Boonstra & Boehmer (1986) reads

$$s_{fd}(\chi, t_d) = \frac{2}{\sqrt{\pi}} e^{-2\sqrt{t_d}} \int_0^{\sqrt{t_d}} e^{\left[2\sqrt{t_d - r'^2} - \frac{\chi^2}{4r'^2}\right]} dr' \qquad (4.28)$$

where

s_{fd} = dimensionless drawdown in the feature [L]
χ = $2 \cdot \alpha \cdot (S/S_f)^{1/2} \cdot (T/T_f)^{1/2}) \cdot r_x/w$ [-]
α = empirical parameter (generally $\alpha = 0.94$) [-]
S = storage coefficient of the matrix of formation [-]
S_f = storage coefficient of the feature [-]
T = matrix or formation transmissivity [L^2T^{-1}]
T_f = feature transmissivity [L^2T^{-1}]
r_x = distance between the pumped well and observation point along the feature[L]
w = feature width [L]
t_d = dimensionless time, $4 \cdot \alpha^2 \cdot (S \cdot T) \cdot t / (w \cdot S_f)^2$ [-]
r' = integration variable

Equation 4.28 is valid up to a pumping time

$$t \approx 0.28 \frac{S \cdot (w \cdot T_f)^2}{4T^3} \qquad (4.29)$$

For longer pumping times the flow in the formation deviates from the parallel flow and develops gradually into the radial-acting flow.

Boonstra & Boehmer (1986) demonstrated that for small values of dimensionless time ($t_d < 0.003$) equation 4.28 at the pumped well reduces to the form

$$s(0,t_d) = \frac{2}{\sqrt{\pi}} \sqrt{t_d} \qquad (4.30)$$

and coincides with the Cinco-Ley & Samaniego (1982) solution for linear fracture flow.

For large values of the dimensionless time ($t_d > 100$) equation 4.28 at the well reduces to the form

$$s(0,t_d) = \sqrt[4]{t_d} \qquad (4.31)$$

Which, for $\alpha = 0.82$, is identical to the equation derived by Cinco-Ley *et al.* (1978) for the bilinear flow case in a fracture of finite length.

4.4.2 Diagnosis

The drawdown curve in a pumped well situated in a vertical feature with finite conductivity, infinite length, and considerable width presents following flow periods:

- linear fracture flow at early time, which shows a typical slope of 0.5 in a log-log plot (Fig. 4.39A) or a straight-line in a lin $t^{1/2}$ plot
- bilinear flow at intermediate time, which shows a typical slope of 0.25 in a log-log plot (Fig. 4.39A) or a straight-line in a lin $t^{1/4}$
- radial flow at late time, which plots as a straight-line in a semi-log plot (Fig. 4.39B)

The drawdown curves show transition periods between all the different flow phases.

In the Boonstra & Boehmer (1986) model the feature has finite conductivity, therefore the reaction in an observation well located in the same feature as the pumped well is not instantaneous like in the infinite conductivity fracture case from Gringarten *et al.* (1974). Thus, at early time the shape of the drawdown in the observation well is different to that of the pumped well like in the Cinco-Ley *et al.* (1978) model (Fig. 4.33).

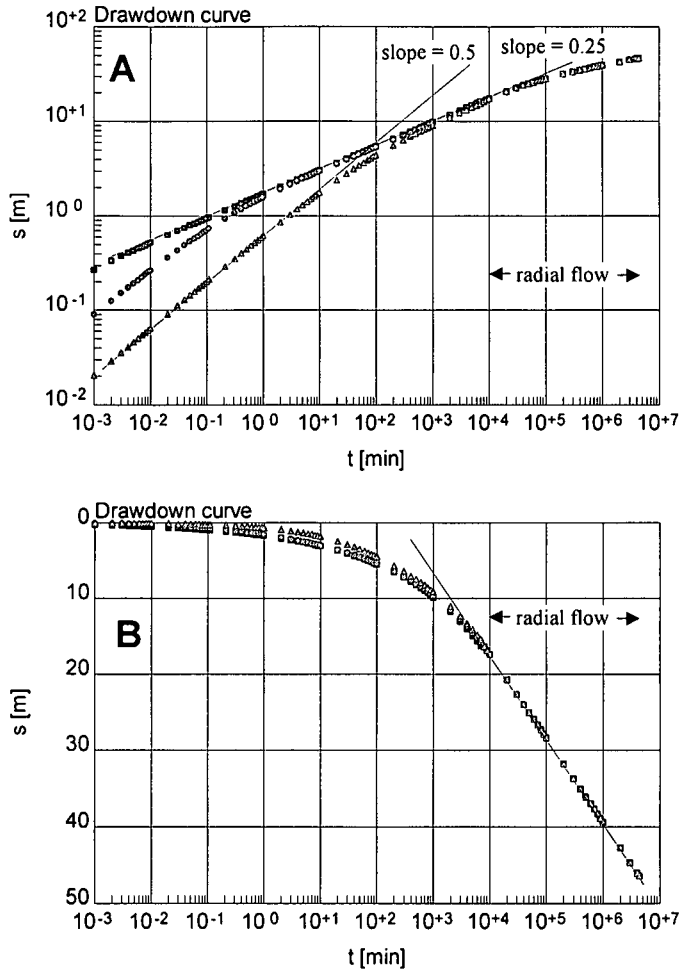

Figure 4.39. Flow periods in drawdown curves from pumped wells located in a vertical finite conductivity feature with infinite length and considerable width. The slope of 0.5 indicates linear fracture flow, the slope of 0.25 bilinear flow, both at early time

Whenever affected by skin, the drawdown in the pumped well develops in the same way as in the infinite conductivity fracture case. In a log-log plot it graphs initially as a horizontal straight-line and after a transition period, it shows the normal radial flow shape (Fig. 4.40 and Fig. 4.41). If the early time data show linear formation flow (slope of 0.5 in a log-log plot), they graph as a straight-line with a positive shift from the origin in a lin $t^{1/2}$ plot (Fig. 4.40). Similarly, the bilinear flow at early time data (slope of 0.25 in a log-log plot) graphs as a straight-line with a positive shift from the origin in a lin $t^{1/4}$ (Fig 4.41). However, the derivative of the drawdown curve can be used to determine the different flow phases because this curve is not affected by skin.

Due to the finite conductivity of the feature, it is not possible to graphically determine the location of the skin following the methodology described in Section 4.2.2 for the infinite conductivity fracture case.

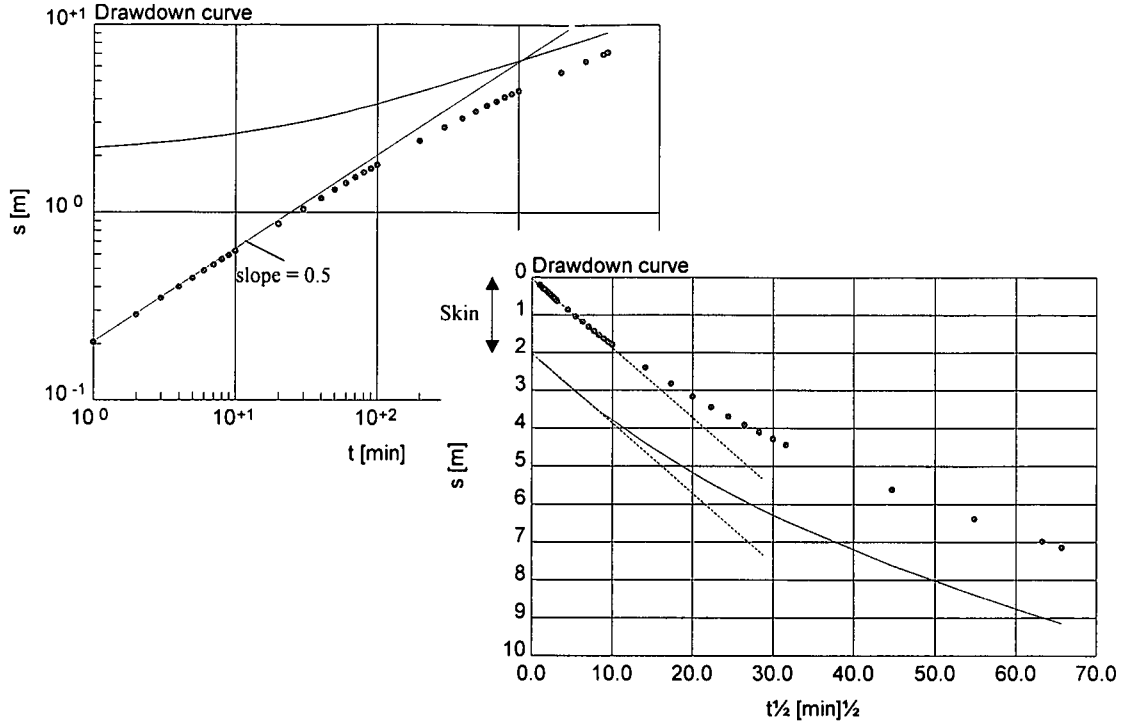

Figure 4.40. Drawdown in a pumped well with linear fracture flow at early time data. The solid line represents the case of skin at the well, while the dots graph the drawdown without skin. The well is located in a finite conductivity vertical feature with finite length and considerable width. The dotted lines in the second graph visualize the linear flow phases

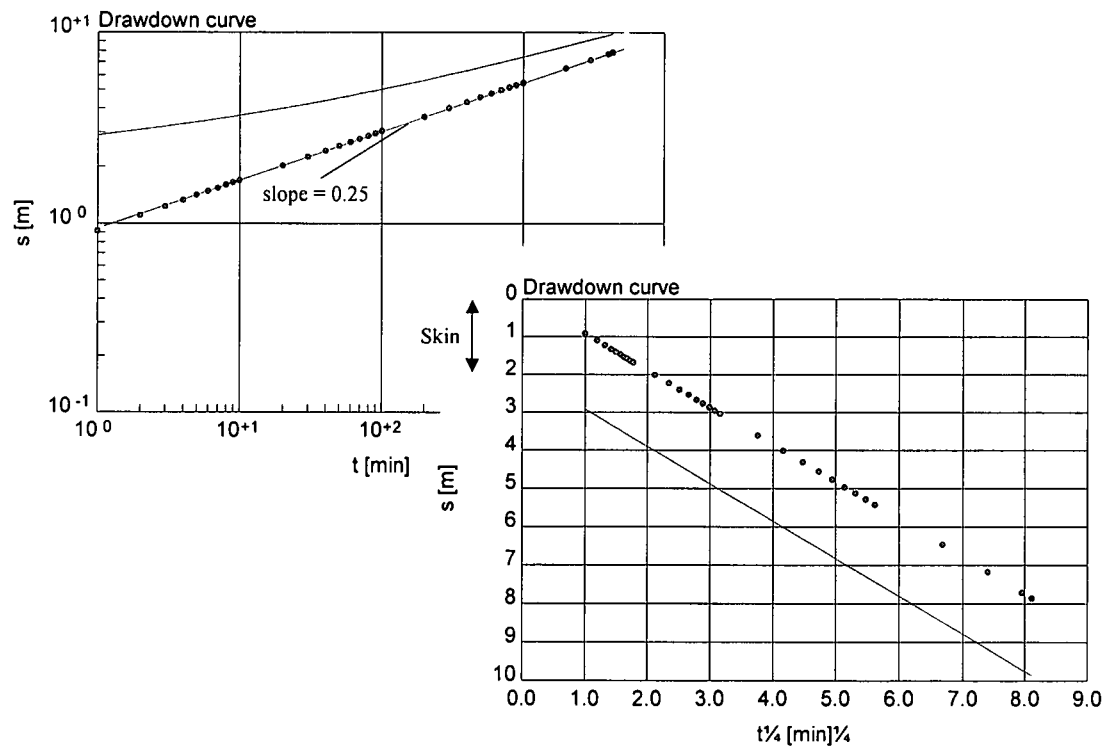

Figure 4.41. Drawdown from a pumped well affected by skin (solid line) and without skin (dots) with bilinear flow at early time data. The well is located in a finite conductivity feature with finite length and considerable width

4.4.3 Method of analysis

Following parameters can be determined using the Boonstra & Boehmer model (1986), if the feature width is known:

- reservoir transmissivity
- reservoir storage coefficient
- feature transmissivity
- feature storage coefficient

Basically two methods of analysis can be used to determine these parameters from the drawdown data: a straight-line method using a semi-log plot and a type curve method using a log-log plot. If recovery (build up) data are available, the recovery method of Theis (1935) or Agarwal (1980) can be utilized. Alternatively, a forward modelling using TPA can be applied to determine the aquifer parameters for both the drawdown and recovery phases in the pumped well.

The methods can be applied, if following conditions are true:

- matrix is infinite
- aquifer (feature and matrix) is confined
- Darcian flow prevails in feature and matrix
- well and feature penetrate the aquifer fully
- well bore storage is negligible
- well bore skin and feature skin are negligible
- straight-line method can be applied only to the radial-acting flow period. Cross-check that the first derivative becomes horizontal

4.4.3.1 Straight-line application

The straight-line application allows the determination of the reservoir transmissivity T using the radial-acting flow phase of drawdown or recovery data in a semi-log plot. Data from pumped well and/or observation well can be used. The approach is similar to the methods of Cooper-Jacob (1946) and Theis (1935). The transmissivity T of the formation can be computed using equation 4.19 (Section 4.2.3.1). In this case, the straight-line method cannot be applied for the estimation of the reservoir storage coefficient S.

The Theis (1935) and Agarwal (1980) recovery methods are applicable for the determination of the formation transmissivity T, if a significant portion of the recovery curve shows radial-acting flow behavior. The handling of the straight-line recovery method is similar to the drawdown approach. The transmissivity of the formation can be determined using equation 4.20 (Section 4.2.3.1).

4.4.3.2 Type curve application

The handling of Boonstra & Boehmer (1986) type curve method is similar to that of the Theis type curve method. After matching the observation well data to a type curve, following parameter products can be calculated by substituting the values for the match point coordinates in following equations:

$$w \cdot T_f = \frac{Q \cdot s_{fd}(\chi, t_d) \cdot r_x}{2 \cdot s(x,t) \cdot \chi} \qquad (4.32)$$

$$w \cdot S_f = \frac{Q \cdot s_{fd}(\chi, t_d) \cdot \chi \cdot t}{2 \cdot s(x,t) \cdot r_x \cdot t_d} \qquad (4.33)$$

$$S \cdot T = \frac{Q^2 \cdot s_{fd}{}^2(\chi, t_d) \cdot \chi^2 \cdot t}{14 \cdot s^2(x,t) \cdot r_x{}^2 \cdot t_d} \qquad (4.34)$$

where
Q = constant discharge rate [L^3T^{-1}]
χ = $2 \cdot \alpha \cdot (S/S_f)^{1/2} \cdot (T/T_f)^{1/2}) \cdot r_x/w$ [-]
t = time [T]
s(x,t) = drawdown [L]

If the radial-acting flow phase is present, the formation transmissivity T can be calculated using the straight-line method. By replacing T in equation 4.34, the formation storage coefficient S can be estimated. If the feature aperture w is known, it is possible to determine the feature's parameters T_f and S_f by replacing w in equations 4.32 and 4.33, respectively.

The type curve fitting using the pumped well data yields following product of parameters:

$$(w \cdot S_f) \cdot (w \cdot T_f) = \frac{\left[\frac{Q \cdot s_{fd}(0, t_d)}{s(0,t)}\right]^2}{\frac{4 \cdot t_d}{t}} \qquad (4.35)$$

$$(w \cdot T_f) \cdot \sqrt{(S \cdot T)} = \frac{\left[\frac{Q \cdot s_{fd}(0, t_d)}{s(0,t)}\right]^2 \cdot \sqrt{\frac{t}{t_d}}}{7.5} \qquad (4.36)$$

Equation 4.35 is valid for those cases where the data curve fits small dimensionless time values (up to t_d approximately 0.003), which indicates linear feature flow and is characterized by a slope of 0.5 in a log-log plot. Equation 4.36 must be used in those cases where the curve fits for t_d in the range of 100, thus, describes bilinear flow and is represented by a slope of 0.25 in a log-log plot.

4.4.3.3 Determination of skin effects

Skin effects can appear at the well (well bore skin), between fracture and matrix (fracture skin), or at both (Cinco-Ley & Samaniego, 1981b). If drawdown data from wells situated in a vertical feature with finite conductivity are obscured by skin effects, the curve shows an almost horizontal drawdown at the early time data followed by a transition and the radial-acting flow periods.

In those cases where the early time data show linear flow (slope of 0.5 in a log-log plot), the total skin factor ξ_t can be graphically determined using the pumped well data represented in a lin $t^{1/2}$ plot (Fig. 4.40) and equation 4.23 (Section 4.2.3.3). The same procedure can be followed for the determination of the skin factor when the early time data show a bilinear flow case (slope of 0.25 in a log-log plot), but the data must be graphed in a lin $t^{1/4}$ plot (Fig. 4.41). However, this method is not applicable, if the early time data do not show linear or bilinear flow.

4.4.3.4 Forward modelling application

If the formation transmissivity is known from the straight-line method, this value should be used as known parameter in the forward modelling to accelerate the fitting process. The Boonstra & Boehmer (1986) model is implemented in TPA for both pumped well and observation well located in the same feature.

In the worst case the known parameters are:

- hydrogeological concept of a single vertical feature with finite transmissivity, infinite extend and considerable width
- transmissivity T of the matrix
- skin factor ξ_t

Following unknown parameters must be estimated:

- storage coefficient S of the matrix
- transmissivity T_f of the feature
- storage coefficient S_f of the feature
- fracture width w

4.4.4 Field example

A published example of a pumping test in a dolerite dyke at Brandwag Tweeeling, Republic of South Africa (Boonstra & Boehmer, 1986 and Boehmer & Boonstra, 1987) is analysed.

The test was performed in a dyke intruded in the Beaufort Series of the Karoo Formation. The test set up consisted of a group of three wells. The pumped well is sited within a 10 m wide dyke, an observation well located 100 m apart from the pumped well within the same dyke, and another observation well situated 20 m from the pumped well perpendicular to the dyke. The test was re-evaluated with TPA using following published parameters:

Discharge rate [m^3/h]	Q	= 50
Formation transmissivity [m^2/d]	T	= 9.3
Formation storage coefficient [-]	S	= 0.000034
Dyke transmissivity [m^2/d]	T_f	= 2390
Dyke storage coefficient [-]	S_f	= 0.000043
Well bore skin factor [-]	ξ	= 0
Dyke skin factor [-]	ξ_f	= 0
Distance of the observation well 1 [m]	r_1	= 200
Distance of the observation well 2 [m]	r_2	= 20

Figure 4.42 shows a very good fitting between the forwards modelling and the published data.

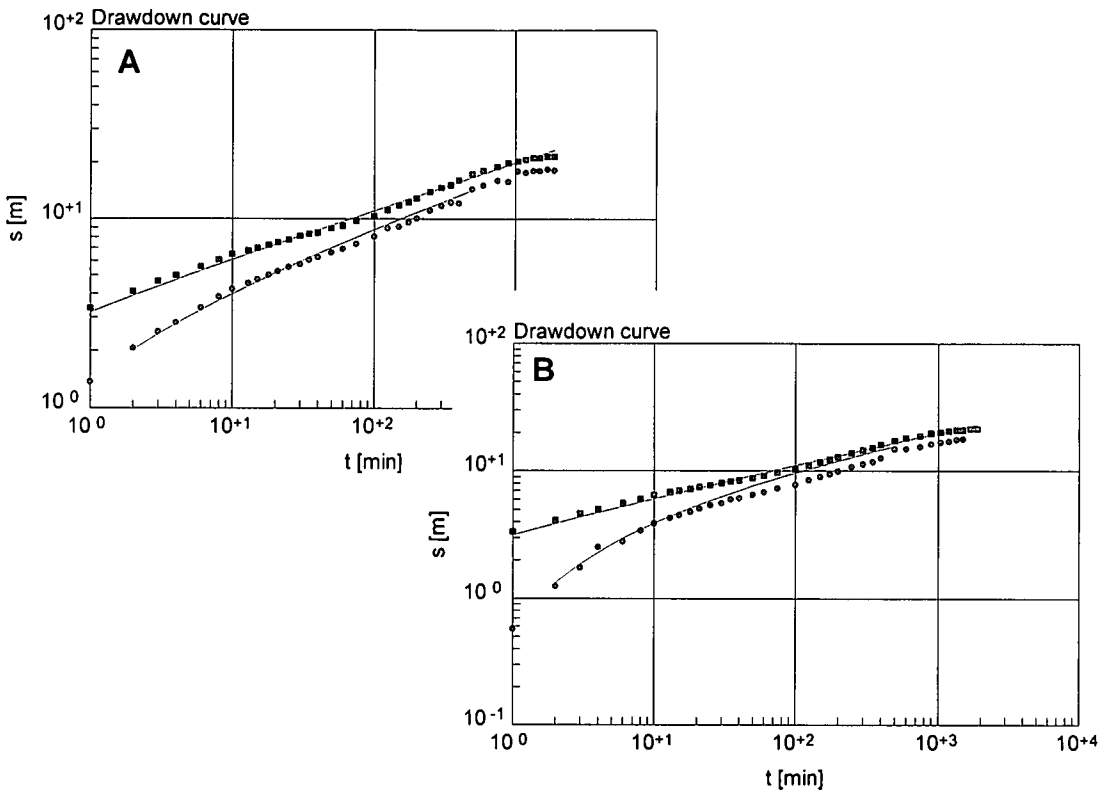

Figure 4.42. Pumping test in a dyke. The upper plot A shows the pumped well (squares) and the observation borehole (dots), both located in the same dyke. The second plot B shows the pumped well (squares) and the observation well (dots) located perpendicular to the dyke

4.5 Bedding plane fracture with infinite conductivity and finite extent (Gringarten & Ramey, 1974)

4.5.1 Theory

Gringarten & Ramey (1974) introduced an analytical model that describes the drawdown in a penny-shape bedding plane fracture of infinite conductivity, finite extension, and uniform flux. The fracture is embedded in an infinite, homogeneous, horizontal matrix that has anisotropic horizontal and vertical conductivities and is limited by upper and lower impermeable boundaries (top and bottom of the aquifer, respectively) (Fig. 4.43). The model considers linear flow followed by a transition period and the radial-acting flow phase.

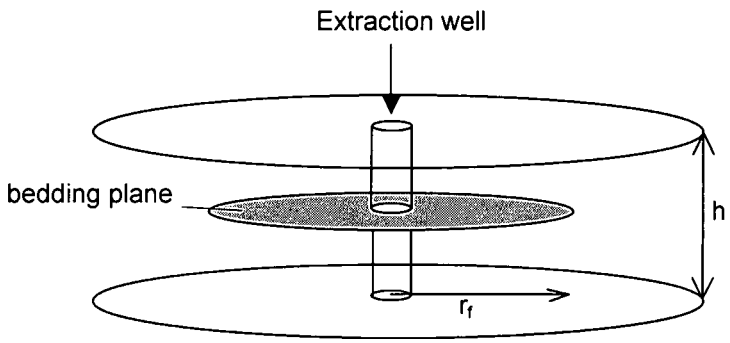

Figure 4.43. Simplification of a penny-shape bedding plane. h = thickness of the aquifer, r_f = radius of the fracture

The equation presented by Gringarten & Ramey (1974) assumes that the flux is constant and uniform along the fracture. It is obtained by means of Green functions and reads:

$$s_{fd}(r_d, z_d, t_d) = \int_0^{t_d} \frac{e^{\left(-\frac{r_d^2}{4t_d'}\right)}}{t_d'} \left[\int_0^1 I_0\left(\frac{r_d r_d'}{2t_d'}\right) \cdot e^{\left(-\frac{4r_d'^2}{4t_d'}\right)} \cdot r_d' \cdot dr_d' \right] \psi \cdot dt_d' \qquad (4.37)$$

with

$$\psi = \left[1 + \frac{4 \cdot h}{\pi \cdot w} \sum_{n=1}^{\infty} \frac{e^{\left(-\frac{n^2 \pi^2 t_d'}{h_d^2}\right)}}{n} \cdot \sin m\pi \frac{w}{2h} \cdot \cos m\pi \frac{z_f}{h} \cdot \cos m\pi \frac{z}{h} \right]$$

where

$$h_d = \frac{h}{r_f} \sqrt{\frac{K_h}{K_v}} \quad [-]$$

$$r_d = \frac{r}{r_f} \quad [-]$$

$$t_d = \frac{K_h \cdot t}{S \cdot r_f^2} \quad [-]$$

$$z_d = \frac{z}{r_f}\sqrt{\frac{K_h}{K_v}} \quad [-]$$

s_{fd} = dimensionless drawdown in the fracture [L]
r = distance of the observation well to the pumped well [L]
r_f = radius of the horizontal penny-shape fracture [L]
z = vertical distance to the reservoir lower boundary [L]
z_f = vertical distance from the fracture to the lower boundary of the reservoir [L]
K_h = horizontal hydraulic conductivity of the formation [LT^{-1}]
K_v = vertical hydraulic conductivity of the formation [LT^{-1}]
t = time [T]
S = storage coefficient of the matrix or formation [-]
I_0 = modified Bessel function of the first kind and zero order
h = formation thickness [L]
w = fracture aperture [L]
r_d', t_d' = dimensionless variables of integration
m = integer value [-]

The meaning of the dimensionless aquifer thickness h_d based on the aquifer geometry is schematically visualized in Figure 4.44, assuming an isotropic aquifer matrix ($K_h = K_v$).

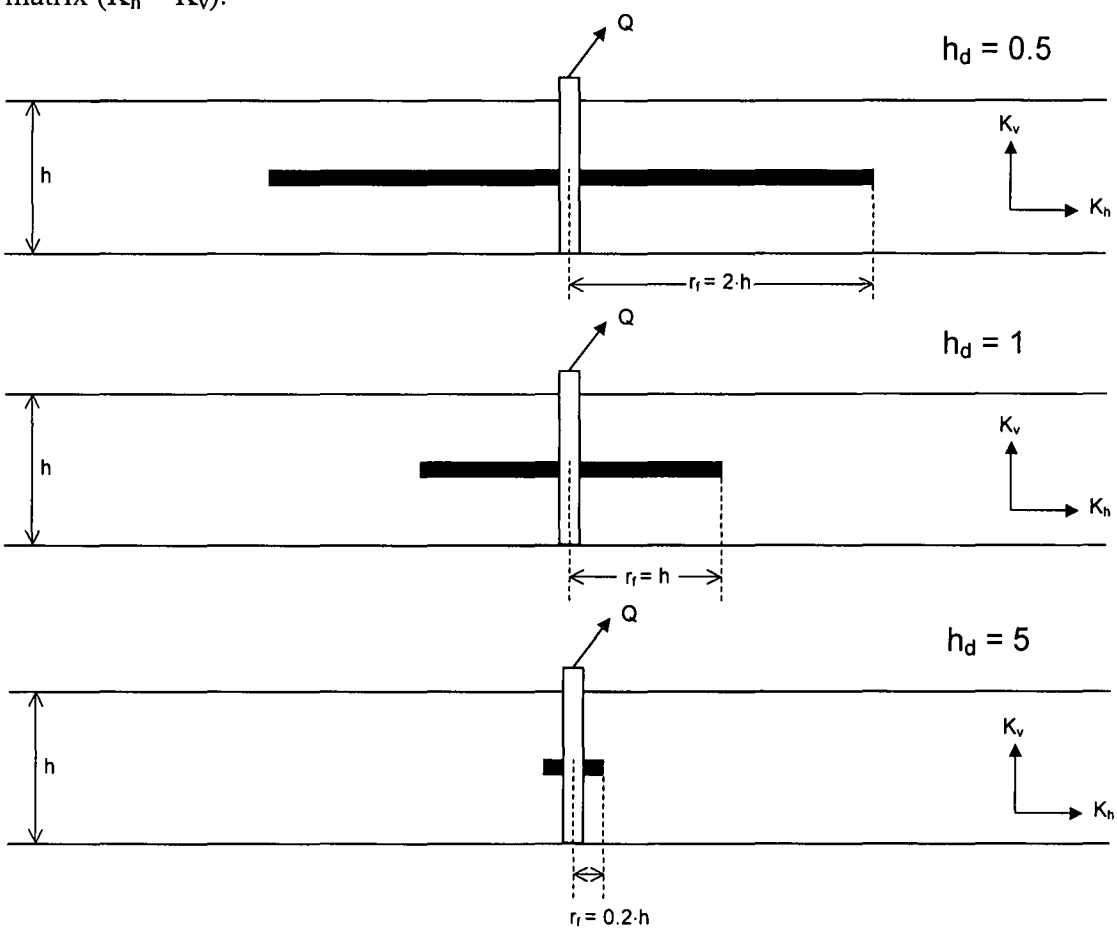

Figure 4.44. Schematic representation of the dimensionless aquifer thickness h_d based on the relationship between the aquifer thickness and fracture radius. The matrix is assumed as isotropic ($K_h = K_v$)

The model is able to describe the following four different flow phases (Gringarten & Ramey, 1974):

- fracture storage flow, which duration depends on the fracture thickness
- linear formation flow, which duration depends on the fracture radius and distance to the upper and lower formation boundaries
- transient flow, which occurrence depends on the dimensionless parameter h_d
  radial-acting flow, which starts at $t_d = 10$

4.5.2 Diagnosis

The drawdown curve in a pumped well situated in a horizontal penny-shape fracture with infinite conductivity, finite extension, and uniform flux can have following flow periods:

- linear formation flow at early time characterized by a slope of 0.5 in a log-log plot (Fig. 4.45) or a straight-line in a lin $t^{1/2}$
- a slope of 1 in a log-log plot (Fig. 4.45) appears for values of $h_d < 1$ when the cone of depression reaches parallel boundaries (the top and bottom of the aquifer). In this case, the linear formation flow (slope of 0.5) is superposed by the closed parallel boundary effect (slope of 0.5) to result in a slope of 1
- radial-acting flow at late time (Fig. 4.45), which plots as a straight-line in a semi-log plot

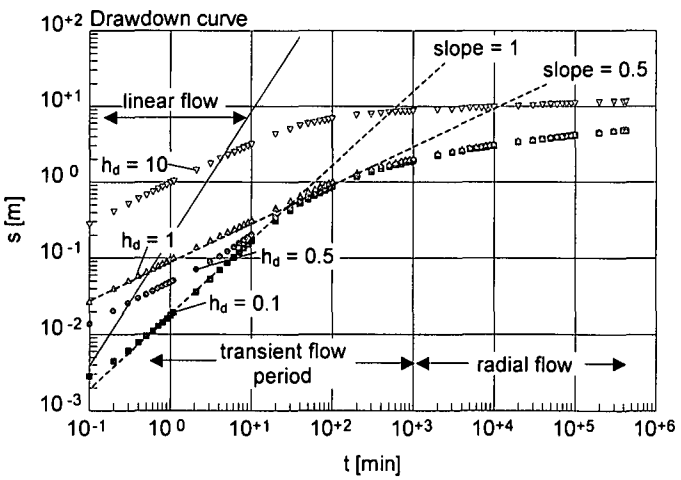

Figure 4.45. Flow periods in pumped wells located in a penny-shape horizontal fracture

The fracture has infinite conductivity, therefore the reaction in an observation well located in the same fracture as the pumped well is instantaneous, as described in the infinite conductivity vertical fracture case (Gringarten *et al.*, 1974). The shape of the drawdown in the observation well at early time is similar to that of the pumped well (Fig. 4.46).

The skin effect can be determined using the method described for the infinite conductivity vertical fracture (Gringarten *et al.*, 1974) as shown in Figure 4.46. The location can be graphically determined following the method presented by Bardenhagen (1999), as described in Section 4.2.2 for the infinite conductivity fracture case. However, this method cannot be applied if the drawdown shows only fracture storage flow.

For small values of h_d (Fig. 4.45), the early time drawdown in horizontal fractures can be misinterpreted as well bore storage because it also shows a slope of 1 in a log-log plot. The real situation can be identified by trying to accommodate the

Papadopulos curve (Theis curve that includes well bore storage) to the test data. Unrealistic large values of S will be obtained, if the field data belong to a horizontal fracture. This methodology can be used to identify horizontal features, even if their presence has not been reported.

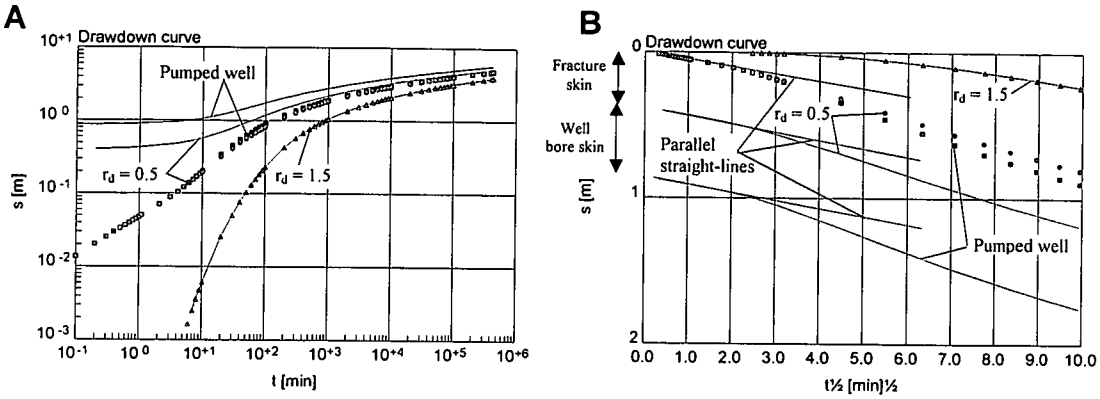

Figure 4.46. Drawdown for h_d = 0.5 in a pumped well (squares) and two observation wells, one at r_d = 0.5 (dots) and the other at r_d = 1.5 (triangles) from the pumped well. The solid lines represent the drawdown in the same wells when affected by well bore and fracture skins. Figure A presents the whole test and figure B shows only the early time data

In the absence of skin effects (well bore skin and fracture skin), a horizontal fracture can be identified by applying the skin factor evaluation for primary aquifers (Section 2.4.2). Negative values of skin are not possible in primary aquifer, but rather indicate the presence of fractures.

4.5.3 Method of analysis

Basically two methods of analysis can be applied in the estimation of the formation or matrix transmissivity T from the drawdown data: a straight-line method using a semi-log plot and a type curve method using a log-log plot. If recovery (build up) data are available, the recovery method of Theis (1935) or Agarwal (1980) can be used as well. Alternatively, a forward modelling with TPA can be applied to estimate the aquifer parameters T and S for both the drawdown and recovery phases. Note that the calculation of the actual fracture transmissivity T_f is not possible because it is a priori considered infinite.

The methods can be applied if following conditions are true:

- matrix is infinite
- aquifer (fracture and matrix) is confined
- Darcian flow prevails in fracture and matrix
- well penetrates the aquifer fully
- well bore storage is negligible
- well bore skin and fracture skin are negligible
- straight-line can be applied if td $\geq$ 10 (linear-acting flow). Cross-check that the first derivative becomes horizontal

4.5.3.1 Straight-line application

The straight-line method allows the determination of the reservoir transmissivity T using the radial-acting flow phase of drawdown data in a semi-log plot. Data from pumped well and/or observation well can be utilized. The approach is similar to the

methods of Cooper-Jacob (1946) and Theis (1935). The transmissivity T of the formation can be determined using equation 4.19 (Section 4.2.3.1). The straight-line method can be applied for the estimation of the reservoir storage coefficient S, if the observation well is located outside of the fracture.

The Theis (1935) and Agarwal (1980) recovery methods are applicable for the determination of the formation transmissivity T, if a significant portion of the recovery curve shows radial-acting flow behavior. The handling of the straight-line recovery method is similar to the drawdown approach. The transmissivity of the formation can be determined using equation 4.20 (Section 4.2.3.1).

4.5.3.2 Type curve application

The handling of the Gringarten & Ramey (1974) type curve method is similar to that of the Theis type curve method. After matching the pumped well data to the type curve, the reservoir transmissivity T can be calculated by substituting the values for the match point coordinates in equation 4.21 (Section 4.2.3.2). The type curve matching also provides the value of h_d, which allows the estimation of the vertical hydraulic conductivity K_v using following equation:

$$K_v = \frac{T \cdot h}{(h_d \cdot r_f)^2} \qquad (4.38)$$

For the given h_d, a different set of curves dependent on r_d can be calculated and graphed on a semi-log plot. A new match of the drawdown data with these curves will provide a value of r_d that permits the calculation of r_f ($r_f = r/r_d$), which is required for the evaluation of the storage coefficient using equation 4.22 (Section 4.2.3.2).

4.5.3.3 Determination of skin effects

Skin effects can appear at the well (well bore skin), between fracture and matrix (fracture skin), or at both (Cinco-Ley & Samaniego, 1981b). If drawdown data from wells situated in a horizontal fracture with infinite conductivity are obscured by skin effects, the curve shows an almost horizontal drawdown at the early time data followed by a transition phase and the radial-acting flow period.

In those cases where the early time data show linear formation flow (slope of 0.5 in a log-log plot), the skin locations and the skin factors can be determined as described in Section 4.2.3.3 for the infinite conductivity vertical fracture case.

4.5.3.4 Forward modelling application

If the formation transmissivity value is known from the straight-line approach, this value should be used as known parameter in the forward modelling to accelerate the fitting process. The Gringarten & Ramey (1974) model is implemented in TPA for both pumped well and observation well.

In the worst case the known parameters are:

- hydrogeological concept of a single horizontal fracture with infinite conductivity
- transmissivity T of the matrix
- skin factor ξ_t

Following unknown parameters must be estimated:

- storage coefficient S of the matrix
- radius of the penny-shape horizontal fracture

- thickness of the fracture
- location of the fracture relative to the upper and lower reservoir boundaries
- vertical reservoir conductivity

4.5.4 Field example

A constant discharge test was performed during 390 minutes in a well located in the test field of the Orange Free State University, Bloemfontein, South Africa. The well intercepts a bedding plane, which is embedded in the Karoo Formation. Due to the shortness of the test, the radial-acting flow was not reached. Therefore the estimated aquifer parameters are relatively uncertain. The test set up consisted of a pumped well and three observation wells. The test evaluation is presented in Figure 4.47. The obtained aquifer characteristics are:

Discharge rate [m^3/h]	Q	= 4.5
Formation transmissivity [m^2/d]	T	= 12
Formation storage coefficient [-]	S	= 0.00002
Formation thickness [m]	h	= 20
Vertical conductivity [m/d]	K_v	= 0.00085
Fracture radius [m]	r_f	= 280
Fracture aperture [m]	w	= 0.2
Fracture elevation [m]	z_f	= 10
Distance of the observation well 1 [m]	r_1	= 5
Distance of the observation well 2 [m]	r_2	= 22
Distance of the observation well 3 [m]	r_3	= 32

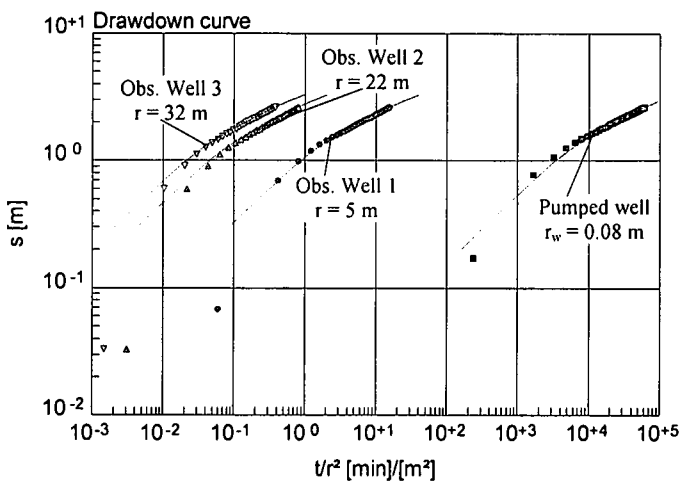

Figure 4.47. Evaluation of a pumping test performed in a well located in the test field of the Orange Free State University, Bloemfontein, South Africa. The data are represented by the symbols and the modelled curves using the Gringarten & Ramey (1974) solution are graphed by solid lines

4.6 Generalised radial flow model for fractured reservoirs (Barker, 1988)

4.6.1 Theory

Barker (1988) introduced an analytical model that describes the drawdown in a fractured aquifer for various flow dimensions including linear, radial, and spherical flows. These flow dimensions are seen as dependent on the fracture connectivity rather than as aquifer dimensions and are described by a factor n. Flow dimensions correspond to aquifer dimensions for integer values of n: for n = 1 the flow is strictly linear, for n = 2 the flow is radial (Theis model), and for n = 3 the flow is spherical. The non-integer values of n describe the excess or lack of fracture connections compared to fracture networks with perfect connections in 1, 2, and 3 dimensions (Leveinen *et al.*, 1998).

The solution is valid for a homogeneous and isotropic fractured medium and considers 1, 2, and 3 dimensional sources with a finite storage capacity. The source dimensions are defined by b^{3-n}, where n = 1 implies a very small cubic source, n = 2 a cylinder source, and n = 3 a sphere source. The model also incorporates the possibility of infinitesimal skin located at the source.

Due to the fact that the model considers the fractured aquifer as an isotropic homogeneous medium, the flow dimension is strictly defined by the dimension of the source. In other words, a one-dimensional flow can be obtained when the aquifer is an infinite strip of a certain aperture and thickness and the source is a surface that intersects the entire strip. The two-dimensional flow is obtained when the aquifer is infinite with a certain thickness and the source is a cylinder of given height that fully penetrates the aquifer. The three-dimensional flow will be obtained whenever the aquifer is infinite in all three directions and the source is a sphere. This effect restricts the use of the method to very few well-defined aquifers and tests, as practically no one-dimensional or three-dimensional flows can extend for an infinite period of time. Naturally, the flow tends to a radial-acting flow (two-dimensional flow) after a certain period of time because most aquifers have a finite thickness compared to the horizontal extent.

Barker introduced two general equations to describe the head in the source and head in the formation both related to the extraction rate (equations 4.39 and 4.40, respectively). The equations obtained by means of the Laplace transformation read

$$\frac{\bar{H}_h(p)}{\bar{Q}(p)} = \frac{\left[1+\xi\cdot\Phi_v(\mu)\right]}{p\cdot S_w + K_f\cdot b^{3-n}\cdot\alpha_n\cdot r_w^{n-2}\cdot\Phi_v(\mu)} \qquad (4.39)$$

$$\frac{\bar{h}_h(r,p)}{\bar{Q}(p)} = \frac{r_d^{\nu}\cdot K_{\nu}(\mu\cdot r_d)}{K_{\nu}(\mu)\cdot\left[r_d\cdot S_w\cdot\left(1+\xi\cdot\Phi_{\nu}(\mu)\right)+K_f\cdot b^{3-n}\cdot\alpha_n\cdot r_w^{n-2}\cdot\Phi_{\nu}(\mu)\right]} \qquad (4.40)$$

where

$\bar{H}_h(p)$ = drawdown at the source in the Laplace space [L]
$\bar{h}_h(p)$ = drawdown in the reservoir in the Laplace space [L]
$\bar{Q}(p)$ = extraction rate in the Laplace space [L^3T^{-1}]
p = Laplace transform variable
n = dimension of the fracture flow system [-]
b = extent of the flow region [L]
r_w = drilled radius or radius of the source [L]
K_f = hydraulic conductivity of the fracture system [LT^{-1}]
S_w = storage capacity of the source [-]

S_{sf} = specific storage of the fracture system [L^{-1}]
ξ = skin factor in the well [-]

$$\alpha_n = \frac{2\pi^{n/2}}{\Gamma(n/2)}$$

r_d = dimensionless distance to the well, r/r_w [-]
μ = λr_w
λ = $(p \cdot S_{sf} / K_f)^{1/2}$
ν = 1-n/2

$$\Phi_\nu(\mu) = \frac{\mu K_{\nu-1}(\mu)}{K_\nu(\mu)}$$

$K_\nu(\mu)$ = modified Bessel function of fractal order
$\Gamma(x)$ = Gamma function

4.6.2 Diagnosis

Based on the Barker (1988) model, following flow characteristics can be observed (Fig. 4.48):

- for n > 2 steady state situation at late time, which shows a typical slope of 0 (horizontal line) in a log-log plot
- the Theis curve corresponds to n = 2, which is characterized by a straight line in a semi-log plot
- for n < 2 straight-lines at late time with slopes of $\nu = 1 - n/2$ in a log-log plot

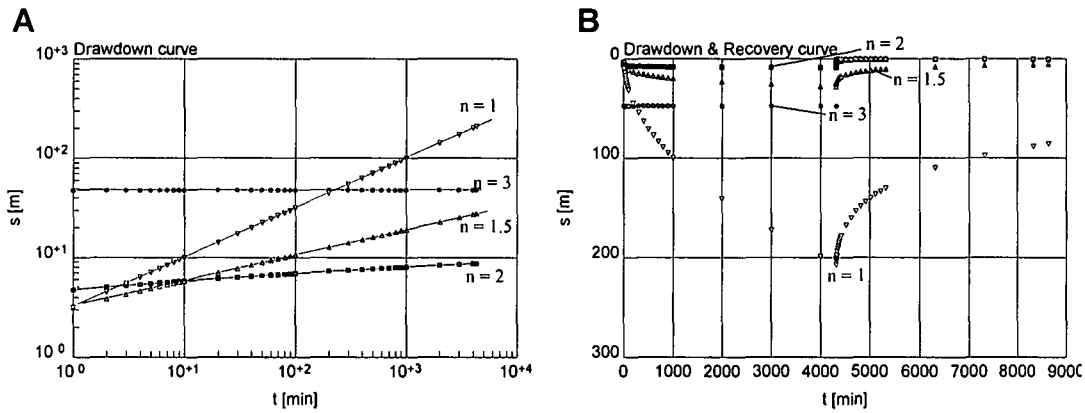

Figure 4.48. Drawdown in a pumped well obtained using the same aquifer parameters for different flow dimensions n in a log-log plot (A). The graph B shows the drawdown and recovery for the same parameters in a linear s vs. t plot

The disadvantages of the method can be summarized as (Fig. 4.49):

- the main difference between the Barker model and the models described before lies in the fact that the Barker model does not provide for radial-acting flow at late time for any $n \neq 2$. This makes difficult the use of the type curve fitting for the evaluation of pumping tests
- additionally, in the case of n = 1 the method provides a drawdown curve that shows a straight-line with slope 0.5 (linear flow), which makes impossible to obtain a unique curve fit

Figure 4.49 shows the type curves drawn for different flow dimensions n. The function F(n, u) is evaluated as

$$F(n,u) = \frac{1}{\nu}\left[\left(\frac{1}{u}\right)^{\nu} - \frac{\Gamma(1-\nu)}{\nu}\right] \qquad (4.41)$$

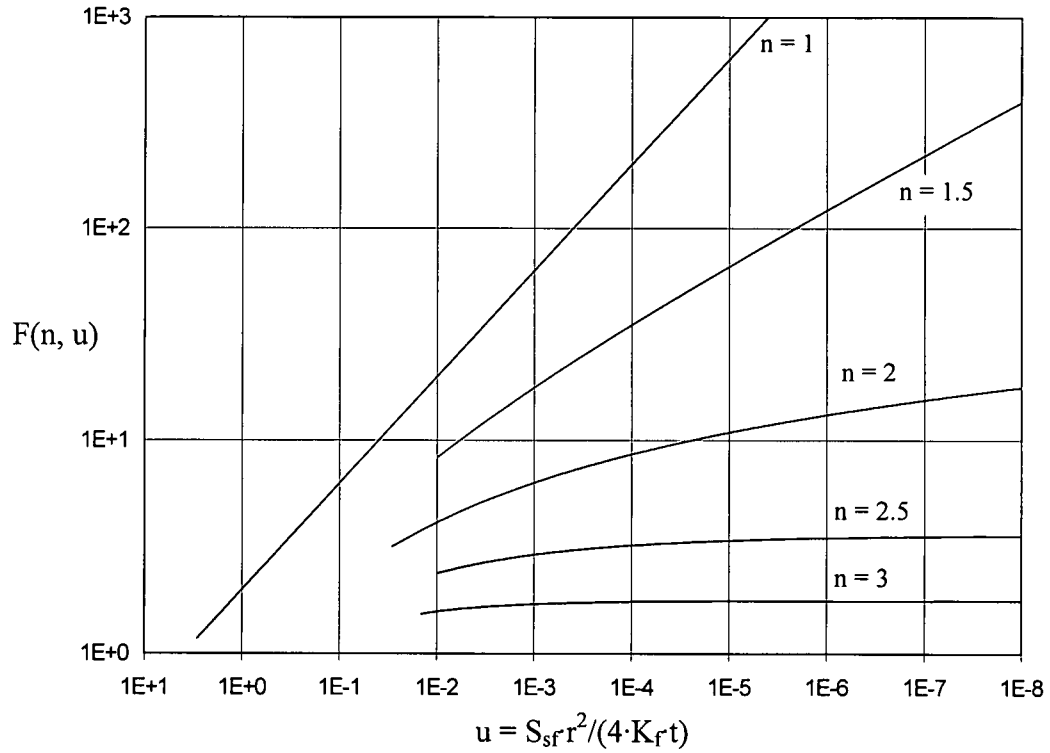

Figure 4.49. Type curves in a pumped well for different flow dimensions (n) based on equation 4.41

4.6.3 Method of analysis

Basically, only the type curve method using a log-log plot or the forward modelling using TPA can be used to determine the formation or matrix transmissivity T from the drawdown data. Common straight-line methods in the semi-log plot can only be applied for the cases where n = 2.

The Barker (1988) method is applicable, if following conditions are true:

- matrix is infinite
- aquifer (fracture and matrix) is confined
- Darcian flow prevails in fracture and matrix
- well bore storage is negligible
- fracture skin is negligible
- straight-line can be applied for n = 2 if u < 0.01 (radial-acting flow). Cross-check that the first derivative becomes horizontal

4.6.3.1 Straight-line application

The straight-line method of Cooper-Jacob (1946) allows the determination of the reservoir transmissivity T using the radial-acting flow phase (n = 2) of drawdown data

in a semi-log plot. Data of pumped well (if the skin effect is negligible) and/or observation well can be utilized. The transmissivity T of the formation can be determined using equation 4.19 (Section 4.2.3.1).

The Theis (1935) and Agarwal (1980) recovery methods are applicable for the determination of the formation transmissivity T, if a significant portion of the recovery curve shows radial-acting flow behavior (n = 2). The handling of the straight-line recovery method is similar to the drawdown approach. The transmissivity of the formation can be determined using equation 4.20 (Section 4.2.3.1).

4.6.3.2 Type curve application

The handling of the Barker type curve method is similar to that of the Theis method. Pumped well data can be used only if the well bore storage and the well bore skin are negligible, but data from observation boreholes can always be analysed using this method.

After matching the data curve of the pumping well with one of the type curves, the product $K_f \cdot b^{3-n}$ (that equals the transmissivity of the fracture system for n = 2) and the diffusivity of the fracture system S_{sf} / K_f can be calculated by substituting the values for the match point coordinates in equations 4.42 and 4.43, respectively.

$$K_f \cdot b^{3-n} = \frac{Q}{4 \cdot \pi^{1-\nu} \cdot s(r,t) \cdot \nu} \left[\left(\frac{4 \cdot K_f \cdot t}{S_{sf}} \right)^{\nu} - \Gamma(1-\nu) \cdot r^{2\nu} \right] \qquad (4.42)$$

$$\frac{S_{sf}}{K_f} = \frac{4 \cdot u \cdot t}{r^2} \qquad (4.43)$$

Barker (1988) suggests that any two of these three parameters (K_f, S_{sf}, or b) can be determined, if the third is either estimated or known.

4.6.3.3 Forward modelling application

If the formation transmissivity value is known from the straight-line approach, this value should be used as known parameter in the forward modelling to accelerate the fitting process. The Barker (1988) model is implemented in TPA for both pumped well and observation well.

In the worst case the known parameters are:

- hydrogeological concept of the aquifer system
- transmissivity T of the matrix
- skin factor ξ_t

Following unknown parameter must be estimated:

- storage coefficient S of the matrix

5. DISCONTINUOUS FRACTURE NETWORK INVESTIGATION WITH NUMERICAL MODELLING

5.1 Introduction

This part of the thesis shows that published analytical and semi analytical solutions can be reproduced using common numerical models in combination with an appropriate model set up. This is first demonstrated using the single vertical fracture case (Gringarten *et al.*, 1974, Cinco-Ley *et al.*, 1978).

Generally, it is assumed that fractures have negligible aperture and storage capacity (Gringarten *et al.*, 1974; Cinco-Ley *et al.*, 1978), but these models are also applicable in the case of wider fault zones, as shown in Section 4.2.4. However, Ramey & Gringarten (1976) developed a series of type curves that take into account the storage of infinite conductivity vertical fractures (Section 4.2.2). Aimed to analyse the influence of wide fault zones with finite extent, which can be considered as homogeneous fractured, the numerical model is applied. Faults with variable apertures in relation to their relative storage capacity (CD_f) are investigated. To analyse the influence of both the fracture shape and the combination of fractures on the drawdown, a vertical crossed fracture case and a bend fracture case are computed.

The drawdown in a single bedding plane (horizontal feature or pancake fracture) is computed to confirm the aptitude of the model to reproduce the semi analytical solution from Valkó & Economides (1997). Further, the effect of the fracture length/aperture relationship as well as the influence of parallel bedding planes on the drawdown are analysed.

Finally, a selection of possible intersections between a vertical fault zone and a bedding plane are studied. To accommodate these scenarios, vertical and horizontal fractures with infinite and/or finite conductivity are simulated. The possible infinite number of conductivity combinations are generally limited to two, an infinite case ($Cr = 1000$) and a finite case ($Cr = 1$). However, in some cases it was necessary to diverge from these standards to be able to highlight special flow situations.

5.2 Model description

The numerical model MODFLOW (Harabaugh *et al.*, 1999) and the pre and post processors Processing MODFLOW PMWin (Chiang & Kinzelbach, 1999) and Visual MODFLOW (Waterloo, 2000) are used for the simulations.

MODFLOW is based on the finite difference method, which has been explained in extension by various authors (Kinzelbach, 1991; Kinzelbach & Rausch, 1995). Therefore, it will not be further described in this work.

The model is built as a cube of 40,000 m by 40,000 m by 20 m with variable grid spacing. A fully penetrating extraction well is located in the centre of the model (Fig. 5.1), which intersects the preferential flow path features. All vertical features are considered as fully penetrating with a maximum total extent of 400 m. The horizontal features are assumed as rectangular with a maximum side length of 400 m. These features are studied as either finite or infinite conductivity and all of them are modelled with an aperture of 0.01 m.

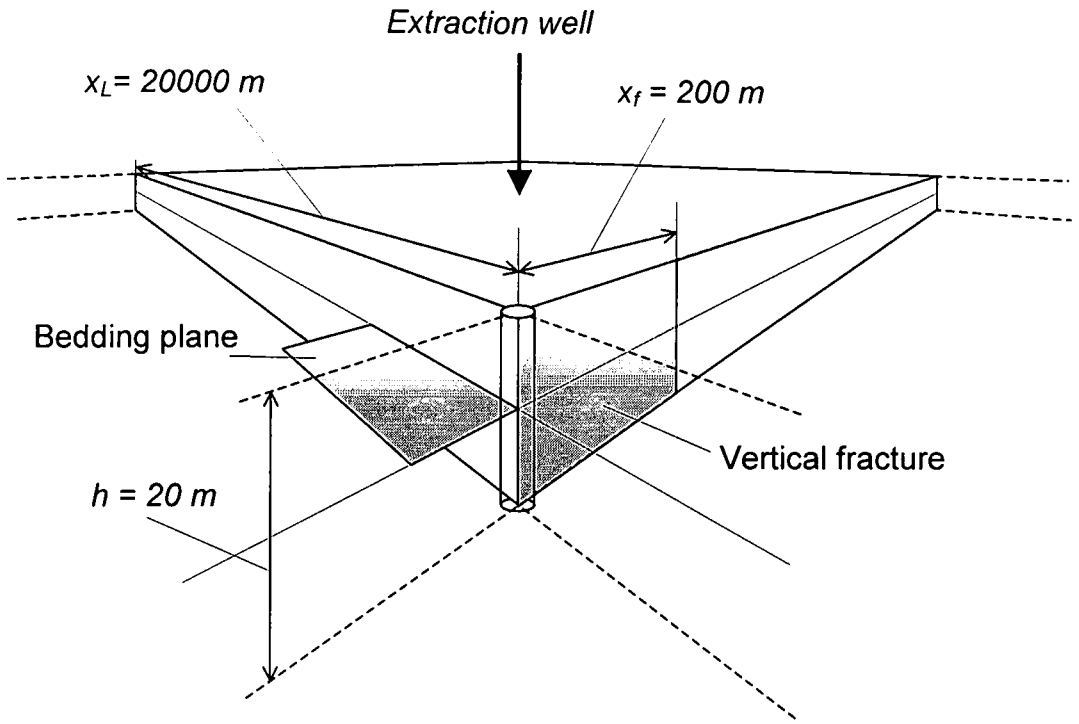

Figure 5.1. Model design and dimension. x_f = fracture half-length, x_L = model half-length, h = model height

5.2.1 Grid design

The grid separation is based on the common rules for refining areas that are characterized by high flow gradients (Fig. 5.2). The fault, or fracture, or bedding plane is designed as a 1 cm wide element, due to the limits of the used preprocessors, with a maximum total length of 400 m, so that the smallest element in the conjunction of a vertical and a horizontal fracture has a volume of just 1 cm^3. An extraction well with a pumping rate of 0.00555 m^3/s (20 m^3/h) is situated in the centre of the fracture or fracture system. The chosen horizontal extent of the model (40,000 m by 40,000 m) allows pumping periods that, with the assumed aquifer parameters, always produce radial acting flow before the cone of depression reaches the model closed boundaries. The aquifer thickness is set at 20 m. Whenever applicable, a quarter of this model with the extraction well in one corner is considered in the calculations to reduce the number of elements and thus, reduce the simulation time.

5.2.2 Model parameters

The matrix is modelled using the following parameters:

- horizontal hydraulic conductivity K_h = 0.00001 m/s or 0.864 m/d
- vertical hydraulic conductivity K_v = 0.0000001 m/s or 0.00864 m/d
- specific storage coefficient S_s = 0.00001 [L^{-1}]

The storage coefficient for preferential flow path features is selected at S_{sf} = 0.00001 and the hydraulic conductivity in the range of 0.001 m/s to 1000 m/s depending weather a finite or infinite conductivity case is considered.

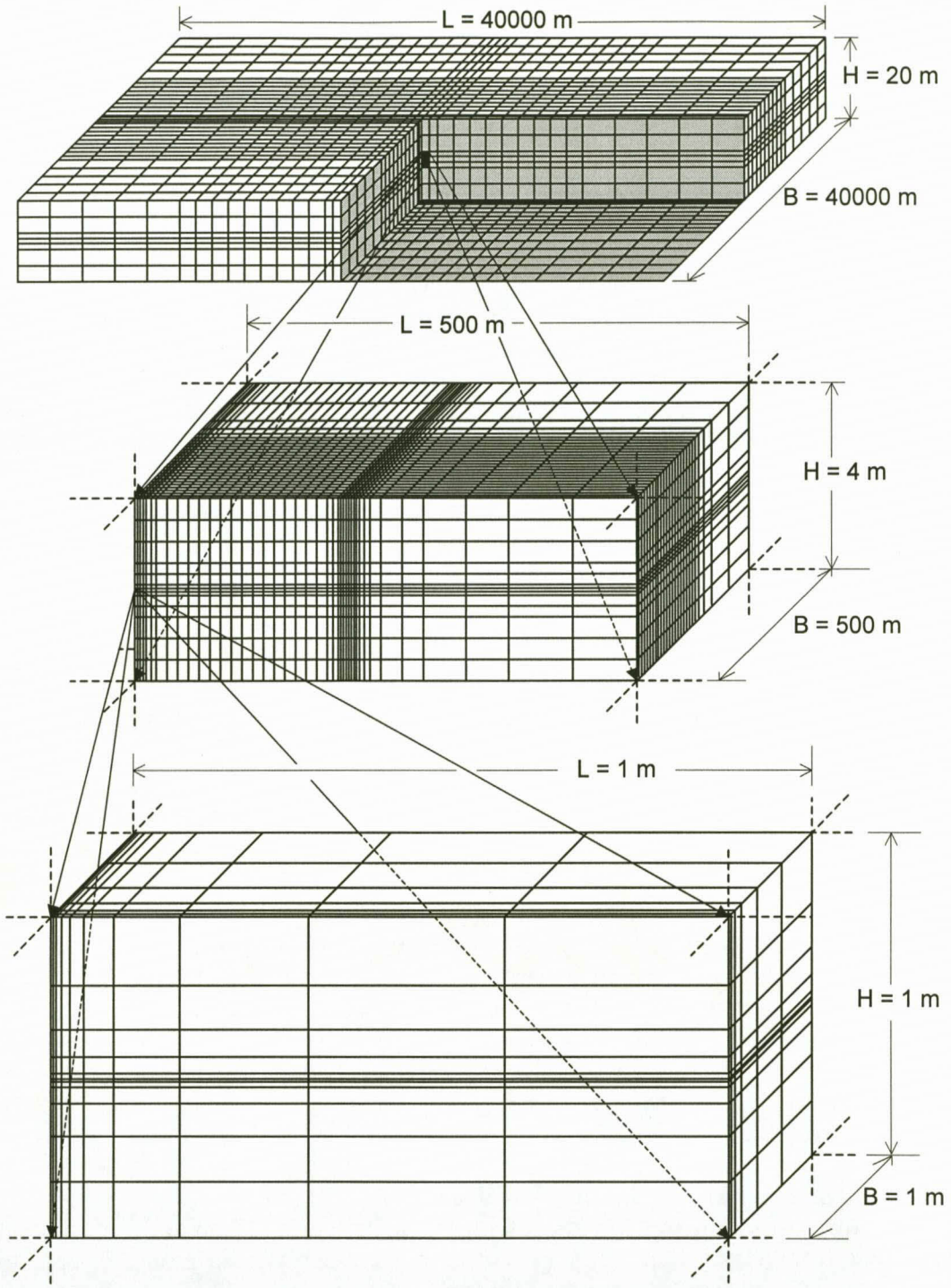

Figure 5.2. Example of a model grid design for the simulation of a vertical fracture that intersects a horizontal bedding plane

5.2.3 Solver

The solver used is PCG (Pre Conjugated Gradient Method) (Harabaugh *et al.*, 1999). In most of the cases, a number of 250 outer iterations and 100 inner iterations is sufficient for convergence. An overall convergence criterion of 0.00001 is adopted.

5.3 Modelling results

The results obtained in the processes of modelling the different geological scenarios are presented and discussed under this section.

5.3.1 Single vertical fracture case

Geological features as fault zones, karstified joints, and dikes as well as vertical fractures produced by artificial hydraulic fracturing can be often approximated as vertical structures (Fig. 5.3). These features are generally long, but usually subdivided into small units by transform faults and/or heterogeneous dissolution processes along the features. Analysis of pumping tests performed in these units show that mathematically, they can be treated as single vertical features (Stober, 1986; Bardenhagen, 1999).

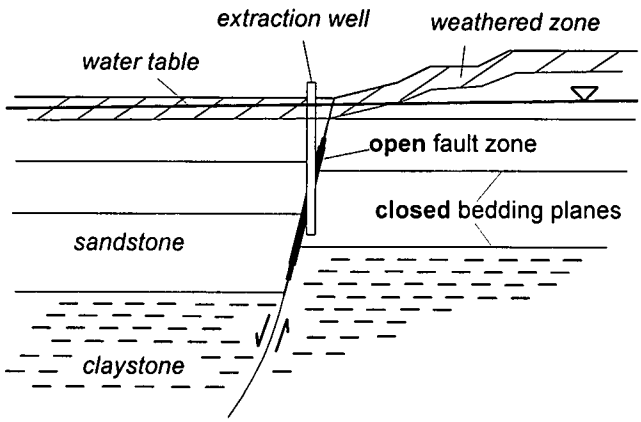

Figure 5.3. Example of a single cross section through a typical tectonic fault situation. The arrows indicate the direction of relative movement. The upper part of the fault (closed to the surface) is assumed to be sealed, due to weathering processes. The bedding planes are supposed to be closed, whereas the vertical fault zone is considered open

To compute the drawdown in a vertical feature, a fully penetrating fracture of 0.01 m aperture is included in the model. The fracture is intersected by a fully penetrating extraction well. The first calculations performed are aimed to investigate the ability of the model set up to reproduce the analytical solutions of Gringarten *et al.* (1974) for an infinite conductivity fracture and Cinco-Ley *et al.* (1978) for a finite conductivity fracture.

5.3.1.1 Infinite conductivity case ($Cr \geq 100$, $Cr = (T_f \cdot w)/(\pi \cdot T \cdot x_f)$)

The comparison of the modelled results with the analytical solutions for uniform and infinite flux from Gringarten *et al.* (1974) demonstrates that the model is able to reproduce the infinite flux, but not the uniform flux case (Fig. 5.4). This is due to the fact that the very high conductivity of the modelled single fracture gives place to a flux distribution that corresponds to the infinite flux case (Fig. 5.5).

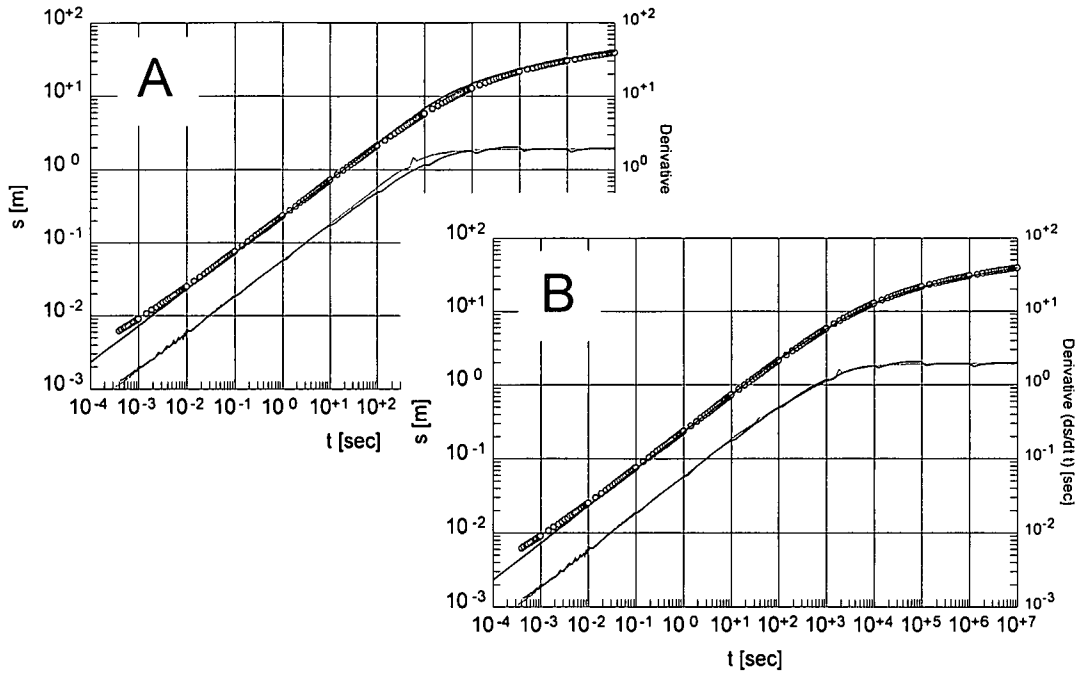

Figure 5.4. Drawdown in a pumped well. Model calculation (dots) (Cr = 1000) versus uniform flux (A) and infinite flux (B) solutions (solid line). After 1 second the modelling results plot identically to both the uniform and infinite flux solutions. From 10 second onwards, the modelling results diverge from the uniform flux solution (A), but coincide with the infinite flux solution (B). Also plotted in the graph are the derivatives of the drawdown curves (solid line curves underneath)

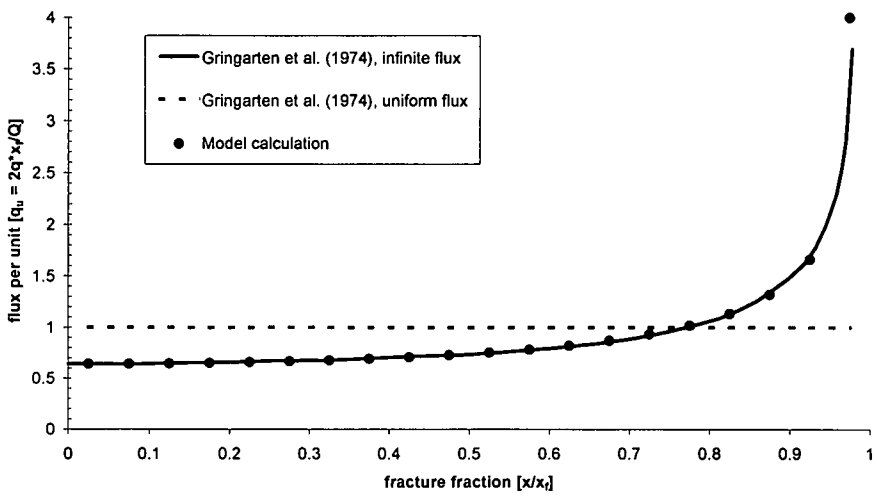

Figure 5.5. Comparison of modelled stabilized influx distribution along a vertical fracture with the uniform and infinite flux distributions of Gringarten *et al.* (1974). The model results fit adequately the infinite flux solution

5.3.1.1.1 Influx along the fracture

One of the advantages of the model is the possibility of visualizing the temporal development of the influx along the fracture (Fig. 5.6 and Fig. 5.9). This analysis shows that the time-dependent flux can be correlated to the flow phases described by Cinco-Ley & Samaniego (1981a). These flow phases are visualized in Figures 5.7 and 5.10, for which $s_d = 2 \cdot \pi \cdot T \cdot s/Q$ and $t_d = T \cdot t / S \cdot x_f^2$. The correlation can be described, as follows:

- for Cr = 100 and very early time ($t_d < 10^{-9}$), most of the extracted water is taken from the fracture in the close surroundings of the well. This period corresponds to the linear fracture flow phase (Figs. 5.6 to 5.8). This phase is followed by a transient phase, in which the influx from the matrix becomes more and more important. As soon as the cone of depression reaches the edge of the fracture, the bilinear flow phase starts. A second transient phase sets, when the contribution of the matrix becomes dominant. The larger the value of Cr (higher contrast between fracture and matrix conductivities), the earlier these phases take place. That is the reason why they cannot be seen in Figures 5.9 to 5.11 for Cr = 10000
- for Cr = 100, the linear formation flow sets at a dimensionless time $t_d = 2 \cdot 10^{-4}$, in which only the matrix supplies water and the fracture acts as a conduit or preferential flow path. This flow phase ends at a dimensionless time $t_d = 10^{-2}$ for both cases of Cr (Cr = 100 and Cr = 10000)
- for t_d between 10^{-2} and 10, the flux in the close surroundings of the well becomes smaller, but increases at the opposite edge of the fracture. This period describes a transient phase in both Cr cases (Cr = 100 and Cr = 10000)
- after $t_d = 10$ the flux distribution stabilizes in both Cr cases (Cr = 100 and Cr = 10000) and the radial flow phase sets. In this phase, the last 30% of the fracture length close to the edge opposite to the well provides about 50% of the extracted water

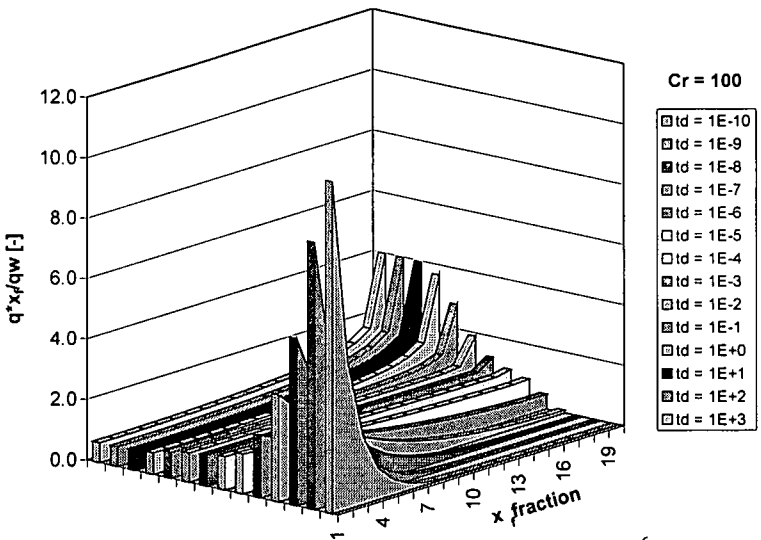

Figure 5.6. Influx distribution along a vertical fracture (Cr = 100 and $CD_f = 10^{-6}$, $CD_f = (S_f \cdot w)/(\pi \cdot S \cdot x_f)$)

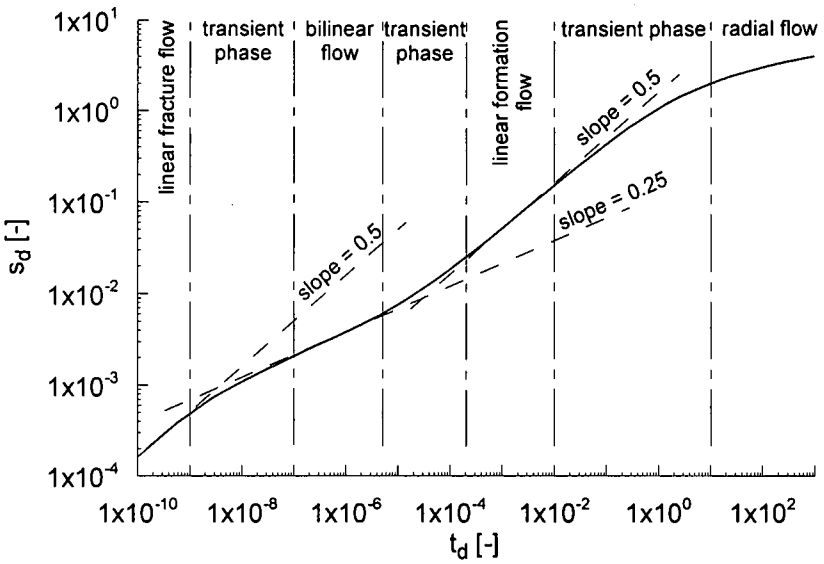

Figure 5.7. Dimensionless drawdown and flow phases in a pumped well located in an infinite conductivity vertical fracture (Cr = 100 and $CD_f = 10^{-6}$, $s_d = 2 \cdot \pi \cdot T \cdot s/Q$, $t_d = T \cdot t / S \cdot x_f^2$)

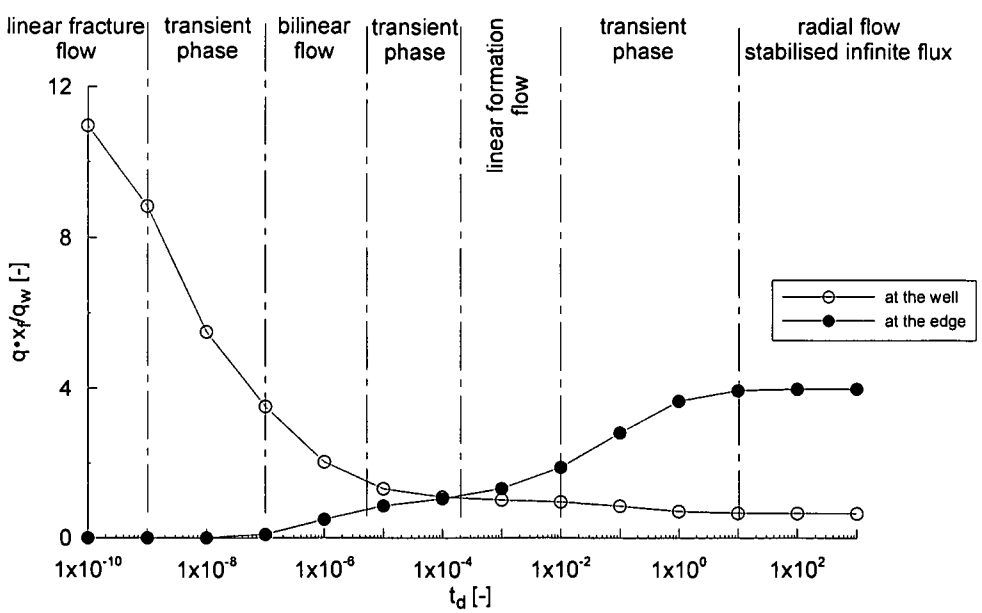

Figure 5.8. Time-dependent influx at the well and at the edge of the fracture (Cr = 100 and $CD_f = 10^{-6}$)

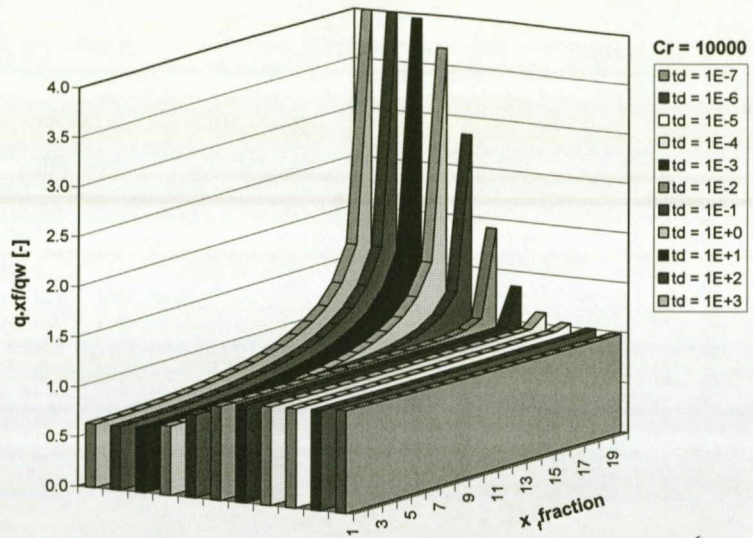

Figure 5.9. Influx distribution along a vertical fracture (Cr = 10000 and $CD_f = 10^{-6}$)

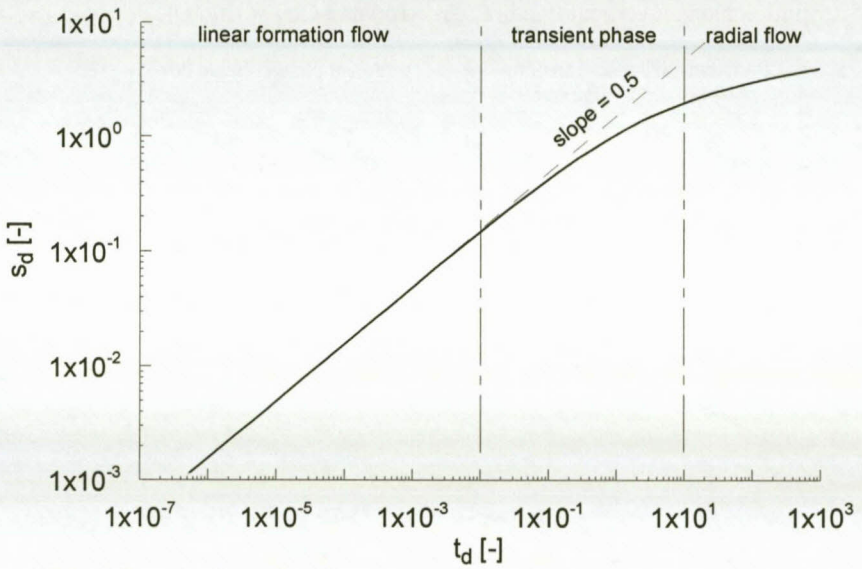

Figure 5.10. Dimensionless drawdown and flow phases in a pumped well located in an infinite conductivity vertical fracture (Cr = 10000 and $CD_f = 10^{-6}$, $s_d = 2 \cdot \pi \cdot T \cdot s/Q$, $t_d = T \cdot t / S \cdot x_f^2$)

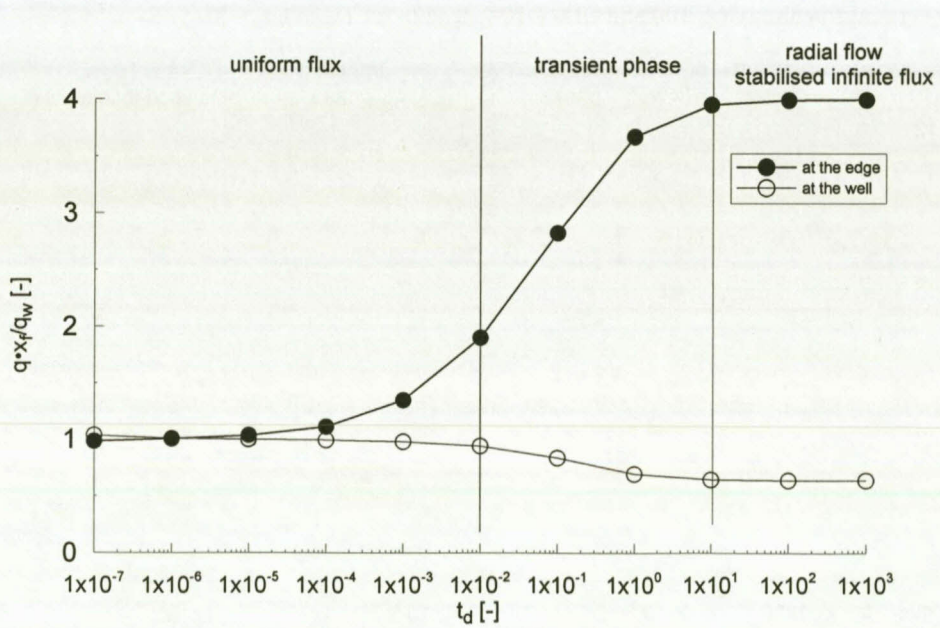

Figure 5.11. Time-dependent influx at the well and at the edge of the fracture (Cr = 10000 and $CD_f = 10^{-6}$)

5.3.1.1.2 Fracture/fault storage and aperture

A variation in the fracture or fault aperture implies a change in the relative storage capacity of the fracture CD_f ($CD_f = (S_f \cdot w)/(\pi \cdot S \cdot x_f)$). Thus, the influence of the fault aperture and the relative storage capacity must be analysed concurrently. Three different apertures are included in the study: 0.02 m, 0.2 m, and 2 m. The three graphs in Figures 5.12 show that, for a given CD_f, all curves have basically the same drawdown for $t_d > 10^{-5}$.

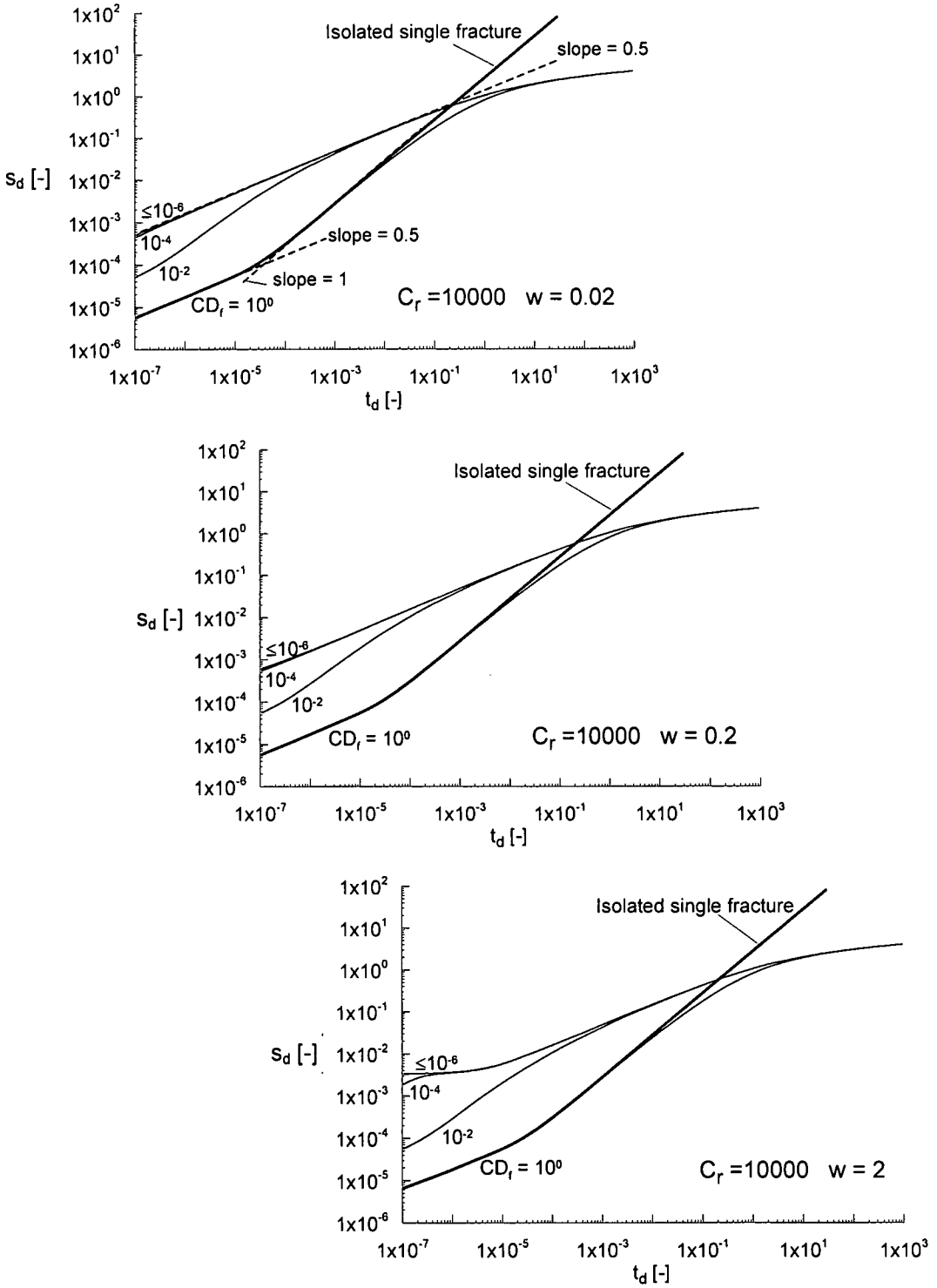

Figure 5.12. Drawdown in a pumped well located in an infinite conductivity vertical fault (Cr = 10000) with finite extent, calculated for various storages and apertures ($s_d = 2 \cdot \pi \cdot T \cdot s/Q$, $t_d = T \cdot t / S \cdot x_f^2$)

Furthermore, for $CD_f < 10^{-4}$ all curves coincide. It is also shown that in broad faults (w = 2m) at very early time ($t_d < 10^{-5}$) and small values of CD_f ($CD_f \leq 10^{-4}$), the drawdown remains practically constant. This is due to the fact that for a short period of time, the matrix, which has a much larger storage capacity than the fault, is able to supply enough water to cover the extraction rate without any significant additional drawdown.

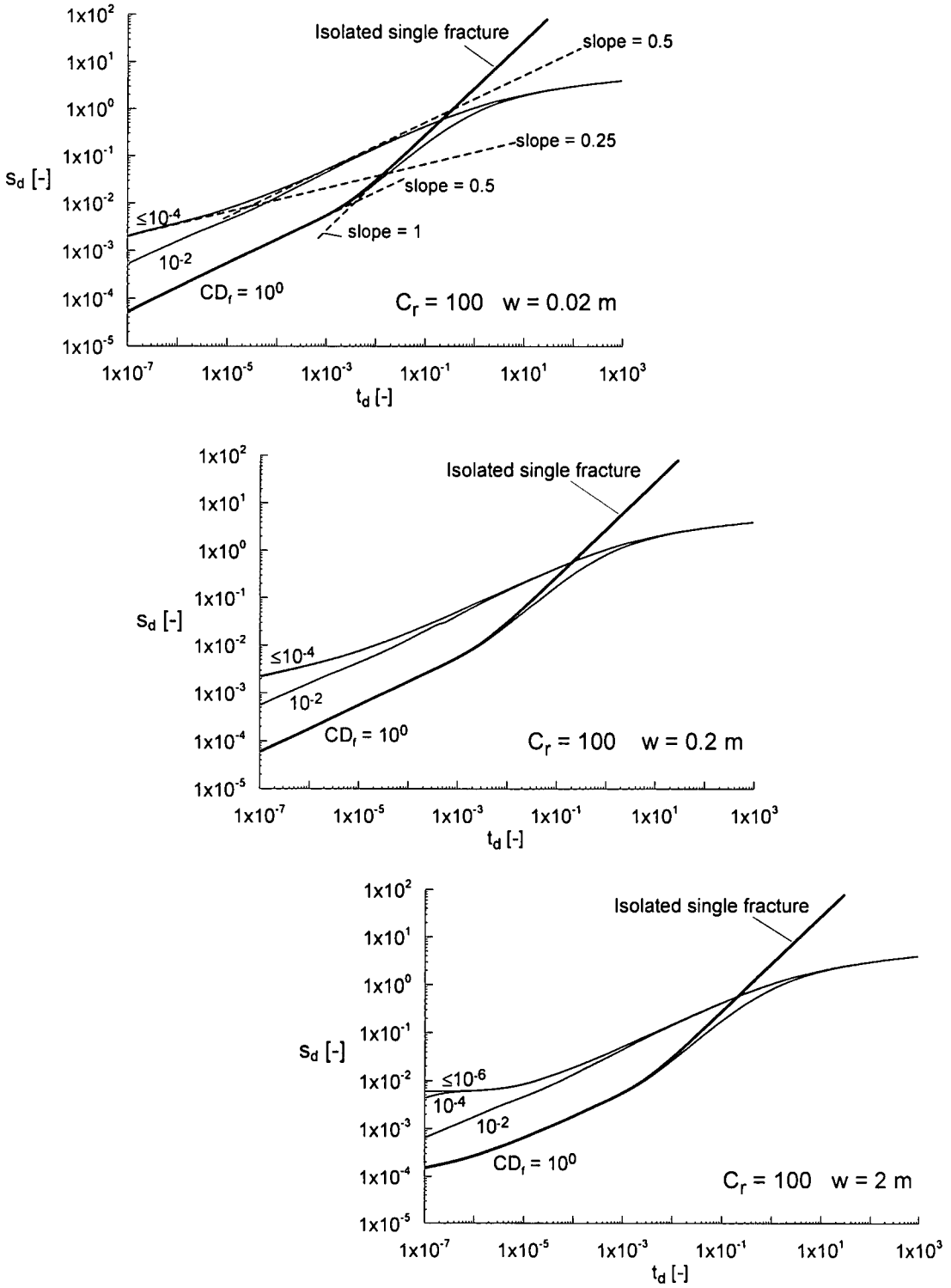

Figure 5.13. Drawdown in a pumped well located in an infinite conductivity vertical fault (Cr = 100) with finite extent, calculated for various storages and apertures ($s_d = 2 \cdot \pi \cdot T \cdot s/Q$, $t_d = T \cdot t / S \cdot x_f^2$)

The drawdown computed within an isolated fault is included in the graph to clearly separate the fault-dominated flow from the matrix-dominated flow. The fault-dominated flow appears for $CD_f > 10^{-4}$. The drawdown for $CD_f = 1$ shows linear fracture flow (slope of 0.5) for early time. At $t_d = 2 \cdot 10^{-5}$ the boundaries of the fault are reached. Thus, the curve shows close boundaries effect (slope of 1). At $t_d = 5 \cdot 10^{-3}$ the flow becomes matrix-dominated. The radial-acting flow sets at $t_d = 10$.

Figure 5.13 visualizes the drawdown curves for different fault storages, fault apertures, and Cr = 100. This Cr value represents the transition between infinite and finite conductivity. Thus, the flow phase are similar to those described above, but shifted towards larger dimensionless time. Furthermore, the transient flow phase for $CD_f = 1$ is not characterized by a slope of 1.

5.3.1.2 Finite conductivity case (Cr < 100)

The good correspondence between the modelled drawdown curve and the semi analytical solutions from Cinco-Ley *et al.* (1978) leads to the conclusion that the case of finite conductivity vertical fracture can be reproduced using numerical modelling with the adopted set up (Fig. 5.14).

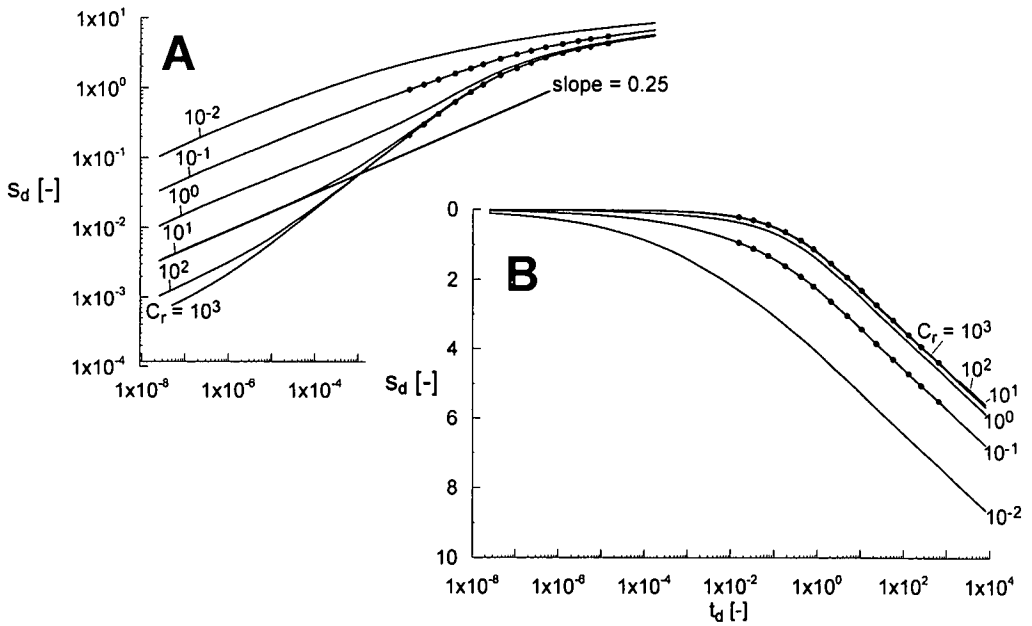

Figure 5.14. Modelled drawdown data in a pumped well calculated for selected values of Cr. The results fit the semi analytical solution from Cinco-Ley *et al.* (1978), which are represented by dots ($s_d = 2 \cdot \pi \cdot T \cdot s/Q$, $t_d = T \cdot t / S \cdot x_f^2$)

5.3.1.2.1 Influx along the fracture

Figure 5.15 shows the time-dependent development of the influx along the fracture for Cr = 0.1 and $CD_f = 10^{-4}$. Following paragraphs describe the correlation between the influx and the flow phases in the drawdown curve[3] published by Cinco-Ley & Samaniego (1981a)

- the dimensionless drawdown graphed in Fig. 5.16 shows an initial linear fracture flow at very early time ($t_d < 5 \cdot 10^{-9}$), which is followed by a transient phase up to

[3] The graphed drawdown curve (Cr = 0.1 and $CD_f = 10^{-4}$) was selected to be able to provide the whole series of known flow phases (compare Fig. 5.16). In addition, this curve demonstrates that the Cinco-Ley & Samaniego (1981a) and the Boehmer & Boonstra (1986) models are equivalent for the linear fracture flow and the bilinear flow phases.

$t_d = 9 \cdot 10^{-6}$. However, no differentiation between those two phases is seen in Figures 5.15 and 5.17, probably due to the subdivision of the fracture half-length into segments, which are necessary for the computation of the water budget (20 segments of equal length)

- bilinear flow (slope of 0.5) sets at $t_d = 9 \cdot 10^{-6}$. In this phase both, the matrix and the fracture provide water
- once the cone of depression overcomes the edge of the fracture, the contribution of the fracture storage decreases gradually ($t_d = 10^{-2}$). This effect results in a transient phase, which is shown in Figures 5.16 and 5.17
- from $t_d = 10$ the influx stabilizes and the radial flow phase sets (Figures 5.16 and 5.17)

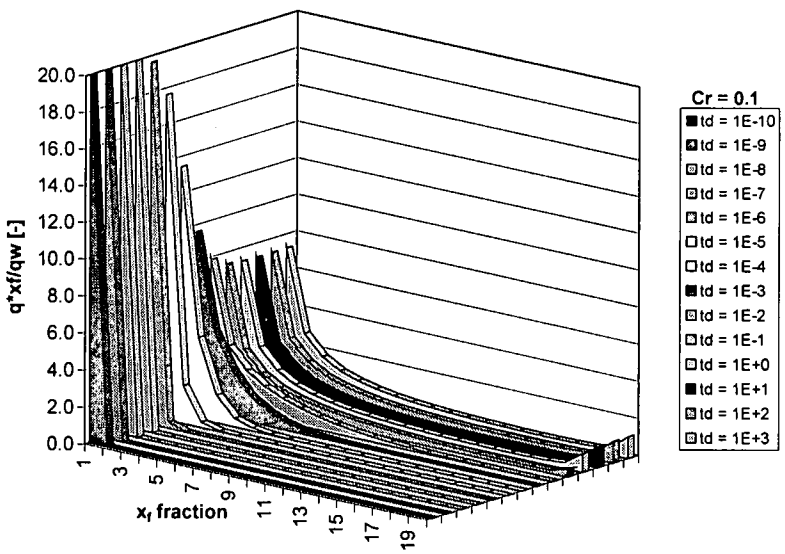

Figure 5.15. Influx distribution along a finite conductivity vertical fracture (Cr = 0.1 and $CD_f = 10^{-4}$)

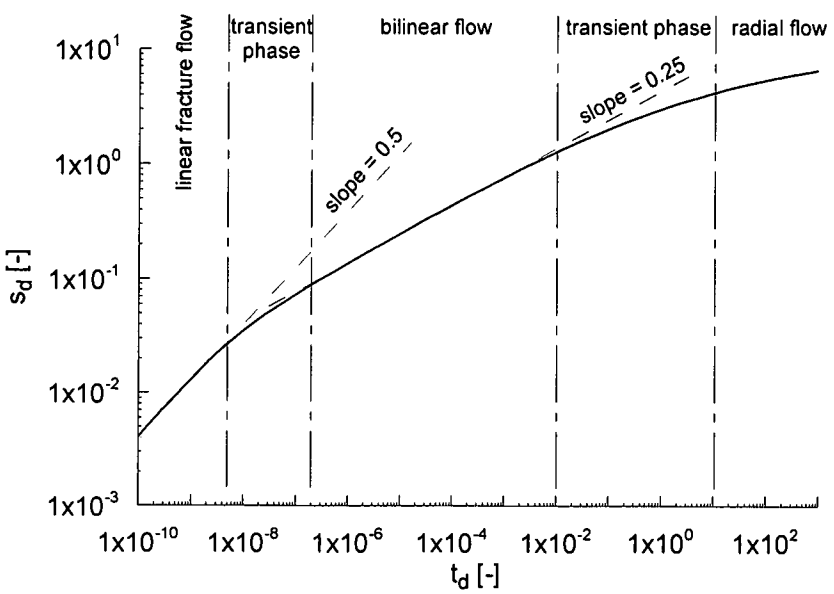

Figure 5.16. Dimensionless drawdown and flow phases in a pumped well located in a finite conductivity vertical fracture (Cr = 0.1 and $CD_f = 10^{-4}$, $s_d = 2 \cdot \pi \cdot T \cdot s/Q$, $t_d = T \cdot t / S \cdot x_f^2$)

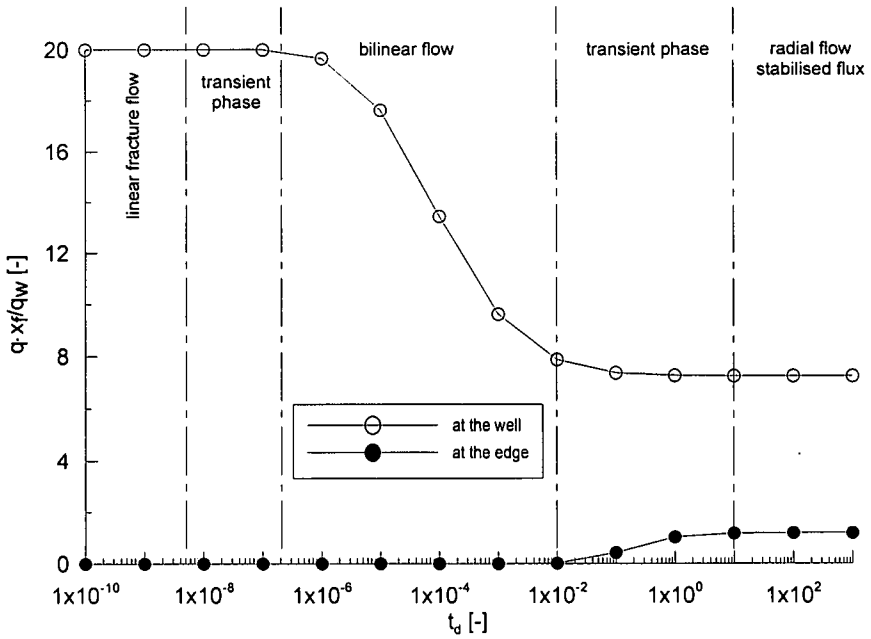

Figure 5.17. Time-dependent influx at the well and at the edge of the fracture (Cr = 0.1 and $CD_f = 10^{-4}$)

5.3.1.2.2 Fracture/fault storage and aperture

Again in this case three different fault apertures are included to investigate the influence of the aperture: 0.02 m, 0.2 m, and 2 m. The results are presented in Figure 5.18, which shows:

- for w = 0.02 m and $CD_f > 10^{-4}$, the curves show a linear fracture flow phase (slope of 0.5) followed by a transient and a radial-acting flow phase. For $CD_f \leq 10^{-4}$ the curves indicate bilinear flow (slope of 0.25) at early time, followed by a transient phase and radial-acting flow at late time
- for w = 0.2 m and $CD_f = 1$, the drawdown curve develops initially a radial flow phase within the fault itself. Once the cone of depression reaches the fault boundaries, a linear fracture flow sets that is followed by a transient period and a radial-acting flow phase in the matrix. Depending on the CD_f values, the other curves show either bilinear flow phase (slope of 0.25 for $CD_f \leq 10^{-4}$) or linear fracture flow phase (slope of 0.5 for $CD_f > 10^{-4}$). Both the linear and bilinear flow phases are followed by a transient phase and a radial formation flow phase
- for w = 2 m, the curves develop initially a radial flow phase within the fault itself. Once the cone of depression reaches the fault boundaries, the drawdown curves show a transient phase that smears both the bilinear and the linear flow phases. This period is followed by a radial formation flow phase

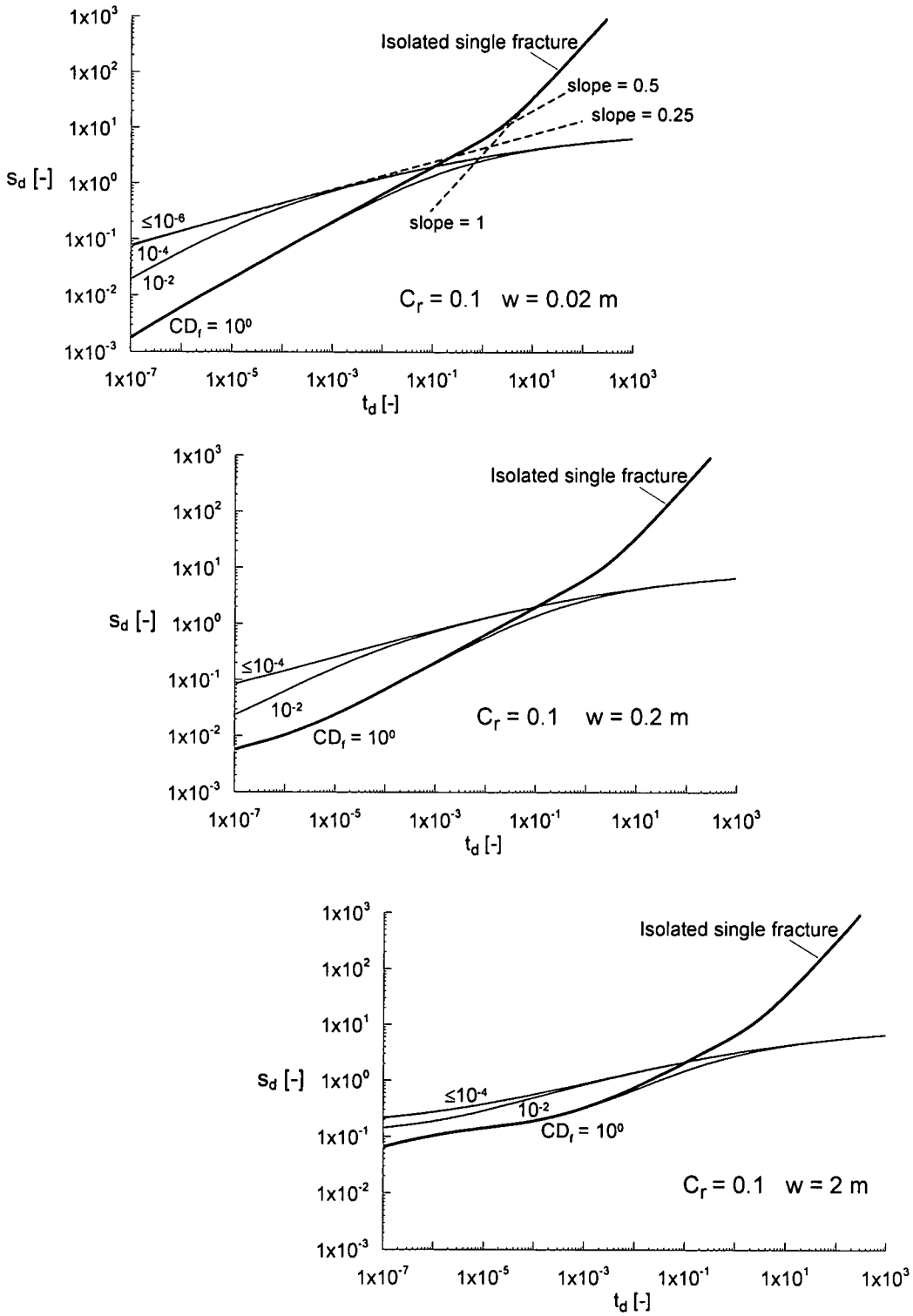

Figure 5.18. Drawdown in a pumped well located in a finite conductivity vertical fault (Cr = 0.1) with finite extent, calculated for various storages and apertures ($s_d = 2 \cdot \pi \cdot T \cdot s/Q$, $t_d = T \cdot t / S \cdot x_f^2$)

5.3.2 Parallel vertical structures

The applicability of the numerical modelling for the representation of single vertical fractures has been demonstrated. In the next sections, numerical modelling is employed to investigate the drawdown behavior in more complicated geological situations, starting with the case of parallel vertical fractures. They appear typically at the edge of grabens, in fault zones (Fig. 5.19), or at the hinge of a normal folded sequence (Hobbs *et al.*, 1976).

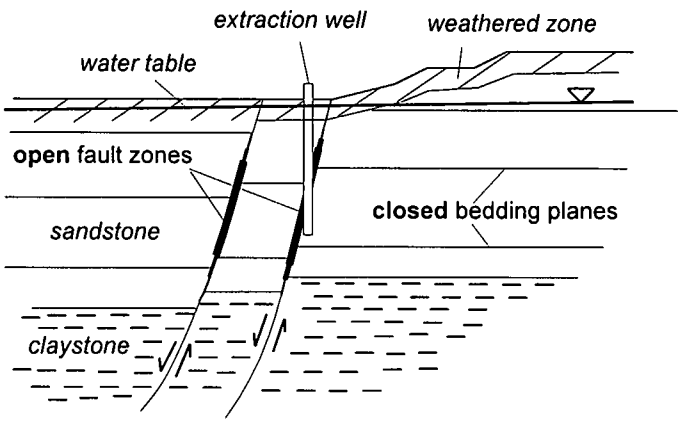

Figure 5.19. Example of a cross section through a typical tectonic fault situation. The arrows indicate the direction of relative movement. The upper part of the fault (closed to the surface) is assumed to be sealed due to weathering processes. The bedding planes are suppose to be closed, whereas the parallel faults are considered open

To study the effects of the separation between such structures, a set of three parallel fractures with equal separation in between was incorporated to the model. The separations vary in the range of 0.50 m to 100 m. A fully penetrating well intersects the central one. To be able to compare the results, the dimensionless relative separation factor s_r is introduced, which is defined as:

$$s_r = \frac{d_f}{x_f} \qquad (5.1)$$

where
d_f = separation between fractures [L]
x_f = fracture half-length [L]

It was found that the presence of parallel structures with infinite (Cr $\geq$ 100) or finite conductivity (Cr < 0.01) does not have any significant influence on the drawdown curve when compared with the single vertical fracture case (Fig. 5.20). However, this situation reverts for Cr between 0.01 and 100. The strongest influence is calculated for parallel fractures separated by s_r less than $5 \cdot 10^{-3}$, where considerable less drawdown than in the single fracture is computed. This difference decreases with increasing separations to disappear at dimensionless relative separations s_r larger than 0.125 (Fig. 5.21).

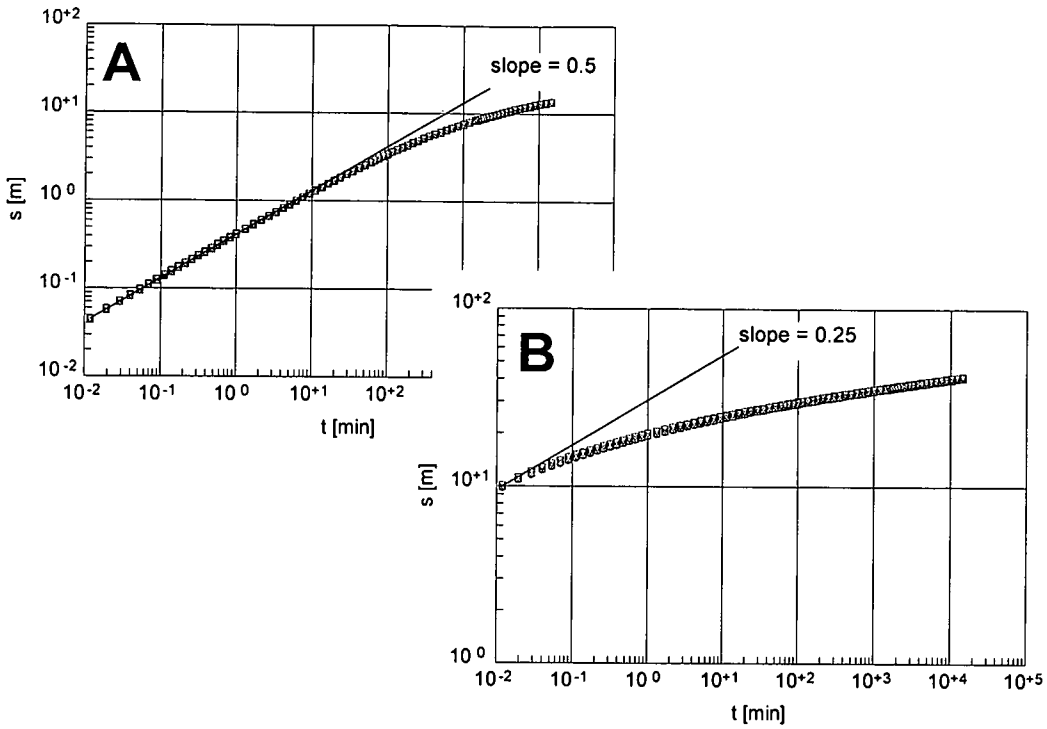

Figure 5.20. Drawdown in a pumped well for various parallel fractures with infinite (Cr ≥ 100) (A) and finite (Cr < 0.01) (B) conductivities. Dimensionless relative separations s_r between fractures of $2.5 \cdot 10^{-3}$, $5 \cdot 10^{-3}$, $2.5 \cdot 10^{-2}$, and $5 \cdot 10^{-2}$ are included. It is seen that the presence of parallel fractures does not have any significant influence on the drawdown

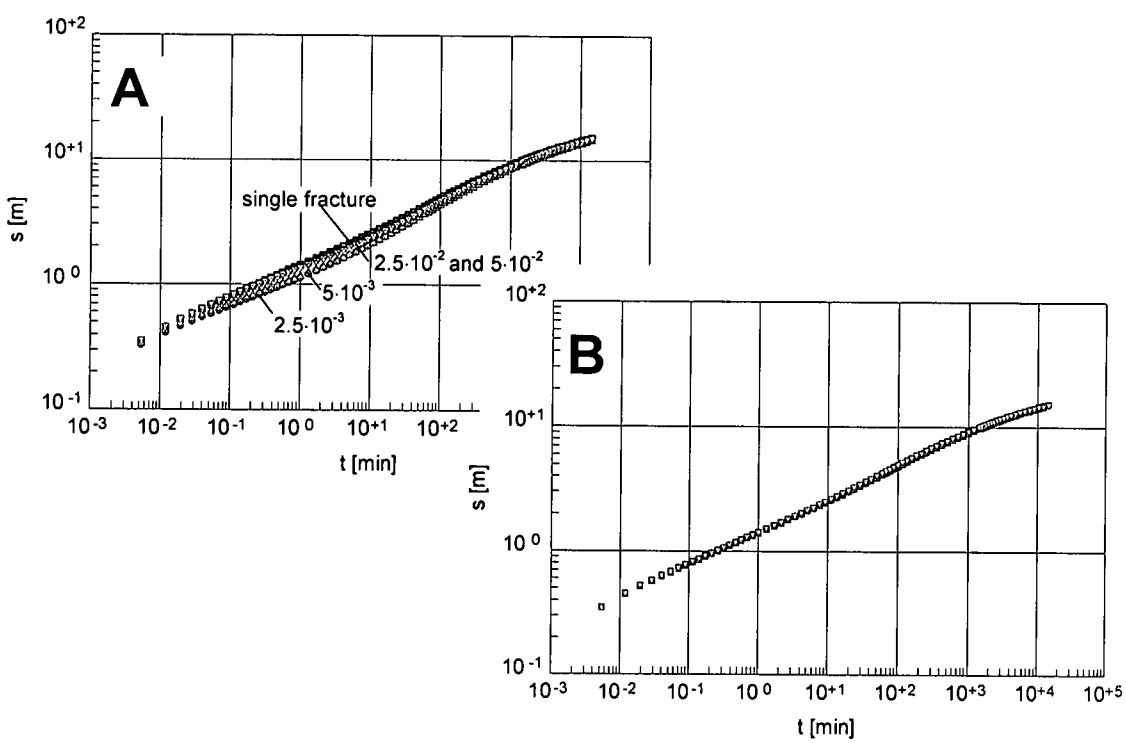

Figure 5.21. Comparison of drawdown in a pumped well in a single fracture and for various parallel fractures for the single fracture case (Cr = 1). Dimensionless relative separations s_r between fractures of $2.5 \cdot 10^{-3}$, $5 \cdot 10^{-3}$, $2.5 \cdot 10^{-2}$, and $5 \cdot 10^{-2}$ are included in the graph A. The strongest differences in the drawdown is observed for s_r of $2.5 \cdot 10^{-3}$ and $5 \cdot 10^{-3}$. Graph B plots the curves for s_r of 0.125, 0.25, and 0.5 which, for practical purposes, do not show any influence on the drawdown

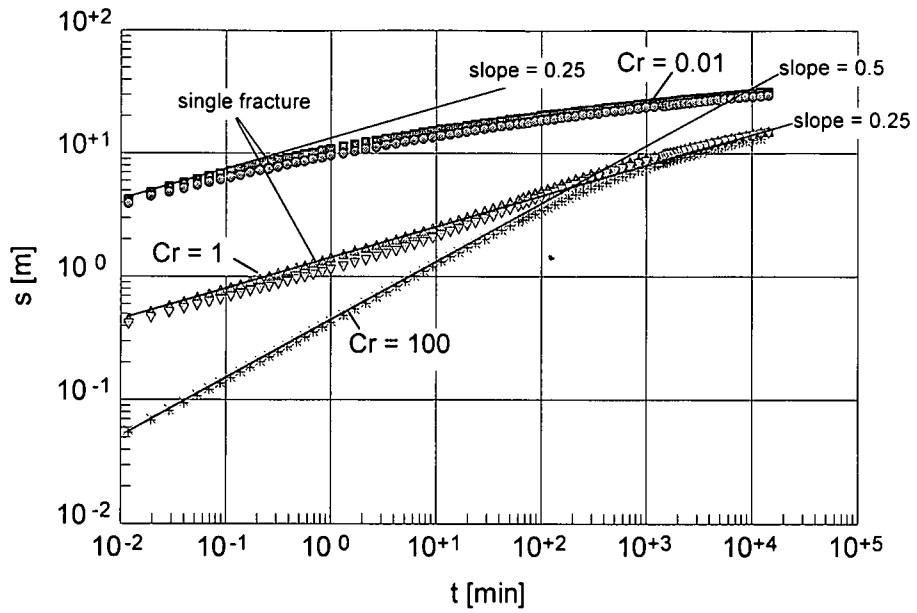

Figure 5.22. Comparison of drawdown in a pumped well for a single fracture and parallel fractures with a relative separation $s_r = 2.5 \cdot 10^{-3}$ for selected Cr. In the case of Cr = 100 the presence of parallel fractures does not influence the drawdown, but for Cr = 1 or 0.01 the presence of parallel fractures leads to less drawdown, except at very early time where the curve coincides with that of the single fracture

In Figure 5.22, the drawdown for selected values of Cr ($Cr = (T_f w)/(\pi \cdot T \cdot x_f)$) calculated for single fractures is compared with the drawdown of parallel fractures separated by $s_r = 2.5 \cdot 10^{-3}$. The case of Cr = 100 shows no difference, as already described. For Cr = 1 and Cr = 0.01, the drawdown at very early time plots almost on the single fracture data, but significant differences appear later.

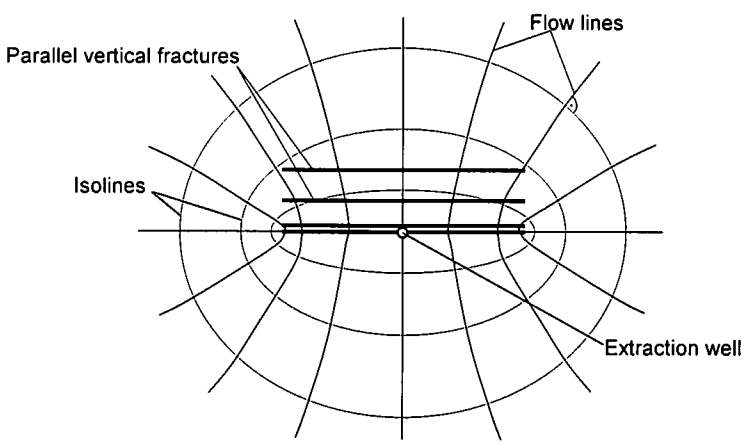

Figure 5.23. Example of the flow situation for parallel vertical infinite conductivity fractures ($Cr \geq 100$). The flow lines directed towards the pumped fracture flow almost perpendicular to all other fractures. Therefore, the whole system acts similar to that of a single fracture embedded in a matrix

The parallel fractures with infinite conductivity ($Cr \geq 100$) have no influence on the drawdown, due to the parallel flow situation (linear formation flow) of the system (Fig 5.23). Because the path lines in the direction of the pumped fracture flow almost perpendicular to all other fractures, the potential lines are parallel to these fractures. There is neither significant gradient along the parallel fractures nor between the series

of fractures. The whole system acts similar to the situation in which there is only one fracture embedded in the matrix.

For values of Cr < 100 gradients develop simultaneously within the pumped fracture and the matrix. When the cone of depression in the matrix reaches the next parallel fracture, it induces a gradient within this fracture towards its centre. As a result, water flows along this fracture and increases the gradient in the central region between the parallel fractures (Fig. 5.24). The potential lines flatten in the areas close to the centres of the parallel fractures.

The smaller the Cr values, the lesser the contrast between matrix and fracture conductivities and the above described effect vanishes. At very small values of Cr (< 0.01) the whole system acts like a homogeneous aquifer and the drawdown curve has no difference with the single vertical fracture curve.

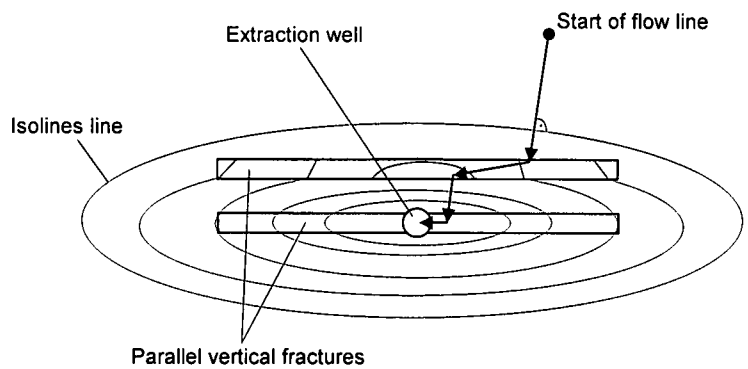

Figure 5.24. Flow situation in a series of parallel vertical finite conductivity fractures (Cr < 100). The flow lines directed to the pumped fracture originate a gradient within the parallel fractures and the matrix. When the cone of depression in the matrix reaches the next parallel fracture, it induces a gradient within this fracture towards its centre. As a result, water flows along this fracture and increases the gradient in the central region between the parallel fractures

5.3.3 Crossed vertical structures

Crossed vertical structures can appear after hydraulic fracturing processes, in the vicinity of granite or salt intrusion plumes, at {0kl} joints in a fold, or in structures associated with wrench faults (Hobbs *et al.*, 1976).

To investigate the influence of crossed vertical structures, two perpendicular fractures are incorporated to the model. A fully penetrating well is located in the intersection of both.

First the infinite conductivity case is analysed. The computed drawdown for a pumped well in the intersection of the fractures is compared with the drawdown modelled for a single vertical feature, both calculated with Cr = 1000 (Fig. 5.25). To be able to compare the results, it is assumed that the influx area is the same in the two cases. In other words, the half-length of the two crossed fractures is 200 m each and the single fracture has a total half-length of 400 m. At early time both cases have the same drawdown, which is characterized by a slope of 0.5 (linear formation flow). During the intermediate phase a stronger drawdown appears for the crossed fracture case. However, the drawdown difference remains constant, once the radial-acting flow is reached.

When compared with the Gringarten *et al.* (1974) solutions, it is seen that the drawdown curve obtained for the crossed fracture case differs significantly from that calculated for a single vertical preferential flow path with infinite flux (Fig. 5.26A). However, it is adequately represented by the uniform flux solution of Gringarten *et al.* (1974), as shown in Figure 5.26B.

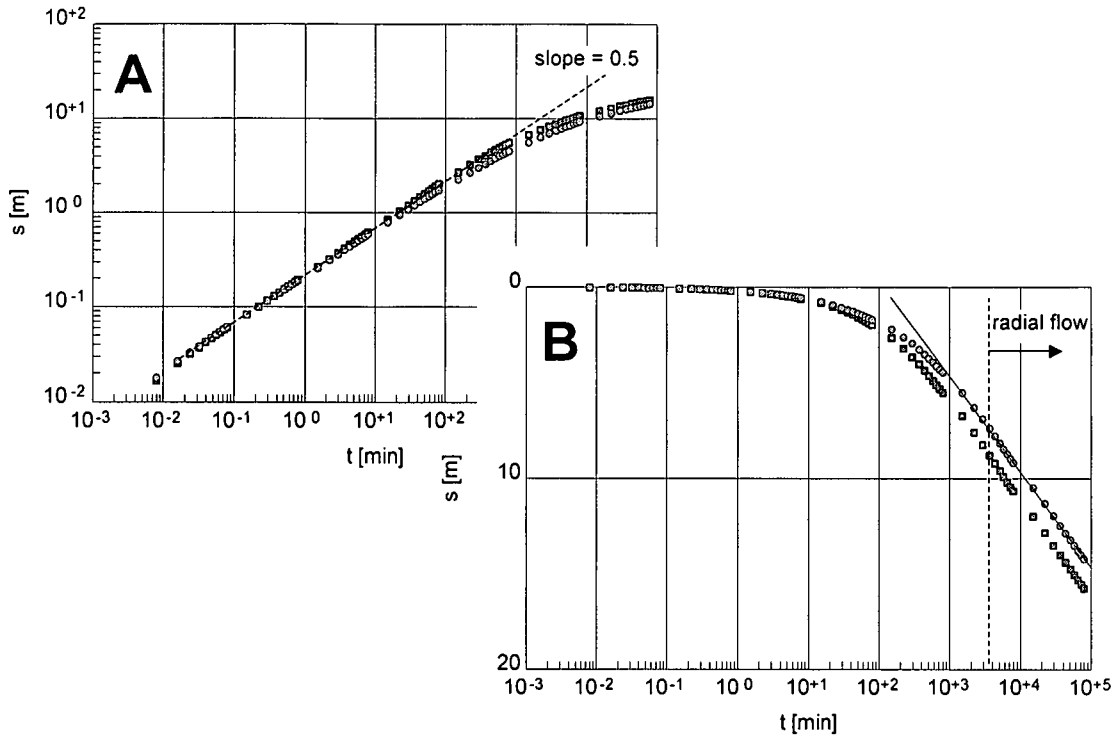

Figure 5.25. Comparison of drawdown in a pumped well obtained with perpendicular crossed infinite conductivity vertical fractures (squares) and a single vertical feature (dots). To be able to obtain the same influx area in both cases each of the crossed fractures is considered with a half-length of 200 m, while the single fracture has a half-length of 400 m. The curves almost coincide at early time, but differ considerably at late time. The crossed vertical fracture case shows a larger drawdown at late time

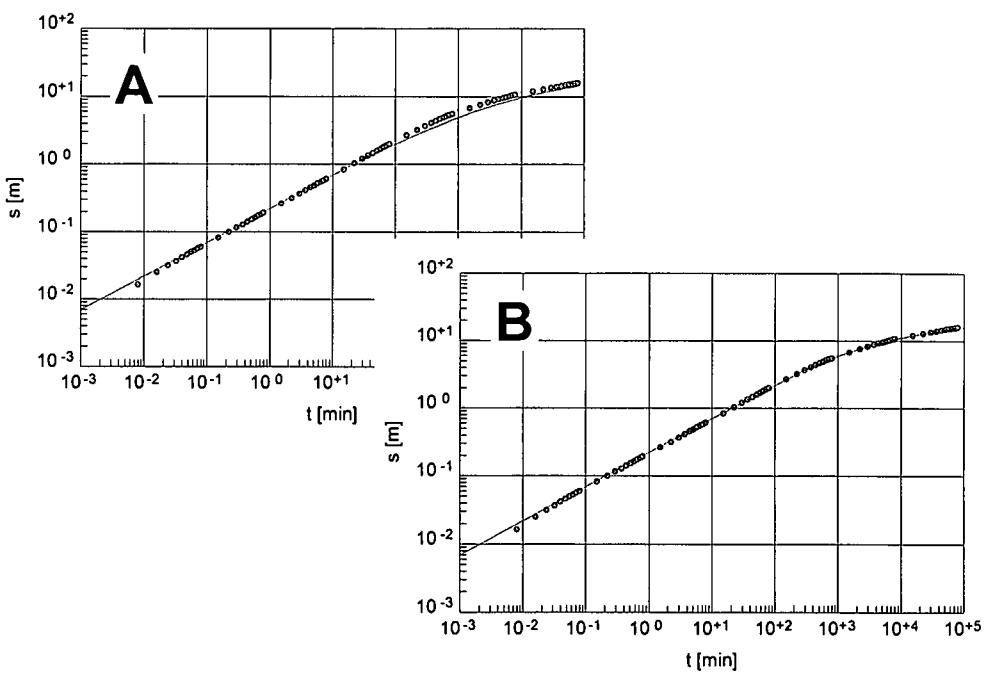

Figure 5.26. Drawdown in a pumped well. Model calculation (dots) (Cr = 1000) versus infinite flux (A) and uniform flux (B) solutions (solid line). The calculated curves fits adequately the uniform flux solution

The case of finite conductivity crossed fractures is also investigated using numerical modelling. Figure 5.27 shows a comparison of the drawdown calculated for a single feature that of crossed fractures for various Cr. An infinite conductivity case (Cr = 1000) is also presented for comparison. For Cr = 1000 (infinite conductivity), the drawdown in the crossed fracture case is larger than in the single fracture case. For Cr = 1 and Cr = 0.001 (finite conductivity), less drawdown is observed in the case of crossed fractures.

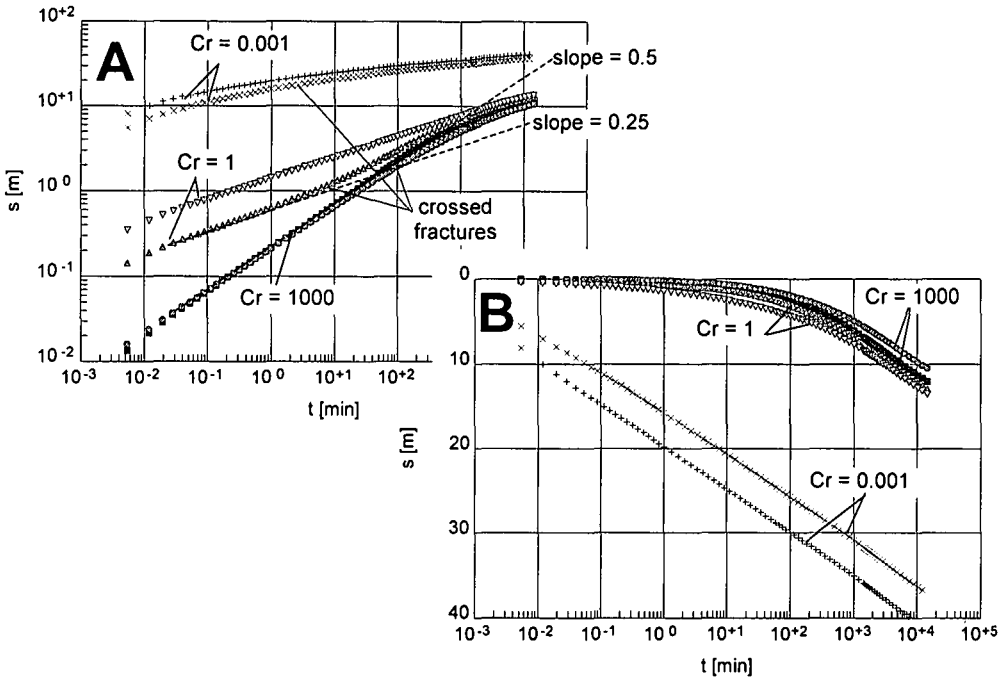

Figure 5.27. Comparison of drawdown in a pumped well calculated with a single vertical feature and with crossed fractures, for selected values of Cr

Figure 5.27 shows that:

- for Cr = 1000 and early time, almost the same drawdown is calculated for both the single fracture case and the crossed fractures. This drawdown is characterized by a slope of 0.5 in a log-log plot, which indicates linear formation flow. During the transient phase the drawdown calculated with the crossed fractures increases over proportionally compared to the drawdown computed for the single fracture case. During the radial flow phase both cases show the same drawdown development and the difference among them remains constant
- for Cr = 1 and early time, lesser drawdown is computed for the crossed fractures than for the single fracture case as a result of a higher water availability in the crossed fractures. However, both curves show bilinear flow phase (slope of 0.25). This difference diminishes during the transient phase, when the extracted water is provided more and more by the matrix and less by the fracture storage. In the radial formation flow phase, both curves are almost equivalent because the whole pumped water is extracted from the matrix
- for Cr = 0.001 and early time, the drawdown calculated for the crossed fracture case is smaller than the calculated with a single fracture, due to the reasons described above. The difference increases during the transient phase to reach a maximum value that remains constant during the radial formation flow phase. In this case the pseudo-skin effect presented in Section 3.1.3 will be enhanced by the presence of crossed fractures

Figure 5.28 shows the time-dependent development of the influx along one of the crossed fractures for Cr = 1000. Each half-length would provide half of the plotted influx. At very early time most of the extracted water is taken from the close surroundings of the well within the fracture. From $t_d = 10^{-5}$ to $t_d = 10$ the peak in the close surroundings to the well decreases slightly, while an increase in the influx at the opposite edge of the fracture is observed, as already described in the single vertical fracture case (Section 5.3.1.1.1). For values of t_d larger than 10 the flux distribution stabilizes and corresponds to the radial flow phase in the drawdown data.

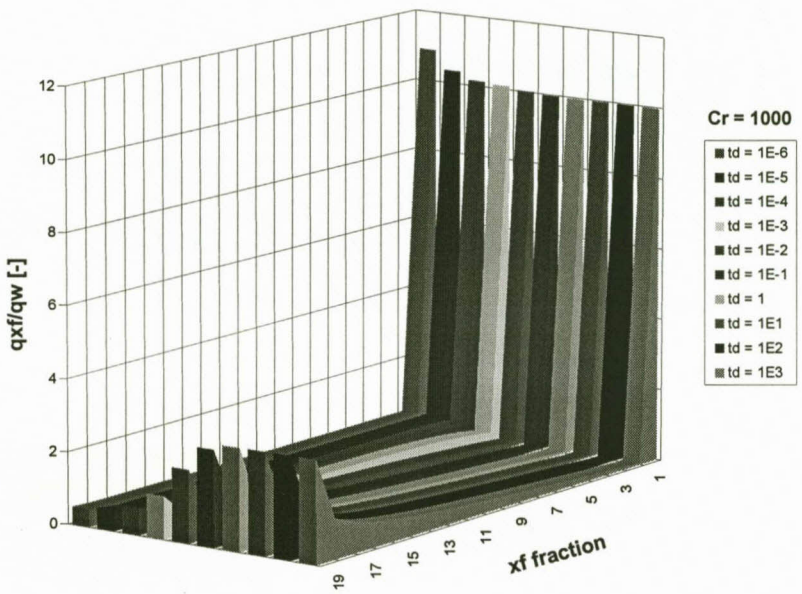

Figure 5.28. Time-dependent development of the fracture influx along one of the crossed fractures with infinite conductivity

Figure 5.29 shows the percentage of the stabilized influx distribution calculated for homogeneous fractions of the fracture half-length. Each half-length would provide half of the plotted percentage.

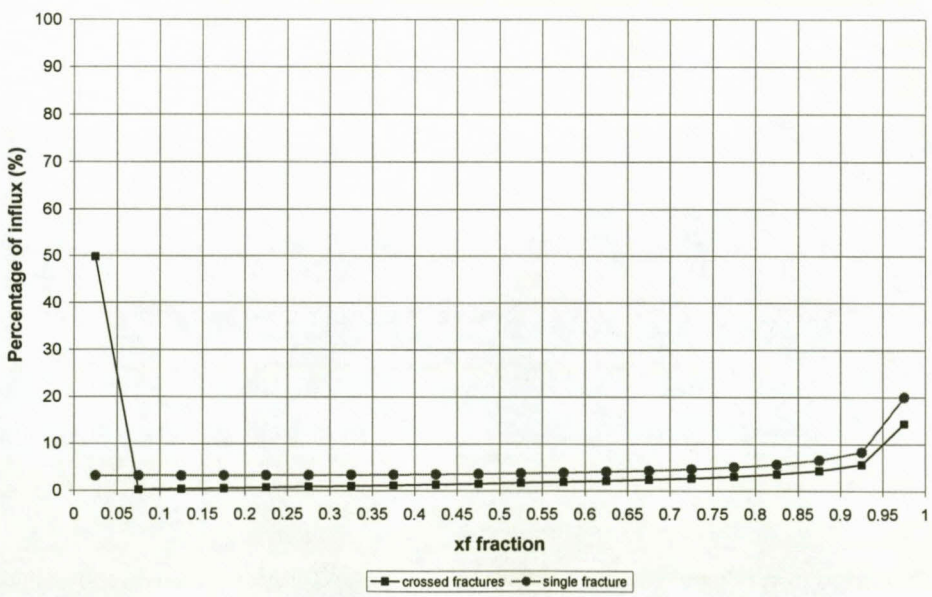

Figure 5.29. Percentage of influx distribution along one fracture for the crossed fractures (squares) and the single vertical fracture (dots), both with infinite conductivity. Each half-length gets half of the plotted percentage

The plot compares the fluxes of both infinite conductivity cases, the crossed fractures and the single vertical fracture. In the crossed fracture case the first segment has an influx slightly higher than 50% of the extracted water. This influx is the sum of the total influx from the perpendicular fracture plus the amount received by the segment itself. Furthermore, the influx distribution is not constant along the fracture. Therefore, it cannot be considered as a uniform flux. However, the drawdown curve coincides exactly with the uniform flux solution from Gringarten *et al.* (1974).

5.3.4 Bend fractures

Another complicated geological situation that is investigated with numerical modelling is the case of a vertical bend fractures. Bend fractures appear typically as associations of faults and transform faults. This case is analysed considering an S-shape fracture (Fig. 5.30). A fully penetrating well intersects the centre of the central branch. The modelled drawdown is compared with the infinite conductivity single vertical case in Figure 5.31. While the curves coincide exactly for early time, the bend case shows a larger drawdown at late time. However, the bend case fits adequately the uniform flux solution from Gringarten *et al.* (1974).

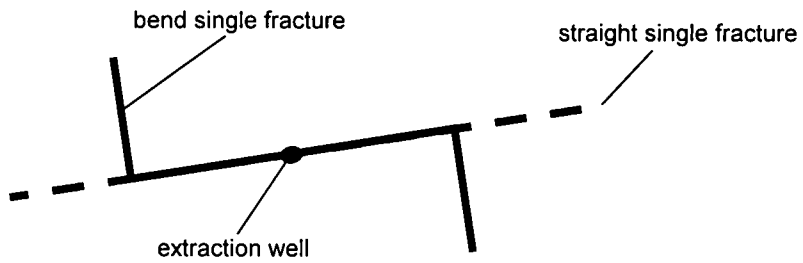

Figure 5.30. Set up used for the analysis of the drawdown in a bend fracture

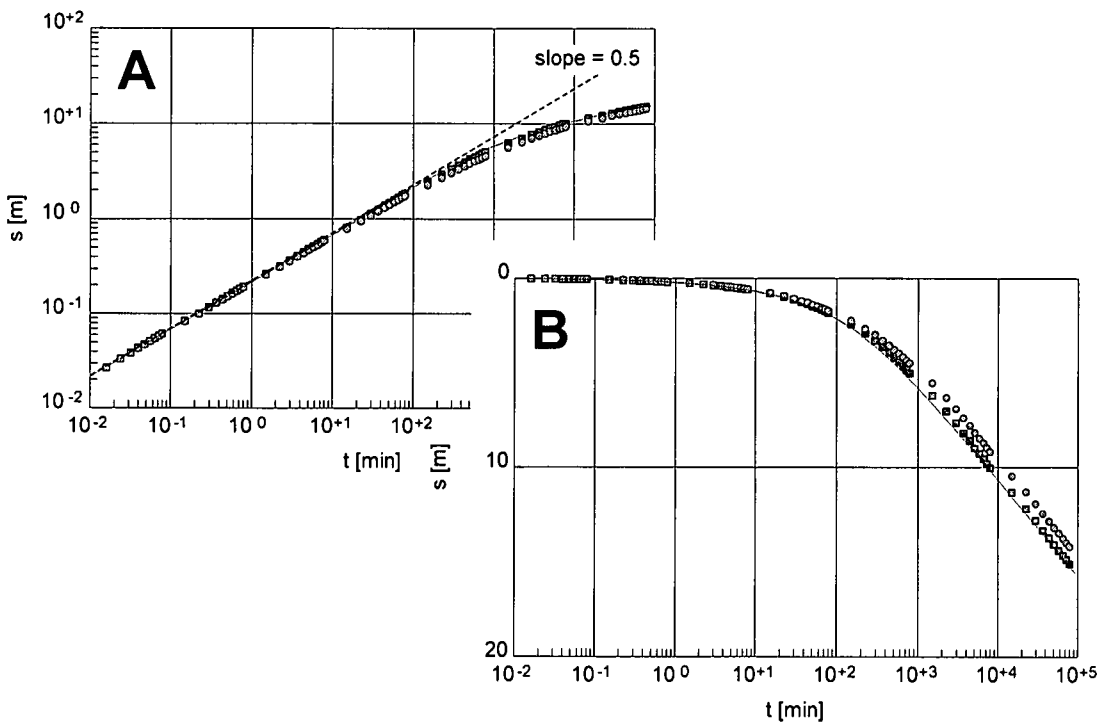

Figure 5.31. Drawdown in a pumped well calculated for Cr = 1000 with a bend fracture (squares) and with a single vertical fracture (dots). The uniform flux solution from Gringarten *et al.* (1974) is additionally plotted as a solid line. It is seen that the bend fracture case coincides with the uniform flux solution

5.3.5 Single horizontal fracture case

Geological structures like bedding planes are the typical case of horizontal fractures. Also horizontal features produced by hydraulic fracturing in shallow formations (Gringarten & Ramey, 1974) are included in this category (Fig. 5.32). Bedding planes are consider as circular fractures in analytical and semi analytical solutions, which are known as penny-shape or pancake bedding planes (Valkó & Economides, 1997).

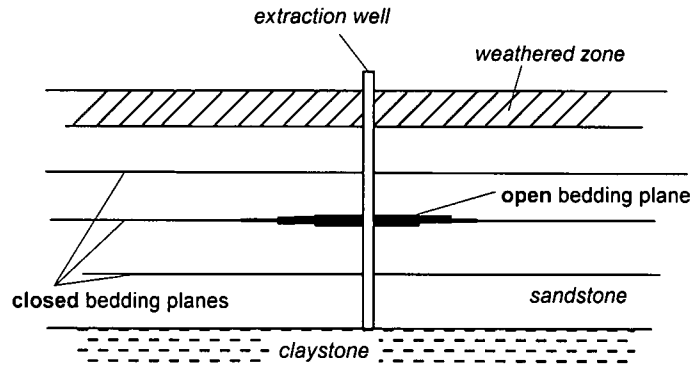

Figure 5.32. Example of an open horizontal bedding plane embedded in a layered sandstone aquifer, intersected by a well

To investigate the ability of the model to represent the horizontal fracture case, a fracture of an aperture of 0.01 m is included in the centre of the cube, half way of the depth. A fully penetrating extraction well is situated in the centre of the model.

The modelled results are first compared with the analytical uniform flux solution from Gringarten & Ramey (1974) (Fig. 5.33). The drawdown curves are coincident at early time within the linear formation flow phase. During the transient phase, the uniform flux solution develops a larger drawdown compared to the infinite solution (modelled data). Once the radial phase is reached, the difference between both solutions remains constant. This effect is similar to that described in the vertical fracture case (Sections 4.2.1 and 5.3.1.1). However, the difference between the uniform flux and the infinite flux solutions for a horizontal fracture with infinite conductivity was already observed by Valkó & Economides (1997).

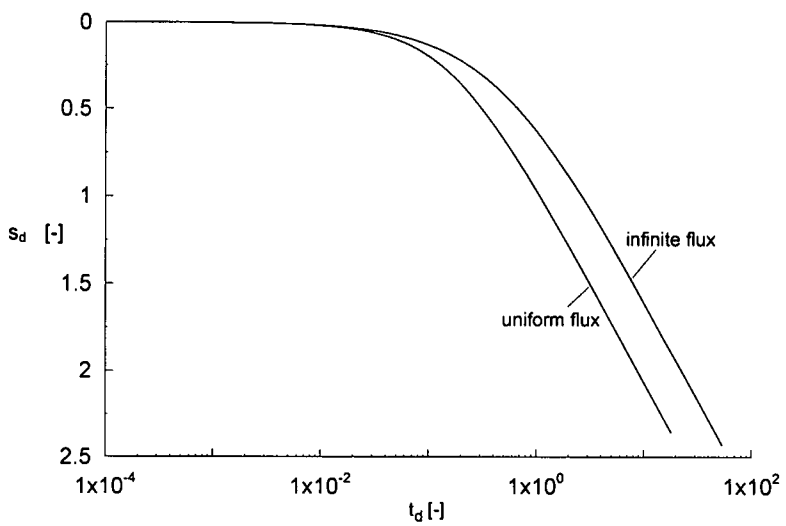

Figure 5.33. Drawdown in a pumped well. Comparison between the modelled data (infinite flux) and the uniform flux analytical solution of Gringarten & Ramey (1974) ($s_d = 2 \cdot \pi \cdot T \cdot s/Q$, $t_d = T \cdot t / S \cdot r_f^2$)

Valkó & Economides (1997) developed a semi analytical solution to calculate the drawdown in a well located in a horizontal pancake fracture with both infinite and finite conductivities. Their model provides solutions for infinite and finite fluxes. They introduced the concept of dimensionless fracture conductivity F_{CD}, which is comparable to the relative conductivity Cr from Cinco-Ley *et al.* (1978) for finite conductivity vertical fractures. F_{CD} is defined as:

$$F_{CD} = \frac{K_f \cdot w}{12 \cdot K_e \cdot r_f} \qquad (5.2)$$

where
K_f = conductivity of the horizontal fracture [LT^{-1}]
w = fracture aperture [L]
K_e = equivalent conductivity, $(K_h^2 \cdot K_v)^{1/3}$ [LT^{-1}]
r_f = radius of the penny-shape fracture [L]

To investigate the ability of the model in representing the Valkó & Economides (1997) semi analytical solution, drawdown in a pancake horizontal fracture was modelled. In Figure 5.34, a series of modelling results for a dimensionless aquifer thickness h_d = 0.1 ($h_d = h/r_f \sqrt{(K_h/K_v)}$) and various F_{CD} is presented. The values published by Valkó & Economides (1997) for $F_{CD} \geq 100$ (infinite conductivity case) and F_{CD} = 0.1 (finite conductivity case) are visualized as dots. The fit is excellent for both cases. However, the curve for F_{CD} = 0.1 is published by Valkó & Economides (1997) as F_{CD} = 1. It is assumed that these data have been erroneously labelled in their publication. For the published dimensionless time range (t_d from 0.01 to 30), the curve corresponding to F_{CD} = 10 almost coincides with the curve for infinite conductivity and they probably missed it. Consequently, the next published curve was wrongly labelled as F_{CD} = 10, although in reality it corresponds to F_{CD} = 1. Progressively, the F_{CD} = 1 curve should be F_{CD} = 0.1.

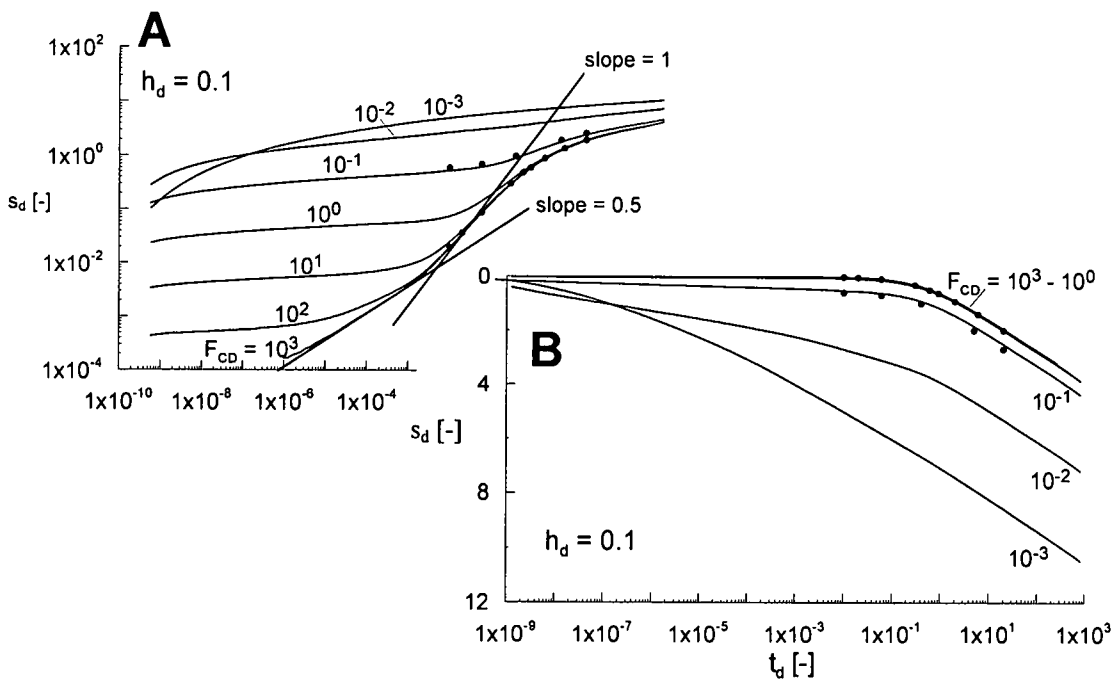

Figure 5.34. Drawdown in a pumped well calculated for the infinite conductivity pancake fracture and selected values of F_{CD} (solid lines). The data published by Valkó & Economides (1997) are represented by dots (F_{CD} = 0.01 and 100). The set of type curves are calculated for h_d = 0.1. For practical purposes, the curves for $F_{CD} \geq 100$ correspond to the infinite conductivity case ($s_d = 2 \cdot \pi \cdot T \cdot s/Q$, $t_d = T \cdot t/S \cdot r_f^2$)

The findings from Figure 5.34 can be summarized as follows:

- at early time, linear flow appears in the infinite conductivity case ($F_{CD} \geq 100$), which is indicated by a slope of 0.5
- the slope of 1 in the transient phase is not fully developed because the value of h_d is not small enough (compare Figure 4.45 in Section 4.5.2)
- if the flow behavior of finite conductivity vertical features is transferred to the horizontal penny-shape fractures, a bilinear flow phase with a slope of 0.25 should appear at early time. However, the drawdown curves for $F_{CD} < 100$ show no characteristic slope
- all curves reach the radial-acting flow at $t_d = 10$

An additional comparison with data published by Valkó & Economides (1997) is presented in Figure 5.35 for $h_d = 1$. Again, the Valkó & Economides (1997) values are visualized with dots. In general the modelled results coincide with the published data, except for the infinite conductivity case ($F_{CD} \geq 100$) at early time, where the slope is larger than 0.5. It is assumed that this published curve corresponds to a dimensionless aquifer thickness $h_d < 1$. Further, the same labelling error explained above is observed in this case.

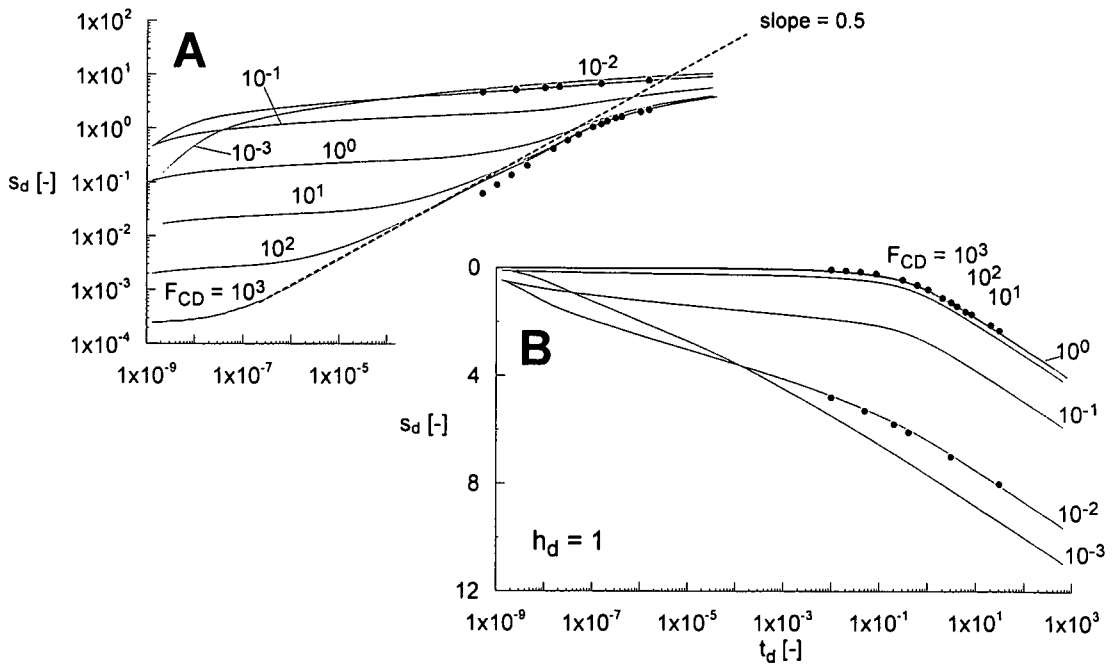

Figure 5.35. Drawdown in a pumped well calculated for the finite conductivity pancake fracture and selected values of F_{CD} (solid lines). The curves published by Valkó & Economides (1997) are represented by dots ($F_{CD} = 0.01$ and 100). A value of $h_d = 1$ was used for the calculations. For practical purposes, the curves for $F_{CD} \geq 100$ corresponds to the infinite conductivity case ($s_d = 2 \cdot \pi \cdot T \cdot s/Q$, $t_d = T \cdot t / S \cdot r_f^2$)

Summarizing, Figure 5.35 shows that:

- drawdown curves for $F_{CD} \leq 1$ could be misinterpreted as double porosity, especially when the early time data are influenced by well bore storage effects
- drawdown for higher values of F_{CD} (≥ 100) are characterized by a linear formation flow (slope of 0.5), which is typical for fractures with infinite conductivity
- all curves reach the radial flow phase at $t_d = 10$

It has been demonstrated that the numerical model is able to reproduce the semi analytical solution from Valkó & Economides (1997) for both finite flux and infinite flux. Due to the fact that the uniform flux solution from Gringarten & Ramey (1974) and the infinite flux solution differ significantly, a new set of type curves for the infinite solution and various h_d is computed and presented in Figure 5.36. This set can be used for the evaluation of pumping test data measured in a horizontal pancake fracture with infinite conductivity and infinite flux.

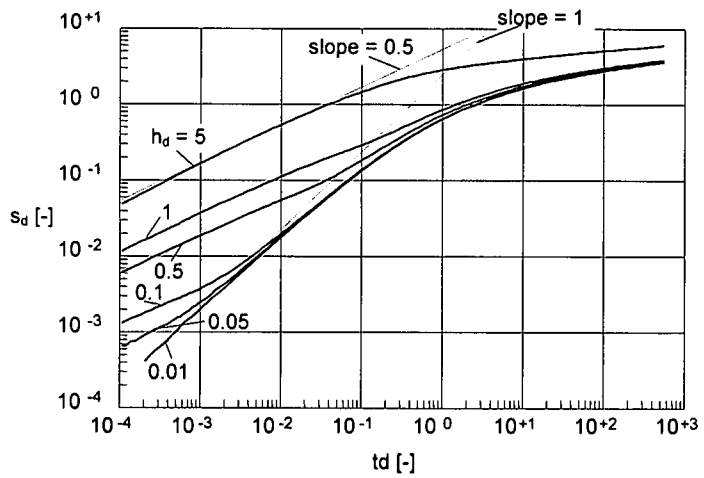

Figure 5.36. Drawdown type curves in a pumped well located in a horizontal penny-shape fracture with infinite conductivity and infinite flux ($s_d = 2 \cdot \pi \cdot T \cdot s/Q$, $t_d = T \cdot t / S \cdot r_f^2$)

5.3.5.1 Influence of fracture geometry

The drawdown curve calculated in a well that intersects a penny-shape fracture is compared with the drawdown modelled for a square fracture with the same influx area (Fig. 5.37). The coincidence of the curves leads to the conclusion that a penny-shape horizontal fracture can be represented by a square fracture, as long as the influx areas are the same (Fig. 5.38) or:

$$\pi \cdot r_f^2 = a \cdot a \qquad (5.3)$$

where
r_f = radius of the penny-shape fracture [L]
a = side length of the square fracture [L]

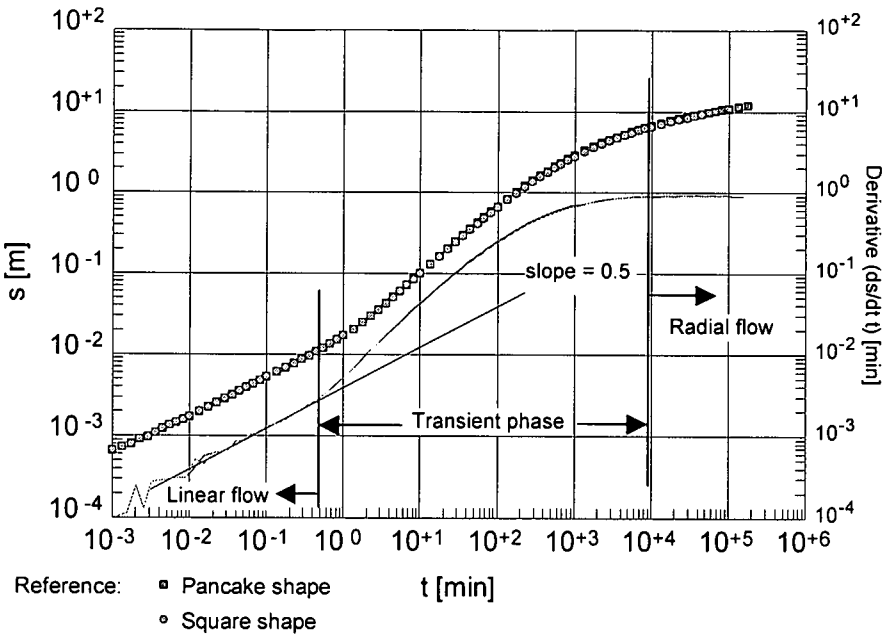

Figure 5.37. Drawdown in a pumped well located in a pancake fracture for h_d = 0.1 and F_{CD} = 1000 compared with the drawdown calculated for a square fracture with the same characteristics and equal influx area. The derivatives are plotted as solid lines in the lower part of the graph

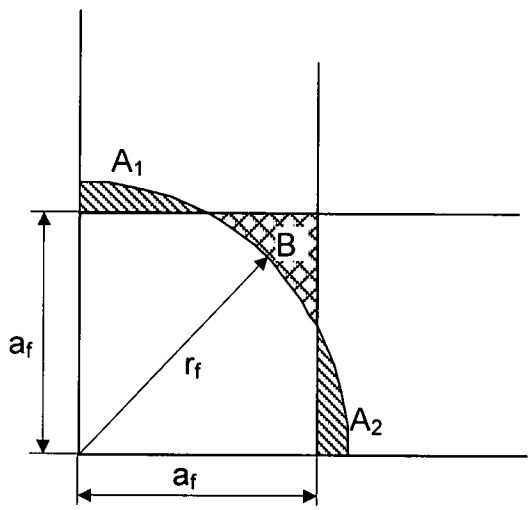

$$A_1 + A_2 = B$$

$$a_f \cdot a_f = \pi \frac{r_f^2}{4}$$

Figure 5.38. Area equivalence between a penny-shape fracture and a square fracture. The sum of the areas A1 and A2 represents the area B, r_f is the radius of the penny-shape fracture, a_f is the half-side length of the square fracture

However, natural bedding planes have not necessarily a penny-shape or a square shape. Due to the heterogeneous genesis, they can have very various shapes. To investigate the influence of the shape on the drawdown in a well, the area of fracture in the centre of the model is varied from a square to a line (one cell row or line fracture) by decreasing the width length a_w. In this process, the aperture (w) and half-length of the fracture (a_f) are maintained constant (Fig. 5.39). Because these

fractures do not have a penny-shape, a new dimensionless aquifer thickness $h_{d\text{-}hor}$ is defined as follows:

$$h_{d-hor} = \frac{h}{a_f}\sqrt{\frac{K_h}{K_v}} \qquad (5.4)$$

where
h = aquifer or formation thickness [L]
a_f = side half-length of a rectangular fracture [L]
K_h = horizontal matrix or formation conductivity [LT^{-1}]
K_v = vertical matrix or formation conductivity [LT^{-1}]

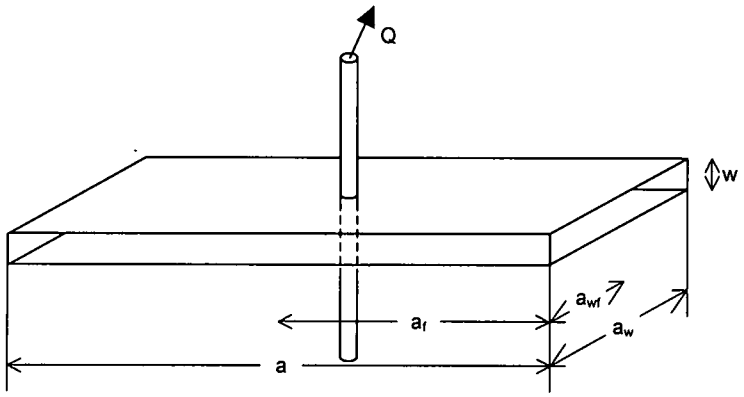

Figure 5.39. Schematic representation of a horizontal rectangular fracture

Figure 5.40 presents drawdown curves, which are computed for dimensionless aquifer thickness $h_{d\text{-}hor}$ = 0.01. An infinite conductivity horizontal fracture is included in the centre of the model. To allow a comparison of the curves, a normalization of the data is performed. This is achieved using the relative fracture half-width b_r that is defined as

$$b_r = \frac{a_{wf}}{a_f} \qquad (5.5)$$

where
a_{wf} = width half-length of a rectangular fracture [L]
a_f = side half-length of a rectangular fracture [L]

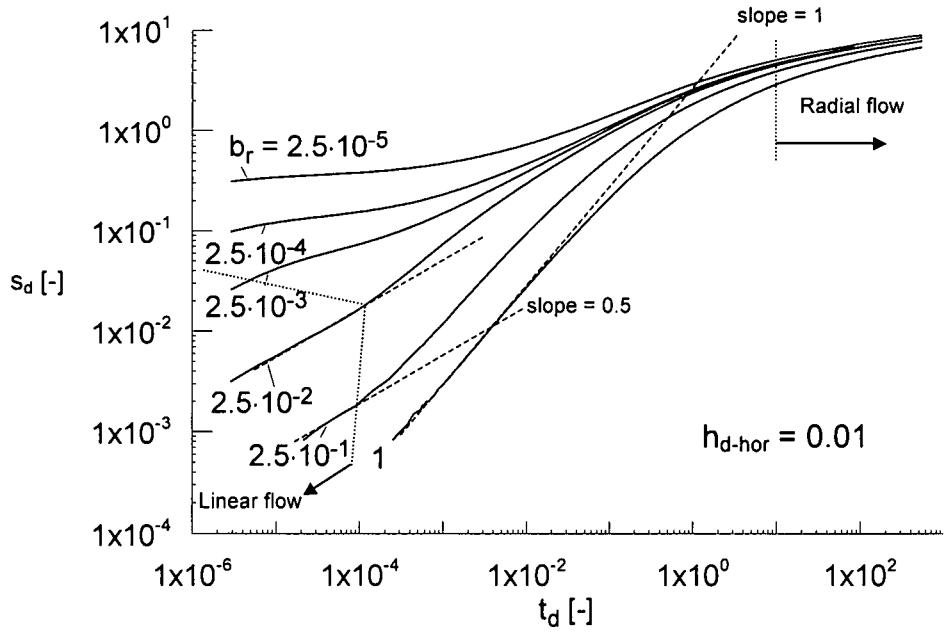

Figure 5.40. Normalized drawdown curves for a pumped well located in an infinite conductivity bedding plane, $h_{d\text{-}hor} = 0.05$, and various relative fracture half-width b_r. The curve for $b_r = 1$ corresponds to the drawdown in the penny-shape horizontal fracture, the curve for $b_r = 0.000025$ is identical to that of a horizontal well with infinite flux. The slope of 0.5 indicates linear flow ($s_d = 2 \cdot \pi \cdot T \cdot s/Q$, $t_d = T \cdot t / S \cdot a_f^2$)

Figure 5.40 can be summarized as follows:

- the drawdown in a well located in a square fracture ($b_r = 1$) is similar to the drawdown of in penny-shape fracture with a radius of $r_f = (4 \cdot b_r x_f / \pi)^{1/2}$
- for very small values of b_r (line fracture), the drawdown is that of a horizontal well. The early time data is dominated by a radial flow around the well axis in the y-z plane followed later by a transient phase and a formation radial flow phase in the x-y plane
- the dotted lines indicate both the end of the linear flow and the start of the radial flow for the different b_r. The area in between represents the transient phase

The influence of the geometry on finite conductivity horizontal fractures is investigated following the same procedure as above. Due to the fact that only the fracture geometry varies for each curve, the value of dimensionless fracture conductivity F_{CD} varies as well. Therefore, it is not possible to set a unique value for the whole graph. The computed curves are visualized in Figure 5.41 for various b_r and $h_{d\text{-}hor} = 0.05$.

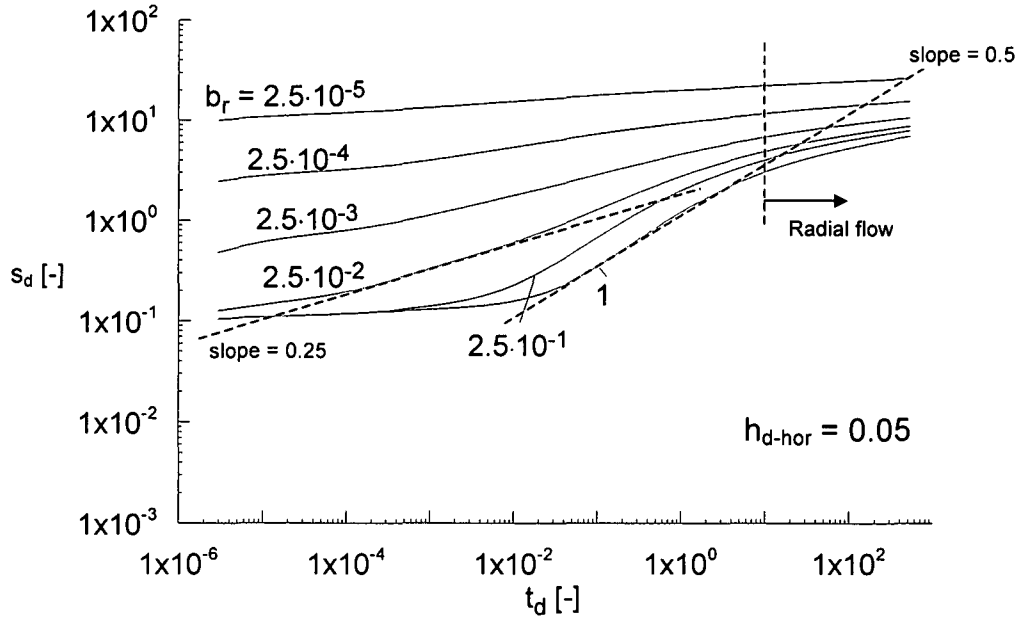

Figure 5.41. Normalized drawdown curves for a pumped well located in a finite conductivity bedding plane, $h_{d\text{-}hor} = 0.05$, and various relative widths b_r. The curve for $b_r = 1$ corresponds to the drawdown in the penny-shape horizontal fracture ($s_d = 2 \cdot \pi \cdot T \cdot s/Q$, $t_d = T \cdot t / S \cdot a_f^2$)

Figure 5.41 can be summarized as follows:

- at very early time, the drawdown curves for large values of b_r (1 and 0.25) show a kind of radial flow within the fracture itself. Once the cone of depression reaches the fracture boundaries, a slope of 0.5 develops that corresponds to linear flow
- for $b_r = 0.025$, a flow phase with a slope of 0.25 typical for bilinear flow appears at early time (t_d between 10^{-4} and 10^{-2}). A plausible explanation for this behavior is that the cone of depression reaches first the closest two boundaries of the relatively narrow fracture and a channel flow type sets (Ehlig-Economides & Economides, 1985), which is superposed by leaky from the matrix. The slope increases later, during the transient phase, when the other two boundaries are reached
- for small values of b_r (0.0025 to 0.000025), the drawdown behavior reminds that of a horizontal line source, where the early time data is dominated by a radial flow around the well axis in the y-z plane followed later by a transient phase and a formation radial flow phase in the x-y plane. However, these curves could be misinterpreted as drawdown curves in double porosity aquifers
- the dotted line at $t_d = 10$ indicates the start of the formation radial flow phase for the different b_r

5.3.5.2 Influence of the horizontal extension of the bedding plane

To investigate the influence of the horizontal extension of the bedding plane on the drawdown development, two computations are performed:

- a finite extent fracture modelled as a square fracture of 800 m x 800 m x 0.01 m located in the centre of the model (the model dimensions are 40,000 m x 40,000 m x 20 m)
- an infinite extent fracture modelled as a fracture that extends throughout the entire model area

The properties used for the matrix-fracture system are:

- a constant specific storage coefficient $S_s = 0.00001\ m^{-1}$ for the whole model
- matrix horizontal hydraulic conductivity $K_h = 10^{-5}$ m/s
- matrix vertical hydraulic conductivity $K_v = 5 \cdot 10^{-7}$ m/s
- fracture horizontal and vertical hydraulic conductivity $K_f = 0.14$ m/s

These values lead to a dimensionless aquifer thickness $h_d = 0.2$ and a dimensionless fracture conductivity $F_{CD} = 0.1$ for the finite fracture. The calculated drawdown curves for both the finite and the infinite extent fractures are presented in Figure 5.42.

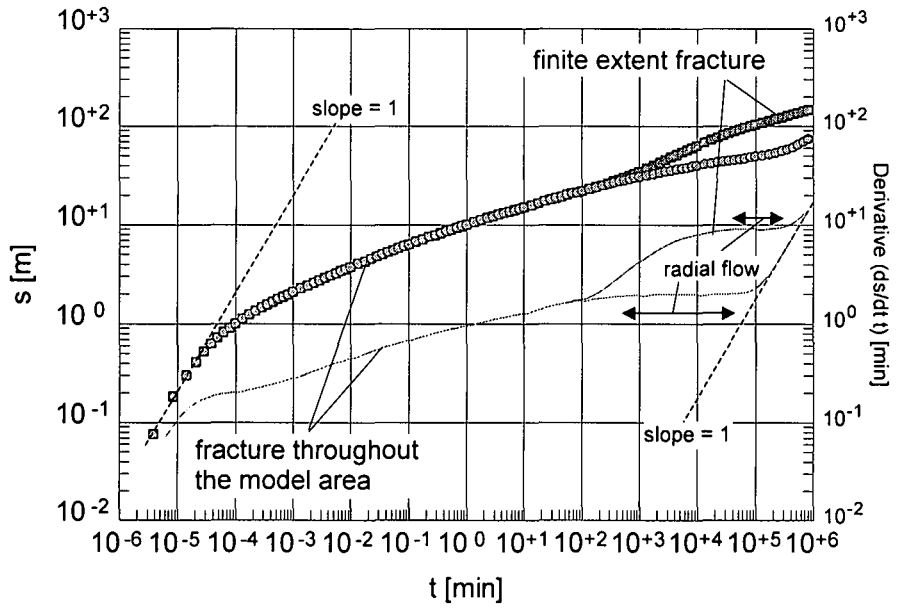

Figure 5.42. Comparison of the drawdown computed for a pumped well located in a bedding plane of limited extent (squares) and a horizontal fracture throughout the model area (dots). Both cases are computed considering finite conductivity fractures. The solid lines indicate the derivatives of the drawdown curves

Summarizing, Figure 5.42 shows that:

- at early time a slope of 1 is observed in both drawdown curves, which is due to cell storage (equivalent to well bore storage)
- after the cell storage, the drawdown curve for both the infinite and finite extent fractures shows a transient phase, which ends at t = 500 minutes. This phase is characteristic for flow in horizontal fractures (compare Fig. 5.34 for finite conductivity and Fig. 5.36 for infinite conductivity)
- from t = 500 minutes, a radial flow phase characterized by a horizontal derivative sets in the case of the infinite extent fracture. The analysis of this radial-acting phase with the common straight-line methods allows the estimation of the fracture-matrix transmissivity, which is the arithmetic mean of each of the system components (Matheron, 1967). The influence of the closed model boundaries (slope of 1) starts at approximately $t = 5 \cdot 10^4$ minutes
- from t = 500 minutes, the finite extent fracture case shows a transition phase up to a time $t = 5 \cdot 10^4$ minutes. Thereafter, a radial-acting flow phase develops within

the matrix. This radial-acting flow phase appears later than in the infinite extent case. The matrix transmissivity can be determined using the radial flow phase and applying the Cooper-Jacob (1946) method. The influence of the closed model boundaries (slope of 1) starts at approximately $3 \cdot 10^5$ minutes

Figure 5.43 shows the drawdown curves obtained applying the same methodology to high conductivity fractures.

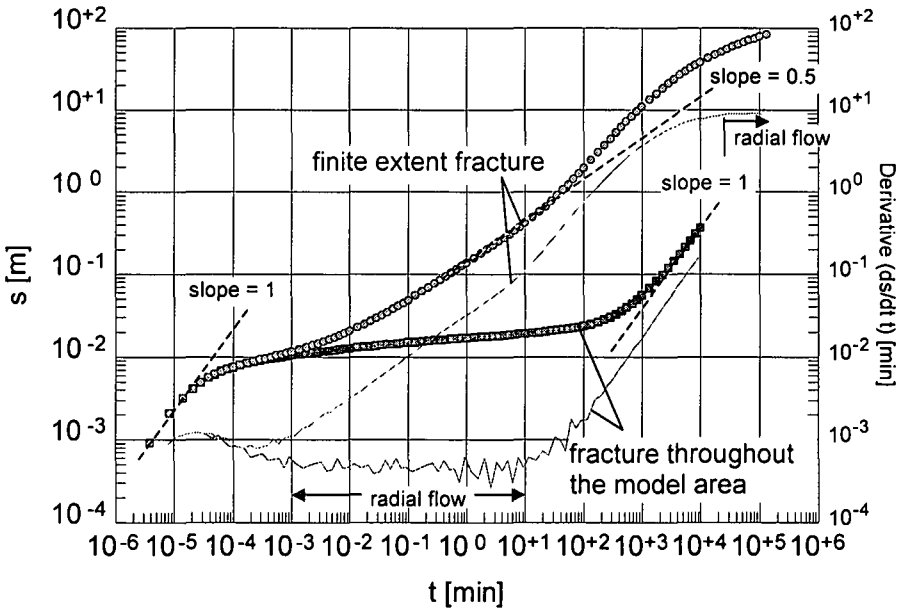

Figure 5.43. Comparison of the drawdown computed for a pumped well located in a bedding plane of limited extent (dots) and a horizontal fracture throughout the model area (squares). Both cases are computed considering high conductivity fractures. The solid lines indicate the derivatives of the drawdown curves

Figure 5.43 can be summarized as follows:

- both curves show an initial cell storage (slope of 1), which is equivalent to the well bore storage. This effect disappears at approximately $t = 3 \cdot 10^{-3}$ minutes
- after the cell storage, the drawdown curve for the infinite extent fracture shows only radial acting flow up to t = 10 minutes, where the influence of the model boundaries becomes visible (slope of 1). A linear flow phase does not develop because the cone of depression within the fracture does not have a lateral limitation and can therefore expand infinitely. The analysis of the radial-acting phase with the Cooper-Jacob (1946) method allows the estimation of the fracture-matrix transmissivity, which is the arithmetic mean of each of the system components (Matheron, 1967)
- after the cell storage, the drawdown curve for the limited fracture shows a linear formation flow characterized by a slope of 0.5. During this phase, the matrix provides the extracted water through the top and bottom of the fracture. A radial-acting flow sets at $t = 5 \cdot 10^4$ minutes. This radial-acting flow phase appears later than in the infinite extent case. The matrix transmissivity can be determined using the radial flow phase and applying the Cooper-Jacob (1946) method. In this case, the closed model boundaries were not reached within the computed time

5.3.6 Parallel horizontal structures

To investigate the influence of parallel horizontal fractures three equidistant bedding planes are included in the centre of the model (Fig. 5.44). A fully penetrating well is considered in the centre of the cube.

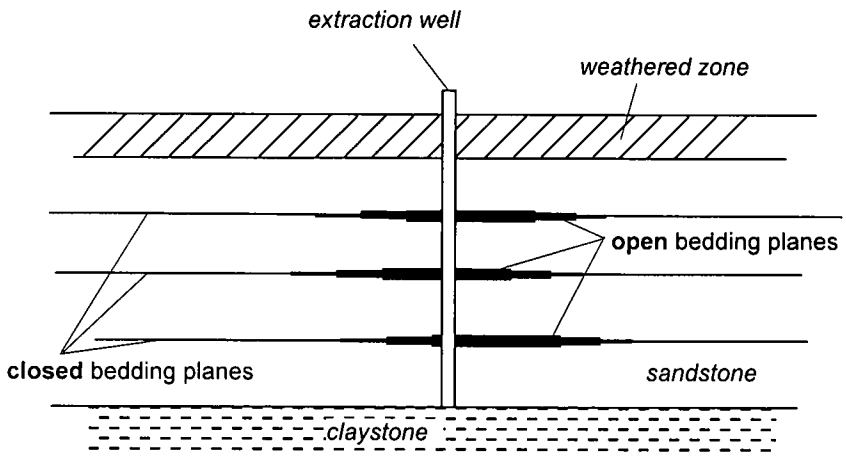

Figure 5.44. Example of parallel horizontal open bedding planes embedded in a layered sandstone aquifer intersected by a well

Figure 5.45 shows a comparison of the drawdown calculated with three parallel infinite conductivity horizontal fractures and the corresponding drawdown in a single bedding plane for $h_d = 0.3$. Each horizontal feature has a dimensionless fracture conductivity $F_{CD} = 250$.

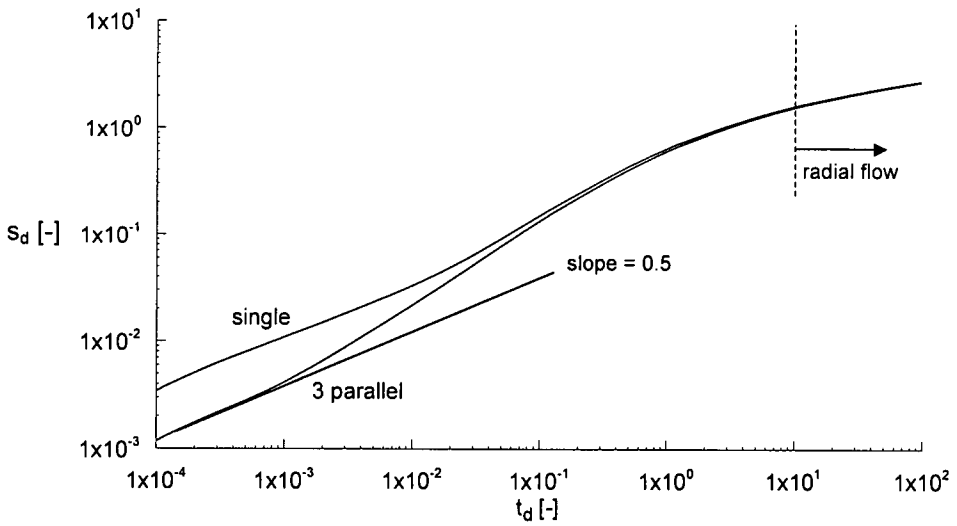

Figure 5.45. Comparison of the drawdown in a pumped well located in a single horizontal bedding plane and that of three horizontal parallel fractures for $h_d = 0.3$. All fractures have infinite conductivity ($F_{CD} = 250$, $s_d = 2 \cdot \pi \cdot T \cdot s/Q$, $t_d = T \cdot t / S \cdot r_f^2$)

Summarizing, Figure 5.45 shows that:

- in both curves, linear flow appears at early time (slope of 0.5), which is followed by a transient phase. The radial-acting flow sets at $t_d = 10$
- lesser drawdown is observed in the three parallel fractures at early time due to the increased conductivity of the fracture-matrix system

- the shape of the drawdown curve in parallel horizontal fractures is equivalent to that of a single bedding plane. Therefore, for a correct evaluation of the test, additional on-site information is required

Due to the lesser drawdown at early time, the fitting of the curve produced by more than one horizontal fracture to a type curve calculated for a single horizontal bedding plane (for example Fig. 5.36) would result in an underestimation of the h_d value ($h_d = h/r_f \cdot \sqrt{(K_h/K_v)}$). Assuming that the aquifer thickness (h) and the horizontal and vertical matrix conductivities (K_h and K_v) are known, the underestimation of h_d will lead to an over estimation of the fracture equivalent radius (r_f).

5.3.7 Combination of vertical and horizontal features

The typical geological structure that can be considered as crossed single fractures is the vertical fault zone connected to open bedding planes (Fig. 5.46).

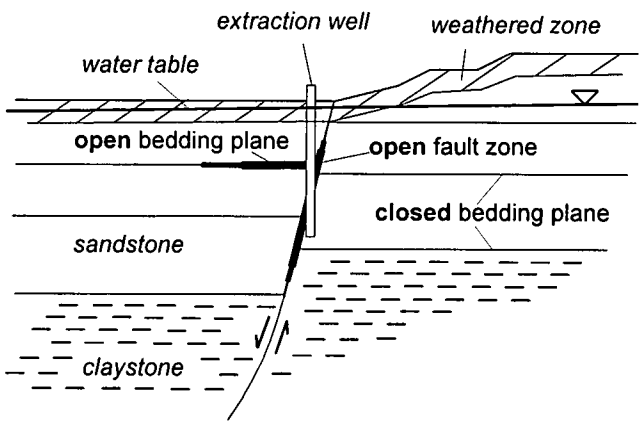

Figure 5.46. Example of a cross section through a typical tectonic fault situation. The arrows indicate the direction of relative movement. The upper part of the fault (closed to the surface) is assumed to be sealed, due to weathering processes. The upper bedding plane is open on the left hand side due to shear forces and closed on the right hand side due to compression forces

The numerical model was applied to this situation with following simplified geometry and basic parameters:

- infinite, homogeneous, confined aquifer
- no recharge
- constant aquifer thickness h = 20 m
- matrix conductivity tensor $K = 10^{-5}$ m/s
- bedding plane location z = 10 m
- bedding plane aperture w = 0.01 m
- bedding plane half-length $a_f = 400$ m
- bedding plane half-width $a_{fw} = 10$ m
- bedding plane conductivity tensor $K_f = 1$ m/s (finite case) or 1000 m/s (infinite case)
- vertical, fully penetrating fault
- fault aperture w = 0.01 m

- fault half-length $x_f = 400$ m
- fault conductivity tensor $K_f = 1$ m/s (finite case) or 1000 m/s (infinite case)
- specific storage coefficient $S_s = 10^{-5}$ [L^{-1}], constant for the whole aquifer system
- extraction rate of the fully penetrating well $Q = 40$ m³/d

The horizontal fracture parameters lead to $b_r = 0.025$ and $h_{d\text{-}hor} = 0.05$. In the case of the vertical fracture $C_r = 0.8$ (finite conductivity case) and $C_r = 800$ (infinite conductivity case).

The results of the calculations are graphed in Figures 5.47 to 5.50. All figures show the drawdown curve of each single case (bedding plane and vertical fault) and the combination of both.

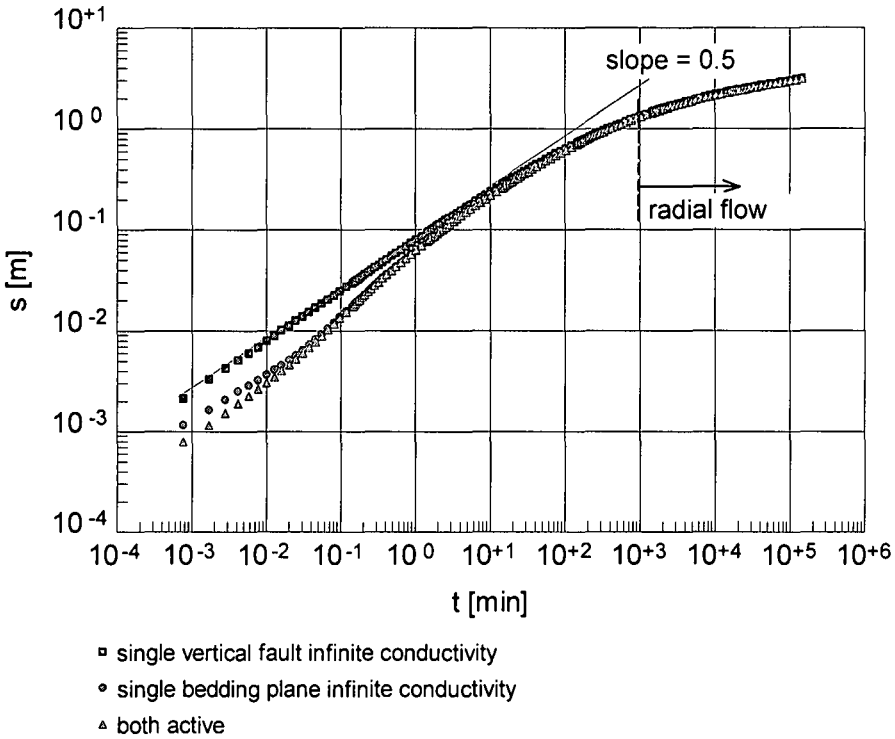

Figure 5.47. Drawdown of a pumped well located in a single vertical fault, a single horizontal bedding plane (both with infinite conductivity), and a combination of both

The findings from Figure 5.47 are:

- the drawdown in the single vertical fault at early time has a slope of 0.5 which, according to Gringarten *et al.* (1974), indicates linear formation flow phase in an infinite conductivity fracture case
- the drawdown in the single bedding plane shows linear flow at very early time (slope of 0.5). The drawdown behavior is similar to that of the type curve for $b_r = 0.025$ and $h_{d\text{-}hor} = 0.05$ in Figure 5.40 (Section 5.3.5.1)
- at very early time, the drawdown in the combination of the single infinite conductivity vertical and the horizontal features is smaller than that of both single drawdown curves. This is due to the increased inflow area in the intersection of the fractures, where the fully penetrating well is located. After 0.1 minutes, the drawdown curve for the intersected features coincides with the drawdown in the single horizontal feature. Therefore, additional information is necessary for a correct evaluation of this combination case

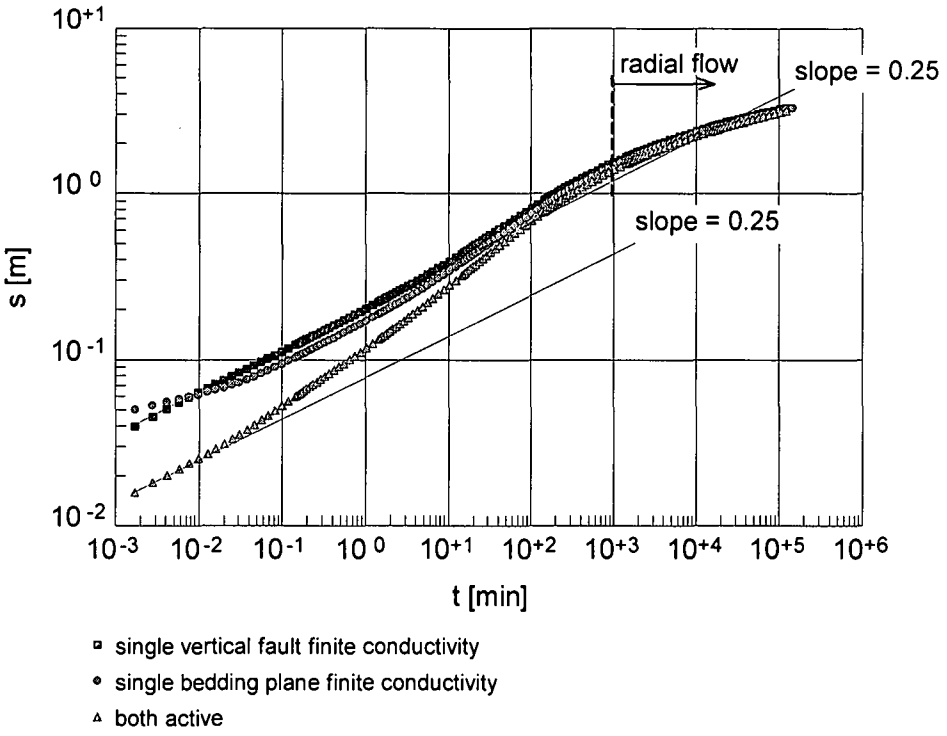

Figure 5.48. Drawdown of a pumped well located in a single vertical fault, a single horizontal bedding plane (both with finite conductivity), and a combination of both

In Figure 5.48, the intersection of single finite conductivity horizontal and vertical features is presented. Following results can be summarized from the graph:

- the drawdown in the single vertical fault at early time shows a slope of 0.25 which, according to Cinco-Ley *et al.* (1978), indicates the bilinear flow phase in a finite conductivity vertical fracture
- the drawdown in the single bedding plane shows a slope of 0.25 which, in this case, means the superposition of channel flow and leakage from the matrix. This effect was described in Section 5.3.5.1 for the finite conductivity type curves (b_r = 0.025 and $h_{d\text{-}hor}$ = 0.05 in Fig. 5.41)
- The drawdown of the combination of both features is significantly smaller than the drawdown of the single cases, due to the increased inflow area. At very early time the curve shows bilinear flow as in the single vertical feature, but the transient period is not similar to any of the two single cases. Again, a correct evaluation of a combination of this type is impossible without additional information from the field

Figure 5.49 shows the drawdown in the intersection of a vertical fracture with infinite conductivity and a finite conductivity bedding plane. Following results can be derived from the graph:

- the drawdown in each of the single cases is already described in Figure 5.47 and Figure 5.48
- the drawdown of the combined case is smaller than each of the single cases, due to the increased inflow area. At very early time, it shows linear flow as in the single vertical case with infinite conductivity. Nevertheless, the overall curve

shape resembles the drawdown in an infinite conductivity horizontal penny-shape fracture for $h_d \leq 1$ and highlights the fact that previous knowledge of the fault situation is necessary for a correct evaluation of the data

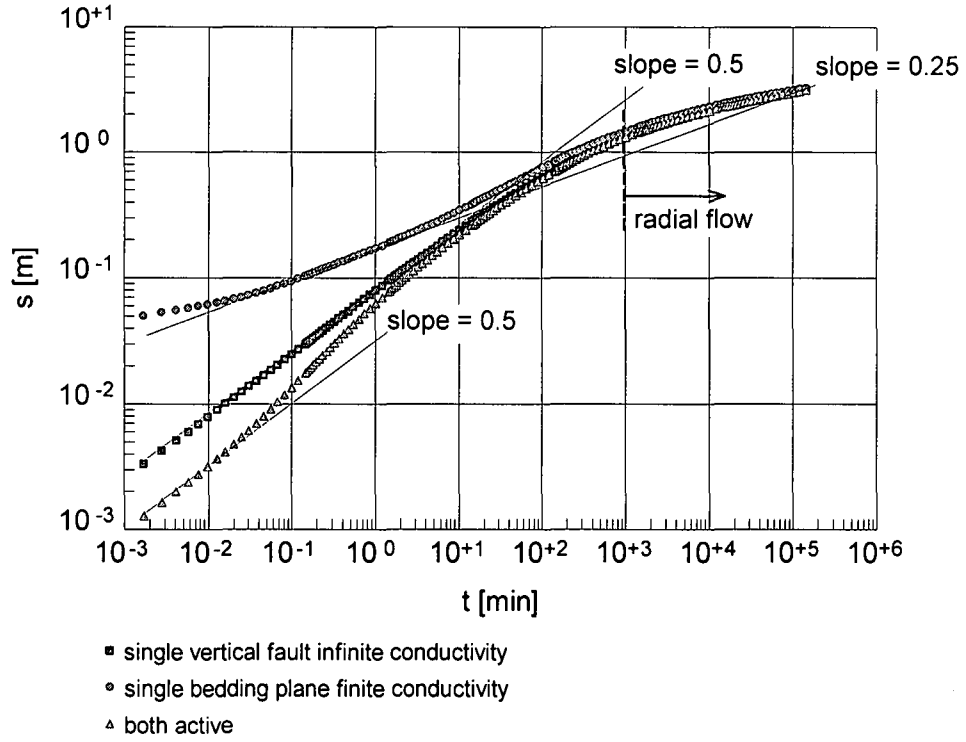

Figure 5.49. Drawdown of a pumped well located in a single vertical fault (with infinite conductivity), a single horizontal bedding plane (with finite conductivity), and a combination of both

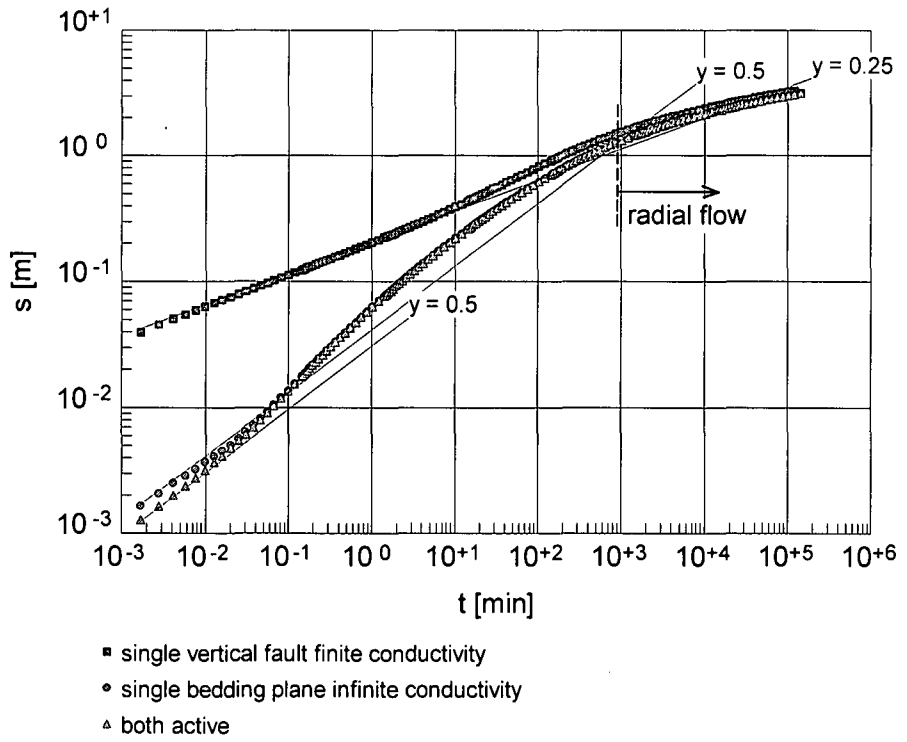

Figure 5.50. Drawdown of a pumped well located in a single vertical fault (with finite conductivity), a single horizontal bedding plane (with infinite conductivity), and a combination of both

Figure 5.50 shows the drawdown in an intersection of a vertical fault with finite conductivity and an infinite conductivity bedding plane. Following results can be derived from the graph:

- the drawdown of the single cases is already described in Figure 5.47 and Figure 5.48
- the drawdown of the combined case is similar to that of the horizontal infinite conductivity bedding plane, but it is slightly smaller at very early time, due to the increased inflow area. Again, additional information from the field is necessary to correctly evaluate such a combination

The calculated examples show that in general it is impossible to draw definite conclusions on the geological set up, if only the produced drawdown curve is observed. Additional on-site information is necessary. Further, following general rules can be summarized:

- if both single features have infinite conductivity, the shape of the drawdown in the intersection of the features is similar to that of the horizontal fracture
- if both features have finite conductivity, the shape of the drawdown in the intersection of the features resembles that of the horizontal bedding plane
- if one of the single features has infinite conductivity and the other finite conductivity, the shape of the drawdown in the intersection of faults is governed by that of the single infinite conductivity case
- in all cases, the matrix transmissivity can be evaluated applying the Cooper-Jacob (1946) method to the radial-acting flow data

5.4 Discussion of results

This part of the thesis was aimed to study whether more complex discontinuous fracture networks have significant influence on drawdown curves. To investigate this issue, various plausible structural situations were modelled and synthetic pumping test curves were computed. Following this methodology, it was found that:

- common numerical modelling are capable of reproducing the analytical and semi analytical solutions for single feature cases. However, due to the long computational time needed (e.g. 3 days were needed for the computation of drawdown in the crossed fractures case), it is not an appropriate method for the day-to-day analysis of pumping tests
- for all practical purposes, the fracture/fault storage does not have influence on the drawdown curve in single vertical fractures with infinite or finite conductivity, if $CD_f \leq 10^{-4}$ ($CD_f = S_f w/(\pi \cdot S \cdot x_f)$). This observation confirm the findings of Cinco-Ley *et al.* (1978)
- drawdown in finite conductivity vertical fracture/faults with considerable width and limited extent present a radial flow phase within the fracture. In cases of larger CD_f, this effect can be misinterpreted with double porosity
- parallel vertical structures with infinite or finite conductivity ($Cr \geq 100$ or $Cr < 0.01$, $Cr = T_f w/(\pi \cdot T \cdot x_f)$) have no influence on the drawdown. Further, parallel vertical structures with Cr in the range of $0.01 \leq Cr < 100$ show minor influences at early time, if the dimensionless relative separation s_r ($s_r = d_f/x_f$) is

less than 0.125. However, for all practical purposes, it can be concluded that parallel vertical fractures do not have influence on the drawdown

- the drawdown computed in the combination of vertical fractures with infinite conductivity (crossed or bend fractures) differs significantly from the drawdown measured in the single straight fracture. However, the results are comparable to the drawdown obtained with the uniform flux solution, although the influx along the fracture is not uniform. Gringarten *et al.* (1974) mentioned that some field data from hydraulic fracturing fit better the uniform flux solution. The results of this work give reasons to believe that such field data are attributed to more complex fracture networks similar to those studied here
- horizontal penny-shape fractures and horizontal square features with equivalent influx area have the same drawdown
- the findings of this part show that infinite flux is common in cases of infinite conductivity horizontal bedding planes. Therefore, a new set of type curves for this kind of influx is presented. Pumping test data can be evaluated using these curves
- horizontal rectangular fracture shapes have a significant influence on the drawdown. In the case of narrow fractures, it is possible to identify channel flow superposed by linear formation flow (leaky) that results in a slope of 0.25 in a log-log plot. Further, it is found that the drawdown in an extremely narrow horizontal fracture is equivalent to that of a horizontal line source (horizontal well)
- if the dimensionless aquifer thickness $h_{d\text{-}hor}$ ($h_{d\text{-}hor} = h/a_f \cdot \sqrt{(K_h/K_v)}$) of a horizontal fracture is known, it is possible to draw a set of type curves that depend on the fracture shape, as shown in Section 5.3.5.1. Consequently, fitting field data to one of these type curves allows the identification of the fracture shape
- drawdown in horizontal finite conductivity bedding planes ($F_{CD} \leq 1$, $F_{CD} = K_f \cdot w/(12 \cdot K_e \cdot r_f)$) can be misinterpreted as double porosity, especially if the drawdown curve is affected by well bore storage. A misinterpretation as double porosity can also occur in the analysis of drawdown curves measured in very narrow horizontal fractures
- the shape of the drawdown curve in parallel horizontal fractures is equivalent to that of the single horizontal bedding plane. Therefore, without additional on-site investigations it is impossible to determine whether the drawdown belongs to a single fracture or to a series of parallel features. Further, the evaluation of the fracture radius depends on h_d ($h_d = h/r_f \cdot \sqrt{(K_h/K_v)}$). If the drawdown curves from parallel fractures are fitted to types curves for single bedding planes, h_d is underestimated which, in turn, results in an overestimation of the fracture radius. This effect is very important, especially for the interpretation and evaluation of transport mechanisms as well as for the design of well protection zones
- the drawdown curve in horizontal bedding planes with infinite extent and infinite conductivity follows the Theis curve, whereas in the case of finite conductivity, the radial flow phase sets after a relatively long transient phase, probably due to the leakage from the matrix. The evaluation of the radial flow phase using the common methods allows the determination of the fracture-matrix transmissivity, which is the arithmetic mean of both components. The correct evaluation of such fracture-matrix systems is of high importance for transport mechanisms and the design of well protection zones

- the results of the calculated examples show that the intersection of vertical and horizontal structures always leads to drawdown curves that could be misinterpreted with drawdown curves of single cases. Drawdown in intersections of vertical and horizontal fractures, where at least one of them has infinite conductivity, plots similar to the infinite single case. If both features have finite or infinite conductivity, the drawdown plots similar to the single horizontal fracture. Therefore, additional on-site information is necessary to identify the real situation. This issue is very important, especially for the interpretation and evaluation of transport mechanisms as well as for the design of well protection zones

6. CONCLUSIONS

Chapter 2: Basics on Reservoirs and Well Effects

The main conclusions that can be drawn from this chapter are:

- a new idea for the interpretation of well bore storage was derived by comparing its effects with the concept of drawdown in a closed aquifer
- it is shown that the time series of the well bore skin plots horizontal during the radial-acting flow phase. This effect can be used as a diagnostic tool to identify this flow period
- if different skins (well bore skin, fracture skin, partial penetration skin, and pseudo-skin) appear simultaneously, their effects are superposed. This means that the positive effects of pseudo-skin (reduced drawdown) could be destroyed by the presence of other skins (for example well bore skin). Therefore, the analysis of skin effects must is very important in the evaluation of pumping test data
- the physical and hydrological processes that take place during fracture dewatering are described and an example is presented. Generally, it is recommended that the test be redone at a lower pumping rate to avoid dewatering, if the estimation of aquifer parameters is of interest

Chapter 3: Flow Diagnostics

The main conclusions from this chapter can be summarized as:

- it is emphasised that the development of the cone of depression is time-dependent, but does not depend on the extraction rate. Therefore, a pumping test aimed to determine the aquifer parameters should be planned to run over relatively long time (2 to 3 days) at a rate that produces a measurable drawdown in the extraction well and the observation wells
- basic instructions for the analysis of pumping test data from fractured media are introduced. It is emphasised that the comparison of the drawdown and the time-corrected recovery curves is a power tool to identify irregularities during the test, for example unreported variations in the extraction rate
- it is shown that in a system composed of a single vertical fracture embedded in a matrix, the correct evaluation of the storage coefficient using the common methods (Jacob or Theis) is only possible, if the observation well is located at a distance of 1.5 to 5 times the half-length of the fracture. This distance depends strongly on the direction of the observation well to the fracture and the relative fracture conductivity Cr (contrast between the fracture transmissivity and the matrix transmissivity). However, for practical purposes, a distance of 3 times the half-length of the fracture is sufficient. This distance is recognised as the limit of the REV. The drawdown in any observation well located further away shows the behavior of the homogeneous media and therefore, leads to the correct evaluation of the storage coefficient

- it is shown that the radial-acting flow in a fracture-matrix system sets once the cone of depression overcomes the REV of this system
- a new method for the determination of skin location in infinite conductivity fractures or faults is presented. It is shown that the location can be uniquely identified, if the pumping well and at least one observation well are located within the same structure

Chapter 4: Analytical Models for Evaluation of Pumping Tests in Fractured Aquifers

The main conclusions from this chapter are:

- the computer program TPA is introduced. The program allows for curve diagnosis, test data evaluation, and forward modelling using the analytical and semi analytical methods that are described in this chapter (homogeneous fractured case, and single vertical and horizontal features with finite and infinite conductivity). The ability of the program to reproduce this solutions is demonstrated on published data and field examples
- a new set of type curves for single vertical fractures with finite conductivity and considerable storage capacity is presented
- it is shown that the presence of a single horizontal fracture can be identified by trying to accommodate the Papadopulos curve (Theis curve that includes well bore storage) to the drawdown data. Due to the pseudo-skin effect, unrealistic large values of S will be obtained, if the field data belong to a horizontal fracture
- it is explained that in the absence of skin effects (well bore skin and fracture skin), a horizontal fracture can also be identified by applying the skin factor evaluation for primary aquifers (Section 2.4.2). Negative values of skin indicate enhanced effective radius of the well which, in fractured rock, is generally related to the presence of open features

Chapter 5: Discontinuous Fracture Network Investigation with Numerical Models

The main conclusions from the fifth chapter are:

- numerical modelling based on laminar flow is able to reproduce the analytical and semi analytical solutions for single fracture cases, if a correct set up is adopted
- at early time and for large CD_f, the drawdown in finite conductivity vertical faults with considerable width show a radial flow phase within the fracture, which can be misinterpreted with double porosity. However, this effect is most likely to appear only under unconfined conditions
- unexpectedly, it was found that parallel vertical structures play a subordinate role in the development of the drawdown in the well
- field data that fits to the uniform flux solution of Gringarten at al. (1974) can be attributed to bend or crossed vertical fractures
- a penny-shape horizontal fracture (pancake) can be replaced by a square fracture with the same influx area

- Gringarten & Ramey (1974) have published type curves for infinite conductivity horizontal penny-shape fracture with uniform flux. However, it is demonstrated that infinite flux is a more appropriate description for this kind of fractures. Therefore, a new set of type curves for infinite flux is presented
- if the cone of depression in an aquifer with open horizontal bedding planes does not reach the boundaries of the fractures during the test, the transmissivity obtained by evaluating the radial flow phase corresponds to the arithmetic mean of both components (matrix and fracture). If the presence of the fracture is not taken into account, the size of a well protection zone or the transport time will be underestimated
- it is shown that the relationship between length and width of a horizontal fracture has a significant influence on the drawdown. Fitting the field data to type curves based on the dimensionless aquifer thickness $h_{d\text{-}hor}$ ($h_{d\text{-}hor} = h/a_f \sqrt{(K_h/K_v)}$) allows the determination of this relationship
- it is shown that many cases of horizontal finite conductivity fractures could be erroneously identified as double porosity cases
- parallel horizontal fractures produce drawdown curves similar to those of single bedding planes. Fitting the drawdown curve of parallel horizontal fractures to the type curve for single horizontal bedding planes leads to an overestimation of the fracture radius
- it is demonstrated that the intersection of vertical and horizontal structures leads to drawdown curves that could be misinterpreted with drawdown curves of single cases. For a correct evaluation, additional on-site information is needed

7. SUMMARY

Fractured aquifers are characterized by the fact that most of the water flows along fractures, faults, open bedding planes, or other geological features. These features are embedded in a matrix that has either porous nature, like in sandstone, or is almost impermeable (inert), as in the case of granite.

It is often observed that in fractured aquifers the measured air lift yield is a strong overestimation of the long-term sustainable yield of the well. The explanation for this effect is that the water extracted initially is provided by a geological feature that is high yielding but limited in its extension, while the long-term sustainable yield is the response of the matrix. Such a geological feature can be among others, a single vertical fracture or a fracture network, which usually acts as a preferential flow path.

Pumping tests in primary and secondary aquifers are widely used by the ground water industry because they provide important information on the reservoir and the well performance. Various researches in the oil and ground water industries have found that the presence of single preferential flow paths results in characteristic drawdown curves. However, a lack of research is encountered, when it comes to more complex fracture networks. This work investigates the behavior of drawdown curves in fracture set ups below the representative elementary volume (REV), which is defined as the smallest volume of aquifer that can be considered as a homogeneous fractured unit. Emphasis is given to the importance of a thorough diagnosis of the data to be able to adequately estimate the aquifer properties.

Chapter 2 of the present work summarizes the basic knowledge on ground water flow in fractured reservoirs, where the REV, fracture connectivity, and conductivity contrast between fracture and matrix are defined and explained. Thereafter, the flow behavior in fractured media (linear, radial, and spherical) are described. This chapter ends with the review of various well and reservoir boundary effects, such as well bore storage, well bore skin, partial penetration skin, fracture skin, pseudo-skin, fracture dewatering, and reservoir boundaries.

Chapter 3 gives practical advice for the planning and performance of pumping tests and stresses the necessity of time correction in the case of variable discharge rate during the test. The importance of the pseudo-skin effect originated by the presence of a single vertical fracture is highlighted. It is shown that pseudo-skin effects are the reason for the apparent dependence of the storage coefficient (S) on the distance between the observation borehole and the single vertical feature, when the common evaluation methods are used for the estimation of S. Furthermore, the radial-acting flow phase and in relation to the REV is explained. This chapter ends with the description of various diagnosis tools, which allow, among others, the determination of the flow phases from pumping test data influenced by preferential flow paths. These tools are included in the computer program **T**est **P**umping **A**nalysis (TPA), which was compiled under the umbrella of this thesis. It is explained that data consistency can be rapidly analysed with the comparison between drawdown and recovery data and any discrepancy must be investigated additionally. The use of straight-lines, especial plots, and curves derivatives is described.

Chapter 4 presents the most important analytical and semi-analytical available solutions for the analysis of pumping test data in fractured aquifers, which are included in TPA. For each case, the mathematical solution is first described. The influence of well bore and reservoir effects are explained using TPA, based on theoretical and field examples. Special emphasis is given to the various skin analyses and to the possible misinterpretation of drawdown curves. The solutions presented are:

- double porosity model of Moench (1984)
- single vertical fracture with infinite conductivity and finite extent of Gringarten *et al.* (1974)
- single vertical fracture with finite conductivity and finite extent of Cinco-Ley *et al.* (1978)
- single vertical dike with finite conductivity and infinite extent of Boonstra & Boehmer (1986)
- bedding plane fracture with infinite conductivity and finite extent of Gringarten & Ramey (1974)
- generalized radial flow model for fractured reservoirs of Barker (1988)

Chapter 5 investigates more complex fracture situations with help of numerical modelling based on the Darcian law. Synthetic pumping tests are simulated and their drawdown behavior is analysed. The single vertical fracture case is first computed to ensure that the model set up leads to the analytical and semi-analytical solutions of Gringarten *et al.* (1974) and Cinco-Ley *et al.* (1978), respectively. To investigate the influence of wider fault zones, which are assumed as a homogeneous fractured zone, faults with increasing width are modelled. It is found that:

- for large storage capacities and finite conductivity, the drawdown at early time shows a radial-acting flow phase within the fault, which could be easily misinterpreted as double porosity. However, this effect occurs most likely under unconfined conditions

The model is then modified to include parallel vertical fractures. It is found that:

- parallel vertical structures with infinite conductivity have no influence on the drawdown at the well
- parallel vertical structures with finite conductivity show minor influences at early time, if the dimensionless relative separation s_r ($s_r = d_f/x_f$) is less than 0.125

Thereafter, the model is modified to represent a crossed fracture case and a bend fracture case, both vertical and with infinite conductivity. The computed drawdown differs significantly from the drawdown measured in the single straight fracture. It is found that:

- this drawdown is comparable to that obtained with the uniform flux solution of Gringarten *et al.* (1974), although the influx along the fracture is not uniform. However, the authors mentioned that some field data from hydraulic fracturing fit better to the uniform flux solution. The results of this work give reasons to believe that such field data are attributed to more complex fracture networks similar to those studied here.

The horizontal bedding plane case is also investigated. First, the model is run to compute the infinite and finite flux solutions from Valkó & Economides (1997). The modelled curves fit adequately the data for their solutions, although a labelling error in the published data is identified. Further, the influence of the fracture geometry is analysed. It is found that:

- horizontal penny-shape fractures and square features with equivalent influx area have the same drawdown
- rectangular horizontal features have a significant influence on the drawdown behavior

The investigation of parallel bedding planes shows that:

- the shape of the drawdown curve in parallel horizontal fractures is equivalent to that of the single horizontal bedding plane. Therefore, without additional on-site investigations (e.g. fluid logging or flow meter measurements) it is impossible to determine whether the drawdown belongs to a single fracture or to a series of parallel features
- The analysis of drawdown curves produced by parallel horizontal fractures using type curves for single horizontal fractures leads to an over estimation of the fracture radius. This effect is important among others, for the design of protection zones

Finally, intersections of a single vertical fracture and a single horizontal bedding plane are modelled. It is found that:

- the obtained drawdown curves could be misinterpreted with drawdown curves of single cases. Therefore, it is concluded that additional information is necessary to correctly identify the geological set up. This issue is highly important for both the design of well protection zones and the estimation of the transport time

8. REFERENCES

Abdassah D. and I. Ershaghi, 1984. Triple Porosity Models for Representing Naturally Fractured Reservoir. PhD Dissertation, USC, USA

Agarwal, R.G., 1980. A New Method to Account for Producing Time Effects when Drawdown Curves are Used to Analyze Pressure Build-up and other Test Data. SPE 9289. Society of Petroleum Engineers of AIME

Agarwal, R.G., R.D. Carter, and C.B. Pollock, 1979. Evaluation and Performance Prediction of Low-Permeability Gas Wells Stimulated by Massive Hydraulic Fracturing. SPE 6838. Society of Petroleum Engineers of AIME. Paper presented at the SPE-AIME 52nd Annual Fall Technical Conference and Exhibition held in Denver, Colorado, 9 – 12 October 1977

Al-Ghamdi A. and I. Ershaghi, 1996. Pressure Transient of Dually Fractured Reservoirs. Society of Petroleum Engineers. SPE 26959, 93 – 100

Bardenhagen, I., 1999. Skin Location at Wells Drilled in a Vertical Fault Zone. Ground Water, Vol. 37, No. 5, 764 – 769

Barenblatt, G.I., Yu.P. Zheltov, and I.N. Kochina, 1960. Basic Concepts in the Theory of Seepage of Homogeneous Liquids in Fissured Rocks. Described in: Well Testing in Heterogeneous Formations. An Exxon Monograph. T.D. Streltsova. John Wiley & Sons, New York, 413 pages

Barker, J.A., 1988. A Generalized Radial Flow Model for Hydraulic Tests in Fractured Rock. Water Resources Res., Vol. 24, No. 10, 1796 – 1804

Birsoy, Y.K. and W.K. Summers, 1980. Determination of Aquifer Parameters from Step Tests and Intermittent Pumping Data. Ground Water, Vol. 18, No. 2, 137 – 146

Boehmer, W.K. and J. Boonstra, 1986. Flow to Wells in Intrusive Dikes. PhD Dissertation, Vrije Universiteit te Amsterdam, the Netherlands

Boehmer, W.K. and J. Boonstra, 1987. Analysis of Drawdown in the Country Rock of Composite Dyke Aquifers. Journal of Hydrology, 94 (1987) 199 - 214

Boonstra, J. and W.K. Boehmer, 1986. Analysis of Data from aquifer and Well Tests in Intrusive Dykes. Journal of Hydrology, 88 (1986) 301 – 317

Boulton, N.S. and T.D. Streltsova, 1977. Unsteady Flow to a Pumped Well in a Fissured Water-bearing Formation. Journal of Hydrology, 35 (1977) 257 – 269

Bourdet, D., 1985. Pressure Behavior of Layered Reservoirs with Cross-Flow. SPE 13628. Society of Petroleum Engineers of AIME. Paper presented at the 1985 SPE California Regional Meeting held in Bakersfield, March 27 – 29

Chiang, W.-H. and W. Kinzelbach, 1999. Processing Modflow. A simulation system for modelling groundwater flow and pollution

Cinco, H., 1982. Evaluation of Hydraulic Fracturing by Transient Pressure Analysis Methods. SPE 10043. Society of Petroleum Engineers of AIME. Paper presented at the International Petroleum Exhibition and Technical Symposium of the Society of Petroleum Engineers held in Beijing, China, 18 – 26 March 1982

Cinco-Ley, H. and F. Samaniego V., 1977. Effect of Wellbore Storage and Damage on the Transient Pressure Behavior of Vertically Fractured Wells. SPE 6752. Society of Petroleum Engineers of AIME. Paper presented at the 52nd Annual Fall Technical Conference and Exhibition of the Society of Petroleum Engineers of AIME held in Denver, Colorado, 9 – 12 October 1977

Cinco-Ley, H. and F. Samaniego V., 1981a. Transient Pressure Analysis for Fractured Wells. SPE 7490. Society of Petroleum Engineers of AIME. Paper presented at the 53rd Annual Technical Conference and Exhibition of the Society of Petroleum Engineers of AIME held in Houston, 1 – 3 October 1978

Cinco-Ley, H. and F. Samaniego V., 1981b. Transient Pressure Analysis: Finite Conductivity Fracture Case Versus Damaged Fracture Case. SPE 10179. Society of Petroleum Engineers of AIME. Paper presented at the 56th Annual Fall Technical Conference and Exhibition of the Society of Petroleum Engineers of AIME held in San Antonio, Texas, 5 – 7 October 1981

Cinco-Ley, H. and F. Samaniego V., 1982. Pressure Transient Analysis for Naturally Fractured Reservoirs. SPE 11026. Society of Petroleum Engineers of AIME. Paper presented at the 57th Annual Fall Technical Conference and Exhibition of the Society of Petroleum Engineers of AIME held in New Orleans, Luisiana, 26 – 29 September 1982

Cinco-Ley, H. and F. Samaniego V., 1985. The Pressure Transient Behavior for Naturally Fractured Reservoirs with Multiple Block Size. SPE 14168. Society of Petroleum Engineers of AIME. Paper presented at the 60th Annual Technical Conference and Exhibition of the Society of Petroleum Engineers held in Las Vegas, NV, 22 – 25 September 1985

Cinco-Ley, H., F. Samaniego V., and N. Dominguez, 1978. Transient Pressure Behavior for a Well with a Finite-Conductivity Vertical Fracture. SPE 6014. Society of Petroleum Engineers of AIME. Paper presented at the 51st Annual Fall Technical Conference and Exhibition held in New Orleans, Luisiana, 3 – 6 October 1976

Cooper H.H. and C.E. Jacob, 1946. A Generalized Graphical Method for Evaluating Formation Constants and Summarizing Well Field History. Am. Geophys. Union Transactions, Vol. 27, 526 - 534

de Marsilly, G., 1986. Quantitative Hydrogeology – Groundwater Hydrogeology for Engineers. Academic Press (London) Ltd., 440 pages

Earlougher, C.R. Jr., 1977. Advances in Well Test Analysis. Monograph Volume 5 of the Henry L. Doherty Series. Second Printing. Society of Petroleum Engineers of AIME. 294 pages

Economides, M. and K.J. Nolte, 1989. Reservoir Simulation. Second Edition. Prentice Hall, Englewood Cliffs, New Jersey 07632

Ehlig-Economides, C. and M. Economides, 1985. Pressure Transient Analysis in an Elongated Linear Flow System. Society of Petroleum Engineers. SPE 12520, 839 – 847

Ferris, J.G., D.B. Knowless, R.H. Brown, and R.W. Stallman, 1962. Theory of Aquifer Tests. U.S. Geological Survey, Water-Supply Paper 1536E, 174 pp

Gringarten, A.C. and H.J. Ramey Jr., 1973. The Use of Source and Green's Functions in Solving Unsteady-Flow Problems in Reservoirs. SPE 3818. SPE Journal, 1973, Vol. 255, 285 – 296

Gringarten, A.C. and H.J. Ramey Jr., 1974. Unsteady-State Pressure Distribution Created by a Well With a Single Horizontal Fracture, Partial Penetration, or Restricted Entry. Society of Petroleum Engineers of AIME. Transactions, Vol. 257, 413 – 426

Gringarten, A.C., H.J. Ramey Jr., and R. Raghavan, 1974. Unsteady-State Pressure Distributions Created by a Well with a Single Infinite-Conductivity Vertical Fracture. SPE 4051. Society of Petroleum Engineers of AIME. Paper presented at the SPE-AIME 47th Annual Fall Meeting held in San Antonio, Texas, 8 – 11 October 1972

Guppy, K.H., H. Cinco-Ley, H.J. Ramey Jr., and F. Samaniego V., 1982. Non-Darcy Flow in Wells with Finite-Conductivity Vertical Fractures. SPE 8281. Society of Petroleum Engineers of AIME

Gustafson, G. and O. Anderson, 1997. Workshop on Borehole Design, Test Pumping and Borehole Rehabilitation held in Windhoek, Namibia, 24 – 28 February 1997

Harabaugh, A.W., E.R. Banta, M.C. Hill and M.G. McDonald, 1999. MODFLOW: The US-Geological Survey Modular Ground-Water Model

Hobbs, B.E., W.D. Means and P.F. Williams, 1976. An Outline of Structural Geology. John Willey and Sons, Inc., New York, Chichester, Brisbane, Toronto, Singapore, 571 pages

Horne, R.N., 1995. Modern Well Test Analysis. A Computer Aided Approach. Second Edition. Petroway, Inc. Palo Alto, CA 94303. 257 pages

Jacob, C.E., 1946. Drawdown Test to Determine Effective Radium of Artesian Well. American Society of Civil Engineers, Transactions, Paper N. 2321

Kawecki, M.W., 1995. Meaningful Interpretation of Step-Drawdown Tests. Ground Water, Vol. 33, No. 1, 23 – 32

Kazemi, H., 1969. Pressure Transient Analysis of Naturally Fractured Reservoirs with Uniform Fracture Distribution. SPE 2156A. Society of Petroleum Engineers. Paper Presented at the 43rd Annual Fall Meeting held in Houston, Texas, 29 September – 2 October 1968

Kinzelbach, W. und R. Rausch, 1995. Grundwassermodellierung. Eine Einführung mit Übungen. Gebrüder Borntraeger Berlin – Stuttgart. 283 Seiten

Kinzelbach, W., 1991. Numerische Methoden zur Modellierung des Transports von Schadstoffen im Grundwasser. 2. Auflage. Gwf – Schriftenreihe Wasser – Abwasser. Oldenbourg Verlag. 343 Seiten

Kruseman, G.P. and N.A. de Ridder, 1991. Analysis and Evaluation of Pumping Test Data. Second Edition. International Institute for Land Reclamation and Improvement. Publication 47. Wageningen, the Netherlands. 377 pages

Leveinen, J., E. Rönkä, J. Tikkanen, and E. Karro, 1998. Fractional Flow Dimensions and Hydraulic Properties of a Fracture-Zone Aquifer, Leppävirta, Finland. IAH Hydrogeology Journal Vol. 6, No. 3, 327 - 340

Long, J.C.S. and P.A. Witherspoon, 1985. The Relationship of the Degree of Interconnection to Permeability in Fracture Networks. J. of Geophysical Research, Vol. 90, No. B4, 3087 – 3098

Long, J.C.S., J.S. Remer, C.R.Wilson and P.A. Witherspoon, 1982. Porous Media Equivalents for Networks of Discontinuous Fractures. Water Resources Res., Vol. 18, No. 3, 645 – 658

Matheron, G., 1967. Eléments pour une théorie des milieux poreux. Masson et Cie, Paris, 166 pages

Mavor, M.J. and H. Cinco-Ley, 1979. Transient Pressure Behavior of Naturally Fractured Reservoirs. SPE 7977. Society of Petroleum Engineers of AIME. Paper presented at the 1979 California Regional Meeting of the Society of Petroleum Engineers of AIME held in Ventura, Calif., 18 – 20 April 1979

Merton, J.G., 1987. Interpretations des Essais de Pompage en Millieu Fisuré. IWACO. Bureau d'Etudes en Eau en Environnement. Rotterdam, Pays-Bas, 120 pages

Moench, A.F. and A. Ogata, 1984. A Numerical Inversion of the Laplace Transform Solution to Radial Dispersion in a Porous Medium. Water Resources Res., Vol. 17, No. 1, 250 – 252

Moench, A.F., 1984. Double-Porosity Models for a Fissured Groundwater Reservoir with Fracture Skin. Water Resources Res., Vol. 20, No. 7, 831 - 846

Olarewaju, J., 1996. Modelling Fractured Reservoirs with Stochastic Fractals. SPE 36207. Society of Petroleum Engineers of AIME. Paper presented at the 7th Abu Dhabi International Petroleum Exhibition Conference held in Abu Dhabi, 13 – 16 October 1996

Olarewaju, J., S. Ghori, A. Fuseni, and M. Wajid, 1997. Stochastic Simulation of Fracture Density for Permeability Field Estimation. SPE 37692. Society of Petroleum Engineers of AIME. Paper presented at the 1997 SPE Middle East Oil Show and Conference held in Manama, Bahrain, 15 – 18 March 1997

Olarewaju, J.S., 1997. Pressure Transient Analysis of Naturally Fractured Reservoirs: A Case Study. Society of Petroleum Engineers. SPE 37801, 357 – 374

Papadopulos, I.S., H.H. Cooper Jr., 1967. Drawdown in a Well of Large Diameter. Water Resources Research. Vol. 3, Nr. 1, pp. 241 – 244

Prats, M., 1961. Effect of Vertical Fractures on Reservoir Behavior – Incompressible Fluid Case. Society of Petroleum Engineers. SPE 1575. Paper presented at 35th Annual Fall Meeting of SPE held in Denver, Colorado, 2 – 5 Oct, 1960

Raghavan, R., A Uraiet, and G.W. Thomas, 1978. Vertical Fracture Height: Effect on Transient Flow Behavior. Society of Petroleum Engineers. SPE 1575. Paper presented at 51th Annual Fall Meeting of SPE held in New Orleans, 3 – 6 Oct, 1976

Ramey Jr., H.J. and A.C. Gringarten, 1976. Effect of High-Volume Fractures on Geothermal Steam Well Behavior. Proceedings Second U. N. Devel. And Use of Geothermal Resources, San Francisco. US Government Printing Office, Washington DC, Vol. 3, 1759 – 1762

Sabet, M.A., 1991. Well Test Analysis. Contributions in Petroleum Geology and Engineering, Volume 8. Gulf Publishing Company, Houston. 460 pages

Spring (2000). Simulation of Processes in Groundwater. Delta h Ingenieurgesellschaft mbH, Bochum

Stehfest, H., 1970. Algorithm 368 – Numerical Inversion of Laplace Transform. Communication of the ASM, Vol. 13, No. 1, 47 – 49

Stober, I., 1986. Strömungsverhalten in Festgesteinsaquiferen mit Hilfe von Pump- und Injektionsversuchen. Geol. Jb., C42, 3 – 204

Streltsova, T.D., 1988. Well Testing in Heterogeneous Formations. An Exxon Monograph. John Wiley & Sons, N.Y., 413 pages

Theis, C.V., 1935. The Relation Between the Lowering of the Piezometric Surface and the Rate and Duration of Discharge of a Well Using Ground-Water Storage. American Geophysical Union, Transactions. Reports and Papers, Hydrology – 1935

Therrien, R. and E.A. Sudicky, 1996. Three-dimensional analysis of variably-saturated flow and solute transport in discretely-fractured porous media. Journal of Contaminant Hydrology, 23, 1 – 44

Valkó, P. and M.J. Economides, 1997. Transient Behavior of Finite Conductivity Horizontal Fractures. SPE 38436. Society of Petroleum Engineers, SPE Journal, Vol. 2, 213 – 222

van Everdingen, A.F., 1952. The Skin Effect and its Influence on the Productive Capacity of a Well. Paper Number 203 G. Society of Petroleum Engineers of AIME. Paper presented at the Fall Meeting of the Petroleum Branch, American Institute of Mining and Metallurgical Engineers, in Houston, Texas, 1 – 3 October, 1952

van Tonder, G., H. Kunstmann, and Y. Xu, 1998. Estimation of the Sustainable Yield of a Borehole Including Boundary Information, Drawdown Derivatives and Uncertainty Propagation

Walton, W.C., 1996. Aquifer Test Analysis with Windows Software. Lewis Publisher, Boca Raton. 301 pages

Warren, J.E. and P.J. Root, 1962. The Behavior of Naturally Fractured Reservoirs. Society of Petroleum Engineers. Paper presented at the Fall Meeting of the Society of Petroleum Engineers held in Los Angeles, 7 – 10 October 1962

Waterloo Hydrogeologic Inc., 2000. Visual MODFLOW User's Manual. The Proven Standard for 3-D Groundwater Flow & Contaminant Transport Modeling using MODFLOW, MODPATH, MT3DMS, and RT3D

Wei, L., J. Hadwin, E. Chaput, K. Rawnsley, and P. Swaby, 1998. Discriminating Fracture Patterns in Fractures Reservoirs by Pressure Transient Tests. SPE 49233. Society of Petroleum Engineers. Paper presented at the 1998 SPE Annual Technical Conference and Exhibition held in New Orleans, Luisiana, 27 – 30 September 1998

Wendland, E.C., 1996. Numerische Simulation von Strömung und hochadvektivem Stofftransport in geklüftetem, porösem Medium. Mitteilung Nr. 96-6. Institut für konstruktiven Ingenieurbau. Ruhr-Universität Bochum

Witherspoon, P.A., C.H. Amick, J.E. Gale and K. Iwai, 1979. Observation of a Potential Size Effect in Experimental Determination of the Hydraulic Properties of Fractures. Water Resources Res., Vol. 15, No. 5, 1142 – 1146

Wollrath, J. and Zielke, W., 1990. FE-Simulation von Strömungen im klüftigen Gestein. Deutsche Gewässerkundliche Mitteilung, Vol. 34, H.1/2, 2-7

Zielke et al. (1984 – 1994). Theorie und Benutzereinleitung zum Programmsystem ROCKFLOW. Institut für Strömungsmechanik und Elektronisches Rechnen im Bauwesen. Universität Hannover, Germany